

# Generalized Quantum Phase Transitions for Quantum-State Engineering in Spinor Bose-Einstein Condensates

Von der QUEST-Leibniz-Forschungsschule  
der Gottfried Wilhelm Leibniz Universität Hannover  
zur Erlangung des akademischen Grades

**Doktorin der Naturwissenschaften**  
**Dr. rer. nat.**

genehmigte Dissertation von

**M. Sc. Polina Feldmann**



2021

Referent: Prof. Dr. Luis Santos (Betreuer)  
Korreferenten: Prof. Dr. Augusto Smerzi (Zweitbetreuer)  
Prof. Dr. Pavel Cejnar  
Vorsitzender der  
Promotionskommission: Prof. Dr. Carsten Klempt  
Tag der Promotion: 12. April 2021

*In memoriam*  
***Alexander Feldmann***



# Abstract

Entanglement lies at the core of emergent quantum technologies such as quantum-enhanced metrology, quantum communication and cryptography, and quantum simulation and computing. Spinor Bose-Einstein condensates (BECs) offer a promising platform for the generation and application of entangled states. For example, a spin-1 BEC has served for the proof-of-principle demonstration of a quantum-enhanced atomic clock. Ferromagnetic spin-1 BECs with zero magnetization exhibit three ground-state quantum phases with different entanglement properties. The control parameter can be tuned by a magnetic field or by microwave dressing. As already experimentally demonstrated, an entangled ground state can be reached from a well accessible, non-entangled one by driving the control parameter across quantum phase transitions (QPTs).

We investigate which of the entangled ground states afford quantum-enhanced interferometry. The interferometric usefulness is quantified by the quantum Fisher information (QFI), which we analyze throughout all ground-state phases. A large QFI at about half the Heisenberg limit, and thus far above the standard quantum limit, is attained by the well-known Twin-Fock state and by the central broken-axisymmetry (CBA) state. We detail how the CBA state can be used as a probe for quantum-enhanced interferometry.

Furthermore, we observe that the large QFI of the CBA state can be traced back to enclosed macroscopic superposition states (MSSs). Measuring the atom number in one out of three modes generates, with high probability and heralded by the measurement outcome, a MSS similar to a NOON state. Our proposal promises NOON-like MSSs of unprecedentedly many atoms.

Both proposed applications of the adiabatically prepared CBA state depend only on existent technology. Our numerical results show that they tolerate a reasonably swift quasiadiabatic passage in the presence of atom loss as well as uncertainties of atom counting.

Excited-state quantum phase transitions (ESQPTs) extend the concept of QPTs beyond the ground state. While they have been extensively investigated theoretically, there are only few experimental results. From the perspective of quantum-state engineering, it is furthermore surprising how rarely order parameters of ESQPTs are discussed in the literature. Mean-field models for spinor BECs imply ESQPTs, to which some experimental observations on the mean-field dynamics can be attributed. However, so far, neither theoretical nor experimental studies have specifically addressed ESQPTs in spinor BECs.

We extend the ground-state phase diagram of ferromagnetic spin-1 BECs with zero magnetization across the spectrum. There are three excited-state phases, corresponding to one ground-state phase each. The ESQPTs are signaled by a diverging density of states. The mean-field phase-space trajectories can be characterized by a winding number that is in one-to-one correspondence to the excited-state phases. We derive a closely related order parameter encoded in the dynamics of coherent states and discuss how this order parameter can be interferometrically measured in current experiments. Remarkably, the mean-field model governing the ESQPTs in spin-1 BECs with zero magnetization is encountered also, e. g., in molecular and nuclear physics. Because of the superior experimental control, spinor BECs can be considered as simulators of the ESQPTs in those systems.

Our results contribute to quantum-state engineering and quantum-enhanced interferometry in spinor BECs and to the characterization of excited-state quantum phases. The latter may, in turn, lead on to applications in quantum-state engineering.

# Keywords

- quantum-state engineering
- spinor Bose-Einstein condensates
- ground-state quantum phase transitions
- excited-state quantum phase transitions
- order parameters
- quantum-enhanced metrology
- quantum-enhanced interferometry
- macroscopic superposition states
- Fisher information
- mean-field convergence

# Contents

<b>List of Abbreviations</b>	<b>9</b>
<b>1 Introduction</b>	<b>11</b>
<b>2 Quantum-State Engineering</b>	<b>15</b>
2.1 Fisher Information and Entanglement	15
2.1.1 Classical Fisher Information	15
2.1.2 Quantum Fisher Information and Optimal Measurements	16
2.1.3 Convexity and Additivity	17
2.1.4 Repeated Experiments	18
2.1.5 Unitary Transformations	19
2.1.6 Optimal Transformations	19
2.1.7 Entanglement Criterion	20
2.1.8 Standard Quantum Limit and Heisenberg Limit	21
2.2 Quantum-Enhanced Interferometry	21
2.2.1 A Minimalist Interferometer	22
2.2.2 The General Interferometer	23
2.2.3 Cramér-Rao Bound and Quantum Enhancement	23
2.3 Macroscopic Superposition States	25
2.3.1 Quantification by Fisher Information	26
<b>3 Spin-1 Bose-Einstein Condensates</b>	<b>27</b>
3.1 Bose-Einstein Condensation	28
3.2 Weakly Interacting Spin-1 Bosons	30
3.3 Single-Mode Approximation	33
3.3.1 Spin Degrees of Freedom	34
3.3.2 Spatial Degrees of Freedom	35
3.4 Collective Transformations	37
3.4.1 Single-Boson Transformations	37
3.4.2 $N$ -Boson Transformations	38
3.4.3 Baker-Campbell-Hausdorff Formula	39
3.5 Interaction with Electromagnetic Radiation	40
3.5.1 Microwave Coupling	41
3.5.2 Radio-Frequency Coupling	44
3.6 Atom Loss	45
3.7 Mean-Field Limit	47
3.7.1 Coherent States	47
3.7.2 Limit of Expectation Values	48
3.7.3 Density of States	50
3.7.4 Equations of Motion	52
3.7.5 Dynamics	54

<b>4</b>	<b>Ground-State Quantum Phase Transitions</b>	<b>55</b>
4.1	Phases . . . . .	56
4.2	Quantum Fisher Information . . . . .	59
4.3	Optimal Measurement . . . . .	62
4.4	Central Broken-Axisymmetry State . . . . .	64
4.5	Macroscopic Superposition States . . . . .	66
4.6	Proposal . . . . .	68
4.7	Experimental Feasibility . . . . .	70
4.7.1	Quasiadiabaticity . . . . .	71
4.7.2	Atom Loss . . . . .	74
4.7.3	Atom-Counting Uncertainty . . . . .	78
4.8	Quenching . . . . .	81
4.9	Conclusion . . . . .	84
<b>5</b>	<b>Excited-State Quantum Phase Transitions</b>	<b>87</b>
5.1	Phases . . . . .	88
5.2	Mean-Field Model . . . . .	89
5.2.1	Phase Space . . . . .	90
5.2.2	Stationary Points . . . . .	90
5.2.3	Energy Hypersurfaces . . . . .	91
5.2.4	Trajectories . . . . .	92
5.2.5	Dynamics . . . . .	93
5.3	Density of States . . . . .	94
5.3.1	Restriction to Magnetization-Free Subspace . . . . .	94
5.3.2	Divergence at Excited-State Quantum Phase Transitions . . . . .	97
5.4	Further Signatures . . . . .	98
5.5	Order Parameter . . . . .	99
5.6	Proposal . . . . .	101
5.7	Experimental Feasibility . . . . .	102
5.7.1	Visibility . . . . .	103
5.7.2	Finite Time . . . . .	104
5.7.3	Finite Size . . . . .	104
5.7.4	Magnetic-Field Fluctuations . . . . .	105
5.8	Bosonic Two-Level Pairing Models . . . . .	106
5.9	Conclusion . . . . .	106
<b>6</b>	<b>Conclusion and Outlook</b>	<b>109</b>
<b>7</b>	<b>Acknowledgment</b>	<b>111</b>
	<b>Bibliography</b>	<b>113</b>
	<b>Curriculum Vitae</b>	<b>129</b>
	<b>List of Publications</b>	<b>131</b>



# List of Abbreviations

BA	broken-axisymmetry
BCH	Baker-Campbell-Hausdorff
BEC	Bose-Einstein condensate
CBA	central broken-axisymmetry
CCRB	classical Cramér-Rao bound
CFI	classical Fisher information
CPTP	completely positive trace-preserving
CRB	Cramér-Rao bound
DOS	density of states
EOM	equation of motion
ESQPT	excited-state quantum phase transition
FI	Fisher information
GHZ	Greenberger-Horne-Zeilinger
HL	Heisenberg limit
LMG	Lipkin-Meshkov-Glick
MCWF	Monte-Carlo wave-function
MSS	macroscopic superposition state
P	polar
POVM	positive operator-valued measurement
QCRB	quantum Cramér-Rao bound
QFI	quantum Fisher information
QPT	quantum phase transition
RHS	right-hand side
RWA	rotating-wave approximation
SLD	symmetric logarithmic derivative
SMA	single-mode approximation
SQL	standard quantum limit
TF	Twin-Fock



# 1 Introduction

The endless, meticulous curves of the sea flamed for an instant and then changed to a deep royal purple flecked with green. The mist lifted in quick, lithe ribbons, and before us lay the island, the mountains as though sleeping beneath a crumpled blanket of brown, the folds stained with the green of olive-groves.

---

G. Durrell  
*in My family and other animals*

Less than one hundred years ago the mere theoretical possibility of quantum entanglement bewildered such great minds as Einstein, Podolsky, Rosen, [1] and Schrödinger [2]. To date, entanglement has matured into a technological resource. Commercial applications of entanglement include quantum annealers [3] and devices for quantum cryptography [4]. On the side of scientific applications, e. g., state-of-the-art interferometers for gravitational-wave detection employ entangled probe states [5–7]. At the same time, entanglement remains a fascinating and active topic of theoretical and experimental research. Much interest is devoted to emerging quantum technologies in the fields of quantum-enhanced metrology [8, 9], quantum communication [10] and cryptography [11, 12], and quantum simulation [13, 14] and computing [15–18]. From the perspective of theoretical physics, e. g., further investigating multipartite entanglement and advancing numerical methods for quantum many-body systems is of outermost importance [19]. The salient long-term goal consists in a fault-tolerant scalable universal quantum computer.

Entangled states need to be designed, prepared, maintained, and characterized. These tasks compose the area of quantum-state engineering. We are especially interested in its application to quantum-enhanced metrology or, more precisely, interferometry [9]. Entangled probes enable interferometric sensitivities that are fundamentally beyond the reach of non-entangled states. The Fisher information (FI) [20] quantifies the interferometric usefulness of entangled states. Furthermore, it is possible to derive an effective size of macroscopic superposition states (MSSs) from the FI [21, 22]. MSSs probe the validity of quantum physics at macroscopic scales and benchmark our ability to prepare and characterize highly entangled states. In Chapter 2, we summarize some mathematical properties of the FI and detail how the FI is related to quantum-enhanced interferometry and MSSs.

We focus on interferometers that rely on the interference of internal atomic states. Notably, this includes atomic clocks, which can measure time with unprecedented precision [23]. So far, high-precision atomic clocks do not exploit entanglement. However, quantum enhancement has been already demonstrated in a number of proof-of-principle experiments [24–27].

In general, cooling is beneficial for precision measurements. At ultra-low temperatures, an ensemble of bosonic atoms can form a Bose-Einstein condensate (BEC) [28]. This phase of matter is characterized by a particularly high occupation of the ground state, which leads to a collective behavior of atoms. The—typically weak—interaction between the atoms gives rise to non-trivial phenomena. An even greater versatility is offered by spinor BECs [29, 30], where the atoms can access several internal or spin states. A quantum-enhanced atomic clock based on a spinor BEC has been demonstrated in Ref. [25]. Moreover, spinor BECs constitute a promising candidate for quantum-enhanced gravity gradiometry [31]. This thesis explores quantum-state engineering in

ferromagnetic spin-1 BECs. Chapter 3 provides an introduction to spinor BECs.

Ferromagnetic spin-1 BECs with zero magnetization exhibit three ground-state quantum phases [32]. The control parameter  $\xi$ , given by the ratio of the quadratic Zeeman energy to the energy of spin-changing collisions, can be tuned by a magnetic field or by microwave dressing [33]. These quantum phases afford adiabatic quantum-state engineering [32]. In the polar (P) phase, the ground state is non-entangled and experimentally well accessible. Highly entangled states are, on the other hand, found in the broken-axisymmetry (BA) and Twin-Fock (TF) phases. According to the adiabatic theorem [34], the ground state at some  $\xi_0$  can be transformed into the ground state at  $\xi_1$  by an infinitely slow change of  $\xi$ . Thus, preparing the P ground state and slowly ramping  $\xi$  into the BA or TF phase gives access to highly entangled states. This method has been successfully used, e. g., to generate a TF state of about 11 000  $^{87}\text{Rb}$  atoms [35].

In Chapter 4, we further investigate the prospects of adiabatic quantum-state engineering in ferromagnetic spin-1 BECs with zero magnetization. First, we analyze the FI throughout the three ground-state quantum phases. The maximal FI is attained by the well-known TF state and by the central broken-axisymmetry (CBA) state. We detail how the CBA state can serve as a probe for quantum-enhanced interferometry. The large FI of the three-mode CBA state can be traced back to constituent two-mode MSSs. More precisely, measuring the atom number in one mode prepares, with high probability and heralded by the measurement outcome, a MSS in the other two modes. These MSSs resemble NOON states, which constitute a paradigmatic example of MSSs. So far, such states were limited to 30 massive particles [36–39], whereas we envisage  $10^2$ - $10^5$  atoms. Both proposed applications of the adiabatically generated CBA state are feasible with current technology.

The proposals in Chapter 4 are based on the ground-state phase diagram of a spin-1 BEC. However, it turns out that their experimental feasibility depends on favorable properties of low-lying excited states. More generally, experimental progress and the current interest in many-body systems out of equilibrium draw increased attention to excited states. Quantum phase transitions (QPTs) concern, by definition, exclusively the ground state [40]. The recently introduced excited-state quantum phase transitions (ESQPTs) generalize this notion [41, 42]. While ESQPTs have been extensively investigated theoretically, the number of experimental results remains unsatisfactory [43–47]. From the perspective of quantum-state engineering, it is furthermore surprising that the literature on ESQPTs scarcely discusses order parameters. The mean-field models for spinor BECs [29] imply ESQPTs, to which some experimental observations on the mean-field dynamics [43, 44, 46] can be attributed. However, so far, neither theoretical nor experimental studies have specifically addressed ESQPTs in spinor BECs. The excellent experimental control offered by spinor BECs makes this omission particularly deplorable.

Chapter 5 extends the ground-state phase diagram of a ferromagnetic spin-1 BEC with zero magnetization across the spectrum. We identify three excited-state phases. At the lowest energy, they turn into the familiar ground-state phases. The ESQPTs are signaled by a divergent density of states (DOS). Moreover, the mean-field phase-space trajectories can be characterized by a winding number that is in one-to-one correspondence to the excited-state phases. This enables us to define an order parameter that is based on the dynamics of coherent states and can be accessed by interferometry. Remarkably, for large particle numbers ferromagnetic spin-1 BECs simulate the ESQPTs in a wide class of quantum models including the Lipkin-Meshkov-Glick (LMG) model, the vibron model for molecules, and the interacting boson model for nuclei. In the present version, the proposed interferometric measurement is feasible but requires an outstanding control over magnetic-field noise. We aim at designing a more robust measurement protocol, if necessary based on an alternative order parameter, in the near future.

In summary, this thesis is devoted to ferromagnetic spin-1 BECs with zero magnetization. We

---

perform a complete analysis of the FI throughout the ground-state phases. Furthermore, we extend the ground-state phase diagram to excited states. In the ground-state domain, we detail how adiabatic quantum-state engineering can be used for quantum-enhanced interferometry and the heralded stochastic generation of MSSs. Regarding ESQPTs, we introduce an order parameter and propose an interferometric measurement for its extraction. We, thus, address the lack of experimental studies on ESQPTs and contribute to the characterization of excited-state phases. In the longer term, we expect that excited-state phase diagrams will enter the rich toolbox of quantum-state engineering.

We conclude and give an outlook on ensuing research topics in Chapter 6.



## 2 Quantum-State Engineering

Entangled quantum states [48] lie at the core of emerging quantum technologies such as quantum-enhanced metrology [8, 9], quantum communication [10] and cryptography [11, 12], and quantum simulation [13, 14] and computing [15–18]. The current progress of these technologies is due to our rapidly increasing ability to control various quantum systems.

Proof-of-principle experiments in quantum-enhanced metrology have been performed, e. g., with spinor Bose-Einstein condensates [25, 49], superconducting qubits coupled to microwave cavities [50], and cold atoms in optical lattices [27]. State-of-the-art photonic interferometers for gravitational-wave detection already benefit from quantum enhancement [6]. Impressive control over single photons has led to commercial quantum cryptography [4]. Related research currently focuses, e. g., on quantum key distribution over large distances [51, 52]. Quantum simulators based on, e. g., Rydberg atoms, have become applicable at the forefront of fundamental physics [53]. Precise control over trapped ions is exploited, e. g., in variational classical-quantum simulation with up to 20 ions [54]. Several large companies have developed universal quantum computers of tens of superconducting qubits, and Google has recently demonstrated quantum supremacy for a specific task [55]. Currently, one of the central goals in these devices is implementing quantum error correction. Meanwhile, commercially available quantum annealers from superconducting qubits [3] are being explored in industry [56].

Quantum-state engineering is the art of designing, preparing, maintaining, and characterizing useful entangled states. The requirements on the design depend on the targeted application. We focus on quantum-enhanced interferometry and macroscopic superposition states (MSSs). Interferometers are widely used for precision measurements in science and industry. In Section 2.2, we discuss how entanglement can fundamentally improve the interferometric precision. MSSs constitute a technological challenge and probe the validity of quantum theory at macroscopic scales. We specify our notion of MSSs in Section 2.3. Since we formulate our design targets in terms of the Fisher information (FI), we start by introducing it in Section 2.1.

### 2.1 Fisher Information and Entanglement

Quantum states may be entangled or non-entangled. However, saying that a many-body quantum state is entangled tells yet little about its properties. Obviously, not all entangled states will be of equal use for a specific task at hand. Hence, understanding the rich structure of multipartite entanglement is crucial for quantum-state engineering. The corresponding classification and quantification can be approached in various ways [57]. In the context of quantum-enhanced interferometry [58–60] and macroscopic superposition states [21], the FI [20] has proven particularly useful. Following Refs. [61, 62], we introduce the FI and discuss some relevant properties.

#### 2.1.1 Classical Fisher Information

We consider a density operator  $\hat{\rho}(\theta)$  which is a differentiable function of a parameter  $\theta \in \mathbb{R}$ . This quantum state becomes subject to a positive operator-valued measurement (POVM). We assume that the possible measurement outcomes  $\mu_j$  are discrete. The POVM assigns to each  $\mu_j$

a Hermitian, positive semi-definite operator  $\hat{M}_j$  with  $\sum_j \hat{M}_j = \mathbb{1}$ . The probability to obtain  $\mu_j$  when applying the POVM to  $\hat{\rho}(\theta)$  is

$$P_\theta(\mu_j) \equiv \text{Tr}[\hat{\rho}(\theta)\hat{M}_j]. \quad (2.1)$$

In the following we will use that, for a given  $\theta$ , there is no  $\mu_j$  with  $P_{\theta+\epsilon}(\mu_j) = 0$  in some neighborhood of  $\theta$ . This can be always achieved by restricting the Hilbert space and, with it, the POVM.

The difference between the probability distributions  $P_\theta$  and  $P_{\theta+\epsilon}$  can be quantified by the Hellinger distance:

$$[d(P_\theta, P_{\theta+\epsilon})]^2 = \frac{1}{2} \sum_j \left( \sqrt{P_\theta(\mu_j)} - \sqrt{P_{\theta+\epsilon}(\mu_j)} \right)^2 \quad (2.2)$$

The corresponding statistical speed [63],

$$\lim_{\epsilon \rightarrow 0} \partial_\epsilon d(P_\theta, P_{\theta+\epsilon}) = \frac{1}{\sqrt{8}} \sqrt{F(\theta)}, \quad (2.3)$$

can be expressed in terms of the classical Fisher information (CFI)

$$F(\theta) \equiv \sum_j \frac{1}{P_\theta(\mu_j)} [\partial_\theta P_\theta(\mu_j)]^2 = \sum_j P_\theta(\mu_j) (\partial_\theta \ln[P_\theta(\mu_j)])^2. \quad (2.4)$$

Thus, the CFI quantifies how fast  $P_\theta$  changes with  $\theta$ .

### 2.1.2 Quantum Fisher Information and Optimal Measurements

The CFI depends on the POVM applied to  $\hat{\rho}(\theta)$ . Maximizing the CFI over all POVMs yields the so-called quantum Fisher information (QFI) [64].

The QFI can be conveniently expressed in terms of the symmetric logarithmic derivative (SLD)  $\hat{L}(\theta)$  of  $\hat{\rho}(\theta)$ , which is defined to be a Hermitian solution<sup>1</sup> of

$$\partial_\theta \hat{\rho}(\theta) = \frac{1}{2} \left( \hat{L}(\theta) \hat{\rho}(\theta) + \hat{\rho}(\theta) \hat{L}(\theta) \right). \quad (2.5)$$

One can show that

$$\begin{aligned} [\partial_\theta P_\theta(\mu_j)]^2 &= \left[ \text{Re} \left( \text{Tr} \left[ \hat{\rho} \hat{L} \hat{M}_j \right] \right) \right]^2 \\ &\leq \left| \text{Tr} \left[ \hat{\rho} \hat{L} \hat{M}_j \right] \right|^2 \\ &\leq \text{Tr} \left[ \hat{\rho} \hat{M}_j \right] \text{Tr} \left[ \hat{L} \hat{\rho} \hat{L} \hat{M}_j \right] = P_\theta(\mu_j) \text{Tr} \left[ \hat{L} \hat{\rho} \hat{L} \hat{M}_j \right], \end{aligned} \quad (2.6)$$

where we have omitted the  $\theta$ -dependence of  $\hat{\rho}$  and  $\hat{L}$  for readability. To get to the last line of Eq. (2.6) we have used the Cauchy-Schwarz inequality  $|\text{Tr}[\hat{A}^\dagger \hat{B}]|^2 \leq \text{Tr}[\hat{A}^\dagger \hat{A}] \text{Tr}[\hat{B}^\dagger \hat{B}]$ . Employing  $\sum_j \hat{M}_j = \mathbb{1}$  yields

$$F(\theta) = \sum_j \frac{1}{P_\theta(\mu_j)} [\partial_\theta P_\theta(\mu_j)]^2 \leq \sum_j \text{Tr} \left[ \hat{L}(\theta) \hat{\rho}(\theta) \hat{L}(\theta) \hat{M}_j \right] = \text{Tr} \left[ \hat{\rho}(\theta) \hat{L}^2(\theta) \right]. \quad (2.7)$$

---

<sup>1</sup>Note that  $\hat{L}(\theta)$  is ambiguous.



The upper bound on the CFI provided by Eq. (2.7) does not depend on the POVM. Let us show that there is a POVM for which  $F(\theta)$  saturates this bound. The left- and right-hand sides of Eq. (2.6) become equal if and only if

$$\text{Im}\left(\text{Tr}\left[\hat{\rho}\hat{L}\hat{M}_j\right]\right) = 0 \quad \text{and} \quad \left(\hat{\rho}\hat{L}\hat{M}_j = 0 \quad \text{or} \quad \exists \lambda \in \mathbb{C} : \hat{\rho}\hat{M}_j = \lambda\hat{\rho}\hat{L}\hat{M}_j\right) \quad (2.8)$$

$$\Leftrightarrow \hat{\rho}\hat{L}\hat{M}_j = 0 \quad \text{or} \quad \exists \lambda \in \mathbb{R} : \hat{\rho}\hat{M}_j = \lambda\hat{\rho}\hat{L}\hat{M}_j. \quad (2.9)$$

Thus,  $F(\theta)$  saturates the bound (2.7) if

$$\forall j : \left(\hat{L}(\theta)\hat{M}_j = 0 \quad \text{or} \quad \exists \lambda_j \in \mathbb{R} : \hat{M}_j = \lambda_j\hat{L}(\theta)\hat{M}_j\right). \quad (2.10)$$

Let us consider the eigenstates  $|j\rangle$  and eigenvalues  $\gamma_j$  of  $\hat{L}(\theta)$ . We can satisfy Eq. (2.10) by setting  $\hat{M}_j = |j\rangle\langle j|$  and, for all  $j$  with  $\gamma_j \neq 0$ ,  $\lambda_j = 1/\gamma_j$ . Hence the QFI can be expressed as

$$F_Q(\theta) \equiv \text{Tr}\left[\hat{\rho}(\theta)\hat{L}^2(\theta)\right]. \quad (2.11)$$

Equation (2.9) can be used to check whether a measurement is optimal, i. e.,  $F(\theta) = F_Q(\theta)$ . For a pure state  $\hat{\rho}(\theta) = |\psi(\theta)\rangle\langle\psi(\theta)|$ , we can set

$$\hat{L}(\theta) = 2\left(|\partial_\theta\psi_\perp(\theta)\rangle\langle\psi(\theta)| + |\psi(\theta)\rangle\langle\partial_\theta\psi_\perp(\theta)|\right), \quad (2.12)$$

where we have introduced  $|\partial_\theta\psi_\perp(\theta)\rangle \equiv (\mathbb{1} - |\psi(\theta)\rangle\langle\psi(\theta)|)|\partial_\theta\psi(\theta)\rangle$  and  $|\partial_\theta\psi(\theta)\rangle \equiv \partial_\theta|\psi(\theta)\rangle$ . If  $\hat{M}_j$  is a one-dimensional projection,  $\hat{M}_j = |\mu_j\rangle\langle\mu_j|$ , condition (2.9) becomes

$$\langle\partial_\theta\psi_\perp(\theta)|\mu_j\rangle = 0 \quad \text{or} \quad \exists \lambda \in \mathbb{R} : \langle\psi(\theta)|\mu_j\rangle = 2\lambda\langle\partial_\theta\psi_\perp(\theta)|\mu_j\rangle \quad (2.13)$$

$$\Leftrightarrow \text{Im}\left(\langle\psi(\theta)|\hat{M}_j|\partial_\theta\psi_\perp(\theta)\rangle\right) = 0. \quad (2.14)$$

In the previous paragraph we have seen that, for any given  $\theta$ , we can construct an optimal measurement. Note however that, in general, a  $\theta$ -independent optimal measurement does not exist [65].

### 2.1.3 Convexity and Additivity

Let us discuss two useful properties of the classical and quantum FI. First, we consider the convex combination of some density matrices  $\hat{\rho}^{(k)}(\theta)$ ,

$$\hat{\rho}(\theta) = \sum_{k=1}^n p_k \hat{\rho}^{(k)}(\theta) \quad \text{with} \quad p_k \geq 0, \quad \sum_k p_k = 1. \quad (2.15)$$

Recall that, though usually not explicitly indicated, both FI depend on the quantum state. It turns out that this dependency is convex:

$$F(\theta) \leq \sum_k p_k F^{(k)}(\theta) \quad \text{and} \quad F_Q(\theta) \leq \sum_k p_k F_Q^{(k)}(\theta) \quad (2.16)$$

Equation (2.16) can be readily demonstrated. For the CFI, we first note that  $P_\theta(\mu_j) = \text{Tr}[\hat{\rho}(\theta)\hat{M}_j] = \sum_k p_k \text{Tr}[\hat{\rho}^{(k)}(\theta)\hat{M}_j] \equiv \sum_k p_k P_\theta^{(k)}(\mu_j)$ . Then the convexity immediately follows from the Cauchy-Schwarz inequality, which yields

$$\begin{aligned} [\partial_\theta P_\theta(\mu_j)]^2 &= \left[\sum_k p_k \partial_\theta P_\theta^{(k)}(\mu_j)\right]^2 \leq \sum_l p_l P_\theta^{(l)}(\mu_j) \sum_k p_k \frac{1}{P_\theta^{(k)}(\mu_j)} \left[\partial_\theta P_\theta^{(k)}(\mu_j)\right]^2 \\ &\Leftrightarrow \frac{1}{P_\theta(\mu_j)} [\partial_\theta P_\theta(\mu_j)]^2 \leq \sum_k p_k \frac{1}{P_\theta^{(k)}(\mu_j)} \left[\partial_\theta P_\theta^{(k)}(\mu_j)\right]^2. \end{aligned} \quad (2.17)$$

To deduce the convexity of the QFI, recall that there is a POVM for which  $F(\theta) = F_Q(\theta)$  and, thus,

$$F_Q(\theta) = F(\theta) \leq \sum_k p_k F^{(k)}(\theta) \leq \sum_k p_k F_Q^{(k)}(\theta). \quad (2.18)$$

Next, we consider the tensor product of some density matrices  $\hat{\rho}^{(k)}(\theta)$ ,

$$\hat{\rho}(\theta) = \bigotimes_k \hat{\rho}^{(k)}(\theta). \quad (2.19)$$

Let us introduce  $\hat{L} \equiv \sum_k \hat{L}^{(k)}$ , where  $\hat{L}^{(k)}$  denotes an SLD of  $\hat{\rho}^{(k)}$ . One can easily check that  $\hat{L}$  is an SLD of  $\hat{\rho}(\theta)$ . Note that, for any density operator  $\hat{\rho}$  and its SLD  $\hat{L}$ ,  $\text{Tr}[\hat{\rho}(\theta)\hat{L}(\theta)] = \partial_\theta \text{Tr}[\hat{\rho}(\theta)] = 0$ . Hence,

$$F_Q(\theta) = \sum_{k,l} \text{Tr}[\hat{\rho}(\theta)\hat{L}^{(k)}(\theta)\hat{L}^{(l)}(\theta)] = \sum_k \text{Tr}[\hat{\rho}^{(k)}(\theta)[\hat{L}^{(k)}(\theta)]^2] = \sum_k F_Q^{(k)}(\theta). \quad (2.20)$$

This is called the additivity of the QFI.

Also the CFI is additive—if the individual subsystems are measured independently. More precisely, each  $\hat{\rho}^{(k)}(\theta)$  is subjected to some POVM with measurement outcomes  $\mu_j^{(k)}$  and operators  $\hat{M}_j^{(k)}$ . Accordingly, the overall POVM admits the measurement outcomes  $\mu_{\mathbf{j}} \equiv (\mu_{j_1}^{(1)}, \mu_{j_2}^{(2)}, \dots)$  corresponding to  $\hat{M}_{\mathbf{j}} = \bigotimes_k \hat{M}_{j_k}^{(k)}$ . Thus,  $P_\theta(\mu_{\mathbf{j}}) = \text{Tr}[\hat{\rho}(\theta)\hat{M}_{\mathbf{j}}] = \prod_k \text{Tr}[\hat{\rho}^{(k)}(\theta)\hat{M}_{j_k}^{(k)}] \equiv \prod_k P_\theta^{(k)}(\mu_{j_k}^{(k)})$  and

$$\begin{aligned} F(\theta) &= \sum_{\mathbf{j}} \prod_i P_\theta^{(i)}(\mu_{j_i}^{(i)}) \sum_{k,l} \left( \partial_\theta \ln[P_\theta^{(k)}(\mu_{j_k}^{(k)})] \right) \left( \partial_\theta \ln[P_\theta^{(l)}(\mu_{j_l}^{(l)})] \right) \\ &= \sum_k \sum_{j_k} P_\theta^{(k)}(\mu_{j_k}^{(k)}) \left( \partial_\theta \ln[P_\theta^{(k)}(\mu_{j_k}^{(k)})] \right)^2 + \sum_{k \neq l} \left( \partial_\theta \sum_{j_k} P_\theta^{(k)}(\mu_{j_k}^{(k)}) \right) \left( \partial_\theta \sum_{j_l} P_\theta^{(l)}(\mu_{j_l}^{(l)}) \right) \\ &= \sum_k F^{(k)}(\theta). \end{aligned} \quad (2.21)$$

Together with Eq. (2.20) this, particularly, entails that an optimal POVM for the entire  $\hat{\rho}(\theta)$  can be realized by independently applying the respective optimal POVMs to all  $\hat{\rho}^{(k)}(\theta)$ .

### 2.1.4 Repeated Experiments

The additivity of the FI has a straightforward consequence on the important case of repeated experiments. We, again, consider a quantum state  $\hat{\rho}(\theta)$  and a POVM with measurement outcomes  $\mu_j$  and corresponding operators  $\hat{M}_j$ . We assume that, at any given  $\theta$ , state preparation and measurement are repeated  $n$  times. This situation is appropriately described by the state  $\hat{\rho}^{[n]}(\theta) \equiv [\hat{\rho}(\theta)]^{\otimes n}$  subjected to the POVM with measurement outcomes  $\mu_{\mathbf{j}} \equiv (\mu_{j_1}, \dots, \mu_{j_n})$  and operators  $\hat{M}_{\mathbf{j}} = \bigotimes_{k=1}^n \hat{M}_{j_k}$ .

Let us denote the FI of a single experiment by  $F$  and  $F_Q$ , respectively, and the FI of the  $n$ -fold experiment by  $F^{[n]}$  and  $F_Q^{[n]}$ . Equations (2.20) and (2.21) immediately yield

$$F^{[n]}(\theta) = nF(\theta) \quad \text{and} \quad F_Q^{[n]}(\theta) = nF_Q(\theta). \quad (2.22)$$

Importantly, the bound  $F^{[n]} \leq F_Q^{[n]}$  can be saturated by optimizing the one-fold POVM.

### 2.1.5 Unitary Transformations

For the remainder of Section 2.1 we assume that  $\hat{\rho}$  depends on  $\theta$  via a unitary transformation of the form

$$\hat{\rho}(\theta) = e^{-i\theta\hat{R}} \hat{\rho}(0) e^{i\theta\hat{R}} \quad (2.23)$$

with  $\hat{R}$  Hermitian. The CFI, thus, becomes

$$F(\theta) = - \sum_j \frac{1}{\text{Tr}[\hat{\rho}(\theta)\hat{M}_j]} \text{Tr}^2[\hat{\rho}(\theta)[\hat{R}, \hat{M}_j]]. \quad (2.24)$$

To specify the QFI, we expand  $\hat{\rho}(\theta)$  in its eigenbasis,  $\hat{\rho}(\theta) = \sum_k p_k |k_\theta\rangle\langle k_\theta|$  with  $|k_\theta\rangle = e^{-i\theta\hat{R}} |k_0\rangle$ . Note that the  $p_k$  do not depend on  $\theta$ . Then the SLD can be expressed as

$$\hat{L}(\theta) = \sum'_{k,l} \frac{2}{p_k + p_l} \langle k_\theta | [\partial_\theta \hat{\rho}(\theta)] | l_\theta \rangle | k_\theta \rangle \langle l_\theta | = 2i \sum'_{k,l} \frac{p_k - p_l}{p_k + p_l} \langle k_\theta | \hat{R} | l_\theta \rangle | k_\theta \rangle \langle l_\theta |, \quad (2.25)$$

where terms with  $p_k + p_l = 0$  are excluded from the summation. The resulting QFI is  $\theta$ -independent and reads

$$F_Q = \text{Tr}[\hat{\rho}(\theta)\hat{L}^2(\theta)] = 2 \sum'_{k,l} \frac{(p_k - p_l)^2}{p_k + p_l} |\langle k_0 | \hat{R} | l_0 \rangle|^2. \quad (2.26)$$

For a pure state  $\hat{\rho}(\theta) = |\psi(\theta)\rangle\langle\psi(\theta)|$  this simplifies to

$$F_Q = 4 \left( \langle \psi(0) | \hat{R}^2 | \psi(0) \rangle - \langle \psi(0) | \hat{R} | \psi(0) \rangle^2 \right) = 4 \Delta^2 \hat{R}, \quad (2.27)$$

where  $\Delta^2 \hat{R}$  denotes the variance of  $\hat{R}$  in the state  $|\psi(0)\rangle$ .

### 2.1.6 Optimal Transformations

Let us have a closer look at the QFI of a pure state  $|\psi(\theta)\rangle = e^{-i\theta\hat{R}} |\psi(0)\rangle$ ,  $F_Q = 4 \Delta^2 \hat{R}$ . Obviously, the QFI can be enlarged by optimizing  $\hat{R}$ . We assume that  $\hat{R}$  is restricted to linear combinations of some  $\hat{R}_k$ ,

$$\hat{R} = \sum_k u_k \hat{R}_k \quad \text{with } u_k \in \mathbb{R}, \sum_k u_k^2 = 1. \quad (2.28)$$

We consider the covariance matrix  $\Gamma$  with elements

$$\Gamma_{kl} = \frac{1}{2} \langle \psi(0) | \hat{R}_k \hat{R}_l + \hat{R}_l \hat{R}_k | \psi(0) \rangle - \langle \psi(0) | \hat{R}_k | \psi(0) \rangle \langle \psi(0) | \hat{R}_l | \psi(0) \rangle. \quad (2.29)$$

Setting  $\mathbf{u} \equiv (u_1, u_2, \dots)$ , we observe that

$$F_Q = 4 \mathbf{u}^T \Gamma \mathbf{u}. \quad (2.30)$$

Let  $\gamma$  be the largest eigenvalue and  $\mathbf{u}^{(\gamma)}$  the corresponding eigenvector of  $\Gamma$ . Equation (2.30) entails that the QFI attains its maximum,  $F_Q = 4\gamma$ , at  $\hat{R} = \sum_k u_k^{(\gamma)} \hat{R}_k$ .

### 2.1.7 Entanglement Criterion

The FI can be used to quantify multipartite entanglement. We consider a system which consists of  $N$  identical subsystems such as, e.g., atoms. There are various notions of multipartite entanglement [57]. We use the following definitions. A pure state is separable or non-entangled if it can be factorized into states of the individual subsystems:

$$|\psi_{sep}\rangle = |\psi_1\rangle \otimes \cdots \otimes |\psi_N\rangle \quad (2.31)$$

Any pure state can be rewritten as a tensor product

$$|\psi\rangle = \bigotimes_j |\psi_j^{(P_j)}\rangle, \quad (2.32)$$

where  $\{P_j\}$  is a partition of  $\{1, 2, \dots, N\}$  and  $|\psi_j^{(P_j)}\rangle$  is a state of the subsystems indicated by  $P_j$ . We denote the number of the respective subsystems, i.e., the cardinality of  $P_j$ , by  $N_j$ . A pure state has an entanglement depth of  $k$  if minimizing  $\max_j N_j$  over all possible decompositions (2.32) yields  $k$ . A maximally entangled state is defined by  $k = N$ . A mixed state is separable if it can be expressed as a convex combination of pure separable states. A mixed state has an entanglement depth of  $k$  if it can be expressed as the convex combination of pure states with entanglement depth  $k' \leq k$  but not with  $k' \leq k - 1$ .

Let us come back to the FI of a state  $\hat{\rho}(\theta)$ . We further restrict the unitary dependence of  $\hat{\rho}$  on  $\theta$ , see Eq. (2.23), to collective local transformations:  $\hat{R} = \sum_{l=1}^N \hat{r}^{(l)}$ , where  $\hat{r}^{(l)}$  is a Hermitian operator  $\hat{r}$  acting on the  $l$ th subsystem. We denote the largest and smallest eigenvalues of  $\hat{r}$  by  $r_+$  and  $r_-$ , respectively, and the corresponding eigenstates by  $|r_+\rangle$  and  $|r_-\rangle$ .

The FI can certify that  $\hat{\rho}(\theta)$  has an entanglement depth greater than  $k$ . Let  $\hat{\rho}(\theta) = |\psi(\theta)\rangle\langle\psi(\theta)|$  be a pure state with entanglement depth  $k$ . We consider the decomposition (2.32) of  $|\psi(\theta)\rangle$ . Then

$$F_Q = \sum_j F_Q^{(j)} = 4 \sum_j \Delta_j^2 \left( \sum_{l \in P_j} \hat{r}^{(l)} \right) \leq (r_+ - r_-)^2 \sum_j N_j^2 \leq (r_+ - r_-)^2 (ak^2 + b^2) \quad (2.33)$$

with  $a = \lfloor N/k \rfloor$  and  $b = N - ak$ . To obtain Eq. (2.33), we have first used the additivity (2.20) of the QFI and expressed the  $F_Q^{(j)}$  according to Eq. (2.27).  $\Delta_j^2$  denotes the variance with respect to  $|\psi_j^{(P_j)}(\theta)\rangle$ . Since the maximal and minimal eigenvalues of the operator  $\sum_{l \in P_j} \hat{r}^{(l)}$  are  $N_j r_+$  and  $N_j r_-$ , respectively, its variance is bounded from above by  $\frac{1}{4}(r_+ - r_-)^2 N_j^2$ . Recall that  $\sum_j N_j = N$  and, for an entanglement depth of  $k$ ,  $N_j \leq k$ .  $\sum_j N_j^2$  is maximized by choosing the  $N_j$  to be as large as possible.

The upper bound from Eq. (2.33) holds, in fact, for the QFI of any, pure or mixed, state with an entanglement depth of  $k$  or less. To confirm this, note that the maximum of  $\sum_j N_j^2$  is a non-decreasing function of  $k$ . This generalizes Eq. (2.33) to pure states with an entanglement depth less than  $k$ . The extension to mixed states immediately follows from the definition of mixed states with entanglement depth  $k$  and from the convexity (2.16) of the QFI. Hence, if  $\hat{\rho}(\theta)$  has an entanglement depth of  $k$  or less, its QFI is bounded by

$$F_Q \leq (r_+ - r_-)^2 (ak^2 + b^2) \quad \text{with } a = \left\lfloor \frac{N}{k} \right\rfloor, b = N - ak. \quad (2.34)$$

Equivalently, if  $F_Q > (r_+ - r_-)^2 (ak^2 + b^2)$ ,  $\hat{\rho}(\theta)$  must have an entanglement depth greater than  $k$ . Since  $F(\theta) \leq F_Q$ , these statements equally apply to  $F(\theta)$ .

The bound (2.34) is tight: for an entanglement depth of  $k$ , it is saturated by the state

$$|\psi(0)\rangle = \frac{1}{\sqrt{2}^{a+1}} \left( |r_+\rangle^{\otimes k} + |r_-\rangle^{\otimes k} \right)^{\otimes a} \otimes \left( |r_+\rangle^{\otimes b} + |r_-\rangle^{\otimes b} \right) \quad (2.35)$$

and the derived  $|\psi(\theta)\rangle$ .

### 2.1.8 Standard Quantum Limit and Heisenberg Limit

Two special cases of Eq. (2.34) are particularly relevant. For separable states, i. e.,  $k = 1$ ,

$$F_Q \leq (r_+ - r_-)^2 N. \quad (2.36)$$

This is the so-called standard quantum limit (SQL). Any quantum state of  $N$  subsystems has at most an entanglement depth of  $N$  and, thus, satisfies

$$F_Q \leq (r_+ - r_-)^2 N^2. \quad (2.37)$$

This is known as the Heisenberg limit (HL). Again, both limits equally apply to  $F(\theta)$ . Typically,  $\hat{r}$  is normalized such that  $r_+ - r_- = 1$ .

## 2.2 Quantum-Enhanced Interferometry

Interferometers are measuring devices which exploit the phenomenon of interference. Most commonly, they are based on interfering electromagnetic waves. The Michelson [66] and Mach-Zehnder [67, 68] configurations are particularly prominent examples. Ramsey spectroscopy [69], instead, relies on the interference of internal atomic states. A sufficiently large de Broglie wavelength enables the observation of interfering matter waves. Accordingly, laser cooling has facilitated a rapid development of atomic matter-wave interferometers [70–72].

Modern science and technology cannot be imagined without interferometry. Laser interferometers are a ubiquitous tool for precise length measurements. Recently, large laser interferometers have enabled the first-ever direct observation of gravitational waves [73]. Ramsey interferometers lie at the core of atomic clocks. The second, as defined by the International System of Units (SI), is realized by atomic clocks referencing a microwave transition [74]. Optical atomic clocks are leading the race for ever better time measurements [23, 75–78]. Atomic matter-wave interferometers have become competitive with or even better than other inertial sensors [79–81]. The technology currently transitions from laboratories into industry [70, 82]. Present research, particularly, targets the ambitious goal of developing atomic sensors for navigation [83, 84]. Because of their striking precision and accuracy, both atomic clocks and matter-wave interferometers increasingly contribute to the search for new physics [85–89].

The interferometric precision is fundamentally limited by the Cramér-Rao bound (CRB) [90–92]. The CRB states the least variance with which a parameter may be estimated. The seminal Ref. [93] introduced a method to improve the interferometric precision exploiting entanglement, and triggered further research in this direction. The theoretical framework of quantum-enhanced metrology was established in Ref. [94]. Particularly, Ref. [94] clarified that, for separable probe states of  $N$  photons or atoms, the CRB scales with  $1/N$ . Like for the FI, see Section 2.1.8, this is called the SQL. Entangled probes, instead, can reach the HL with a CRB proportional to  $1/N^2$ .

Today’s gravitational-wave detectors routinely use squeezed light to exceed the SQL [5–7]. Quantum-enhanced atomic clocks have been demonstrated in a number of proof-of-principle experiments [24–27]. Applying entanglement to improve cutting-edge atomic clocks is targeted

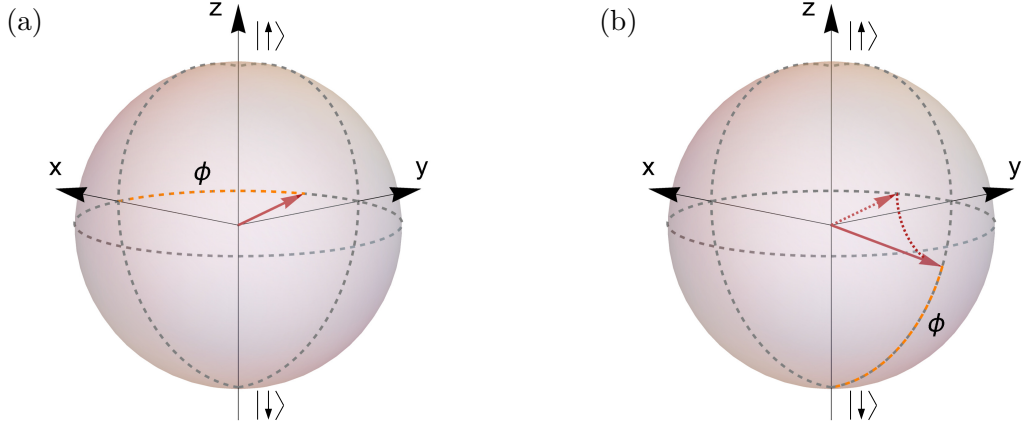


**Figure 2.1:** Bloch-sphere representation of a minimalist single-qubit interferometer. (a) State  $|\psi(\pi/2, \phi)\rangle$  whose phase  $\phi$  is sought. (b) A rotation around the  $y$ -axis encodes  $\phi$  in the probability of  $|\uparrow\rangle$ .

in Refs. [95, 96]. So far, atomic inertial sensors are limited by technical noise. However, particularly gradiometers are approaching the SQL, and prospects of quantum-enhancement are being investigated [31, 97–99]. Note that beating the SQL is not per se useful. Instead, the optimal advancement of a specific device depends on the particular goals and constraints, which requires a detailed analysis [94, 100, 101].

Below, we illustrate the concept of an interferometer. Following Refs. [9, 61, 62], we detail our mathematical framework, derive the CRB, and discuss its relation to the FI. This enables us to elaborate on the concept of quantum-enhanced interferometry.

### 2.2.1 A Minimalist Interferometer

To set the stage we start with a minimalist example of an interferometer. Consider a two-level quantum system—a qubit. We choose two orthonormal basis states and denote them by  $|\uparrow\rangle$  and  $|\downarrow\rangle$ . Any pure state of a single qubit can be parameterized in the following way:

$$|\psi(\theta, \phi)\rangle = \cos\left(\frac{\theta}{2}\right) |\uparrow\rangle + e^{i\phi} \sin\left(\frac{\theta}{2}\right) |\downarrow\rangle, \quad \theta \in [0, \pi], \quad \phi \in [-\pi, \pi] \quad (2.38)$$

Hence,  $|\psi(\theta, \phi)\rangle$  can be represented by a point with spherical coordinates  $(\theta, \phi)$  on a sphere, which, in this context, is called the Bloch sphere.

Figure 2.1a depicts a state with  $\theta = \pi/2$ ,

$$|\psi(\pi/2, \phi)\rangle = \frac{1}{\sqrt{2}} (|\uparrow\rangle + e^{i\phi} |\downarrow\rangle). \quad (2.39)$$

The interferometric task is to determine  $\phi$ . To this end, one applies  $e^{-i\frac{\pi}{2}\hat{\sigma}_y}$  with  $\hat{\sigma}_y \equiv \frac{1}{2i}(|\uparrow\rangle\langle\downarrow| - |\downarrow\rangle\langle\uparrow|)$ . Since

$$e^{-i\frac{\pi}{2}\hat{\sigma}_y} |\uparrow\rangle = \frac{1}{\sqrt{2}} (|\uparrow\rangle + |\downarrow\rangle), \quad e^{-i\frac{\pi}{2}\hat{\sigma}_y} |\downarrow\rangle = \frac{1}{\sqrt{2}} (|\downarrow\rangle - |\uparrow\rangle), \quad (2.40)$$

$e^{-i\frac{\pi}{2}\hat{\sigma}_y}$  is called an (internal-state) beamsplitter. On the Bloch sphere, it induces a rotation around the  $y$ -axis, see Fig. 2.1b. Equation (2.40) yields

$$e^{-i\frac{\pi}{2}\hat{\sigma}_y} |\psi(\pi/2, \phi)\rangle = \frac{1}{2} [(1 - e^{i\phi})|\uparrow\rangle + (1 + e^{i\phi})|\downarrow\rangle]. \quad (2.41)$$

For a qubit in the state (2.41), the probability to find it in  $|\uparrow\rangle$  is

$$p_{\uparrow} \equiv |\langle \uparrow | e^{-i\frac{\pi}{2}\hat{\sigma}_y} |\psi(\pi/2, \phi)\rangle|^2 = \sin^2\left(\frac{\phi}{2}\right). \quad (2.42)$$

To estimate  $p_{\uparrow}$ , one repeatedly prepares  $|\psi(\pi/2, \phi)\rangle$  and measures  $\hat{\sigma}_z \equiv \frac{1}{2}(|\uparrow\rangle\langle\uparrow| - |\downarrow\rangle\langle\downarrow|)$ . Then  $\phi$  is deduced via Eq. (2.42). The precision of the result is finite and increases with the number of experimental cycles.

### 2.2.2 The General Interferometer

We define a general interferometric protocol in terms of four steps. First, a probe state  $\hat{\rho}(0)$  is prepared. Second, the probe interacts with its environment. We assume that the interaction can be parameterized by  $\theta \in \mathbb{R}$  and yields a differentiable  $\hat{\rho}(\theta)$ . We say that a phase  $\theta$  is imprinted on  $\hat{\rho}$ . If the corresponding transformation is unitary,  $\hat{\rho}(\theta) = e^{-i\theta\hat{R}} \hat{\rho}(0) e^{i\theta\hat{R}}$  with  $\hat{R}$  Hermitian, we call  $\hat{R}$  the phase imprinting operator. Third,  $\hat{\rho}(\theta)$  is measured by a POVM. Any measurement outcome  $\mu_j$  is obtained with some probability  $P_{\theta}(\mu_j)$ . Multiple experimental cycles can be treated as if they were performed in parallel. For  $n$  repetitions,  $\hat{\rho}(\theta)$  becomes  $[\hat{\rho}(\theta)]^{\otimes n}$ , and  $\mu_{\mathbf{j}} \equiv (\mu_{j_1}, \dots, \mu_{j_n})$  comprises the  $n$  successive measurement outcomes. Note that, so far, our framework is the same as in Section 2.1.

Forth,  $\theta$  has to be deduced from the  $n$  measurement outcomes summarized in  $\mu_{\mathbf{j}}$ . This is done by means of an estimator  $\Theta(\mu_{\mathbf{j}})$ , which assigns a presumable value  $\Theta$  of  $\theta$  to any  $\mu_{\mathbf{j}}$ .  $\Theta$  follows a probability distribution which is determined by  $P_{\theta}(\mu_{\mathbf{j}})$ . At a given  $\theta$ , its expectation value and variance are

$$\langle \Theta \rangle_{\theta} = \sum_{\mathbf{j}} P_{\theta}(\mu_{\mathbf{j}}) \Theta(\mu_{\mathbf{j}}), \quad (2.43)$$

$$\Delta_{\theta}^2 \Theta = \sum_{\mathbf{j}} P_{\theta}(\mu_{\mathbf{j}}) (\Theta(\mu_{\mathbf{j}}) - \langle \Theta \rangle_{\theta})^2. \quad (2.44)$$

An estimator with

$$\langle \Theta \rangle_{\theta} = \theta \quad (2.45)$$

is called unbiased. Note that Eq. (2.45) implies  $\partial_{\theta} \langle \Theta \rangle_{\theta} = 1$ .

To improve the precision of an interferometer one has to minimize  $\Delta_{\theta}^2 \Theta$ .

### 2.2.3 Cramér-Rao Bound and Quantum Enhancement

The precision of an interferometer is, unfortunately, fundamentally limited by the CRB:  $\Delta_{\theta}^2 \Theta \geq \Delta_{\theta}^2 \Theta_{\text{CR}}$ . Interestingly, the classical Cramér-Rao bound (CCRB) is a simple function of the CFI<sup>2</sup>. For the case of  $n$  experimental cycles and an unbiased estimator, it reads

$$\Delta_{\theta}^2 \Theta_{\text{CR}} = \frac{1}{F^{[n]}(\theta)} = \frac{1}{nF(\theta)}. \quad (2.46)$$

<sup>2</sup>See Eq. (2.4) for the definition of the CFI.

As in Section 2.1.4,  $F^{[n]}(\theta)$  and  $F(\theta)$  denote the CFI of  $[\hat{\rho}(\theta)]^{\otimes n}$  and  $\hat{\rho}(\theta)$ , respectively. Equation (2.46) follows from the Cauchy-Schwarz inequality:

$$\begin{aligned}
 \Delta_{\theta}^2 \Theta \cdot F^{[n]}(\theta) &= \sum_{\mathbf{j}} P_{\theta}(\mu_{\mathbf{j}}) (\Theta(\mu_{\mathbf{j}}) - \theta)^2 \sum_{\mathbf{k}} P_{\theta}(\mu_{\mathbf{k}}) (\partial_{\theta} \ln[P_{\theta}(\mu_{\mathbf{k}})])^2 \\
 &\geq \left| \sum_{\mathbf{j}} P_{\theta}(\mu_{\mathbf{j}}) (\Theta(\mu_{\mathbf{j}}) - \theta) \partial_{\theta} \ln[P_{\theta}(\mu_{\mathbf{k}})] \right|^2 \\
 &= \left| \partial_{\theta} \sum_{\mathbf{j}} P_{\theta}(\mu_{\mathbf{j}}) \Theta(\mu_{\mathbf{j}}) - \theta \partial_{\theta} \sum_{\mathbf{k}} P_{\theta}(\mu_{\mathbf{k}}) \right|^2 \\
 &= |\partial_{\theta} \langle \Theta \rangle_{\theta}|^2 = 1.
 \end{aligned} \tag{2.47}$$

How can we enlarge  $F(\theta)$  and thereby reduce  $\Delta_{\theta}^2 \Theta_{\text{CR}}$ ? First, we may optimize the measurement. As we know from Section 2.1.2, the CFI is bounded by the QFI,  $F(\theta) \leq F_{\text{Q}}(\theta)$ . For an optimal POVM,<sup>3</sup>  $F(\theta) = F_{\text{Q}}(\theta)$ . The corresponding CRB is called the quantum Cramér-Rao bound (QCRB),

$$\Delta_{\theta}^2 \Theta_{\text{QCR}} = \frac{1}{F_{\text{Q}}^{[n]}(\theta)} = \frac{1}{n F_{\text{Q}}(\theta)}. \tag{2.48}$$

Second, we may optimize the phase imprinting. We have discussed the case of a pure probe state and unitary phase imprinting in Section 2.1.6.

Third, we may optimize the probe state. As in Section 2.1.7, we consider a probe which consists of  $N$  identical subsystems such as, e. g., atoms. The phase imprinting is unitary and generated by a collective local phase-imprinting operator  $\hat{R} = \sum_{l=1}^N \hat{r}^{(l)}$ , where  $\hat{r}^{(l)}$  is a Hermitian operator  $\hat{r}$  acting on the  $l$ th subsystem. Recall that the corresponding QFI does not depend on  $\theta$ . We denote the largest and smallest eigenvalues of  $\hat{r}$  by  $r_+$  and  $r_-$ , respectively. Then we know from Section 2.1.8 that, for a separable state, the FI is bounded by the SQL:

$$F_{\text{Q}} \leq (r_+ - r_-)^2 N \Rightarrow \Delta^2 \Theta_{\text{QCR}} \geq \frac{1}{n(r_+ - r_-)^2 N} \tag{2.49}$$

For a general quantum state, the FI can instead reach the HL:

$$F_{\text{Q}} \leq (r_+ - r_-)^2 N^2 \Rightarrow \Delta^2 \Theta_{\text{QCR}} \geq \frac{1}{n(r_+ - r_-)^2 N^2} \tag{2.50}$$

The same statements hold for  $F(\theta)$  and  $\Delta_{\theta}^2 \Theta_{\text{CR}}$ . The limits on the CRB are, again, called SQL and HL, respectively.

The HL can be saturated, see Section 2.1.7. Hence, there are entangled states which facilitate a better interferometric precision than any separable probe. This is the foundation of quantum enhanced interferometry. We call the entanglement of a probe state interferometrically useful if the corresponding CRB is below the SQL and thus beyond the reach of any separable probe. Crucially, entanglement turns out to be interferometrically useful if and only if the FI exceeds the SQL.

We have discussed that we can reduce the CRB by optimizing the probe state, the phase imprinting, and the POVM. But can the CRB, at all, be attained? The best general statement we can make is that, for large  $n$ , the CRB is asymptotically saturated by the maximum likelihood estimator [20, 61, 62, 102].

<sup>3</sup>Recall that a  $\theta$ -independent optimal POVM usually does not exist. This problem can be addressed by adaptive measurements [65].



Let us finally remark that, in practice, neither the probe, nor the phase imprinting, nor the POVM can be chosen at will. Restrictions are posed, particularly, by the actual interferometric task, i. e., by the physical quantity of interest which has to be encoded in  $\theta$ , and by limited experimental control.

## 2.3 Macroscopic Superposition States

We know quantum theory as a precise description of the microscopic world. By contrast, at the macroscopic scale Schrödinger’s famous thought experiment commonly known as Schrödinger’s Cat [103] demonstrates the apparent absurdity of quantum phenomena. Indeed, a cat being in the superposition of “dead” and “alive” strongly contradicts our everyday experience. How can we reconcile this with the fact that this same cat consists of microscopic objects obeying quantum theory? A crucial observation is that, unlike in classical physics, typical macroscopic quantum systems cannot be treated as being isolated [104]. The decoherence due to interactions with the environment may render macroscopic quantum phenomena hardly observable [105]. On the other hand, quantum theory might be just incomplete. Collapse models extend the Schrödinger equation by adding nonlinear stochastic terms. While these models reproduce the standard quantum theory at microscopic scales, they, at the same time, circumvent paradoxical predictions for macroscopic objects [106]. Collapse models may be motivated by various underlying theories. A particularly intriguing speculation is their relation to quantum gravity [107–110]. It is of obvious fundamental interest to test the validity of quantum theory at macroscopic scales. Therefore, physicists strive for MSSs, of which Schrödinger’s Cat is a paradigmatic example.

From the perspective of quantum-state engineering, MSSs benchmark our ability to control large quantum systems. Progress in preparing, maintaining, and characterizing MSSs brings us substantially closer to quantum-enhanced technologies such as quantum metrology or computing. The preparation of photonic MSSs is typically based on spontaneous parametric down-conversion or the coupling of an electromagnetic cavity field to a well-controlled quantum system—for instance, a transmon. The first method has been used, e. g., to prepare 15 dB squeezed vacuum states [111], while the second one led to superpositions of coherent states [112]. With massive particles, the preparation of Greenberger-Horne-Zeilinger (GHZ) states of 20 Rydberg atoms [37], 24 ions [38], or 27 superconducting qubits [39] has been recently demonstrated. Collectively addressing cold atoms produced 20 dB of spin squeezing [26]. Spinor Bose-Einstein condensates with atom numbers of the order of  $10^4$  have served, e. g., for preparing Twin-Fock states [113] with at least 450 entangled atoms [35]. Instead of entangling internal degrees of freedom, matter-wave interferometry targets large spatial separations of heavy particles. A particularly large separation of half a meter has been realized with atoms [114], and masses beyond 10 000 Da have been achieved with molecules [115]. Recently, significant experimental progress has raised the interest in optomechanical systems [116–118]. This list of achievements intends only to give a flavor of the current state of play.

From a theoretical point of view, first of all we have to define MSSs. Similarity to Schrödinger’s Cat is, obviously, a somewhat vague requirement. Furthermore, we would like to have a figure of merit—some measure of macroscopic quantumness—by which we can order MSSs and compare different experimental settings. Both the definition and the figure of merit should reflect our central question—if quantum theory is valid at macroscopic scales. A first formalization has been attempted in Ref. [119], whereupon many further proposals followed, see Ref. [22] for a review. Some definitions restrict MSSs to states of the form  $|\psi\rangle \propto |\mathcal{A}\rangle + |\mathcal{D}\rangle$  [119], while others admit general density matrices [120]. The figure of merit may be composed, in various proportions, from the quantumness of the overall state [121], the quantumness of  $|\psi\rangle$  as opposed to  $|\mathcal{A}\rangle$  and

$|\mathcal{D}\rangle$  [122], and the difference between  $|\mathcal{A}\rangle$  and  $|\mathcal{D}\rangle$  [123]. Macroscopicity typically enters as a prerequisite for a large quantumness or distinguishability. Quantumness may be defined, e.g., in terms of unconventional theories which can be ruled out by a given experiment [124], in terms of GHZ states that can be attained by local operations and classical communication [125], or in terms of the Wigner function [126]. Distinguishability may refer, e.g., to expectation values of extensive observables [119] or to coarse-grained measurements [127].

### 2.3.1 Quantification by Fisher Information

Reference [21] suggests to quantify macroscopic quantumness by means of the QFI. Let  $\hat{\rho}$  be the  $N$ -particle state of interest. We consider collective local unitary transformations  $\hat{\rho}(\theta) = e^{-i\theta\hat{R}} \hat{\rho} e^{i\theta\hat{R}}$  with  $\hat{R} = \sum_{l=1}^N \hat{r}^{(l)}$  and  $\hat{r}^{(l)}$  acting as  $\hat{r}$  on particle  $l$ , cf. Sections 2.1.7 and 2.2.3. Similarly to Ref. [21], we define the effective size of  $\hat{\rho}$  as

$$\mathcal{N}(\hat{\rho}) \equiv \frac{1}{N} \max_{\hat{r}: \|\hat{r}\|=1/2} F_{\text{Q}}[\hat{\rho}, \hat{r}]. \quad (2.51)$$

For clarity, we explicitly indicate that the QFI  $F_{\text{Q}}$  of  $\hat{\rho}(\theta)$  depends on  $\hat{\rho}$  and  $\hat{r}$ . The maximization is restricted to operators  $\hat{r}$  with operator norm  $\|\hat{r}\| = 1/2$ <sup>4</sup>. Note that  $\mathcal{N}$  is a lower bound to the effective size defined in Ref. [21], where the  $\hat{r}^{(l)}$  may differ from each other and may affect more than one particle. According to Eq. (2.34),  $\mathcal{N}(\hat{\rho}) > k$  implies that  $\hat{\rho}$  has an entanglement depth greater than  $k$ <sup>5</sup>. Hence, a large  $\mathcal{N}$  certifies many entangled particles and thus macroscopic quantumness. Recall, at this occasion, that  $\mathcal{N} \leq N$  and that this bound can be saturated, see Eq. (2.35).

A figure of merit for MSSs becomes particularly appealing if it corresponds to a useful quantum effect. As we have seen in Section 2.2, the QFI  $F_{\text{Q}}[\hat{\rho}, \hat{r}]$  quantifies the ultimate precision of a quantum-enhanced interferometer which estimates  $\theta$  from  $\hat{\rho}(\theta)$ , see Section 2.2.3. Particularly, the precision of any interferometer with probe state  $\hat{\rho}$  provides a lower bound to  $\mathcal{N}(\hat{\rho})$ . Alternative ways to experimentally access the QFI exploit further lower bounds, such as the tightly bounding CFI [128] or functions of few collective measurements [113, 129]. Reference [130] compares lower bounds on the effective size of MSSs obtained in various experiments.

We define MSSs  $\hat{\rho}$  by  $1 \ll \mathcal{N}(\hat{\rho}) \ll N$ , where  $\ll$  means “not much less than”. Note that this especially requires  $N \gg 1$ . For completeness, let us mention that Ref. [21] reserves the term MSS for  $|\psi\rangle = \frac{1}{\sqrt{2}}(|\mathcal{A}\rangle + |\mathcal{D}\rangle)$  with a large *relative* QFI

$$\mathcal{N}_r(|\psi\rangle\langle\psi|) \equiv \frac{2\mathcal{N}(|\psi\rangle\langle\psi|)}{\mathcal{N}(|\mathcal{A}\rangle\langle\mathcal{A}|) + \mathcal{N}(|\mathcal{D}\rangle\langle\mathcal{D}|)}. \quad (2.52)$$

General states with a large  $\mathcal{N}$  are called macroscopic quantum states, instead. We refrain from this distinction.

<sup>4</sup>Let  $r_{\pm}$  be the largest and smallest eigenvalues of  $\hat{r}$ , respectively. Note that the constraint  $\|\hat{r}\| = 1/2$  in Eq. (2.51) could be equivalently replaced by  $r_{+} - r_{-} = 1$ . Since  $F_{\text{Q}}[\hat{\rho}, \alpha\hat{r} + \beta] = |\alpha|^2 F_{\text{Q}}[\hat{\rho}, \hat{r}]$ , see Eq. (2.26), the maximum of  $F_{\text{Q}}$  under the restriction  $\|\hat{r}\| = 1/2$  is always attained at  $r_{+} = -r_{-} = 1/2$ .

<sup>5</sup>Note that  $\lfloor \frac{N}{k} \rfloor k^2 + (N - \lfloor \frac{N}{k} \rfloor)^2 \leq Nk$ .

### 3 Spin-1 Bose-Einstein Condensates

When the temperature of a Bose gas, i.e. a gas of bosons, approaches the absolute zero, there may be a critical temperature below which the ground-state occupation drastically increases. This phase transition is called Bose-Einstein condensation and has been predicted by Einstein in 1925 [131].

The discovery of superfluid helium [132, 133] significantly boosted the interest in Bose-Einstein condensation, which was supposed to provide a key to understanding superfluidity [134, 135]. The theory of Bose-Einstein condensation evolved hand in hand with the theories of superfluidity and superconductivity [136]. Let us, however, stress that these phenomena are related but distinct.

Observing Bose-Einstein condensation in a weakly interacting gas was a long-lasting problem. 1995 was a breakthrough year, marked by the Bose-Einstein condensation of three different species of alkali atoms:  $^{23}\text{Na}$  [137],  $^7\text{Li}$  [138], and  $^{87}\text{Rb}$  [139]. The experiments with  $^{23}\text{Na}$  and  $^{87}\text{Rb}$  have been awarded the Nobel prize. Before, Bose-Einstein condensation had been observed in superfluid helium, see Ref. [140] for a review, and in semiconductor excitons [141]. However, Bose-Einstein condensates (BECs) of alkali atoms have a number of conceptual and experimental advantages. Therefore, their first preparation led to an explosion of interest in ultracold atoms. Meanwhile, many more atomic species [142] and even small molecules [143, 144] have been successfully condensed. Besides this, also BECs of, e.g., exciton-polaritons and photons [145] or quantum magnets [146] are experimentally investigated.

The first BECs of atomic gases were trapped magnetically and therefore consisted of atoms in a single spin state. However, the spin-independent confinement of optical dipole traps was soon used for preparing BECs with spin degrees of freedom—so-called spinor BECs [147]. The additional degrees of freedom lead to a plethora of exciting phenomena. Spinor BECs exhibit a variety of ground-state quantum phases, whose number further increases in the presence of a magnetic field [29, 30, 32, 33, 148]. The interparticle interaction leads to a coherent spin dynamics [43, 46, 149]. Both the quantum phases and spin dynamics can be employed for the preparation of entangled states. In the first case, a separable ground state is quasiadiabatically driven into the entangled ground state of another quantum phase [32, 35, 150]. In the second case, the evolution of a dynamically unstable separable state produces a spin-squeezed state [151–153] that is a superposition of Twin-Fock states [113, 154]. Entangled states of both kinds have been used for proof-of-principle demonstrations of quantum-enhanced metrology [25, 49]. Further methods for creating entanglement in spinor BECs are provided, e.g., by quantum nondemolition measurements [155] or an analog of the dynamical Casimir effect [156]. Recently, entanglement has been successfully transferred from spin to momentum states, thus approaching quantum-enhanced matter-wave interferometry [31]. Other exciting studies with spinor BECs concern, e.g., topological defects [157], synthetic spin-orbit coupling [158], the quantum Zeno effect [159], quantum droplets [160], dynamical phase transitions [161], and magnetometry [162]. For a review of spinor BECs see Refs. [29, 30].

We are particularly interested in ferromagnetic spin-1 BECs such as obtained from  $^{87}\text{Rb}$  atoms in their ground state with hyperfine spin 1 [163]. Below we first detail, in Section 3.1, the concept of Bose-Einstein condensation. In Section 3.2 we review the Hamiltonian describing a gas of weakly interacting spin-1 bosons. Under some conditions, the spatial and spin degrees of freedom of a spinor BEC can be separated by means of the single-mode approximation (SMA).

In Section 3.3, we apply the SMA, derive the corresponding spin Hamiltonian, and show that the spatial degrees of freedom are governed by the Gross-Pitaevskii equation. We review the collective unitary transformations in a spin-1 system in Section 3.4 and employ them to describe the manipulation of spinor BECs by the interaction with electromagnetic radiation in Section 3.5. Real BECs are subject to atom loss, which can significantly impair entangled states. We study the precise impact by means of the Monte-Carlo wave-function method described in Section 3.6. The identification of quantum phases strongly relies on the limit of an infinite particle number. Therefore, we close by considering this mean-field limit in Section 3.7.

### 3.1 Bose-Einstein Condensation

In this section we consider an ideal Bose gas, i. e., free, non-interacting, identical bosons. For simplicity we assume that the bosons have spin zero. Let  $N$  bosons occupy a three-dimensional cube with edge length  $L$  and volume  $V = L^3$ . The single-particle energy eigenstates can be uniquely labeled by  $\mathbf{q} \equiv (q_x, q_y, q_z)$  with  $q_i \in \mathbb{N}$ , and the corresponding eigenenergies read

$$E_{\mathbf{q}} = \frac{\hbar^2 \pi^2}{2mL^2} (q^2 - 3), \quad (3.1)$$

where  $m$  is the mass of a boson and  $q^2 \equiv q_x^2 + q_y^2 + q_z^2$ . Note that we have deliberately set the ground-state energy  $E_{(1,1,1)}$  to zero. At thermal equilibrium, the expectation value of the particle number  $\hat{N}_{\mathbf{q}}$  in the  $\mathbf{q}$ -th eigenstate obeys the Bose-Einstein distribution [164, 165]:

$$\langle \hat{N}_{\mathbf{q}} \rangle = \frac{1}{e^{\beta(E_{\mathbf{q}} - \mu)} - 1}, \quad (3.2)$$

where  $\beta \equiv \frac{1}{k_B T}$ ,  $T$  is the temperature, and  $k_B$  denotes the Boltzmann constant. The chemical potential  $\mu < 0$  is implicitly fixed by

$$\sum_{\mathbf{q}} \langle \hat{N}_{\mathbf{q}} \rangle = N \quad (3.3)$$

and, thus, depends on  $N$  and  $\beta$ . One can easily ascertain that  $\mu$  is a strictly increasing function of  $\beta$ .

To reveal the concept of Bose-Einstein condensation [28, 131, 165–167], we study the thermodynamic limit, which is defined by  $N \rightarrow \infty$  at constant  $\rho \equiv N/V$ . We will use the following lemma, which provides an upper bound on the error of approximating sums by integrals:

**Lemma 1.** *Let  $f : \mathbb{R}_{\geq 0} \rightarrow \mathbb{R}_{\geq 0}$  be a continuous, absolutely bounded, non-increasing function with*

$$\exists I \in \mathbb{R} : \int_0^{\infty} dx f(x) = I. \quad (3.4)$$

*Then*

$$\left| I - \sum_{x=0}^{\infty} f(x) \right| \leq f(0). \quad (3.5)$$

*Proof.* As illustrated in Fig. 3.1a,

$$\sum_{x=1}^{\infty} f(x) \leq I \leq \sum_{x=0}^{\infty} f(x) \Rightarrow -f(0) \leq I - \sum_{x=0}^{\infty} f(x) \leq 0. \quad (3.6)$$

□

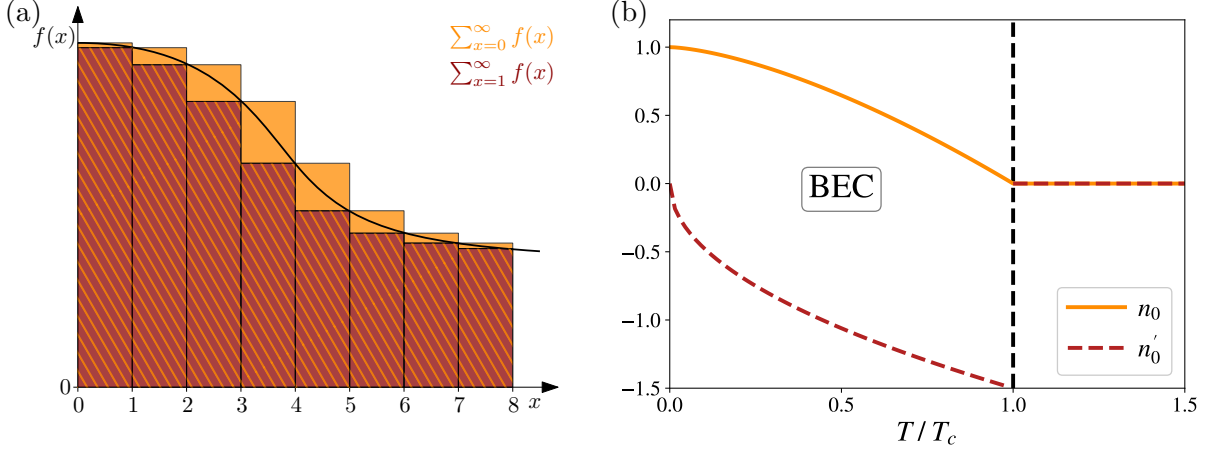


**Figure 3.1:** Bose-Einstein condensation. (a) Illustration for the proof of Lemma 1. The area  $I$  under  $f(x)$  satisfies  $\sum_{x=1}^{\infty} f(x) \leq I \leq \sum_{x=0}^{\infty} f(x)$ . (b) The condensed fraction  $n_0$  of an ideal Bose gas in the thermodynamic limit as a function of  $T/T_c$ . The derivative  $n'_0(T)$  exhibits a jump discontinuity at  $T_c$ .

We denote the chemical potential in the thermodynamic limit by  $\mu_\infty$  and conclude from the properties of  $\mu$  at finite  $N$  that  $\mu_\infty \leq 0$  and that  $\mu_\infty$  is a non-decreasing function of  $\beta$ . First, we assume that  $\beta$  is sufficiently small such that  $\mu_\infty < 0$ . We consider the thermodynamic limit of the normalization condition in Eq. (3.3),

$$1 = \lim_{N \rightarrow \infty} \sum_{\mathbf{q}} \frac{1}{N(e^{\beta(E_{\mathbf{q}} - \mu_\infty)} - 1)}. \quad (3.7)$$

Employing Lemma 1 one can show that in the thermodynamic limit the sum in Eq. (3.7) can be replaced by the respective integral<sup>1</sup>. Thus,

$$\begin{aligned} 1 &= \lim_{N \rightarrow \infty} \frac{1}{N} \int_1^\infty d^3q \frac{1}{e^{\beta \left( \frac{\hbar^2 \pi^2}{2mL^2} (q^2 - 3) - \mu_\infty \right)} - 1} \quad \left| \mathbf{k} \equiv \frac{\pi}{L} \mathbf{q} \right. \\ &= \lim_{N \rightarrow \infty} \frac{L^3}{\pi^3 N} \int_{\pi/L}^\infty d^3k \frac{1}{e^{\beta \left( \frac{\hbar^2}{2m} \left( k^2 - \frac{3\pi^2}{L^2} \right) - \mu_\infty \right)} - 1} \quad \left| L = \sqrt[3]{\frac{N}{\rho}} \right. \\ &= \frac{1}{\pi^3 \rho} \int_0^\infty d^3k \frac{1}{e^{\beta \left( \frac{\hbar^2}{2m} k^2 - \mu_\infty \right)} - 1} \\ &= \frac{1}{2\pi^2 \rho} \int_0^\infty dk \frac{k^2}{e^{\beta \left( \frac{\hbar^2}{2m} k^2 - \mu_\infty \right)} - 1}. \end{aligned} \quad (3.8)$$

This establishes the relation between  $\beta$  and  $\mu_\infty$  when  $\mu_\infty < 0$ . To determine the critical  $\beta_c$  at which  $\mu_\infty$  approaches zero, we have to solve

$$1 = \frac{1}{2\pi^2 \rho} \int_0^\infty dk \frac{k^2}{e^{\beta \frac{\hbar^2}{2m} k^2} - 1} = \frac{1}{\pi^2 \hbar^3 \rho} \sqrt{\frac{m^3}{2\beta^3}} \Gamma(3/2) \zeta(3/2), \quad (3.9)$$

<sup>1</sup>Lemma 1 can be subsequently applied to each  $q_i$ . In the thermodynamic limit the upper bound on the overall error vanishes.

where  $\Gamma$  and  $\zeta$  denote the gamma function and the Riemann zeta function, respectively. This yields the critical temperature

$$T_c = \frac{2\pi\hbar^2}{k_B m} \left( \frac{\rho}{\zeta(3/2)} \right)^{2/3} \quad (3.10)$$

with  $\zeta(3/2) \approx 2.612$ . Hence  $T > T_c$  goes along with  $\mu_\infty < 0$  and  $T \leq T_c$  with  $\mu_\infty = 0$ .

For  $T > T_c$  and thus  $\mu_\infty < 0$  the Bose-Einstein distribution (3.2) implies that the relative occupation of the ground state—and, actually, of any particular eigenstate—vanishes in the thermodynamic limit:

$$n_0 \equiv \lim_{N \rightarrow \infty} \frac{\langle \hat{N}_{(1,1,1)} \rangle}{N} = 0 \quad \forall T > T_c. \quad (3.11)$$

For  $T \leq T_c$ , instead, we cannot determine  $n_0$  from Eq. (3.2) without specifying how, precisely,  $\mu$  approaches zero when  $N \rightarrow \infty$ . As a consequence, our proof that the sum in Eq. (3.7) can be replaced by an integral breaks down. However, excluding the ground state from the sum, we can show that<sup>2</sup>

$$\lim_{N \rightarrow \infty} \sum_{\mathbf{q} \neq (1,1,1)} \frac{1}{N(e^{\beta E_{\mathbf{q}}} - 1)} = \frac{1}{2\pi^2 \rho} \int_0^\infty dk \frac{k^2}{e^{\beta \frac{\hbar^2}{2m} k^2} - 1} = \frac{\zeta(3/2)}{\hbar^3} \sqrt{\frac{m^3}{8\pi^3}} \frac{1}{\rho \sqrt{\beta^3}}. \quad (3.12)$$

Hence, by Eqs. (3.7) and (3.10),

$$n_0 = 1 - \frac{\zeta(3/2)}{\hbar^3} \sqrt{\frac{m^3}{8\pi^3}} \frac{1}{\rho \sqrt{\beta^3}} = 1 - \left( \frac{T}{T_c} \right)^{3/2} \quad \forall T \leq T_c. \quad (3.13)$$

This macroscopic accumulation of bosons in the ground state is called condensation. Figure 3.1b depicts  $n_0(T)$ . At the critical temperature  $T_c$  the derivative of  $n_0(T)$  becomes discontinuous. Thus, Bose-Einstein condensation is a phase transition with the order parameter  $n_0(T)$ .

As we see from Eqs. (3.10) and (3.13), Bose-Einstein condensation requires high densities at low temperatures. Recall, furthermore, that we have assumed that the bosons do not interact with each other. Reconciling these requirements is non-trivial.

## 3.2 Weakly Interacting Spin-1 Bosons

Let  $\hat{\mathbf{F}} \equiv (\hat{F}_x, \hat{F}_y, \hat{F}_z)$  be a spin operator and  $|f, m\rangle$  denote the joint eigenstates of  $\hat{\mathbf{F}}^2 \equiv \hat{F}_x^2 + \hat{F}_y^2 + \hat{F}_z^2$  and  $\hat{F}_z$  with  $\hat{\mathbf{F}}^2 |f, m\rangle = \hbar^2 f(f+1) |f, m\rangle$ ,  $\hat{F}_z |f, m\rangle = \hbar m |f, m\rangle$ ,  $f \in \mathbb{N}_0/2$ , and  $m \in \{f, f-1, \dots, -f\}$  [168]. The states  $|f, m\rangle$  constitute an orthonormal basis of the spin space. Hence, a boson with spin  $f = 1$  has three internal states labeled by  $m \in \{1, 0, -1\}$ . In analogy, bosons with three internal states that do not correspond to a physical spin of 1 are called pseudospin-1 bosons. Our general discussion equally applies to spin-1 and pseudospin-1 bosons. Occasionally, we will refer to the exemplary case of  $^{87}\text{Rb}$  atoms in their ground state  $5^2S_{1/2}$  with hyperfine spin  $f = 1$  [169, 170].

In the following, we construct the second-quantized Hamiltonian [171] for weakly interacting spin-1 bosons [29]. The field operators  $\hat{\psi}_m(\mathbf{r})$  and  $\hat{\psi}_m^\dagger(\mathbf{r})$  correspond, respectively, to the annihilation and creation of a boson in the spin state  $m$  at position  $\mathbf{r}$ . They fulfill the canonical bosonic commutation relations

$$[\hat{\psi}_m(\mathbf{r}), \hat{\psi}_l(\mathbf{r}')] = [\hat{\psi}_m^\dagger(\mathbf{r}), \hat{\psi}_l^\dagger(\mathbf{r}')] = 0 \quad \text{and} \quad [\hat{\psi}_m(\mathbf{r}), \hat{\psi}_l^\dagger(\mathbf{r}')] = \delta_{ml} \delta(\mathbf{r} - \mathbf{r}'), \quad (3.14)$$

<sup>2</sup>We observe that  $\lim_{N \rightarrow \infty} \langle \hat{N}_{\mathbf{q}} \rangle / N = 0$  for all  $\mathbf{q} \neq (1, 1, 1)$ . We set  $a_{\mathbf{q}} \equiv \langle \hat{N}_{\mathbf{q}} \rangle / N$ ,  $b_{\mathbf{q}} \equiv a_{\mathbf{q}} \forall \mathbf{q} \neq (1, 1, 1)$ , and  $b_{(1,1,1)} \equiv a_{(1,1,1)}$ . Then  $\lim_{N \rightarrow \infty} \sum_{\mathbf{q} \neq (1,1,1)} a_{\mathbf{q}} = \lim_{N \rightarrow \infty} \sum_{\mathbf{q}} b_{\mathbf{q}}$ . That the sum in  $\lim_{N \rightarrow \infty} \sum_{\mathbf{q}} b_{\mathbf{q}}$  can be replaced by an integral can be shown as in the case of  $\mu_\infty < 0$ .

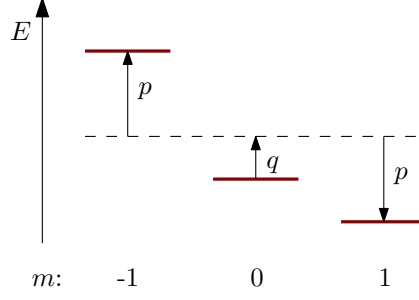


**Figure 3.2:** Relative energy  $E$  of the spin states  $|1, m\rangle$  parameterized by the effective linear ( $p$ ) and quadratic ( $q$ ) Zeeman effect.

where the first  $\delta$  denotes a Kronecker delta and the second one a Dirac delta distribution. We assume that the bosons experience a spin-independent external potential  $V_e(\mathbf{r})$ . Together with the kinetic energy, this contributes

$$\hat{H}_0 = \sum_m \int d^3r \hat{\psi}_m^\dagger(\mathbf{r}) \left[ -\frac{\hbar^2 \nabla^2}{2M} + V_e(\mathbf{r}) \right] \hat{\psi}_m(\mathbf{r}) \quad (3.15)$$

with the boson mass  $M$  to the total Hamiltonian. Typically,  $V_e$  is a confining potential which can be well approximated by a three-dimensional harmonic oscillator:

$$V_e(\mathbf{r}) = \frac{m}{2}(\omega_x^2 x^2 + \omega_y^2 y^2 + \omega_z^2 z^2) \quad (3.16)$$

For cold neutral atoms, such a potential can be realized by an optical dipole trap [25, 172].

In general the internal states differ in energy. For three spin states the spacing of the energy levels  $E_m$  can be parameterized by  $p \equiv \frac{1}{2}(E_{-1} - E_1)$  and  $q \equiv \frac{1}{2}(E_1 + E_{-1}) - E_0$ , see Fig. 3.2. Including these energy shifts into  $\hat{H}_0$  yields

$$\hat{H}'_0 = \sum_m \int d^3r \hat{\psi}_m^\dagger(\mathbf{r}) \left[ -\frac{\hbar^2 \nabla^2}{2M} + V_e(\mathbf{r}) - pm + qm^2 \right] \hat{\psi}_m(\mathbf{r}). \quad (3.17)$$

The energy splitting can be due to a magnetic field, in which case  $p$  and  $q$  are called the linear and quadratic Zeeman effect, respectively. Let us focus on atomic states with electronic spin  $s = 1/2$  and orbital angular momentum  $l = 0$ , which includes the hyperfine ground state of  $^{87}\text{Rb}$ . Then the energy shifts induced by a z-directed homogeneous magnetic field with magnitude  $B$  are provided by the Breit-Rabi formula [169, 170, 173]. Neglecting the nuclear magneton and Taylor expanding in  $B$  yields

$$p = (-1)^{f-i+1/2} \frac{g_j \mu_B B}{2i+1} \quad \text{and} \quad q = (-1)^{f-i+1/2} \frac{2(g_j \mu_B B)^2}{(2i+1)^2 \Delta E_{\text{hf}}}, \quad (3.18)$$

where  $i$  is the nuclear spin,  $\mu_B$  the Bohr magneton,  $\Delta E_{\text{hf}}$  the hyperfine splitting<sup>3</sup>, and  $g_j$  the Landé g-factor. Approximating the electron spin g-factor  $g_s$  by 2 gives  $g_j = 2$ . The Zeeman effect is not the only way to tune the relative energy of atomic spin states. Off-resonant electromagnetic dressing [46, 174] constitutes an important experimental technique to vary  $q$  independently

<sup>3</sup> $\Delta E_{\text{hf}}$  is the energy difference between states with hyperfine spin  $f = i + 1/2$  and  $f = i - 1/2$  at  $B = 0$ . For the ground state of  $^{87}\text{Rb}$ ,  $\Delta E_{\text{hf}}/\hbar \approx 6.835 \times 2\pi \text{ GHz}$  [29].



of  $p$ . Note that the sign of the quadratic Zeeman effect is fixed by  $f$  and  $i$ . Conveniently, electromagnetic dressing faces no restrictions on the sign of  $q$ . Independently of their specific physical origin, we will henceforth call  $p$  and  $q$  the effective linear and quadratic Zeeman effect, respectively.

Finally, we include an isotropic short-range interaction among the bosons. We assume that the gas is sufficiently dilute to consider only binary collisions. Since we focus on extremely low temperatures, we can restrict ourselves to s-wave scattering [168]. An interaction range that is negligible compared with the mean interparticle distance allows us to approximate the spatial dependence of the interaction potential by  $\delta(\mathbf{r})$ .

For binary s-wave collisions, conservation of the total angular momentum turns into conservation of the total spin  $\mathcal{F}$  of any two colliding bosons. For spin-1 particles we, in general, have  $\mathcal{F} \in \{2, 1, 0\}$ . Since the two colliding particles are bosons, their total state has to be symmetric under particle exchange. S-wave scattering implies a symmetric spatial wave function and, hence, requires a symmetric spin state  $|\mathcal{F}, \mathcal{M}\rangle$ . The latter can be expressed in terms of the states  $|m_1, m_2\rangle \equiv |f, m_1\rangle \otimes |f, m_2\rangle$ ,

$$|\mathcal{F}, \mathcal{M}\rangle = \sum_{m_1, m_2} \langle m_1, m_2 | \mathcal{F}, \mathcal{M} \rangle |m_1, m_2\rangle, \quad (3.19)$$

where  $\langle m_1, m_2 | \mathcal{F}, \mathcal{M} \rangle$  are known as the Clebsch-Gordan coefficients<sup>4</sup> [29, 168, 175] and satisfy

$$\langle m_1, m_2 | \mathcal{F}, \mathcal{M} \rangle = (-1)^{\mathcal{F}-2f} \langle m_2, m_1 | \mathcal{F}, \mathcal{M} \rangle. \quad (3.20)$$

Property (3.20) implies that spin states with  $\mathcal{F} \in \{0, 2\}$  are symmetric, while those with  $\mathcal{F} = 1$  are antisymmetric.

A scalar operator which describes a binary interaction with a spatial dependence of the form  $\delta(\mathbf{r})$  and conserves  $\mathcal{F} \in \{0, 2\}$  must be of the following form [29]:

$$\begin{aligned} \hat{H}_{\text{int}} &= \frac{1}{2} \sum_{\mathcal{F} \in \{0, 2\}} g_{\mathcal{F}} \sum_{\mathcal{M} = -\mathcal{F}}^{\mathcal{F}} \int d^3r \hat{A}_{\mathcal{F}, \mathcal{M}}^\dagger(\mathbf{r}) \hat{A}_{\mathcal{F}, \mathcal{M}}(\mathbf{r}) \quad \text{with} \\ \hat{A}_{\mathcal{F}, \mathcal{M}}(\mathbf{r}) &\equiv \sum_{m, l} \langle \mathcal{F}, \mathcal{M} | m, l \rangle \hat{\psi}_m(\mathbf{r}) \hat{\psi}_l(\mathbf{r}) \quad \text{and} \quad g_{\mathcal{F}} \equiv \frac{4\pi\hbar^2 a_{\mathcal{F}}}{M} \end{aligned} \quad (3.21)$$

The scattering lengths  $a_{\mathcal{F}}$  can be determined experimentally. Plugging the explicit Clebsch-Gordan coefficients for  $f = 1$  into Eq. (3.21) and adding  $\hat{H}_{\text{int}}$  to  $\hat{H}'_0$  yields [176]

$$\begin{aligned} \hat{H}_{\text{tot}} &= \sum_m \int d^3r \hat{\psi}_m^\dagger \left[ -\frac{\hbar^2 \nabla^2}{2M} + V_e(\mathbf{r}) - pm + qm^2 \right] \hat{\psi}_m \\ &+ \frac{c_0}{2} \sum_{m, l} \int d^3r \hat{\psi}_m^\dagger \hat{\psi}_l^\dagger \hat{\psi}_m \hat{\psi}_l \\ &+ \frac{c_1}{2} \int d^3r \left( \hat{\psi}_1^\dagger \hat{\psi}_1^\dagger \hat{\psi}_1 \hat{\psi}_1 + \hat{\psi}_{-1}^\dagger \hat{\psi}_{-1}^\dagger \hat{\psi}_{-1} \hat{\psi}_{-1} + 2\hat{\psi}_1^\dagger \hat{\psi}_0^\dagger \hat{\psi}_1 \hat{\psi}_0 + 2\hat{\psi}_{-1}^\dagger \hat{\psi}_0^\dagger \hat{\psi}_{-1} \hat{\psi}_0 - 2\hat{\psi}_1^\dagger \hat{\psi}_{-1}^\dagger \hat{\psi}_1 \hat{\psi}_{-1} \right. \\ &\quad \left. + 2\hat{\psi}_0^\dagger \hat{\psi}_0^\dagger \hat{\psi}_1 \hat{\psi}_{-1} + 2\hat{\psi}_1^\dagger \hat{\psi}_{-1}^\dagger \hat{\psi}_0 \hat{\psi}_0 \right), \end{aligned} \quad (3.22)$$

<sup>4</sup>The numeric values of Clebsch-Gordan coefficients depend on phase conventions. We assume the Condon-Shortley convention for  $|f, m\rangle$  and  $|\mathcal{F}, \mathcal{M}\rangle$ , which is equivalent to requiring that  $\gamma$  in  $(\hat{F}_x + i\hat{F}_y)|f, m\rangle = \gamma|f, m+1\rangle$  be positive and the analogous condition for  $|\mathcal{F}, \mathcal{M}\rangle$ . As is common practice, we set the Clebsch-Gordan coefficients to be real.



where  $c_0 \equiv \frac{1}{3}(g_0 + 2g_2)$ ,  $c_1 \equiv \frac{1}{3}(g_2 - g_0)$ , and we have omitted the  $\mathbf{r}$ -dependence of the field operators  $\hat{\psi}_m^{(\dagger)}$  for readability. Interaction terms of the form  $\hat{\psi}_m^\dagger \hat{\psi}_l^\dagger \hat{\psi}_m \hat{\psi}_l$  are called spin preserving, while the spin-changing collisions in the Hamiltonian (3.22) are given by

$$c_1 \int d^3r \left( \hat{\psi}_0^\dagger \hat{\psi}_0^\dagger \hat{\psi}_1 \hat{\psi}_{-1} + \hat{\psi}_1^\dagger \hat{\psi}_{-1}^\dagger \hat{\psi}_0 \hat{\psi}_0 \right). \quad (3.23)$$

Note that we do not consider the dipolar interaction of the bosons since it is typically—and, particularly, for the hyperfine ground state of  $^{87}\text{Rb}$ —negligible with respect to the short-range interaction.

### 3.3 Single-Mode Approximation

To obtain a BEC, the kinetic energy of the Bose gas is reduced, e. g., by laser and evaporative cooling [142, 177]. We might expect that this drives the Bose gas into its many-body ground state<sup>5</sup>. However, since the cooling addresses only the spatial degrees of freedom, attaining the overall ground state requires that the spin and spatial degrees of freedom thermalize. If the characteristic energies of the spatial and spin excitations have a different order of magnitude, thermalization gets inhibited. Particularly, if the energy scale of the spatial degrees of freedom is significantly larger, we can argue that, approximately, cooling ultimately prepares the Bose gas in the spatial ground state without restricting the spin degrees of freedom.

In the following we assume that, indeed, the total energy of a Bose gas described by the Hamiltonian (3.22) is essentially given by the kinetic energy and the spin-preserving collisions proportional to  $c_0$ . A large relative kinetic energy can be ensured by a sufficiently weak trap<sup>6</sup> [178], and  $|c_0| \gg |c_1|$  is fulfilled for a range of species, including the hyperfine ground state of  $^{87}\text{Rb}$ . Under this condition, we can approximate the quantum state of the BEC by assuming that the bosons share a common, spin-independent spatial wave function  $\psi(\mathbf{r})$  [176]. This is known as the SMA.

The field operators can be always expanded as

$$\hat{\psi}_m^{(\dagger)}(\mathbf{r}) = \sum_j \phi_j^{(*)}(\mathbf{r}) \hat{a}_{mj}^{(\dagger)}, \quad (3.24)$$

where the  $\phi_j(\mathbf{r})$  constitute an orthonormal basis of the space of square-integrable functions,  $\hat{a}_{mj}^\dagger$  creates a boson in the state  $\phi_j(\mathbf{r})|1, m\rangle$ , and  $[\hat{a}_{mj}, \hat{a}_{lk}] = [\hat{a}_{mj}^\dagger, \hat{a}_{lk}^\dagger] = 0$ ,  $[\hat{a}_{mj}, \hat{a}_{lk}^\dagger] = \delta_{ml}\delta_{jk}$ . Under the SMA, the spatial degrees of freedom are frozen and Eq. (3.24) reduces to

$$\hat{\psi}_m^{(\dagger)}(\mathbf{r}) = \psi^{(*)}(\mathbf{r}) \hat{a}_m^{(\dagger)}. \quad (3.25)$$

Below we assume that almost all  $N \gg 1$  bosons are condensed and apply the SMA to the Hamiltonian (3.22). In Section 3.3.1 we derive an effective Hamiltonian for the spin degrees of freedom, and in Section 3.3.2 we introduce the Gross-Pitaevskii equation that determines the spatial wave function  $\psi(\mathbf{r})$ .

Before proceeding we note that the SMA is not always applicable to typical experiments on spinor BECs [179]. However, in our case of interest, where  $c_1 < 0$ , there is strong theoretical evidence that the SMA is appropriate [180]. Furthermore, the SMA has been successfully employed to describe experimental setups closely related to those studied in the present thesis [25].

<sup>5</sup>Note that, in the presence of a symmetry, i. e., of an operator  $\hat{S}$  that commutes with the Hamiltonian  $\hat{H}$ , an eigenstate of  $\hat{S}$  can reach only the lowest-energy state within the respective eigenspace.

<sup>6</sup>Naively, one might expect that the trap should be tight since this increases the energy gap  $\Delta E$  between the ground state and the first excited state of a particle in the trap  $V_e(\mathbf{r})$ . However, for a harmonic trap with trapping frequency  $\omega$ ,  $\Delta E \propto \omega$  grows slower with  $\omega$  than the energy of the  $c_1$ -interaction, see Eq. (3.43).

### 3.3.1 Spin Degrees of Freedom

Plugging  $\hat{\psi}_m(\mathbf{r}) = \psi(\mathbf{r})\hat{a}_m$  into the Hamiltonian (3.22) yields

$$\begin{aligned} \hat{H}_{\text{tot}} = & \int d^3r \psi^*(\mathbf{r}) \left[ -\frac{\hbar^2 \nabla^2}{2M} + V_e(\mathbf{r}) + \frac{c_0}{2} |\psi(\mathbf{r})|^2 (\hat{N} - 1) \right] \psi(\mathbf{r}) \hat{N} \\ & + \sum_m (qm^2 - pm) \hat{a}_m^\dagger \hat{a}_m \\ & + \frac{\lambda}{2} \left( \hat{a}_1^\dagger \hat{a}_1^\dagger \hat{a}_1 \hat{a}_1 + \hat{a}_{-1}^\dagger \hat{a}_{-1}^\dagger \hat{a}_{-1} \hat{a}_{-1} + 2\hat{a}_1^\dagger \hat{a}_0^\dagger \hat{a}_1 \hat{a}_0 + 2\hat{a}_{-1}^\dagger \hat{a}_0^\dagger \hat{a}_{-1} \hat{a}_0 - 2\hat{a}_1^\dagger \hat{a}_{-1}^\dagger \hat{a}_1 \hat{a}_{-1} \right. \\ & \left. + 2\hat{a}_0^\dagger \hat{a}_0^\dagger \hat{a}_1 \hat{a}_{-1} + 2\hat{a}_1^\dagger \hat{a}_{-1}^\dagger \hat{a}_0 \hat{a}_0 \right) \quad \text{with } \lambda \equiv c_1 \int d^3r |\psi(\mathbf{r})|^4, \end{aligned} \quad (3.26)$$

where  $\hat{N}_m \equiv \hat{a}_m^\dagger \hat{a}_m$  counts the bosons in the spin state  $|1, m\rangle$  and  $\hat{N} \equiv \sum_m \hat{N}_m$  is the conserved total boson number. Since pure quantum states of massive particles always have a definite particle number  $N$ , it is sufficient to consider a single eigenspace of  $\hat{N}$  with an arbitrary eigenvalue  $N \in \mathbb{N}$ . Then the term in the first line of Eq. (3.26) becomes proportional to the identity operator and thus has no influence on the evolution of the BEC. The dynamics of the spin degrees of freedom is, hence, governed by [176]

$$\hat{H}_{\text{spin}} = q(\hat{N}_1 + \hat{N}_{-1}) - p\hat{D} + \lambda \left[ \hat{a}_0^{\dagger 2} \hat{a}_1 \hat{a}_{-1} + \hat{a}_1^\dagger \hat{a}_{-1}^\dagger \hat{a}_0^2 + \hat{N}_0 \left( \hat{N}_1 + \hat{N}_{-1} + \frac{1}{2} \right) + \frac{\hat{D}^2}{2} \right] \quad (3.27)$$

with  $\hat{D} \equiv \hat{N}_1 - \hat{N}_{-1}$ . One can readily check that  $\hat{H}_{\text{spin}}$  commutes with  $\hat{D}$  and  $\hat{I} \equiv (-1)^{\hat{N}_0} = e^{i\pi\hat{N}_0}$ ,  $[\hat{H}_{\text{spin}}, \hat{D}] = [\hat{H}_{\text{spin}}, \hat{I}] = 0$ , which means that  $\hat{D}$  and  $\hat{I}$  are conserved during the evolution.

The properties of the BEC strongly depend on the sign of  $\lambda$ , which is identical to the sign of the scattering-length difference  $a_2 - a_0$ . Let us illustrate this by considering the ground-state in the absence of an effective Zeeman effect. We introduce the collective spin-1 operator  $\hat{\mathbf{L}} \equiv (\hat{L}_x, \hat{L}_y, \hat{L}_z)$  that is defined by  $\hat{L}_i \equiv \sum_{j=1}^N \hat{F}_i^{(j)}$ , where  $\hat{F}_i^{(j)}$  denotes the  $i$ -th component of the single-boson spin-1 operator acting on the  $j$ -th boson. As we detail in Section 3.4, the components of  $\hat{\mathbf{L}}$  can be expressed as

$$\begin{aligned} \hat{L}_x &= \frac{1}{\sqrt{2}} (\hat{a}_0^\dagger \hat{a}_1 + \hat{a}_0^\dagger \hat{a}_{-1} + \hat{a}_1^\dagger \hat{a}_0 + \hat{a}_{-1}^\dagger \hat{a}_0), \\ \hat{L}_y &= \frac{1}{i\sqrt{2}} (\hat{a}_0^\dagger \hat{a}_1 - \hat{a}_0^\dagger \hat{a}_{-1} - \hat{a}_1^\dagger \hat{a}_0 + \hat{a}_{-1}^\dagger \hat{a}_0), \\ \hat{L}_z &= \hat{a}_{-1}^\dagger \hat{a}_{-1} - \hat{a}_1^\dagger \hat{a}_1. \end{aligned} \quad (3.28)$$

The  $\hat{L}_i$  obey the defining commutation relation for dimensionless angular momentum operators,  $[\hat{L}_\alpha, \hat{L}_\beta] = i \sum_\gamma \epsilon_{\alpha\beta\gamma} \hat{L}_\gamma$ , where  $\epsilon_{\alpha\beta\gamma}$  is the Levi-Civita symbol. Notably,

$$\hat{H}_{\text{spin}} = q(\hat{N}_1 + \hat{N}_{-1}) - p\hat{D} + \lambda \hat{\mathbf{L}}^2 \quad (3.29)$$

with  $\hat{\mathbf{L}}^2 = \hat{L}_x^2 + \hat{L}_y^2 + \hat{L}_z^2$ . Hence, for  $q = p = 0$  the eigenstates of  $\hat{H}_{\text{spin}}$  are the eigenstates of  $\hat{\mathbf{L}}^2$ . The symmetric eigenstates<sup>7</sup> of  $\hat{\mathbf{L}}^2$  have eigenvalues  $l(l+1)$  with  $0 \leq l \in \{N, N-2, \dots\}$  [176]. Thus, for  $\lambda > 0$  the spin ground state of the BEC goes along with the smallest possible value of  $l$ , while for  $\lambda < 0$  the ground state has a maximal collective spin of  $N$ . Therefore, a spin-1 BEC

<sup>7</sup>The joint symmetric eigenstates of  $\hat{\mathbf{L}}^2$  and  $\hat{L}_z$  are sometimes called spin-1 Dicke states.

with  $\lambda < 0$  is called ferromagnetic. The present thesis is devoted to ferromagnetic BECs as have been realized, e. g., with  $^{87}\text{Rb}$  atoms in their hyperfine ground state.

Since  $\hat{D}$  is a conserved quantity, the effective linear Zeeman effect  $p\hat{D}$  induces a trivial evolution, which we can absorb into a rotating frame. We define  $\hat{a}'^{(\dagger)} \equiv \hat{U}\hat{a}^{(\dagger)}\hat{U}^\dagger$  with  $\hat{U} = e^{ip\hat{D}t/\hbar}$ , which is a function of the time  $t$ . Then  $\hat{a}'^\dagger$  creates a boson in the ‘‘rotating’’ state  $e^{ipmt/\hbar}|1, m\rangle$ . Expressing an operator  $\hat{A}$  in terms of the  $\hat{a}'^{(\dagger)}$  and omitting the primes yields  $\hat{A}' = \hat{U}^\dagger\hat{A}\hat{U}$ . Importantly, we want to treat the new creation and annihilation operators as not explicitly time dependent. At the same time, we intend to preserve the standard form of the Heisenberg equations of motion [168],

$$\frac{d}{dt}\hat{A}_H = \frac{i}{\hbar}[\hat{H}_{\text{spin}}, \hat{A}_H] + (\partial_t\hat{A})_H, \quad (3.30)$$

where the subscript  $H$  indicates the transition to the Heisenberg picture. Hence, we define the spin Hamiltonian in the rotating frame,  $\hat{H}$ , by requiring [177]

$$\frac{i}{\hbar}[\hat{H}, \hat{A}'_H] + (\partial_t\hat{A}')_H = \hat{U}^\dagger \left( \frac{i}{\hbar}[\hat{H}_{\text{spin}}, \hat{A}_H] + (\partial_t\hat{A})_H \right) \hat{U}. \quad (3.31)$$

Equation (3.31) can be satisfied by setting  $\hat{H} = \hat{U}^\dagger\hat{H}_{\text{spin}}\hat{U} + i\hbar(\partial_t\hat{U}^\dagger)\hat{U}$ . To confirm this we observe that  $\hat{U}^\dagger\hat{U} = \hat{U}\hat{U}^\dagger = \mathbb{1}$  is the identity operator and  $0 = \partial_t(\hat{U}^\dagger\hat{U}) = (\partial_t\hat{U}^\dagger)\hat{U} + \hat{U}^\dagger(\partial_t\hat{U})$ . Since  $\hat{H}_{\text{spin}}$  commutes with  $\hat{D}$  and, thus, with  $\hat{U}$ , evaluating  $\hat{H}$  is straightforward and yields

$$\hat{H} = q(\hat{N}_1 + \hat{N}_{-1}) + \lambda \left[ \hat{a}_0^{\dagger 2}\hat{a}_1\hat{a}_{-1} + \hat{a}_1^\dagger\hat{a}_{-1}^\dagger\hat{a}_0^2 + \hat{N}_0 \left( \hat{N}_1 + \hat{N}_{-1} + \frac{1}{2} \right) + \frac{\hat{D}^2}{2} \right]. \quad (3.32)$$

To study how various properties of the BEC scale with  $N$ , we have to specify the  $N$ -dependence of  $q$  and  $\lambda$ . We set  $\lambda = c/N$  and assume that  $q$  and  $c$  do not depend on  $N$ . This ensures a sensible treatment of the thermodynamic limit  $N \rightarrow \infty$ , see Sections 3.3.2 and 3.7. As will become obvious in Section 3.3.2, the spatial wave function  $\psi$  and, thus,  $\lambda$  is fixed by the trapping potential  $V_e$  and the particle number  $N$ . To obtain the desired scaling of  $\lambda$ , the trap has to be adjusted with  $N$ .

We summarize that the Hamiltonian

$$\hat{H} = q(\hat{N}_1 + \hat{N}_{-1}) + \frac{c}{N} \left[ \hat{a}_0^{\dagger 2}\hat{a}_1\hat{a}_{-1} + \hat{a}_1^\dagger\hat{a}_{-1}^\dagger\hat{a}_0^2 + \hat{N}_0 \left( \hat{N}_1 + \hat{N}_{-1} + \frac{1}{2} \right) + \frac{\hat{D}^2}{2} \right] \quad (3.33)$$

describes the spin degrees of freedom of a spin-1 BEC in a rotating frame. It conserves the magnetization  $\hat{D} \equiv \hat{N}_1 - \hat{N}_{-1}$  and the parity  $\hat{I} \equiv (-1)^{\hat{N}_0}$ . We will study the ferromagnetic case, which is characterized by a negative interaction strength  $c < 0$ . Of course, Eq. (3.33) is meaningful only in the scope of the SMA.

### 3.3.2 Spatial Degrees of Freedom

As we see from Eq. (3.26), the spatial wave function  $\psi(\mathbf{r})$  contributes

$$E = \int d^3r \psi^*(\mathbf{r}) \left[ -\frac{\hbar^2\nabla^2}{2M} + V_e(\mathbf{r}) + \frac{c_0}{2}|\psi(\mathbf{r})|^2N \right] \psi(\mathbf{r}) \quad (3.34)$$

to the total energy of the BEC. Note that we have replaced  $\hat{N}$  by  $N$ , as discussed in the previous section, and approximated  $N - 1$  by  $N$  since  $N \gg 1$ . Because  $\psi(\mathbf{r})$  shall describe the ground state of the Bose gas, we require that it minimizes  $E$ :

$$\delta_{\psi^*} \left( E - \mu N \int d^3r |\psi(\mathbf{r})|^2 \right) = 0, \quad (3.35)$$

where  $\delta_{\psi^*}$  denotes the variation with respect to  $\psi^*(\mathbf{r})$ , and the chemical potential  $\mu$  constitutes a Lagrange multiplier which ensures that  $\psi$  is normalized,

$$\int d^3r |\psi(\mathbf{r})|^2 = 1. \quad (3.36)$$

Applying the calculus of variations [181] yields

$$\left[ -\frac{\hbar^2 \nabla^2}{2M} + V_e(\mathbf{r}) + \frac{c_0}{2} |\psi(\mathbf{r})|^2 N \right] \psi(\mathbf{r}) = \mu \psi(\mathbf{r}). \quad (3.37)$$

This is the time-independent form of the famous Gross-Pitaevskii equation [28, 182–184]. In general, Eq. (3.37) admits multiple solutions. The ground state of the Bose gas is described by the solution with the lowest energy<sup>8</sup>. We will consider only repulsive short-range interactions, for which  $c_0 > 0$ <sup>9</sup>.

If the interaction energy is sufficiently large, the kinetic energy in Eq. (3.34) can be neglected, such that Eq. (3.37) becomes

$$\left[ V_e(\mathbf{r}) + \frac{c_0}{2} |\psi(\mathbf{r})|^2 N \right] \psi(\mathbf{r}) = \mu \psi(\mathbf{r}). \quad (3.38)$$

This is known as the Thomas-Fermi limit [28]. Typically, this approximation can be applied when the characteristic length scale of the condensate-density variations is much larger than the average distance between two bosons. The lowest-energy solution of Eq. (3.38) is [185]

$$|\psi(\mathbf{r})|^2 = \begin{cases} \frac{2}{c_0 N} [\mu - V_e(\mathbf{r})] & \text{for } \mu \geq V_e(\mathbf{r}) \\ 0 & \text{otherwise} \end{cases}, \quad (3.39)$$

where  $\mu$  is fixed by the normalization condition (3.36).

Let us apply the Thomas-Fermi approximation to the important case of a spherical harmonic trap,

$$V_e(r) = \frac{M}{2} \omega^2 r^2, \quad r \equiv |\mathbf{r}|. \quad (3.40)$$

$V_e(R) = \mu$  defines the Thomas-Fermi radius  $R$ , in terms of which

$$|\psi(\mathbf{r})|^2 = \begin{cases} \frac{M\omega^2 R^2}{c_0 N} \left(1 - \frac{r^2}{R^2}\right) & \text{for } r \leq R \\ 0 & \text{otherwise} \end{cases}. \quad (3.41)$$

The normalization condition (3.36) yields

$$R = \left( \frac{15c_0 N}{8\pi M\omega^2} \right)^{1/5}. \quad (3.42)$$

We can now, e. g., compute the higher moments of the probability distribution  $|\psi(\mathbf{r})|^2$ :

$$\begin{aligned} \int d^3r |\psi(\mathbf{r})|^4 &= \frac{32\pi}{105} \left( \frac{M\omega^2}{c_0 N} \right)^2 R^7 = \frac{32\pi}{105} \left( \frac{15}{8\pi} \right)^{7/5} \left( \frac{M\omega^2}{c_0 N} \right)^{3/5}, \\ \int d^3r |\psi(\mathbf{r})|^6 &= \frac{64\pi}{315} \left( \frac{M\omega^2}{c_0 N} \right)^3 R^9 = \frac{64\pi}{315} \left( \frac{15}{8\pi} \right)^{9/5} \left( \frac{M\omega^2}{c_0 N} \right)^{6/5} = \frac{7}{6} \left( \int d^3r |\psi(\mathbf{r})|^4 \right)^2 \end{aligned} \quad (3.43)$$

<sup>8</sup>The “excited” solutions of the time-independent Gross-Pitaevskii equation are also physically relevant. A famous example is the vortex solution, which describes the ground state of a fast rotating Bose gas [28].

<sup>9</sup>As can be easily imagined, for attractive interactions the BEC may collapse.

Note that  $N \int d^3r |\psi(\mathbf{r})|^4$  and  $N^2 \int d^3r |\psi(\mathbf{r})|^6$  are the average of the particle number density  $N|\psi(\mathbf{r})|^2$  and of its square, respectively.

In the previous section we have introduced the interaction strength  $c = \lambda N$  and have required  $c$  to not depend on  $N$ . Recalling the definition of  $\lambda$ , see Eq. (3.26), we observe that in the Thomas-Fermi limit this is equivalent to fixing the average density of the BEC. Therefore, taking  $N$  to infinity at constant  $c$  corresponds to the usual definition of the thermodynamic limit [186]. According to Eq. (3.43),  $c$  becomes independent of  $N$  if the trap is widened with increasing particle number as  $\omega \propto 1/N^{1/3}$ . Note that, hence, increasing  $N$  at constant  $c$  eventually violates the assumptions of the SMA. However, this does not devalue the thermodynamic limit, whose relevance is not based on its exact attainability but on its applicability to large but finite systems.

## 3.4 Collective Transformations

In Chapter 2 we have repeatedly referred to unitary transformations generated by collective local operators,

$$\hat{U} = e^{-i\theta\hat{R}} \quad \text{with} \quad \hat{R} = \sum_{k=1}^N \hat{r}^{(k)}, \quad \theta \in \mathbb{R}, \quad (3.44)$$

where  $\hat{r}^{(k)}$  denotes a Hermitian single-particle operator  $\hat{r}$  acting on the  $k$ -th particle. We call  $\hat{U}$  a collective transformation and  $\hat{R}$  a collective generator. In the present section we review the collective transformations on the spin space of  $N$  indistinguishable spin-1 bosons. We consider only the spin degrees of freedom because the SMA restricts the spinor BEC to a definite spatial wave function, see Section 3.3. Collective transformations are particularly important since they describe typical experimental manipulations of spinor BECs, as we will see in the following section.

### 3.4.1 Single-Boson Transformations

We start by considering a single boson. The spin states  $|1, m\rangle$  with  $m \in \{1, 0, -1\}$  form an orthonormal basis of the corresponding Hilbert space  $\mathcal{H}$ . The unitary transformations on  $\mathcal{H}$  constitute the Lie group [187–189]  $U(3)$ . Any element  $\hat{u} \in U(3)$  can be expressed as  $\hat{u} = e^{-i\hat{r}}$ , where  $\hat{r}$  is a Hermitian operator on  $\mathcal{H}$ . In turn, any Hermitian operator  $\hat{r}$  on  $\mathcal{H}$  generates a  $\hat{u} = e^{-i\hat{r}} \in U(3)$ . The 9-dimensional vector space of Hermitian operators on  $\mathcal{H}$  constitutes the Lie algebra  $\mathfrak{u}(3)$ .

The Lie algebra  $\mathfrak{su}(3)$  consists of the traceless Hermitian operators on  $\mathcal{H}$ . It generates the special unitary group  $SU(3)$  of unitary operators with determinant 1. Any  $\hat{u} \in U(3)$  can be expressed as  $\hat{u} = e^{i\phi} \hat{v}$  with  $\phi \in \mathbb{R}$  and  $\hat{v} \in SU(3)$ . Recall that quantum theory is gauge invariant under global phase shifts. Hence, it is sufficient to consider  $SU(3)$  when studying the unitary transformations on a three-dimensional Hilbert space.

The Gell-Mann operators<sup>10</sup> provide a common basis of  $\mathfrak{su}(3)$ :

$$\begin{aligned} \hat{e}_1 &\equiv \frac{1}{2}(|1, -1\rangle\langle 1, 0| + |1, 0\rangle\langle 1, -1|), & \hat{e}_2 &\equiv \frac{1}{2i}(|1, -1\rangle\langle 1, 0| - |1, 0\rangle\langle 1, -1|), \\ \hat{e}_3 &\equiv \frac{1}{2}(|1, -1\rangle\langle 1, -1| - |1, 0\rangle\langle 1, 0|), \\ \hat{e}_4 &\equiv \frac{1}{2}(|1, 1\rangle\langle 1, -1| + |1, -1\rangle\langle 1, 1|), & \hat{e}_5 &\equiv \frac{1}{2i}(|1, -1\rangle\langle 1, 1| - |1, 1\rangle\langle 1, -1|), \\ \hat{e}_6 &\equiv \frac{1}{2}(|1, 0\rangle\langle 1, 1| + |1, 1\rangle\langle 1, 0|), & \hat{e}_7 &\equiv \frac{1}{2i}(|1, 0\rangle\langle 1, 1| - |1, 1\rangle\langle 1, 0|), \\ \hat{e}_8 &\equiv \frac{1}{2\sqrt{3}}(|1, -1\rangle\langle 1, -1| + |1, 0\rangle\langle 1, 0| - 2|1, 1\rangle\langle 1, 1|). \end{aligned} \quad (3.45)$$

<sup>10</sup>Usually, the Gell-Mann operators are defined as twice the  $\hat{e}_j$ .

To obtain a basis of  $\mathfrak{u}(3)$ , they can be augmented by

$$\hat{e}_0 \equiv \frac{1}{\sqrt{6}} \left( |1, -1\rangle\langle 1, -1| + |1, 0\rangle\langle 1, 0| + |1, 1\rangle\langle 1, 1| \right), \quad (3.46)$$

which is proportional to the identity. The operators  $\sqrt{2}\hat{e}_j$  are orthonormal in the sense that  $\text{Tr}[\hat{e}_j^\dagger \hat{e}_k] = \delta_{jk}/2$ .

The algebra  $\mathfrak{u}(3)$  is a vector space over  $\mathbb{R}$ . Admitting the multiplication by complex numbers yields the complexification of  $\mathfrak{u}(3)$ , which is the algebra  $\mathfrak{gl}(3, \mathbb{C})$  of all complex-valued linear operators on  $\mathcal{H}$ . For  $\mathfrak{gl}(3, \mathbb{C})$ , we can use the simple basis elements  $\hat{b}_{ml} \equiv |1, m\rangle\langle 1, l|$  with  $m, l \in \{1, 0, -1\}$  instead of the Gell-Mann operators.

### 3.4.2 N-Boson Transformations

The Hilbert space  $\mathcal{H}_N$  for  $N \in \mathbb{N}$  indistinguishable spin-1 bosons is obtained by restricting  $\mathcal{H}^{\otimes N}$  to the totally symmetric states [168]. A convenient basis of  $\mathcal{H}_N$  consists of the Fock states  $|N_1, N_0, N_{-1}\rangle$ , where  $N_m$  indicates the occupation of  $|1, m\rangle$  and  $\sum_m N_m = N$ . The operators  $\hat{E}_j \equiv \sum_{k=1}^N \hat{e}_j^{(k)}$  constitute a basis of the  $N$ -particle collective generators  $\hat{R}$  in Eq. (3.44). To express the  $\hat{E}_j$  in terms of creation and annihilation operators, we have to replace each  $|1, m\rangle$  in  $\hat{e}_j$  by  $\hat{a}_m^\dagger$  and each  $\langle 1, m|$  by  $\hat{a}_m$ . This yields

$$\begin{aligned} \hat{E}_0 &= \frac{\hat{a}_{-1}^\dagger \hat{a}_{-1} + \hat{a}_0^\dagger \hat{a}_0 + \hat{a}_1^\dagger \hat{a}_1}{\sqrt{6}}, & \hat{E}_1 &= \frac{\hat{a}_{-1}^\dagger \hat{a}_0 + \hat{a}_0^\dagger \hat{a}_{-1}}{2}, & \hat{E}_2 &= \frac{\hat{a}_{-1}^\dagger \hat{a}_0 - \hat{a}_0^\dagger \hat{a}_{-1}}{2i}, \\ \hat{E}_3 &= \frac{\hat{a}_{-1}^\dagger \hat{a}_{-1} - \hat{a}_0^\dagger \hat{a}_0}{2}, & \hat{E}_4 &= \frac{\hat{a}_1^\dagger \hat{a}_{-1} + \hat{a}_{-1}^\dagger \hat{a}_1}{2}, & \hat{E}_5 &= \frac{\hat{a}_{-1}^\dagger \hat{a}_1 - \hat{a}_1^\dagger \hat{a}_{-1}}{2i}, \\ \hat{E}_6 &= \frac{\hat{a}_0^\dagger \hat{a}_1 + \hat{a}_1^\dagger \hat{a}_0}{2}, & \hat{E}_7 &= \frac{\hat{a}_0^\dagger \hat{a}_1 - \hat{a}_1^\dagger \hat{a}_0}{2i}, & \hat{E}_8 &= \frac{\hat{a}_{-1}^\dagger \hat{a}_{-1} + \hat{a}_0^\dagger \hat{a}_0 - 2\hat{a}_1^\dagger \hat{a}_1}{2\sqrt{3}}. \end{aligned} \quad (3.47)$$

The collective  $\hat{E}_j$  obey the same commutation relations as the single-particle  $\hat{e}_j$ . Therefore, the vector space over  $\mathbb{R}$  spanned by the  $\hat{E}_j$  represents the algebra  $\mathfrak{u}(3)$  or, if  $\hat{E}_0$  is excluded from the basis,  $\mathfrak{su}(3)$ . Accordingly, the collective (special) unitary transformations in Eq. (3.44) represent  $U(3)$  or  $SU(3)$ . These representations are faithful and are called Schwinger representations [168, 190]. We have derived them as representations on  $\mathcal{H}_N$  with an arbitrary  $N \in \mathbb{N}$ . However, they can be just as well regarded as representations on the Fock space  $\mathcal{H}_F \equiv \bigoplus_{N=0}^{\infty} \mathcal{H}_N$ . In this latter setting it is useful to note that all representing operators commute with  $\hat{N}$ .

The operators  $\hat{b}_{ml}$  give rise to

$$\hat{B}_{ml} \equiv \sum_{k=1}^N \hat{b}_{ml}^{(k)} = \hat{a}_m^\dagger \hat{a}_l. \quad (3.48)$$

Let us introduce the set  $\mathcal{P}$  of complex polynomials in the  $\hat{B}_{ml}$ .  $\mathcal{P}$  represents the universal enveloping algebra of  $\mathfrak{gl}(3, \mathbb{C})$  [188, 189]. Regarded as operators on  $\mathcal{H}_F$ , the elements of  $\mathcal{P}$ , again, commute with  $\hat{N}$ . A large part of the operators we will encounter throughout this thesis belongs to  $\mathcal{P}$ .

The algebra  $\mathfrak{su}(3)$  contains  $\mathfrak{su}(2)$  as a subalgebra. One can choose different bases of  $\mathfrak{su}(2)$  in  $\mathfrak{su}(3)$ . Let us introduce the symmetric ( $g$ ) and antisymmetric ( $h$ ) creation and annihilation operators

$$\hat{g}^{(\dagger)} \equiv \frac{1}{\sqrt{2}} (\hat{a}_1^{(\dagger)} + \hat{a}_{-1}^{(\dagger)}), \quad \hat{h}^{(\dagger)} \equiv \frac{1}{\sqrt{2}} (\hat{a}_1^{(\dagger)} - \hat{a}_{-1}^{(\dagger)}). \quad (3.49)$$

The operators  $\hat{a}_0^{(\dagger)}$ ,  $\hat{g}^{(\dagger)}$ , and  $\hat{h}^{(\dagger)}$  obey the standard commutation relations for three independent bosonic modes. We employ the following four bases  $\{\hat{R}_x, \hat{R}_y, \hat{R}_z\}$  of  $\mathfrak{su}(2)$  within the Schwinger representation of  $\mathfrak{su}(3)$ :

$$\begin{aligned}
 \hat{S}_x &\equiv \frac{\hat{a}_0^\dagger \hat{g} + \hat{g}^\dagger \hat{a}_0}{2} = \frac{\hat{E}_6 + \hat{E}_1}{\sqrt{2}}, & \hat{A}_x &\equiv \frac{\hat{a}_0^\dagger \hat{h} + \hat{h}^\dagger \hat{a}_0}{2} = \frac{\hat{E}_6 - \hat{E}_1}{\sqrt{2}}, \\
 \hat{S}_y &\equiv \frac{\hat{a}_0^\dagger \hat{g} - \hat{g}^\dagger \hat{a}_0}{2i} = \frac{\hat{E}_7 - \hat{E}_2}{\sqrt{2}}, & \hat{A}_y &\equiv \frac{\hat{a}_0^\dagger \hat{h} - \hat{h}^\dagger \hat{a}_0}{2i} = \frac{\hat{E}_7 + \hat{E}_2}{\sqrt{2}}, \\
 \hat{S}_z &\equiv \frac{\hat{a}_0^\dagger \hat{a}_0 - \hat{g}^\dagger \hat{g}}{2} = \frac{\sqrt{3}\hat{E}_8 - 2\hat{E}_4 - 3\hat{E}_3}{4}, & \hat{A}_z &\equiv \frac{\hat{a}_0^\dagger \hat{a}_0 - \hat{h}^\dagger \hat{h}}{2} = \frac{\sqrt{3}\hat{E}_8 + 2\hat{E}_4 - 3\hat{E}_3}{4}, \\
 \\ 
 \hat{J}_x &\equiv \frac{\hat{a}_1^\dagger \hat{a}_{-1} + \hat{a}_{-1}^\dagger \hat{a}_1}{2} = \hat{E}_4, & \hat{L}_x &\equiv \frac{1}{\sqrt{2}}(\hat{a}_0^\dagger \hat{a}_1 + \hat{a}_0^\dagger \hat{a}_{-1} + \hat{a}_1^\dagger \hat{a}_0 + \hat{a}_{-1}^\dagger \hat{a}_0) = 2\hat{S}_x, \\
 \hat{J}_y &\equiv \frac{\hat{a}_1^\dagger \hat{a}_{-1} - \hat{a}_{-1}^\dagger \hat{a}_1}{2i} = -\hat{E}_5, & \hat{L}_y &\equiv \frac{1}{i\sqrt{2}}(\hat{a}_0^\dagger \hat{a}_1 - \hat{a}_0^\dagger \hat{a}_{-1} - \hat{a}_1^\dagger \hat{a}_0 + \hat{a}_{-1}^\dagger \hat{a}_0) = 2\hat{A}_y, \\
 \hat{J}_z &\equiv \frac{\hat{a}_1^\dagger \hat{a}_1 - \hat{a}_{-1}^\dagger \hat{a}_{-1}}{2} = -\frac{\sqrt{3}\hat{E}_8 + \hat{E}_3}{2}, & \hat{L}_z &\equiv \hat{a}_{-1}^\dagger \hat{a}_{-1} - \hat{a}_1^\dagger \hat{a}_1 = -2\hat{J}_z.
 \end{aligned} \tag{3.50}$$

All  $\hat{\mathbf{R}} \equiv (\hat{R}_x, \hat{R}_y, \hat{R}_z)$  introduced in Eq. (3.50) satisfy the defining commutation relation for dimensionless angular momentum operators,

$$[\hat{R}_\alpha, \hat{R}_\beta] = i \sum_\gamma \epsilon_{\alpha\beta\gamma} \hat{R}_\gamma, \tag{3.51}$$

where  $\epsilon_{\alpha\beta\gamma}$  is the Levi-Cevita symbol.  $\hat{\mathbf{S}}$ ,  $\hat{\mathbf{A}}$ , and  $\hat{\mathbf{J}}$  are related to each other through collective unitary transformations: there is, e. g., a collective  $\hat{U}$  such that  $\hat{U}^\dagger \hat{S}_\alpha \hat{U} = \hat{A}_\alpha$  for all  $\alpha \in \{x, y, z\}$ . Regarding  $\hat{\mathbf{S}}$  as an operator on  $\mathcal{H}_N$ , we can write  $\hat{S}_\alpha \equiv \sum_{k=1}^N \hat{s}_\alpha^{(k)}$  and, by that, define a single-particle operator  $\hat{\mathbf{s}}$ . The non-trivial action of  $\hat{\mathbf{s}}$  is restricted to the subspace of  $\mathcal{H}$  that is spanned by  $|1, 0\rangle$  and  $|g\rangle \equiv \frac{1}{\sqrt{2}}(|1, 1\rangle + |1, -1\rangle)$ . On this subspace,  $\hat{\mathbf{s}}$  defines a pseudospin-1/2 representation of  $\mathfrak{su}(2)$ , where the prefix ‘‘pseudo’’ indicates that the physical spin of the considered bosons is not 1/2. Therefore, we call  $\hat{\mathbf{S}}$  and, by the same arguments,  $\hat{\mathbf{A}}$  and  $\hat{\mathbf{J}}$  collective pseudospin-1/2 operators. By contrast,  $\hat{\mathbf{L}}$  is a collective spin-1 operator since it arises from a spin-1 representation of  $\mathfrak{su}(2)$  on  $\mathcal{H}$ .

### 3.4.3 Baker-Campbell-Hausdorff Formula

The Baker-Campbell-Hausdorff (BCH) formula<sup>11</sup> is a central tool for explicitly applying collective transformations to operators and states:<sup>12</sup>

$$e^{\hat{A}} \hat{B} e^{-\hat{A}} = \sum_{j=0}^{\infty} \frac{1}{j!} [\hat{A}, \hat{B}]_j \quad \text{with} \quad [\hat{A}, \hat{B}]_0 \equiv \hat{B}, \quad [\hat{A}, \hat{B}]_j \equiv [\hat{A}, [\hat{A}, \hat{B}]_{j-1}] \tag{3.52}$$

Let us, e. g., introduce  $\hat{S}_\theta \equiv \cos(\theta)\hat{S}_x + \sin(\theta)\hat{S}_y$ . Equation (3.52) yields the useful relations

$$\begin{aligned}
 e^{-ix\hat{S}_\theta} \hat{a}_0^\dagger e^{ix\hat{S}_\theta} &= \cos\left(\frac{\chi}{2}\right) \hat{a}_0^\dagger + e^{+i(\theta-\pi/2)} \sin\left(\frac{\chi}{2}\right) \hat{g}^\dagger, \\
 e^{-ix\hat{S}_\theta} \hat{g}^\dagger e^{ix\hat{S}_\theta} &= \cos\left(\frac{\chi}{2}\right) \hat{g}^\dagger + e^{-i(\theta+\pi/2)} \sin\left(\frac{\chi}{2}\right) \hat{a}_0^\dagger.
 \end{aligned} \tag{3.53}$$

<sup>11</sup>See Proposition 3.35 in Ref. [189].

<sup>12</sup>More precisely, Eq. (3.52) represents a lemma which is typically employed in the proof of the BCH formula.



Let  $T(\mathbf{n}, \chi)$  denote the rotation matrix that induces a rotation by the angle  $\chi$  around the axis pointing along the unit vector  $\mathbf{n}$ . For example,

$$T((0, 0, 1), \chi) = \begin{pmatrix} \cos \chi & -\sin \chi & 0 \\ \sin \chi & \cos \chi & 0 \\ 0 & 0 & 1 \end{pmatrix}. \quad (3.54)$$

A vector operator  $\hat{\mathbf{V}} \equiv (\hat{V}_x, \hat{V}_y, \hat{V}_z)$  with respect to the angular momentum operator  $\hat{\mathbf{R}}$  is defined by [168]

$$e^{i\chi\mathbf{n}\cdot\hat{\mathbf{R}}} \hat{V}_\alpha e^{-i\chi\mathbf{n}\cdot\hat{\mathbf{R}}} = \sum_{\beta} T_{\alpha\beta}(\mathbf{n}, \chi) \hat{V}_\beta, \quad (3.55)$$

where  $\mathbf{n} \cdot \hat{\mathbf{R}} \equiv \sum_{\alpha} n_{\alpha} \hat{R}_{\alpha}$ . The BCH formula implies that the left-hand side of Eq. (3.55) is completely determined by the commutation relation of  $\hat{\mathbf{V}}$  with  $\hat{\mathbf{R}}$ . Considering infinitesimal transformations proves that Eq. (3.55) is equivalent to

$$[\hat{V}_{\alpha}, \hat{R}_{\beta}] = i \sum_{\gamma} \epsilon_{\alpha\beta\gamma} \hat{V}_{\gamma}. \quad (3.56)$$

Hence,  $\hat{\mathbf{R}}$  itself is a vector operator and transforms according to Eq. (3.55). We can use this to conveniently evaluate transformations of the collective (pseudo-)spin operators introduced in the previous section.

### 3.5 Interaction with Electromagnetic Radiation

Transitions between internal atomic states can be driven by electromagnetic waves [177]. We consider a classical monochromatic electromagnetic field that is almost resonant with a couple of atomic transitions and relatively far detuned from the others. This permits us to neglect the off-resonant transitions and to describe the atoms as few-level systems. The transitions we consider correspond to wavelengths of at least several centimeters, which significantly exceeds the typical size of a BEC. Therefore, we describe the electromagnetic wave in the region of the BEC as a homogeneous oscillating field. This is known as the long-wavelength or dipole approximation. Typically, the electromagnetic pulses are short in comparison with the characteristic time scale of atomic collisions [25]. We, hence, neglect the collisions and consider an ensemble of identical independent atoms—or, actually, a single atom—interacting with the electromagnetic field.

It is often sufficient to consider only the electric component of the electromagnetic field because the coupling to the magnetic component is suppressed by the fine structure constant  $\alpha \approx 1/137$ . The interaction of the atom with the electric field  $\mathbf{E}$  can be described by  $-\hat{\mathbf{d}} \cdot \mathbf{E}$ , where  $\hat{\mathbf{d}}$  is the atomic dipole moment [177]. However, we are concerned with transitions between atomic states with orbital angular momentum  $l = 0$ . In this case, the dipole moment vanishes and the transitions are driven by the oscillating magnetic field

$$\mathbf{B} = \frac{B_0}{2} (\mathbf{u} e^{-i\omega t} + \mathbf{u}^* e^{i\omega t}), \quad (3.57)$$

where  $B_0 > 0$ , and the unit vector  $\mathbf{u} \in \mathbb{C}^3$  determines the  $t = 0$  phase and the polarization of  $\mathbf{B}$ . The interaction Hamiltonian becomes [191]

$$\hat{H}_{\text{int}} = g_s \mu_B \hat{\Sigma} \cdot \mathbf{B}, \quad (3.58)$$

where  $g_s \approx 2$  is the electron spin g-factor,  $\mu_B$  is the Bohr magneton, the nuclear magneton has been neglected, and  $\hat{\Sigma}$  denotes the electron spin operator. The ground state of  $^{87}\text{Rb}$  atoms



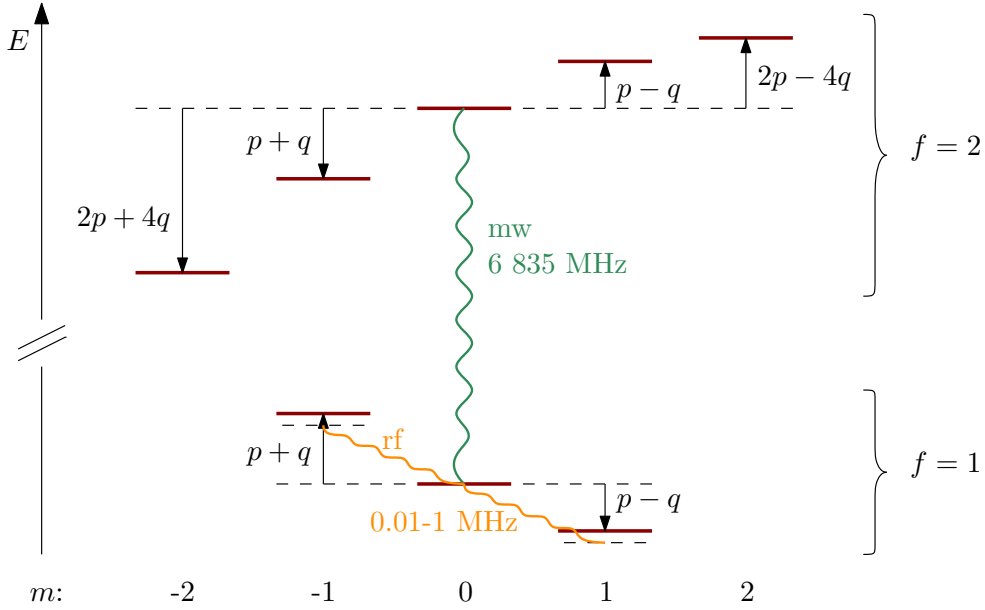


**Figure 3.3:** Hyperfine structure of the electronic ground state  $5^2S_{1/2}$  of  $^{87}\text{Rb}$  in a weak magnetic field. The states are labeled by the hyperfine quantum numbers  $f$  and  $m$ , and  $p$  and  $q$  denote the linear and quadratic Zeeman effect for  $f = 1$ , respectively. The arrows indicate typical microwave (mw) and radio-frequency (rf) transitions and the corresponding frequencies [25, 191, 192]. The spacing in energy  $E$  is not to scale.

corresponds to  $l = 0$ , an electron spin of  $s = 1/2$ , and a nuclear spin of  $i = 3/2$  [29]. For  $l = 0$  the hyperfine spin  $\hat{\mathbf{F}}$  becomes the operator sum of  $\hat{\mathbf{S}}$  and the nuclear spin  $\hat{\mathbf{I}}$ , such that  $f \in \{1, 2\}$  and  $f = 1$  in the hyperfine ground state [169, 170]. In the following we elaborate on the transitions<sup>13</sup> indicated in Fig. 3.3. Our discussion can be easily transferred to other atomic states.

### 3.5.1 Microwave Coupling

In this section we model the atom as a two-level system with the ground state  $|g\rangle \equiv |f = 1, m = 0\rangle$  and the excited state  $|e\rangle \equiv |f = 2, m = 0\rangle$ . The energy difference  $\hbar\omega_0$  between  $|g\rangle$  and  $|e\rangle$  is in the microwave range, see Fig. 3.3. Adding the free evolution of the internal atomic states to the interaction Hamiltonian (3.58), we obtain

$$\begin{aligned} \hat{H} &= \hbar\omega_0|e\rangle\langle e| + g_s\mu_B\mathbf{B} \cdot \hat{\mathbf{S}} \\ &= \hbar\omega_0|e\rangle\langle e| + g_s\mu_B\mathbf{B} \cdot \left[ \langle g|\hat{\mathbf{S}}|g\rangle|g\rangle\langle g| + \langle e|\hat{\mathbf{S}}|e\rangle|e\rangle\langle e| + \langle g|\hat{\mathbf{S}}|e\rangle|g\rangle\langle e| + \langle e|\hat{\mathbf{S}}|g\rangle|e\rangle\langle g| \right]. \end{aligned} \quad (3.59)$$

To identify the matrix elements of  $\hat{\mathbf{S}}$ , we expand the states  $|g\rangle$  and  $|e\rangle$  in the eigenstates  $|m_s; m_i\rangle$  of  $\hat{S}_z$  and  $\hat{I}_z$ . The Clebsch-Gordan coefficients<sup>14</sup> [168, 175] for  $s = 1/2$  and  $i = 3/2$  yield

$$|g\rangle = -\frac{1}{\sqrt{2}}|1/2; -1/2\rangle + \frac{1}{\sqrt{2}}|-1/2; 1/2\rangle, \quad |e\rangle = \frac{1}{\sqrt{2}}|1/2; -1/2\rangle + \frac{1}{\sqrt{2}}|-1/2; 1/2\rangle. \quad (3.60)$$

<sup>13</sup>Note that lifting the degeneracy of  $\hat{F}_z$ -eigenstates fixes the z-direction.

<sup>14</sup>We use the same conventions as in Section 3.2. Note that the Condon-Shortley convention refers to definite directions of the x- and y-axis.

The components of  $\hat{\Sigma}$  expressed in terms of the eigenstates  $|m_s\rangle$  of  $\hat{\Sigma}_z$  are

$$\begin{aligned}\hat{\Sigma}_x &= \frac{1}{2} \left( |1/2\rangle\langle -1/2| + |-1/2\rangle\langle 1/2| \right), \\ \hat{\Sigma}_y &= \frac{1}{2i} \left( |1/2\rangle\langle -1/2| - |-1/2\rangle\langle 1/2| \right), \\ \hat{\Sigma}_z &= \frac{1}{2} \left( |1/2\rangle\langle 1/2| - |-1/2\rangle\langle -1/2| \right).\end{aligned}\tag{3.61}$$

Plugging in Eqs. (3.60) and (3.61) simplifies the Hamiltonian (3.59) to

$$\hat{H} = \hbar\omega_0|e\rangle\langle e| - \frac{1}{2}g_s\mu_B B_z \left[ |g\rangle\langle e| + |e\rangle\langle g| \right].\tag{3.62}$$

Note that only the z-component of the magnetic field contributes to the interaction.

Typically  $\hbar\omega_0 \gg g_s\mu_B B_0$ , where  $B_0$  is defined in Eq. (3.57). We can therefore expect that the dynamics governed by the Hamiltonian (3.59) consist of a fast contribution due to the free evolution of the internal atomic states and a slow contribution due to the interaction with the magnetic field. The free evolution leaves  $|g\rangle$  invariant and transforms  $|e\rangle$  into  $e^{-i\omega_0 t}|e\rangle$ . This suggests to move into the rotating frame [177] with basis states  $|g\rangle$  and  $e^{-i\omega_0 t}|e\rangle$  to extract the slow evolution associated with the magnetic field. It turns out to be more convenient to choose  $|g'\rangle \equiv |g\rangle$  and  $|e'\rangle \equiv e^{-i\omega t}|e\rangle$  as the rotating basis, where  $\omega$  is the frequency of the magnetic field, see Eq. (3.57). Recall that restricting the atom to two internal states relies on a small detuning  $\Delta \equiv \omega - \omega_0$ . Therefore,  $|e'\rangle$  and  $e^{-i\omega_0 t}|e\rangle$  are equally suited to capture the fast evolution. The change into the rotating basis is provided by the unitary operator  $\hat{U} = e^{-i\omega t|e\rangle\langle e|}$ , which satisfies  $|g'\rangle = \hat{U}|g\rangle$  and  $|e'\rangle = \hat{U}|e\rangle$ . As in Section 3.3.1, we define the Hamiltonian (3.62) in the rotating frame, with the primes of the new basis states omitted, by

$$\hat{H}_{\text{rot}} \equiv \hat{U}^\dagger \hat{H} \hat{U} + i\hbar(\partial_t \hat{U}^\dagger) \hat{U}.\tag{3.63}$$

Then

$$\begin{aligned}\hat{H}_{\text{rot}} &= -\hbar\Delta|e\rangle\langle e| - \frac{1}{2}g_s\mu_B B_z \left[ e^{-i\omega t}|g\rangle\langle e| + e^{i\omega t}|e\rangle\langle g| \right] \\ &= -\hbar\Delta|e\rangle\langle e| - \frac{1}{4}g_s\mu_B B_0 \left( u_z e^{-i\omega t} + u_z^* e^{i\omega t} \right) \left[ e^{-i\omega t}|g\rangle\langle e| + e^{i\omega t}|e\rangle\langle g| \right],\end{aligned}\tag{3.64}$$

where we have used Eq. (3.57) to make the time dependence of the magnetic field explicit. Expanding the product in Eq. (3.64) shows that the terms in  $\hat{H}_{\text{rot}}$  are either time-independent<sup>15</sup> or proportional to  $e^{\pm 2i\omega t}$ . In the rotating-wave approximation (RWA), the latter, rapidly oscillating, terms are replaced by their zero average value. This is justified by the common interest in the relatively slow interaction dynamics. Furthermore, when neglecting all but two internal atomic states, we have, in fact, already made an approximation very similar to the RWA. Therefore, keeping the rapidly oscillating terms in the Hamiltonian (3.64) would be even inconsistent [177]. Hence, we describe the magnetic microwave coupling of  $|g\rangle = |1, 0\rangle$  and  $|e\rangle = e^{-i\omega t}|2, 0\rangle$  by the time-independent Hamiltonian

$$\hat{H}_{\text{MW}} = -\hbar\Delta|e\rangle\langle e| + \frac{\hbar\Omega_{\text{MW}}}{2} \left( e^{-i\phi}|g\rangle\langle e| + e^{i\phi}|e\rangle\langle g| \right)\tag{3.65}$$

with  $u_z \equiv |u_z|e^{i\phi}$  and the Rabi frequency  $\Omega_{\text{MW}} \equiv -\frac{1}{2\hbar}g_s\mu_B B_0|u_z|$ .

<sup>15</sup>We refer here to the explicit time dependence of  $\hat{H}_{\text{rot}}$ , ignoring the implicit time dependence of the rotating basis state  $|e\rangle$ .

Let us analyze the dynamics of a general pure atomic state  $c_g(t)|1, 0\rangle + c_e(t)e^{-i\omega t}|2, 0\rangle$ . The state coefficients in the rotating frame,  $c_g(t)$  and  $c_e(t)$ , obey the equations of motion

$$\partial_t c_g = -i e^{-i\phi} \frac{\Omega_{\text{MW}}}{2} c_e, \quad (3.66)$$

$$\partial_t c_e = i\Delta c_e - i e^{i\phi} \frac{\Omega_{\text{MW}}}{2} c_g. \quad (3.67)$$

To solve Eqs. (3.66) and (3.67), we differentiate Eq. (3.67) with respect to  $t$  and insert Eq. (3.66), obtaining

$$\partial_t^2 c_e = i\Delta \partial_t c_e - \frac{\Omega_{\text{MW}}^2}{4} c_e. \quad (3.68)$$

We observe that Eq. (3.68) is equivalent to

$$\left( \partial_t^2 - i\Delta \partial_t + \frac{\Omega_{\text{MW}}^2}{4} \right) c_e = \left( \partial_t - i\frac{\Delta}{2} + i\frac{\tilde{\Omega}_{\text{MW}}}{2} \right) \left( \partial_t - i\frac{\Delta}{2} - i\frac{\tilde{\Omega}_{\text{MW}}}{2} \right) c_e = 0 \quad (3.69)$$

with  $\tilde{\Omega}_{\text{MW}} \equiv \sqrt{\Omega_{\text{MW}}^2 + \Delta^2}$ . Equation (3.69) is satisfied by any solution of

$$\left( \partial_t - i\frac{\Delta}{2} + i\frac{\tilde{\Omega}_{\text{MW}}}{2} \right) c_e = 0 \quad \text{or} \quad \left( \partial_t - i\frac{\Delta}{2} - i\frac{\tilde{\Omega}_{\text{MW}}}{2} \right) c_e = 0. \quad (3.70)$$

Therefore, we can set

$$c_e(t) = e^{i\Delta t/2} \left( \alpha e^{i\tilde{\Omega}_{\text{MW}} t/2} + \beta e^{-i\tilde{\Omega}_{\text{MW}} t/2} \right) \quad (3.71)$$

with  $\alpha, \beta \in \mathbb{C}$  and obtain  $c_g(t)$  by integrating Eq. (3.66). Expressing the coefficients  $\alpha$  and  $\beta$  through the initial conditions  $c_g(0)$  and  $c_e(0)$  leads on to the Rabi oscillation

$$\begin{aligned} c_g(t) &= e^{i\Delta t/2} \left[ c_g(0) \cos \frac{\tilde{\Omega}_{\text{MW}} t}{2} - \frac{i}{\tilde{\Omega}_{\text{MW}}} \left( \Delta c_g(0) + e^{-i\phi} \Omega_{\text{MW}} c_e(0) \right) \sin \frac{\tilde{\Omega}_{\text{MW}} t}{2} \right], \\ c_e(t) &= e^{i\Delta t/2} \left[ c_e(0) \cos \frac{\tilde{\Omega}_{\text{MW}} t}{2} + \frac{i}{\tilde{\Omega}_{\text{MW}}} \left( \Delta c_e(0) - e^{+i\phi} \Omega_{\text{MW}} c_g(0) \right) \sin \frac{\tilde{\Omega}_{\text{MW}} t}{2} \right]. \end{aligned} \quad (3.72)$$

In the particular case of a  $2\pi$  pulse, i. e., a pulse with duration  $T = 2\pi/\tilde{\Omega}_{\text{MW}}$ ,

$$c_g(T) = -e^{i\pi\Delta/\tilde{\Omega}_{\text{MW}}} c_g(0), \quad c_e(T) = -e^{i\pi\Delta/\tilde{\Omega}_{\text{MW}}} c_e(0). \quad (3.73)$$

Note that

$$\frac{\Delta}{\tilde{\Omega}_{\text{MW}}} = \frac{\Delta}{\sqrt{\Omega_{\text{MW}}^2 + \Delta^2}} \quad (3.74)$$

can, in principle, attain any value between  $\pm 1$ . Values close to  $\pm 1$  require a sufficiently large  $|\Delta|$  or a sufficiently small  $\tilde{\Omega}_{\text{MW}}$ . Recall that we have assumed both a small detuning—to restrict the atom to two internal states, and a large  $\tilde{\Omega}_{\text{MW}}$ —to neglect the atomic collisions during the electromagnetic pulse. If  $\Delta/\tilde{\Omega}_{\text{MW}} \approx 1$  is accessible without violating these assumptions, a  $2\pi$  microwave pulse can be used to arbitrarily set the phase of  $c_g$ . This is pointless if the atom is, indeed, in the two-level superposition  $c_g(t)|1, 0\rangle + c_e(t)e^{-i\omega t}|2, 0\rangle$  because, according to Eq. (3.73), the interaction merely changes the global phase of the state. However, if the superposition comprises further internal atomic states, the  $2\pi$  microwave pulse allows to tune the relative phase between  $c_g$  and  $c_e$  on the one and all other coefficients on the other hand. Particularly, a superposition  $|\psi\rangle$  of the internal states  $|1, m\rangle$  gets transformed into  $e^{i\theta|1,0\rangle\langle 1,0|} |\psi\rangle$  with  $\theta = \pi(1 + \Delta/\tilde{\Omega}_{\text{MW}})$ . The corresponding collective operator is  $e^{i\theta\hat{N}_0}$ , cf. Section 3.4.

### 3.5.2 Radio-Frequency Coupling

We consider now the three internal atomic states  $|1, m\rangle$  with  $m \in \{1, 0, -1\}$ . Their free evolution obeys

$$\hat{H}_0 = (-p + q)|1, 1\rangle\langle 1, 1| + (p + q)|1, -1\rangle\langle 1, -1|, \quad (3.75)$$

where  $p$  and  $q$  are the linear and quadratic effective Zeeman shift, respectively. We assume that  $|p| \gg |q|$  and  $\hbar\omega \approx p$ , such that the electromagnetic field almost resonantly couples  $|1, 0\rangle$  to  $|1, \pm 1\rangle$ , see Fig. 3.3. This implies that  $\omega$  is in the radio-frequency range. The Hamiltonian including the interaction with the magnetic field is

$$\begin{aligned} \hat{H} &= \hat{H}_0 + g_s \mu_B \hat{\Sigma} \cdot \mathbf{B} \\ &= \left( -p + q - \frac{1}{4} g_s \mu_B B_z \right) |1, 1\rangle\langle 1, 1| + \left( p + q + \frac{1}{4} g_s \mu_B B_z \right) |1, -1\rangle\langle 1, -1| \\ &\quad - \frac{1}{4\sqrt{2}} g_s \mu_B \left( B_x \left[ |1, 0\rangle\langle 1, 1| + |1, 0\rangle\langle 1, -1| + |1, 1\rangle\langle 1, 0| + |1, -1\rangle\langle 1, 0| \right] \right. \\ &\quad \left. + i B_y \left[ |1, 0\rangle\langle 1, 1| - |1, 0\rangle\langle 1, -1| - |1, 1\rangle\langle 1, 0| + |1, -1\rangle\langle 1, 0| \right] \right), \end{aligned} \quad (3.76)$$

where we have again used the Clebsch-Gordan coefficients to evaluate the matrix elements of  $\hat{\Sigma}$ . Next, we move to the rotating frame with basis states  $\hat{U}|1, m\rangle$  and  $\hat{U} = \exp(-i\omega t[|1, -1\rangle\langle 1, -1| - |1, 1\rangle\langle 1, 1|])$ . We apply the RWA, neglecting terms proportional to  $e^{\pm i\omega t}$  or  $e^{\pm 2i\omega t}$ , and obtain the time-independent Hamiltonian

$$\begin{aligned} \hat{H}_{\text{RF}} &= (q + \hbar\Delta)|1, 1\rangle\langle 1, 1| + (q - \hbar\Delta)|1, -1\rangle\langle 1, -1| \\ &\quad + \frac{\hbar\Omega_{\text{RF}}}{2\sqrt{2}} \left[ e^{i\phi} |1, 0\rangle\langle 1, 1| + e^{-i\phi} |1, 0\rangle\langle 1, -1| + e^{-i\phi} |1, 1\rangle\langle 1, 0| + e^{i\phi} |1, -1\rangle\langle 1, 0| \right] \end{aligned} \quad (3.77)$$

with  $\Delta \equiv \omega - p/\hbar$ ,  $u_{xy} \equiv u_x + iu_y \equiv |u_{xy}| e^{i\phi}$ , and  $\Omega_{\text{RF}} \equiv -\frac{1}{4\hbar} g_s \mu_B B_0 |u_{xy}|$ .

The collective operator arising from  $\hat{H}_{\text{RF}}$  is

$$\hat{H}_{\text{RF}} = (q + \hbar\Delta)\hat{N}_1 + (q - \hbar\Delta)\hat{N}_{-1} + \hbar\Omega_{\text{RF}} \left[ \cos(\phi)\hat{S}_x - \sin(\phi)\hat{A}_y \right] \quad (3.78)$$

with the collective pseudospin operators  $\hat{S}_x$  and  $\hat{A}_y$  defined in Eq. (3.50). Typically,  $q$  and  $\hbar\Delta$  are negligible with respect to  $\hbar\Omega_{\text{RF}}$ , such that we can use

$$\hat{H}_{\text{RF}} \approx \hbar\Omega_{\text{RF}} \left[ \cos(\phi)\hat{S}_x - \sin(\phi)\hat{A}_y \right]. \quad (3.79)$$

Note that

$$\cos(\phi)\hat{S}_x - \sin(\phi)\hat{A}_y = \cos(\phi)\hat{L}_x - \sin(\phi)\hat{L}_y = e^{i\phi\hat{L}_z} \hat{L}_x e^{-i\phi\hat{L}_z} = e^{-i\phi\hat{D}} \hat{L}_x e^{i\phi\hat{D}}, \quad (3.80)$$

where we have used the definition of  $\hat{\mathbf{L}}$  in Eq. (3.50) and the transformation rule in Eq. (3.55). For  $\Delta = 0$  the rotating frame of  $\hat{H}_{\text{RF}}$  coincides with the rotating frame in which we have expressed the Hamiltonian (3.33) for the spin degrees of freedom of the BEC.

Let us remark that the direct transition between  $|1, 1\rangle$  and  $|1, -1\rangle$  is forbidden because  $\langle 1, 1|\hat{\Sigma}_\alpha|1, -1\rangle = 0$  for all  $\alpha \in \{x, y, z\}$ . This complicates the experimental realization of the pseudospin operators  $\hat{J}_{x/y}$ , which we have introduced in Eq. (3.50) along with  $\hat{\mathbf{S}}$  and  $\hat{\mathbf{A}}$ . Similarly to Ref. [113], the states  $|1, \pm 1\rangle$  can be coupled via  $|2, 0\rangle$ . In general, this method requires circularly polarized microwave radiation to avoid cross-couplings. The necessary experimental techniques have been demonstrated in Ref. [191]. Alternatively,  $|1, \pm 1\rangle$  may be coupled by a stimulated Raman transition [177].

### 3.6 Atom Loss

We are interested in the preparation of highly entangled quantum states. Such states can be very sensitive to particle loss. Therefore, it is essential to model the atom loss experienced by a BEC. Typical sources of atom loss are elastic collisions with the background gas in the vacuum chamber and inelastic collisions within the Bose gas [193]. We assume that the thermal fraction of the BEC is negligible. Collisions involving  $k$  condensed atoms lead to a depletion of the total atom number  $N$  according to

$$\frac{d}{dt}N = -G_k \langle n^{k-1} \rangle N \equiv -\Gamma_k N, \quad (3.81)$$

where  $n(\mathbf{r}) \equiv N|\psi(\mathbf{r})|^2$  denotes the particle density of the BEC,  $\langle n^{k-1} \rangle \equiv \int d^3r |\psi(\mathbf{r})|^2 [n(\mathbf{r})]^{k-1}$ , and  $\Gamma_k$  is called the  $k$ -body loss rate.  $\Gamma_1 = G_1$  depends on the vacuum quality and can, in principle, be made arbitrarily small as technology advances. Conversely, the rate constants  $G_{k \neq 1}$  depend only on the condensed species. Both loss rates and rate constants can be determined experimentally [194, 195]. Recall that we consider weakly interacting, dilute Bose gases. Therefore, we have to account only for few-body collisions. For a BEC confined in an optical trap, inelastic collisions involve at least three atoms. Two of them form a dimer and release a binding energy that suffices to expel the dimer and the third atom from the trap. The additional atom is indispensable for momentum conservation<sup>16</sup>.

A BEC that experiences atom loss is an open quantum system [196, 197]. Its density matrix  $\hat{\rho}$  can be obtained from the total density matrix  $\hat{\rho}_{\text{tot}}$  of the BEC and its environment by taking the partial trace over the environmental degrees of freedom,  $\hat{\rho} = \text{Tr}_{\text{env}}[\hat{\rho}_{\text{tot}}]$ . The evolution of a reduced density matrix is given by a completely positive trace-preserving (CPTP) map. We assume that the CPTP map has the Markov property, which means that  $\frac{d}{dt}\hat{\rho}(t)$  does not depend on  $\hat{\rho}(t')$  with  $t' \neq t$ . This assumption is reasonable if the environment retains information on  $\hat{\rho}(t' < t)$  only on a time-scale where  $\hat{\rho}(t') \approx \hat{\rho}(t)$ . A Markovian evolution obeys a master equation in Lindblad form [198, 199]:

$$\frac{d}{dt}\hat{\rho} = \frac{1}{i\hbar}[\hat{H}, \hat{\rho}] - \frac{1}{2} \sum_l \{ \hat{L}_l^\dagger \hat{L}_l, \hat{\rho} \} + \sum_l \hat{L}_l \hat{\rho} \hat{L}_l^\dagger, \quad (3.82)$$

where  $\hat{H}$  is Hermitian, the  $\hat{L}_l$  are called Lindblad operators, all operators may depend on time, and  $\{ \cdot, \cdot \}$  denotes the anticommutator. In the absence of Lindblad operators, Eq. (3.82) reduces to the Schrödinger equation with the Hamilton operator  $\hat{H}$ . In fact, we can identify  $\hat{H}$  with the Hamiltonian of the BEC under fairly general assumptions, regarding mainly the weak coupling of the BEC to its environment. The Lindblad operators accounting for one-body loss with a spin-independent loss rate  $\Gamma$  are  $\hat{L}_m = \sqrt{\Gamma} \hat{a}_m$  [200].

Equation (3.82) can be addressed by different numerical methods [201]. One of the most prominent techniques for computing the dynamics of  $\hat{\rho}$  is the Monte-Carlo wave-function (MCWF) or quantum jump method introduced in Ref. [200]. The central strength of the MCWF method is that it subsequently propagates individual wave functions instead of directly processing an entire density matrix. Therefore, the computational cost scales just linearly with the dimensionality of the Hilbert space. Furthermore, the method is particularly suited for parallelization.

Recall that any density matrix is an ensemble of pure states,  $\hat{\rho} = \sum_k p_k |\psi_k\rangle \langle \psi_k|$ . Since Eq. (3.82) is linear in  $\hat{\rho}$ , it is sufficient to discuss the evolution of an arbitrary pure state  $\hat{\rho}(0) = |\psi(0)\rangle \langle \psi(0)|$ . We discretize the time into steps of length  $\Delta t$ . Each step begins with

<sup>16</sup>In a magnetic trap, atoms can be also lost by two-body spin relaxation.

computing the quantum jump probabilities  $j_l(t) \equiv \langle \psi(t) | \hat{L}_l^\dagger(t + \Delta t/2) \hat{L}_l(t + \Delta t/2) | \psi(t) \rangle \Delta t$  and  $j(t) \equiv \sum_l j_l(t)$ . Note that  $\Delta t$  should be chosen such that  $j(t) \ll 1$ . We introduce the unnormalized state  $|\phi(t + \Delta t)\rangle$  and set, with probability  $1 - j(t)$ ,

$$\begin{aligned} |\phi(t + \Delta t)\rangle &= \exp \left[ - \left( \frac{i\hat{H}(t + \Delta t/2)}{\hbar} + \frac{\sum_l \hat{L}_l^\dagger(t + \Delta t/2) \hat{L}_l(t + \Delta t/2)}{2} \right) \Delta t \right] |\psi(t)\rangle \\ &\equiv e^{-i\hat{H}_{\text{eff}}(t + \Delta t/2)\Delta t/\hbar} |\psi(t)\rangle. \end{aligned} \quad (3.83)$$

With probability  $j_l(t)$  we, instead, apply the respective quantum jump,

$$|\phi(t + \Delta t)\rangle = \hat{L}_l(t + \Delta t/2) |\psi(t)\rangle. \quad (3.84)$$

We obtain  $|\psi(t + \Delta t)\rangle$  by normalizing  $|\phi(t + \Delta t)\rangle$ . The stochastic evolution of  $|\psi(0)\rangle$  is repeated  $r$  times, yielding  $r$  independent  $|\psi_k(t)\rangle$  and, finally,

$$\hat{\rho}(t) = \frac{1}{r} \sum_k |\psi_k(t)\rangle \langle \psi_k(t)|. \quad (3.85)$$

Let us confirm that, for  $r \rightarrow \infty$  and  $\Delta t \rightarrow 0$ ,  $\hat{\rho}(t)$  in Eq. (3.85) solves the Lindblad equation (3.82). It is sufficient to consider the step from a pure initial state  $\hat{\rho}(0)$  to  $\hat{\rho}(\Delta t)$ . For  $r \rightarrow \infty$ , the MCWF method yields

$$\begin{aligned} \hat{\rho}(\Delta t) &= \frac{1 - j(0)}{\text{Tr}[\hat{\rho}(0) e^{i\hat{H}_{\text{eff}}^\dagger(\Delta t/2)\Delta t/\hbar} e^{-i\hat{H}_{\text{eff}}(\Delta t/2)\Delta t/\hbar}]} e^{-i\hat{H}_{\text{eff}}(\Delta t/2)\Delta t/\hbar} \hat{\rho}(0) e^{i\hat{H}_{\text{eff}}^\dagger(\Delta t/2)\Delta t/\hbar} \\ &+ \sum_l \frac{j_l}{\text{Tr}[\hat{\rho}(0) \hat{L}_l^\dagger(\Delta t/2) \hat{L}_l(\Delta t/2)]} \hat{L}_l(\Delta t/2) \hat{\rho}(0) \hat{L}_l^\dagger(\Delta t/2) \\ &= \hat{\rho}(0) + \frac{1}{i\hbar} [\hat{H}(\Delta t), \hat{\rho}(0)] \Delta t - \frac{1}{2} \sum_l \left\{ \hat{L}_l^\dagger(\Delta t/2) \hat{L}_l(\Delta t/2), \hat{\rho}(0) \right\} \Delta t \\ &+ \sum_l \hat{L}_l(\Delta t/2) \hat{\rho}(0) \hat{L}_l^\dagger(\Delta t/2) \Delta t + \mathcal{O}(\Delta t^2). \end{aligned} \quad (3.86)$$

Taking the limit  $\Delta t \rightarrow 0$  of  $(\hat{\rho}(\Delta t) - \hat{\rho}(0))/\Delta t$  reproduces the Lindblad equation (3.82).

Let us conclude by focusing on the spin-independent one-body loss from a spin-1 BEC, for which  $\hat{L}_m = \sqrt{\Gamma} \hat{a}_m$  with  $m \in \{1, 0, -1\}$ . The stochastically evolving wave function  $|\psi(t)\rangle$  remains, at any time, an eigenstate of the particle number operator  $\hat{N}$ ,  $\hat{N}|\psi(t)\rangle = N(t)|\psi(t)\rangle$ . The jump probabilities are  $j_m(t) = \Gamma \langle \psi(t) | \hat{N}_m | \psi(t) \rangle \Delta t$  and  $j(t) = \sum_m j_m(t) = \Gamma N(t) \Delta t$ . Explicitly normalizing the states  $|\phi(t + \Delta t)\rangle$  in Eqs. (3.83) and (3.84) yields

$$|\psi(t + \Delta t)\rangle = \exp \left[ -i\hat{H}(t + \Delta t/2)\Delta t/\hbar \right] |\psi(t)\rangle \quad (3.87)$$

in the absence of a quantum jump and

$$|\psi(t + \Delta t)\rangle = \frac{\hat{a}_m}{\sqrt{\langle \psi(t) | \hat{N}_m | \psi(t) \rangle}} |\psi(t)\rangle \quad (3.88)$$

otherwise. The operator  $\hat{H}(t)$  in Eq. (3.87) refers to the Hamiltonian (3.33) for the spin degrees of freedom of the BEC with potentially time-dependent parameters.

### 3.7 Mean-Field Limit

The mean-field limit [202–207] is the limit of an infinite particle number  $N$ . It provides a classical model for a BEC of  $N \rightarrow \infty$  particles. This model captures central properties of a BEC with  $N \gg 1$ . Furthermore, phase transitions can be defined via singularities in the mean-field limit.

As before, we consider only the spin degrees of freedom. More precisely, we focus on the Hamiltonian density

$$\begin{aligned} \hat{h} &\equiv \frac{\hat{H}}{N} - \frac{q}{2} \\ &= \frac{q}{N} \left( \frac{N}{2} - \hat{N}_0 \right) + \frac{c}{N^2} \left[ \hat{a}_0^\dagger \hat{a}_1 \hat{a}_{-1} + \hat{a}_1^\dagger \hat{a}_{-1}^\dagger \hat{a}_0^2 + \hat{N}_0 \left( \hat{N}_1 + \hat{N}_{-1} + \frac{1}{2} \right) + \frac{\hat{D}^2}{2} \right], \end{aligned} \quad (3.89)$$

where  $\hat{H}$  is the Hamiltonian (3.33) and we have subtracted  $q/2$  for computational convenience. We introduce a separable basis of the  $N$ -particle Hilbert space  $\mathcal{H}_N$ , see Section 3.7.1, and subsequently study the  $N \rightarrow \infty$  limit of expectation values in the basis states. This yields a mean-field Hamiltonian (Section 3.7.2), from which we can compute the density of states (DOS, Section 3.7.3), the equations of motion (EOMs, Section 3.7.4), and the dynamics (Section 3.7.5) in the mean-field limit. Wherever possible, we discuss the general case of bosons with (pseudo-)spin  $j \in \mathbb{N}_0/2$  before specializing to the Hamiltonian density (3.89).

We closely follow our supplemental material for Ref. [208].

#### 3.7.1 Coherent States

Any pure state of a single (pseudo-)spin- $j$  boson is of the form

$$|\boldsymbol{\alpha}\rangle \equiv \sum_{m=-j}^j \alpha_m |j, m\rangle, \quad (3.90)$$

where  $\boldsymbol{\alpha} \in \mathbb{C}^{2j+1}$  comprises the  $\alpha_m$  and  $\sum_m |\alpha_m|^2 = 1$ . Our mean-field limit relies on the  $N$ -boson coherent states [188, 207]

$$|\boldsymbol{\alpha}, N\rangle \equiv |\boldsymbol{\alpha}\rangle^{\otimes N} = \frac{1}{\sqrt{N!}} \left( \sum_m \alpha_m \hat{a}_m^\dagger \right)^N |0\rangle. \quad (3.91)$$

We will often use the parameterization  $\alpha_m \equiv \sqrt{n_m} e^{i\phi_m}$  with  $n_m \geq 0$ ,  $\phi_m \in \mathbb{R} \bmod 2\pi$ , and  $\sum_m |\alpha_m|^2 = \sum_m n_m = 1$ .

Let us review some properties of the coherent states  $|\boldsymbol{\alpha}, N\rangle$ . They are, by definition, pure symmetric product states and therefore exactly the pure separable states of an  $N$ -boson system. Direct computation reveals that

$$\hat{a}_m |\boldsymbol{\alpha}, N\rangle = \sqrt{N} \alpha_m |\boldsymbol{\alpha}, N-1\rangle. \quad (3.92)$$

Crucially, the coherent states form a basis of the  $N$ -particle Hilbert space  $\mathcal{H}_N$ , since

$$\begin{aligned} C_N \int \mathcal{D}\boldsymbol{\alpha} |\boldsymbol{\alpha}, N\rangle \langle \boldsymbol{\alpha}, N| &= \mathbb{1}_N \quad \text{with} \\ \mathcal{D}\boldsymbol{\alpha} &\equiv \frac{1}{(2\pi)^{2j+1}} \prod_m dn_m d\phi_m \delta\left(\sum_m n_m - 1\right), \quad C_N = \frac{(N+2j)!}{N!}. \end{aligned} \quad (3.93)$$

$\mathbb{1}_N$  denotes the identity operator on  $\mathcal{H}_N$ . To confirm the resolution of the identity, we recall the Fock states  $|N_j, N_{j-1}, \dots, N_{-j}\rangle$ , which are labeled by the eigenvalues  $N_m$  of  $\hat{N}_m$ . The Fock states with  $\sum_m N_m = N$  form an orthonormal basis of  $\mathcal{H}_N$ . Therefore, Eq. (3.93) holds if and only if

$$C_N \int \mathcal{D}\alpha \langle N_j, N_{j-1}, \dots, N - \sum_{m=-j+1}^j N_m | \alpha, N \rangle \langle \alpha, N | N'_j, N'_{j-1}, \dots, N - \sum_{m=-j+1}^j N'_m \rangle = \prod_m \delta_{N_m, N'_m}. \quad (3.94)$$

The integral can be evaluated with the help of Eq. (3.92) and generalized spherical coordinates. The coherent basis is overcomplete, as can be concluded from its cardinality. The definition (3.91) of  $|\alpha, N\rangle$  immediately entails that coherent states with the same  $N$  are connected by collective unitary transformations, cf. Section 3.4.

### 3.7.2 Limit of Expectation Values

We want to study

$$\lim_{N \rightarrow \infty} \langle \alpha, N | \hat{A} | \alpha, N \rangle \quad (3.95)$$

for operators  $\hat{A}$  that act on the Fock space  $\mathcal{H}_F$  and satisfy  $[\hat{A}, \hat{N}] = 0$ . In general, this limit does not exist. We focus on operators from the set  $\mathcal{A}$ :

**Definition 1.**  $\hat{A} : \mathcal{H}_F \rightarrow \mathcal{H}_F$  is an element of  $\mathcal{A}$  if the restrictions of  $\hat{A}$  to  $\mathcal{H}_N$  with  $N \in \mathbb{N}_0$ ,  $\hat{A}_N : \mathcal{H}_N \rightarrow \mathcal{H}_F$ , satisfy:

1.  $\hat{A}_0 = 0$ .
2. The  $\hat{A}_N$  with  $N \geq 1$  are given by a polynomial in  $\hat{a}_m^\dagger \hat{a}_l / N$  with coefficients  $c_k(N)$ .
3.  $\forall k \exists d_k \in \mathbb{R}, e_k \in \mathbb{C} : |c_k(N)| \leq d_k \forall N$  and  $\lim_{N \rightarrow \infty} c_k(N) = e_k$ .

Let us review some properties of  $\mathcal{A}$ :

**Lemma 2.**

1.  $\mathcal{A}$  is a  $\mathbb{C}$ -algebra with the usual addition and multiplication of operators.
2.  $\hat{A} \in \mathcal{A} \Rightarrow [\hat{A}, \hat{N}] = 0$  and  $\hat{A}_N : \mathcal{H}_N \rightarrow \mathcal{H}_N$ .
3.  $\hat{A}, \hat{B} \in \mathcal{A} \Rightarrow \hat{N}[\hat{A}, \hat{B}] \in \mathcal{A}$ .
4.  $\hat{A} \in \mathcal{A} \Rightarrow \exists c \in \mathbb{R} : \|\hat{A}_N\| \leq c \forall N$ , where  $\|\cdot\|$  denotes the spectral norm.

*Proof.*

1. The algebra axioms can be easily verified.
2.  $[\hat{a}_m^\dagger \hat{a}_l, \hat{N}] = 0$ .
3. To confirm the third property in Definition 1, one may iteratively apply

$$[\hat{D}\hat{E}, \hat{F}] = [\hat{D}, \hat{F}]\hat{E} + \hat{D}[\hat{E}, \hat{F}] \quad \text{and} \quad [\hat{D}, \hat{E}\hat{F}] = [\hat{D}, \hat{E}]\hat{F} + \hat{E}[\hat{D}, \hat{F}], \quad (3.96)$$

which holds for any operators  $\hat{D}$ ,  $\hat{E}$ , and  $\hat{F}$ . This yields a finite number of terms, each of which contains a single elementary commutator,  $[\hat{a}_m / \sqrt{N}, \hat{a}_l^\dagger / \sqrt{N}] = \delta_{ml} / N$ . The coefficients of these terms have the desired property.



4.  $\|\cdot\|$  is sub-additive and sub-multiplicative, and the norm of  $\hat{a}_m^{(\dagger)}$  restricted to  $\mathcal{H}_N$  equals  $\sqrt{N}$ . Hence,  $c$  can be chosen to be the (finite) sum of the  $d_k$  introduced in the third property in Definition 1.

□

The mean-field limit of expectation values can be expressed in terms of the mean-field symbol:

**Definition 2.** Let us first substitute the  $\hat{a}_m$  and  $\hat{a}_m^\dagger$  in the restriction  $\hat{A}_N$ ,  $N \geq 1$ , of  $\hat{A} \in \mathcal{A}$  by  $\sqrt{N}\alpha_m$  and  $\sqrt{N}\alpha_m^*$ , respectively, and then take the limit  $N \rightarrow \infty$ . This yields the mean-field symbol  $A_{\text{mf}}(\alpha)$ .

To evaluate  $\lim_{N \rightarrow \infty} \langle \alpha, N | \hat{A} | \alpha, N \rangle$  for  $\hat{A} \in \mathcal{A}$ , we first consider the normal ordering  $:\hat{A}:$  of  $\hat{A}$ . Applying Eq. (3.92) and using that  $\lim_{N \rightarrow \infty} \frac{N-k}{N} = 1$  for  $k \in \mathbb{N}_0$ , we obtain

$$\lim_{N \rightarrow \infty} \langle \alpha, N | : \hat{A} : | \alpha, N \rangle = A_{\text{mf}}(\alpha). \quad (3.97)$$

Note that, since the  $\alpha_m$  commute, it does not matter whether we derive the mean-field symbol from  $:\hat{A}:$  or  $\hat{A}$ . The scaling of  $[\hat{a}_m/\sqrt{N}, \hat{a}_m^\dagger/\sqrt{N}] = 1/N$  with  $N$  entails that  $\lim_{N \rightarrow \infty} \langle \alpha, N | \hat{A} - : \hat{A} : | \alpha, N \rangle = 0$ . This leads to the following

**Lemma 3.** For  $\hat{A}, \hat{B} \in \mathcal{A}$ ,

1.  $\lim_{N \rightarrow \infty} \langle \alpha, N | \hat{A} | \alpha, N \rangle = A_{\text{mf}}(\alpha)$ ,
2.  $\lim_{N \rightarrow \infty} \langle \alpha, N | \hat{A} \hat{B} | \alpha, N \rangle = A_{\text{mf}}(\alpha) B_{\text{mf}}(\alpha)$ .

We will also encounter operators that are constructed from elements of  $\mathcal{A}$  but do not belong to  $\mathcal{A}$ . We can evaluate the mean-field limit of such operators with the help of the following

**Theorem 1** (Tannery [209]). Consider the sequence  $a_k(n) \in \mathbb{C}$  with  $k \in \mathbb{N}_0, n \in \mathbb{N}$  and assume that for any  $k$  there are  $b_k, c_k$  such that  $\lim_{n \rightarrow \infty} a_k(n) = b_k$ ,  $|a_k(n)| \leq c_k \forall n$ , and  $\sum_k c_k < \infty$ . Then  $\lim_{n \rightarrow \infty} \sum_k a_k(n) = \sum_k b_k$ .

Let us summarize some useful mean-field limits:

**Lemma 4.** We consider arbitrary  $\hat{A}, \hat{B}, \hat{C} \in \mathcal{A}$ ,  $z \in \mathbb{C}$ , and  $f \in \mathcal{C}(\mathcal{A})$ , where  $\mathcal{C}(\mathcal{A})$  denotes the (not explicitly  $N$ -dependent) complex analytic functions on  $\mathcal{A}$ . Then

1.  $\lim_{N \rightarrow \infty} \langle \alpha, N | e^{z\hat{A}} | \alpha, N \rangle = e^{zA_{\text{mf}}(\alpha)}$ ,
2.  $\lim_{N \rightarrow \infty} \langle \alpha, N | f(\hat{A}) | \alpha, N \rangle = f(A_{\text{mf}}(\alpha))$ ,
3.  $\lim_{N \rightarrow \infty} \langle \alpha, N | e^{zN\hat{A}} \hat{B} e^{-zN\hat{A}} | \alpha, N \rangle = \sum_k \frac{z^k}{k!} K_{\text{mf}}^{(k)}(\alpha)$   
with  $\hat{K}^{(0)} \equiv \hat{B}$ ,  $\hat{K}^{(k)} \equiv N[\hat{A}, \hat{K}^{(k-1)}]$ ,
4.  $\lim_{N \rightarrow \infty} \langle \alpha, N | e^{zN\hat{A}} \hat{B} \hat{C} e^{-zN\hat{A}} | \alpha, N \rangle$   
 $= \left( \lim_{N \rightarrow \infty} \langle \alpha, N | e^{zN\hat{A}} \hat{B} e^{-zN\hat{A}} | \alpha, N \rangle \right) \left( \lim_{N \rightarrow \infty} \langle \alpha, N | e^{zN\hat{A}} \hat{C} e^{-zN\hat{A}} | \alpha, N \rangle \right)$ .

*Proof.*

1. We know from Lemma 3 that  $\lim_{N \rightarrow \infty} \langle \alpha, N | \hat{A}^k | \alpha, N \rangle = A_{\text{mf}}^k(\alpha) \forall k \in \mathbb{N}_0$ . Tannery's theorem ensures that we can pull the  $N \rightarrow \infty$  limit into the exponential series. Its assumptions are fulfilled since, by Property 4 in Lemma 2, there is some  $c \in \mathbb{R}$  such that  $|\langle \alpha, N | \hat{A}^k | \alpha, N \rangle| \leq c^k \forall N$ , and  $\sum_k \frac{|zc|^k}{k!} = e^{|zc|}$  is finite.

2. The preceding proof can be immediately generalized to arbitrary  $f \in \mathcal{C}(\mathcal{A})$ .
3. This result relies on the BCH formula (3.52) and Tannery's theorem. The key step is to demonstrate that we can find a suitable  $N$ -independent bound on  $\|\hat{K}^{(k)}\|$ . First, we construct upper bounds  $c_A$  and  $c_B$  on  $\|\hat{A}\|_N$  and  $\|\hat{B}\|_N$  as suggested in the proof of Property 4 in Lemma 2. Iteratively applying the relation (3.96), we find that  $\|\hat{K}^{(k)}\| \leq 2^{r_B} c_B (2^{r_A} c_A)^k$ , where  $r_A$  and  $r_B$  are the polynomial degrees of  $\hat{A}$  and  $\hat{B}$ , respectively.
4. Using Eq. (3.96) and Lemma 3 we observe that

$$K_{\text{mf}}^{(n)}[\hat{B}\hat{C}] = \sum_{l=0}^n \binom{n}{l} K_{\text{mf}}^{(l)}[\hat{B}] K_{\text{mf}}^{(n-l)}[\hat{C}], \quad (3.98)$$

where the argument of  $K_{\text{mf}}^{(k)}$  specifies the operator  $\hat{K}^{(0)}$ , and  $\hat{K}^{(k)}$  ensues inductively as defined in the preceding result. Then the desired result follows from the preceding one.  $\square$

When constructing an entire mean-field model, we require that the Hamiltonian density is a Hermitian element of  $\mathcal{A}$ . This is indeed the case for our Hamiltonian density (3.89). By Definition 2 the mean-field symbol  $h_{\text{mf}}$  of  $\hat{h}$ , which we usually call the mean-field Hamiltonian, is

$$\begin{aligned} \frac{h_{\text{mf}}}{|c|} &= \xi(1 - 2n_0) \\ &+ \text{sg}(c) n_0 \left[ 1 - n_0 + \sqrt{(1 - n_0)^2 - (n_1 - n_{-1})^2 \cos(2\phi)} \right] + \frac{\text{sg}(c)}{2} (n_1 - n_{-1})^2, \end{aligned} \quad (3.99)$$

where we have introduced  $\xi \equiv \frac{q}{2|c|}$ ,  $\phi \equiv \phi_0 - (\phi_1 + \phi_{-1})/2$ , and  $\text{sg}(c) \equiv c/|c|$ . The conservation of  $\hat{I} \equiv (-1)^{\hat{N}_0}$  by the Hamiltonian density (3.89) gives rise to the symmetry  $h_{\text{mf}}(\phi \pm \pi) = h_{\text{mf}}(\phi)$  of the mean-field Hamiltonian. Furthermore, we observe that  $h_{\text{mf}}(-\phi) = h_{\text{mf}}(\phi)$ . Since we will mainly consider  $n_1 = n_{-1}$ , we immediately add that this simplifies  $h_{\text{mf}}$  to

$$\frac{h_{\text{mf}}}{|c|} = \xi(1 - 2n_0) + \text{sg}(c) 2n_0(1 - n_0) \cos^2(\phi). \quad (3.100)$$

Note that, for  $n_1 = n_{-1}$ , positive and negative values of  $\xi$  turn out to be related by  $h_{\text{mf}}(-\xi, 1 - n_0) = h_{\text{mf}}(\xi, n_0)$ .

### 3.7.3 Density of States

We denote the energy per particle by  $\epsilon$  and define the DOS  $\nu_N(\epsilon)$  in the  $N$ -particle Hilbert space  $\mathcal{H}_N$  by way of its Fourier transform:

$$\mathcal{F}[\nu_N](\zeta) \equiv \int d\epsilon e^{i\zeta\epsilon} \nu_N(\epsilon) \equiv \text{Tr}_N e^{i\zeta\hat{h}}, \quad \zeta \in \mathbb{R}, \quad (3.101)$$

where the trace is taken over  $\mathcal{H}_N$  and  $\hat{h} \in \mathcal{A}$  is a Hermitian Hamiltonian density. To obtain the DOS in the mean-field limit, we argue that

$$\lim_{N \rightarrow \infty} \frac{1}{N^{2j}} \text{Tr}_N e^{i\zeta\hat{h}} = \lim_{N \rightarrow \infty} \frac{C_N}{N^{2j}} \int \mathcal{D}\alpha \langle \alpha, N | e^{i\zeta\hat{h}} | \alpha, N \rangle \quad (3.102a)$$

$$= \int \mathcal{D}\alpha e^{i\zeta h_{\text{mf}}(\alpha)} \quad (3.102b)$$

$$= \int d\epsilon e^{i\zeta\epsilon} \int \mathcal{D}\alpha \delta(h_{\text{mf}}(\alpha) - \epsilon) \quad (3.102c)$$

and conclude that

$$\lim_{N \rightarrow \infty} \frac{\nu_N(\epsilon)}{N^{2j}} = \int \mathcal{D}\alpha \delta(h_{\text{mf}}(\alpha) - \epsilon). \quad (3.103)$$

In the following we comment on some details of this derivation.

First of all, note that  $\nu_N(\epsilon)$  is well defined by Eq. (3.101). For any  $N$ , the inverse Fourier transform of  $\text{Tr}_N e^{i\zeta\hat{h}}$  is a unique tempered distribution,  $\nu_N \in \mathcal{S}'(\mathbb{R})$ .

Next, we discuss each step of Eq. (3.102). Equality (3.102a) follows from the resolution of the identity (3.93) in terms of coherent states:

$$\text{Tr}_N \hat{A} = \text{Tr}_N \left[ C_N \int \mathcal{D}\alpha |\alpha, N\rangle \langle \alpha, N| \cdot \hat{A} \right] = C_N \int \mathcal{D}\alpha \langle \alpha, N | \hat{A} | \alpha, N \rangle \quad (3.104)$$

for any operator  $\hat{A}$ .

Equality (3.102b) comprises several steps. First, we note that  $\lim_{N \rightarrow \infty} C_N/N^{2j} = 1$ . Second, we apply Result 1 of Lemma 4 to the integrand:

$$\lim_{N \rightarrow \infty} \langle \alpha, N | e^{i\zeta\hat{h}} | \alpha, N \rangle = e^{i\zeta h_{\text{mf}}(\alpha)} \quad (3.105)$$

The third and last step employs Lebesgue's dominated convergence theorem:

**Theorem 2** (Lebesgue [210]). *Let  $f_n : U \subset \mathbb{R}^d \rightarrow \mathbb{C}$ ,  $n \in \mathbb{N}$  be Lebesgue integrable functions which, for  $n \rightarrow \infty$ , converge pointwise to a function  $f$  and are dominated by some Lebesgue integrable function  $g$ , i. e.,  $|f_n(x)| \leq g(x) \forall n \in \mathbb{N}, x \in U$ . Then  $f$  is integrable and*

$$\lim_{n \rightarrow \infty} \int_U dx f_n(x) = \int_U dx f(x). \quad (3.106)$$

This theorem allows us to interchange the  $N \rightarrow \infty$  limit with the integration. To check the assumptions of the theorem it is helpful to note that the domain of integration is compact,  $\langle \alpha, N | e^{i\zeta\hat{h}} | \alpha, N \rangle$  is a continuous function of  $\alpha$ , and that  $|\langle \alpha, N | e^{i\zeta\hat{h}} | \alpha, N \rangle| \leq \|e^{i\zeta\hat{h}_N}\| \leq 1 \forall N$ .

The last step of Eq. (3.102), Equality (3.102c), is essentially a change of variables. Some caution is needed at values of  $\alpha$  where the gradient of  $h_{\text{mf}}(\alpha)$  vanishes. For measurable sets of  $\alpha$  with  $h_{\text{mf}}(\alpha) = c$  the equality can be proven directly. Measure-zero sets with  $\nabla h_{\text{mf}}(\alpha) = 0$ , e. g., isolated stationary points of  $h_{\text{mf}}$ , can be excluded from the integration.

Finally, to arrive at Eq. (3.103) we demonstrate that, for any sequence of tempered distributions  $f_N \in \mathcal{S}'(\mathbb{R})$ ,

$$\lim_{N \rightarrow \infty} f_N = f \Leftrightarrow \lim_{N \rightarrow \infty} \mathcal{F}[f_N] = \mathcal{F}[f]. \quad (3.107)$$

Since the  $f_N$  are distributions, we can demand convergence only in the following weak sense:

$$\lim_{N \rightarrow \infty} f_N = f \Leftrightarrow \lim_{N \rightarrow \infty} \int dx f_N(x) t(x) = \int dx f(x) t(x) \quad (3.108)$$

for all test functions  $t \in \mathcal{S}(\mathbb{R})$ . Similarly, the Fourier transform of any  $g \in \mathcal{S}'(\mathbb{R})$  is defined by

$$\int dx \mathcal{F}[g](x) t(x) \equiv \int dx g(x) \mathcal{F}[t](x) \quad \forall t \in \mathcal{S}(\mathbb{R}). \quad (3.109)$$

Since the Fourier transformation is an automorphism on  $\mathcal{S}(\mathbb{R})$ , we can replace the arbitrary test function  $t(x)$  in Eq. (3.108) by its Fourier transform  $\mathcal{F}[t](x)$ . This connects Eq. (3.108) with Eq. (3.109) and yields Eq. (3.107).

### 3.7.4 Equations of Motion

We consider the Heisenberg representation [168]  $\hat{A}_H(t) \equiv e^{i\hat{H}t/\hbar} \hat{A} e^{-i\hat{H}t/\hbar}$  of a Hermitian, not explicitly time-dependent operator  $\hat{A} \in \mathcal{A}$ . As before, we assume that the Hamiltonian  $\hat{H}$  corresponds to a Hermitian Hamiltonian density  $\hat{h} \in \mathcal{A}$ ,  $\hat{H} = \hat{N}\hat{h}$ . The Heisenberg EOM for  $\langle \boldsymbol{\alpha}, N | \hat{A}_H(t) | \boldsymbol{\alpha}, N \rangle$  reads

$$\frac{d}{dt} \langle \boldsymbol{\alpha}, N | \hat{A}_H(t) | \boldsymbol{\alpha}, N \rangle = \frac{i}{\hbar} \langle \boldsymbol{\alpha}, N | [\hat{H}, \hat{A}_H(t)] | \boldsymbol{\alpha}, N \rangle. \quad (3.110)$$

This section contains three results. We demonstrate that

$$\lim_{N \rightarrow \infty} \langle \boldsymbol{\alpha}, N | \hat{A}_H(t) | \boldsymbol{\alpha}, N \rangle = A_{\text{mf}}(\boldsymbol{\alpha}_t), \quad (3.111)$$

where  $\boldsymbol{\alpha}_0 \equiv \boldsymbol{\alpha}$  and  $\boldsymbol{\alpha}_t$  comprises  $\alpha_m(t) \equiv \sqrt{n_m(t)} e^{i\phi_m(t)}$  with  $n_m(t) \geq 0$ ,  $\phi_m(t) \in \mathbb{R} \bmod 2\pi$ , and  $\sum_m n_m(t) = 1$ . Furthermore, we prove that the dynamics of  $A_{\text{mf}}(\boldsymbol{\alpha}_t)$  is governed by

$$\frac{d}{dt} A_{\text{mf}}(\boldsymbol{\alpha}_t) = \frac{i}{\hbar} K_{\text{mf}}(\boldsymbol{\alpha}_t) \quad \text{with} \quad \hat{K} \equiv [\hat{H}, \hat{A}]. \quad (3.112)$$

We conclude with the mean-field EOMs for the Hamiltonian density (3.89).

To derive Eq. (3.111), we recall that  $\hat{A}$  is a polynomial in  $\hat{a}_m^\dagger \hat{a}_l / N$  with coefficients  $c_k(N)$ , see Definition 1. Let us introduce  $\hat{\lambda}^{(ml)} \equiv \hat{a}_m^\dagger \hat{a}_l / N$  and  $\lambda_{ml}(t) \equiv \lim_{N \rightarrow \infty} \langle \boldsymbol{\alpha}, N | \hat{\lambda}_H^{(ml)}(t) | \boldsymbol{\alpha}, N \rangle$ . According to Result 4 of Lemma 4,  $\lim_{N \rightarrow \infty} \langle \boldsymbol{\alpha}, N | \hat{A}_H(t) | \boldsymbol{\alpha}, N \rangle$  is a polynomial in  $\lambda_{ml}(t)$  with coefficients  $\lim_{N \rightarrow \infty} c_k(N)$ . We argue now that  $\lambda_{ml}(t)$  can be parameterized, without loss of generality, by  $\sqrt{n_m(t)n_l(t)} e^{-i(\phi_m(t) - \phi_l(t))}$ . At  $t = 0$  this parametrization is obviously correct. For  $m = l$ ,  $\lambda_{mm}(t) = n_m(t)$  is a valid parameterization since  $\lambda_{mm}(t) \geq 0$  and  $\sum_m \lambda_{mm}(t) = \lim_{N \rightarrow \infty} \frac{1}{N} \langle \boldsymbol{\alpha}, N | \hat{N}_H(t) | \boldsymbol{\alpha}, N \rangle = 1$ . Employing, again, Result 4 of Lemma 4, we find

$$\begin{aligned} \lambda_{ml}(t) \lambda_{lm}(t) &= \lim_{N \rightarrow \infty} \langle \boldsymbol{\alpha}, N | \hat{\lambda}_H^{(ml)}(t) \hat{\lambda}_H^{(lm)}(t) | \boldsymbol{\alpha}, N \rangle \\ &= \lim_{N \rightarrow \infty} \langle \boldsymbol{\alpha}, N | \hat{\lambda}_H^{(mm)}(t) \hat{\lambda}_H^{(ll)}(t) + \hat{\lambda}_H^{(mm)}(t) / N | \boldsymbol{\alpha}, N \rangle = n_m(t) n_l(t). \end{aligned} \quad (3.113)$$

Together with  $\lambda_{ml}(t) = \lambda_{lm}^*(t)$  this entails  $|\lambda_{ml}(t)| = |\lambda_{lm}(t)| = \sqrt{n_m(t)n_l(t)}$ . The phases of all  $\lambda_{ml}(t)$  with  $m \neq l$  can be deduced from the phases of  $\lambda_{0l}(t)$  by using the relations  $\lambda_{ml}(t) = \lambda_{lm}^*(t)$  and  $\lambda_{ml}(t) \lambda_{lk}(t) \lambda_{km}(t) = n_m(t) n_l(t) n_k(t) \in \mathbb{R}$ . The parameterization  $\lambda_{ml}(t) = \sqrt{n_m(t)n_l(t)} e^{-i(\phi_m(t) - \phi_l(t))}$  reflects these relations without constraining the  $\lambda_{ml}(t)$  any further.

To obtain the mean-field EOM (3.112), we take the  $N \rightarrow \infty$  limit of Eq. (3.110). In any time interval  $[t_1, t_2]$ , we can interchange the limit with the time derivative thanks to the following

**Theorem 3.** [211] *Let  $f_n : [a, b] \rightarrow \mathbb{R}$ ,  $n \in \mathbb{N}$  be continuously differentiable functions which, for  $n \rightarrow \infty$ , converge pointwise to  $f$ . Let the sequence of derivatives  $f'_n : [a, b] \rightarrow \mathbb{R}$  converge uniformly. Then  $f$  is differentiable and*

$$f'(x) = \lim_{n \rightarrow \infty} f'_n(x) \quad \forall x \in [a, b]. \quad (3.114)$$

The right-hand side (RHS) of Eq. (3.110) is continuous in  $t$ . Let us prove that it uniformly converges for  $N \rightarrow \infty$ . According to Result 3 of Lemma 4 the pointwise limit of

$$f_N(t) \equiv \langle \boldsymbol{\alpha}, N | [\hat{H}, \hat{A}_H(t)] | \boldsymbol{\alpha}, N \rangle = \sum_k \frac{(it/\hbar)^k}{k!} \langle \boldsymbol{\alpha}, N | \hat{K}^{(k+1)} | \boldsymbol{\alpha}, N \rangle \quad (3.115)$$

with  $\hat{K}^0 \equiv \hat{A}$  and  $\hat{K}^k \equiv [\hat{H}, \hat{K}^{(k-1)}]$  is

$$\lim_{N \rightarrow \infty} f_N(t) \equiv f(t) = \sum_k \frac{(it/\hbar)^k}{k!} K_{\text{mf}}^{(k+1)}(\boldsymbol{\alpha}). \quad (3.116)$$

It is sufficient to show that for  $t \in [t_1, t_2]$  the RHS of

$$|f_N(t) - f(t)| \leq \sum_k \frac{|t/\hbar|^k}{k!} \left| \langle \boldsymbol{\alpha}, N | \hat{K}^{(k+1)} | \boldsymbol{\alpha}, N \rangle - K_{\text{mf}}^{(k+1)}(\boldsymbol{\alpha}) \right| \quad (3.117)$$

uniformly converges to zero as  $N \rightarrow \infty$ . Similarly to the proof of Result 3 in Lemma 4, we can find some  $c, \tilde{c} \in \mathbb{R}$  such that

$$|\langle \boldsymbol{\alpha}, N | \hat{K}^{(k+1)} | \boldsymbol{\alpha}, N \rangle| \leq \tilde{c} c^k \forall N \Rightarrow \left| \langle \boldsymbol{\alpha}, N | \hat{K}^{(k+1)} | \boldsymbol{\alpha}, N \rangle - K_{\text{mf}}^{(k+1)}(\boldsymbol{\alpha}) \right| \leq 2\tilde{c} c^k \forall N. \quad (3.118)$$

This allows us to apply **Tannery's** theorem, which reveals that the RHS of Eq. (3.117) converges to zero pointwise. The RHS of Eq. (3.117) is a strictly increasing function of  $|t|$ . Let us assume, without loss of generality, that  $|t_2| \geq |t_1|$ . Then, for any  $N$ , the RHS of Eq. (3.117) is absolutely bounded by its value at  $t_2$  and the pointwise convergence to zero in  $t_2$  implies uniform convergence.

We derive the mean-field EOMs for the Hamiltonian density (3.89) by applying Eq. (3.112) to the operators  $\hat{N}_0/N$ ,  $(\hat{a}_0^\dagger \hat{a}_1 \hat{a}_{-1} + \hat{a}_1^\dagger \hat{a}_{-1}^\dagger \hat{a}_0^2)/N^2$ ,  $\hat{D}/N$ ,  $(\hat{a}_1^\dagger \hat{a}_{-1} + \hat{a}_{-1}^\dagger \hat{a}_1)/N$ , and  $i(\hat{a}_1^\dagger \hat{a}_{-1} - \hat{a}_{-1}^\dagger \hat{a}_1)/N$ , obtaining [29]

$$\frac{d}{d\tau} n_0 = -\text{sg}(c) 2n_0 \sqrt{(1-n_0)^2 - d^2} \sin(2\phi) = \frac{\partial}{\partial \phi} \frac{h_{\text{mf}}}{|c|}, \quad (3.119a)$$

$$\frac{d}{d\tau} \phi = 2\xi - \text{sg}(c)(1-2n_0) - \text{sg}(c) \frac{(1-n_0)(1-2n_0) - d^2}{\sqrt{(1-n_0)^2 - d^2}} \cos(2\phi) = -\frac{\partial}{\partial n_0} \frac{h_{\text{mf}}}{|c|}, \quad (3.119b)$$

$$\frac{d}{d\tau} d = 0 = \frac{\partial}{\partial \Delta\phi} \frac{h_{\text{mf}}}{|c|}, \quad (3.119c)$$

$$\frac{d}{d\tau} \Delta\phi = -\text{sg}(c) \left( 1 - \frac{n_0}{\sqrt{(1-n_0)^2 - d^2}} \cos(2\phi) \right) d = -\frac{\partial}{\partial d} \frac{h_{\text{mf}}}{|c|}, \quad (3.119d)$$

where we have introduced  $d \equiv n_1 - n_{-1}$ ,  $\Delta\phi \equiv (\phi_1 - \phi_{-1})/2$ , and the dimensionless time  $\tau \equiv |c|t/\hbar$ . Note that the EOMs are Hamilton's equations for the Hamiltonian function  $h_{\text{mf}}/|c|$  of the generalized coordinates  $n_0, d$  and conjugate momenta  $\phi, \Delta\phi$ . This is, indeed, a general result [204, 205]. The mean-field conservation of  $d$  reflects the quantum conservation of  $\hat{D}$ . For  $d = 0$  the EOMs become

$$\frac{d}{d\tau} n_0 = -\text{sg}(c) 4n_0(1-n_0) \cos(\phi) \sin(\phi) = \frac{\partial}{\partial \phi} \frac{h_{\text{mf}}}{|c|}, \quad (3.120a)$$

$$\frac{d}{d\tau} \phi = 2\xi - \text{sg}(c) 2(1-2n_0) \cos^2(\phi) = -\frac{\partial}{\partial n_0} \frac{h_{\text{mf}}}{|c|}, \quad (3.120b)$$

$$\frac{d}{d\tau} d = 0 = \frac{\partial}{\partial \Delta\phi} \frac{h_{\text{mf}}}{|c|}, \quad (3.120c)$$

$$\frac{d}{d\tau} \Delta\phi = 0 = -\frac{\partial}{\partial d} \frac{h_{\text{mf}}}{|c|}. \quad (3.120d)$$

### 3.7.5 Dynamics

The EOM for  $n_0$ , Eq. (3.119a), can be solved analytically [29, 149]. The dynamics conserves the relative energy  $\eta$ ,

$$\frac{h_{\text{mf}}}{|c|} = \xi(1 - 2n_0) + \text{sg}(c) n_0 \left[ 1 - n_0 + \sqrt{(1 - n_0)^2 - d^2} \cos(2\phi) \right] + \frac{\text{sg}(c)}{2} d^2 = \eta \quad (3.121)$$

and  $\frac{d}{d\tau}\eta = 0$ . Equation (3.121) serves us to bring the square of Eq. (3.119a) into the form

$$\left( \frac{d}{d\tau} n_0 \right)^2 = -\text{sg}(c) 16\xi(n_0 - z_1)(n_0 - z_2)(n_0 - z_3). \quad (3.122)$$

We deliberately set  $z_1 \leq z_2 \leq z_3$ .

According to Refs. [29, 149],

$$n_0(\tau) = \begin{cases} z_2 + (z_3 - z_2) \text{cn}^2 \left( 2\sqrt{|\xi|(z_3 - z_1)}\tau + u, \frac{z_3 - z_2}{z_3 - z_1} \right) & \text{for } \xi c > 0, \\ z_2 - (z_2 - z_1) \text{cn}^2 \left( 2\sqrt{|\xi|(z_3 - z_1)}\tau + v, \frac{z_2 - z_1}{z_3 - z_1} \right) & \text{for } \xi c < 0, \end{cases} \quad (3.123)$$

where  $\text{cn}(w; k^2)$  is the Jacobi elliptic cosine and  $u, v$  account for the initial conditions. One can easily verify that Eq. (3.123) solves Eq. (3.122).

The evolution of  $n_0$  is periodic with period

$$\mathcal{T} = \begin{cases} \frac{1}{\sqrt{|\xi|(z_3 - z_1)}} K \left( \frac{z_3 - z_2}{z_3 - z_1} \right) & \text{for } \xi c > 0, \\ \frac{1}{\sqrt{|\xi|(z_3 - z_1)}} K \left( \frac{z_2 - z_1}{z_3 - z_1} \right) & \text{for } \xi c < 0, \end{cases} \quad (3.124)$$

where  $K(k^2) = \int_0^{\pi/2} d\gamma \sqrt{1 - k^2 \sin^2 \gamma}^{-1}$  is the complete elliptic integral of the first kind.

## 4 Ground-State Quantum Phase Transitions

Quantum-state engineering can clearly benefit from classifying the accessible states of matter. A phase diagram categorizes the states of a given system into phases [212]. Assume that we can prepare a certain type of states—e. g., thermal equilibrium states or Hamiltonian eigenstates, and that we can manipulate the preparation by specifying the values of some control parameters—e. g., Hamiltonian coefficients or temperature. Each control parameter defines an axis of the phase diagram. To divide the states corresponding to different points of the phase diagram into phases, one has to specify the defining signatures of phase transitions<sup>1</sup>. With engineering in mind, it is natural to group the states by common properties. This is formalized by order parameters—quantities that qualitatively distinguish different subsets of states. A typical order parameter is zero in one phase and non-zero in an adjacent phase. Particularly often, phase transitions are defined by singularities of thermodynamic potentials. Another important signature relies on the observation that a point of the phase diagram may correspond to an entire state space instead of a single state. Changes in the dimensionality of the state space can be identified with phase transitions [213]. Note that, strictly speaking, phase diagrams are defined only for infinite systems. However, sufficiently large systems are usually well described by this limit.

Ground-state quantum phase transitions [40]—usually called just quantum phase transitions (QPTs)—classify the ground state of a quantum system depending on a set of control parameters. In phase diagrams for thermal equilibrium states, ground-state QPTs are phase transitions at zero temperature. There are various reasons for the interest in ground states. The thermal state at temperature  $T$  of a system with Fermi temperature  $T_F \gg T$  is well approximated by the  $T = 0$  state. This applies, particularly, to metals at room temperature. Moreover, ground states play a central role in the field of quantum-state engineering. In general, the states at our disposal are thermal with  $T > 0$ . It is conceptually clear that cooling ultimately transforms a thermal state into the ground state. In contrast to thermal states, ground states are pure. Thus, they exhibit quantum but no classical fluctuations, which is an obvious advantage when aiming at high experimental control. Dealing with ground states is also facilitated by their stationarity. Finally, ground states cannot decay—e. g., by spontaneous emission—into eigenstates of lower energy.

Let us concretize the above signatures of phase transitions for the case of ground-state QPTs: we focus on order parameters, singularities of ground-state energy, and changes of ground-state degeneracy. If the low-lying energy spectrum is discrete, an increase in ground-state degeneracy is associated with a closing gap between the lowest and the next higher eigenenergy. Often, a Hamiltonian symmetry is spontaneously broken in one phase and respected by the ground states in the other. This leads to a higher ground-state degeneracy throughout the phase with symmetry breaking. The symmetry operator can be used to define an order parameter. However, symmetry breaking is not necessary for QPTs, and the degeneracy may differ only at the QPT itself.

Quantum phases give an overview of the available ground-state properties. However, they can also be directly employed for quantum-state engineering. Imagine that it is experimentally feasible to prepare a ground state in phase A, and that a ground state in phase B exhibits

---

<sup>1</sup>Different standard signatures often yield the same phases.



some desired properties such as strong entanglement. The adiabatic theorem [34] says that an infinitely slow change of control parameters transforms the ground state in phase A into the ground state in phase B. Accordingly, the final state of a sufficiently slow sweep is expected to have a high fidelity with the desired state. Adiabatic passages are widely used in different areas of physics. Recently, numerous methods summarized under the term “shortcuts to adiabaticity” have been developed to cope with the typically short coherence times of quantum experiments [214]. However, QPTs conflict with adiabaticity. The Landau-Zener formula reveals that a closing gap prohibits adiabatic transitions within finite time [177, 215–218]. Luckily, finite systems feature a residual gap that may suffice for an adiabatic passage of feasible duration. For example, the beautiful experiment presented in Ref. [219] adiabatically takes ultracold atoms in an optical lattice from the superfluid to the Mott insulator phase.

Spinor Bose-Einstein condensates (BECs) exhibit QPTs [29, 30] useful for quantum-state engineering. Reference [32] proposed to generate strongly entangled states by adiabatically crossing QPTs in spin-1 BECs with zero magnetization. A feasibility analysis revealed that hundreds of atoms could be genuinely entangled under realistic conditions. We call the target state in Ref. [32] the central broken-axisymmetry (CBA) state. Reference [150] reported the adiabatic crossing of a QPT in a ferromagnetic BEC of  $^{87}\text{Rb}$  atoms with hyperfine spin 1. Shortly after, a highly entangled Twin-Fock (TF) state was produced by adiabatically driving the  $^{87}\text{Rb}$  BEC through two QPTs [35]. As detailed in Section 2.2.3, entanglement useful for quantum-enhanced interferometry can be quantified by the quantum Fisher information (QFI). The QFI of TF states exhibits Heisenberg scaling [9]. A large ground-state QFI has been, furthermore, predicted for spin-1 BECs with antiferromagnetic interactions [220] or a large magnetization [221]. However, a complete analysis of the ground-state QFI for the experimentally relevant case of a ferromagnetic spin-1 BEC with zero magnetization has been missing.

In the following, we review the quantum phases of a ferromagnetic spin-1 BEC with zero magnetization (Section 4.1) and determine the ground-state FI for optimal collective unitary phase imprinting (Section 4.2). We find that the CBA state exhibits an essentially equally large QFI as the ground state of the TF phase. In Section 4.3, we prove that the metrological gain of the CBA and the TF state can be accessed by counting the atoms in different spin modes, which is a standard experimental technique. We provide some mathematical details on the CBA state in Section 4.4. Seeking to understand the large QFI of the CBA state, we observe (Section 4.5) that the three-mode CBA state hosts two-mode macroscopic superposition states (MSSs) resembling NOON states. Hence, in Section 4.6 we propose two applications of the adiabatically prepared CBA state. First, it can serve as the probe state for quantum-enhanced interferometry. Second, it can be used for the heralded stochastic generation of MSSs. Remarkably, both proposals rely only on existent technology and, as demonstrated in Section 4.7, are feasible under realistic conditions. Finally, we compare the adiabatic generation of states with a large QFI to the widely used method of quenching (Section 4.8). We conclude in Section 4.9.

The results presented in this chapter are published in Refs. [222, 223].

## 4.1 Phases

We consider the spin Hamiltonian from Eq. (3.33) with a ferromagnetic interaction  $c < 0$ ,

$$\frac{\hat{H}}{|c|} = 2\xi(\hat{N}_1 + \hat{N}_{-1}) - \frac{1}{N} \left[ \hat{a}_0^{\dagger 2} \hat{a}_1 \hat{a}_{-1} + \hat{a}_1^{\dagger} \hat{a}_{-1}^{\dagger} \hat{a}_0^2 + \hat{N}_0 \left( \hat{N}_1 + \hat{N}_{-1} + \frac{1}{2} \right) + \frac{\hat{D}^2}{2} \right], \quad (4.1)$$



where  $\xi \equiv \frac{q}{2|c|}$  and  $q$  is the effective quadratic Zeeman shift. Following Ref. [32], we assume that the  $N$ -particle BEC is initially prepared in the separable, coherent state

$$|(\alpha_1 = 0, \alpha_0 = 1, \alpha_{-1} = 0), N\rangle = \frac{1}{\sqrt{N!}} \hat{a}_0^{\dagger N} |0\rangle = |N_1 = 0, N_0 = N, N_{-1} = 0\rangle. \quad (4.2)$$

This state is a zero-magnetization eigenstate of the magnetization operator  $\hat{D} \equiv \hat{N}_1 - \hat{N}_{-1}$ ,  $\hat{D} \hat{a}_0^{\dagger N} |0\rangle = D \hat{a}_0^{\dagger N} |0\rangle$  with  $D = 0$ . Recall that the spin dynamics preserves the magnetization,  $[\hat{H}, \hat{D}] = 0$ . Therefore, we focus on the  $D = 0$  subspace of the  $N$ -particle Hilbert space  $\mathcal{H}_N$ . This subspace is spanned by the Fock states  $|N_1 = k, N_0 = N - 2k, N_{-1} = k\rangle$  with  $k \in \{0, 1, \dots, \lfloor N/2 \rfloor\}$ .

Quantum de-Finetti theorems ensure that the ground-state  $|\psi_0^{(N)}\rangle$  of a bosonic system with a large particle number  $N$  is well approximated by the coherent state  $|\alpha_0, N\rangle$  that minimizes the energy density  $\langle \alpha, N | \hat{H} / N | \alpha, N \rangle$  [224]. More precisely, for an arbitrary operator  $\hat{A} \in \mathcal{A}$ , see Definition 1,

$$\left| \langle \alpha_0, N | \hat{A} | \alpha_0, N \rangle - \langle \psi_0^{(N)} | \hat{A} | \psi_0^{(N)} \rangle \right| \in \mathcal{O}(1/N). \quad (4.3)$$

Note that we are interested in the ground state within an eigenspace of the symmetry operator  $\hat{D}$  with a certain eigenvalue  $D$ . It is commonly assumed that, to account for this constraint, it is sufficient to restrict the coherent states to those with  $\langle \alpha, N | \hat{D} | \alpha, N \rangle = D$  [148]. The mean-field energy density of  $\hat{H} - qN/2^2$  obtained from coherent states satisfying  $\langle \alpha, N | \hat{D} | \alpha, N \rangle = 0$  is, see Eq. (3.100),

$$\frac{h_{\text{mf}}}{|c|} = \xi(1 - 2n_0) - 2n_0(1 - n_0) \cos^2(\phi). \quad (4.4)$$

Minimizing  $h_{\text{mf}}$  as a function of  $0 \leq n_0 \leq 1$  and  $\phi \in [0, 2\pi)$  yields  $\phi \in \{0, \pi\}$ ,

$$n_0 = \begin{cases} 0 & \text{for } \xi \leq -1 \\ \frac{1}{2}(\xi + 1) & \text{for } -1 < \xi < 1, \\ 1 & \text{for } \xi \geq 1 \end{cases} \quad (4.5)$$

and the dimensionless ground-state energy density in the mean-field limit

$$\eta_0 \equiv \min_{n_0, \phi} \frac{h_{\text{mf}}}{|c|} = \begin{cases} \xi & \text{for } \xi \leq -1 \\ -\frac{1}{2}(\xi^2 + 1) & \text{for } -1 < \xi < 1. \\ -\xi & \text{for } \xi \geq 1 \end{cases} \quad (4.6)$$

From the above arguments we can expect that

$$\eta_0 = \lim_{N \rightarrow \infty} \frac{1}{|c|} \langle \psi_0^{(N)} | \hat{H} / N | \psi_0^{(N)} \rangle - \xi, \quad n_0 = \lim_{N \rightarrow \infty} \langle \psi_0^{(N)} | \hat{N}_0 / N | \psi_0^{(N)} \rangle. \quad (4.7)$$

The second  $\xi$ -derivative of  $\eta_0$  is discontinuous in  $\xi = \pm 1$ , see Fig. 4.1a. This indicates that there are two ground-state QPTs at  $\xi = \pm 1$ . The relative occupation  $n_0$  of the spin state  $|f = 1, m = 0\rangle$  is a suitable order parameter for these QPTs, see Fig. 4.1b.

Let us have a closer look at the  $\xi$ -dependent ground state  $|\psi_0^{(N)}\rangle$  with  $N \gg 1$ . For  $\xi \geq 1$ , we have  $n_0 \approx 1$  and hence  $|\psi_0^{(N)}\rangle \approx |0, N, 0\rangle$ . This coincides with the observation that for  $|\xi| \gg 1$  the Hamiltonian becomes

$$\frac{\hat{H}}{|c|} \approx 2\xi(\hat{N}_1 + \hat{N}_{-1}), \quad (4.8)$$

<sup>2</sup>Recall that we shift  $\hat{H}$  by  $qN/2$  for computational convenience.

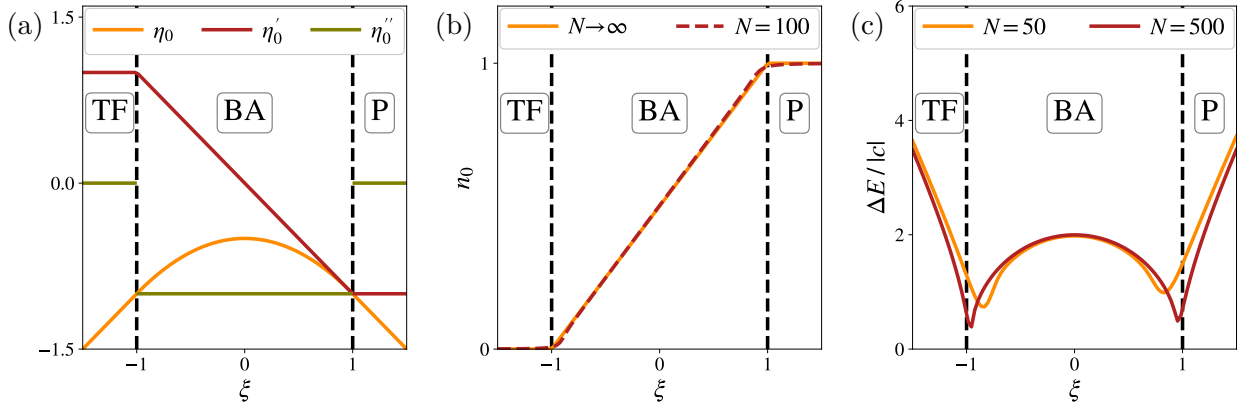


**Figure 4.1:** Ground-state quantum phases in the magnetization-free subspace of a ferromagnetic spin-1 BEC. The control parameter is the dimensionless effective quadratic Zeeman shift  $\xi$ . There are three phases: the TF phase for  $\xi < -1$ , the BA phase for  $-1 < \xi < 1$ , and the P phase for  $\xi > 1$ . (a) Dimensionless ground-state energy density  $\eta_0$  and its derivatives with respect to  $\xi$ . The second derivative of  $\eta_0$  is discontinuous at the two QPTs. (b) The ground-state expectation value of the relative atom number  $n_0$  in the spin state  $|f = 1, m = 0\rangle$  is a suitable order parameter for the QPTs. (c) Dimensionless energy gap  $\Delta E/|c|$  between the ground state and the first excited state. For  $N \rightarrow \infty$  the gap vanishes at the QPTs but remains finite everywhere else.

which is diagonal in the Fock states  $|k, N - 2k, k\rangle$ . For  $\xi > 0$ , the minimal eigenvalue obviously corresponds to  $k = 0$ . The state  $|0, N, 0\rangle$  is called polar (P), and the quantum phase at  $\xi \geq 1$  is known as the P phase, accordingly. For  $\xi \leq -1$ ,  $n_0 \approx 0$  entails  $|\psi_0^{(N)}\rangle \approx |N/2, 0, N/2\rangle$  for even  $N$  and  $|\psi_0^{(N)}\rangle \approx |[N/2], 1, [N/2]\rangle$  for odd  $N$ . Again, these are indeed the respective ground states of the Hamiltonian (4.8) for  $\xi < 0$ . The quantum phase at  $\xi \leq -1$  is named after the TF state  $|N/2, 0, N/2\rangle$ .

Between the TF and P phases,  $|\psi_0^{(N)}\rangle$  strongly depends on the precise value of  $-1 < \xi < 1$ . In Eq. (3.50) we have introduced the collective spin-1 operator  $\hat{\mathbf{L}}$ . For  $\xi = 0$ , the Hamiltonian (4.1) becomes [176]

$$\frac{\hat{H}}{|c|} = -\frac{1}{N}\hat{\mathbf{L}}^2. \quad (4.9)$$

Since  $\hat{L}_z = -\hat{D}$  and the maximal eigenvalue of  $\hat{\mathbf{L}}^2$  is  $l(l+1)$  with  $l = N$ , we can conclude that  $|\psi_0^{(N)}\rangle = |l = N, m_l = 0\rangle$ . This state plays a central role in the present chapter.

The quantum phase at  $-1 < \xi < 1$  is called the broken-axisymmetry (BA) phase. This name is derived from the observation that  $\lim_{N \rightarrow \infty} \langle \alpha_0, N | \hat{L}_{x/y} / N | \alpha_0, N \rangle \neq 0$ , where  $\alpha_0$  corresponds to the values of  $n_0$  and  $\phi$  that minimize the mean-field energy density in Eq. (4.4). A ground state with  $\langle \hat{L}_{x/y} \rangle \neq 0$  would break the  $\hat{L}_z$ - or, equivalently,  $\hat{D}$ -symmetry of the Hamiltonian (4.1). However, this is an example where the mean-field limit has to be treated with caution. Of course, the ground state within an eigenspace of  $\hat{D}$  does not break the  $\hat{D}$ -symmetry. The contradicting mean-field result is probably due to the fact that we study an eigenspace of  $\hat{D}$  in terms of coherent states which, in general, are no eigenstates of  $\hat{D}$ . Nevertheless, we stick to the common name of the quantum phase, and call the ground state  $|\psi_0^{(N)}\rangle$  at  $\xi = 0$  the CBA state  $|\text{CBA}\rangle \equiv |l = N, m_l = 0\rangle$ .

The three ground-state quantum phases in the  $D = 0$  subspace of a ferromagnetic spin-1 BEC have been confirmed numerically [32] and already explored experimentally [31, 35, 150]. It has

been particularly shown that, at  $\xi = \pm 1$ , the energy gap  $\Delta E$  between the ground state and the first excited state amounts to  $\Delta E/|c| \approx 7.4N^{-1/3}$  [32]. Thus, for  $N \rightarrow \infty$  the energy gap at the QPTs vanishes. Remarkably, at all other values of  $\xi$  the gap remains finite, cf. Fig. 4.1c. This implies that the ground states at  $\xi \neq \pm 1$  do not break any symmetry of the Hamiltonian—neither at finite  $N$ , nor in the  $N \rightarrow \infty$  limit.

## 4.2 Quantum Fisher Information

Second-generation quantum technologies rely on entanglement. Particularly, entangled probes can provide quantum-enhanced interferometry, see Section 2.2.3. The CBA and TF states are maximally entangled [32, 225]. The interferometric usefulness of entanglement can be quantified by the QFI. Therefore, we investigate the QFI of the ground state  $|\psi_0^{(N)}\rangle$  at arbitrary  $\xi$ .

The QFI depends on the transformation that imprints the interferometric phase  $\theta$  on the probe state  $\hat{\rho} = |\psi_0^{(N)}\rangle\langle\psi_0^{(N)}|$ . We assume a collective unitary transformation:  $\hat{\rho}(\theta) = e^{-i\theta\hat{R}} \hat{\rho} e^{i\theta\hat{R}}$ , where the phase-imprinting operator  $\hat{R}$  is a collective generator, see Section 3.4. Since  $|\psi_0^{(N)}\rangle$  is a spin state of spin-1 bosons,  $\hat{R}$  must be a linear combination of the collective Gell-Mann operators  $\hat{E}_j$  introduced in Eq. (3.47),  $\hat{R} = \sum_j u_j \hat{E}_j$  with  $u_j \in \mathbb{R}$  and  $\mathbf{u} \equiv (u_1, \dots, u_8)$ . As discussed in Section 2.1.6, the corresponding QFI equals

$$F_Q = 4 \mathbf{u}^T \Gamma \mathbf{u}, \quad (4.10)$$

where  $\Gamma$  is the covariance matrix with the elements

$$\Gamma_{kl} = \frac{1}{2} \langle \psi_0^{(N)} | \hat{E}_k \hat{E}_l + \hat{E}_l \hat{E}_k | \psi_0^{(N)} \rangle - \langle \psi_0^{(N)} | \hat{E}_k | \psi_0^{(N)} \rangle \langle \psi_0^{(N)} | \hat{E}_l | \psi_0^{(N)} \rangle. \quad (4.11)$$

Since the QFI is proportional to  $\|\mathbf{u}\|_2^2$ , we fix  $\|\mathbf{u}\|_2 = 1$ . Then the maximal QFI is determined by the largest eigenvalue  $\gamma$  of  $\Gamma$ ,  $F_Q = 4\gamma$ . The corresponding eigenvector  $\mathbf{u}^{(\gamma)}$  defines the optimal phase-imprinting operator.

Our goal is, thus, to diagonalize  $\Gamma$ . Let us expand  $|\psi_0^{(N)}\rangle$  in the Fock basis of the magnetization-free subspace,

$$|\psi_0^{(N)}\rangle = \sum_k c_k |k, N - 2k, k\rangle, \quad \sum_k |c_k|^2 = 1. \quad (4.12)$$

The restriction to  $D = 0$  entails that  $\Gamma$  is block diagonal:

$$\Gamma = \Gamma^{(4)} \oplus \Gamma^{(2)} \oplus \Delta^2 \hat{E}_4 \oplus \Delta^2 \hat{E}_5, \quad (4.13)$$

where  $\Gamma^{(4)}$  and  $\Gamma^{(2)}$  denote the covariance matrices of  $\{\hat{E}_1, \hat{E}_2, \hat{E}_6, \hat{E}_7\}$  and  $\{\hat{E}_3, \hat{E}_8\}$ , respectively, and  $\Delta^2 \hat{E}_j$  is the variance of  $\hat{E}_j$ .

$\Gamma^{(4)}$  has the doubly degenerate eigenvalues

$$\lambda_{\pm} = A \pm |B| \quad (4.14)$$

with

$$A \equiv \frac{1}{4} \left( N + \sum_{k=0}^{\lfloor N/2 \rfloor} |c_k|^2 k (2N - 4k - 1) \right), \quad (4.15)$$

$$B \equiv \frac{1}{2} \sum_{k=0}^{\lfloor N/2 - 1 \rfloor} c_k^* c_{k+1} (k+1) \sqrt{(N-2k)(N-2k-1)}.$$

For  $|B| \neq 0$ , the corresponding eigenvectors are

$$\begin{aligned}
 \mathbf{u}_+^{(1)} &= \frac{1}{\sqrt{2}|B|} \begin{pmatrix} \text{Im}(B), & \text{Re}(B), & 0, & |B| \end{pmatrix}, \\
 \mathbf{u}_+^{(2)} &= \frac{1}{\sqrt{2}|B|} \begin{pmatrix} \text{Re}(B), & -\text{Im}(B), & |B|, & 0 \end{pmatrix}, \\
 \mathbf{u}_-^{(1)} &= \frac{1}{\sqrt{2}|B|} \begin{pmatrix} -\text{Im}(B), & -\text{Re}(B), & 0, & |B| \end{pmatrix}, \\
 \mathbf{u}_-^{(2)} &= \frac{1}{\sqrt{2}|B|} \begin{pmatrix} -\text{Re}(B), & \text{Im}(B), & |B|, & 0 \end{pmatrix}.
 \end{aligned} \tag{4.16}$$

Note that if all  $c_k \in \mathbb{R}$ ,  $\text{Im}(B)$  vanishes and  $\Gamma^{(4)}$  further decomposes into the covariance matrices  $\Gamma'$  of  $\{\hat{E}_1, \hat{E}_6\}$  and  $\Gamma''$  of  $\{\hat{E}_2, \hat{E}_7\}$ ,  $\Gamma^{(4)} = \Gamma' \oplus \Gamma''$ . The doubly degenerate eigenvalues

$$\tilde{\lambda}_{\pm} = A \pm B \tag{4.17}$$

then correspond to the eigenvectors

$$\begin{aligned}
 \tilde{\mathbf{u}}_+^{(1)} &= \frac{1}{\sqrt{2}}(0, 1, 0, 1), & \tilde{\mathbf{u}}_+^{(2)} &= \frac{1}{\sqrt{2}}(1, 0, 1, 0), \\
 \tilde{\mathbf{u}}_-^{(1)} &= \frac{1}{\sqrt{2}}(0, -1, 0, 1), & \tilde{\mathbf{u}}_-^{(2)} &= \frac{1}{\sqrt{2}}(-1, 0, 1, 0).
 \end{aligned} \tag{4.18}$$

If  $|B| = 0$ ,  $\Gamma^{(4)}$  becomes proportional to the 4-dimensional identity matrix.

The eigenvalues and eigenvectors of  $\Gamma^{(2)}$  are

$$\begin{aligned}
 \lambda_0 &= 0, & \lambda_1 &= 3 \left( \sum_{k=0}^{\lfloor N/2 \rfloor} |c_k|^2 k^2 - \left( \sum_{k=0}^{\lfloor N/2 \rfloor} |c_k|^2 k \right)^2 \right), \\
 \mathbf{u}_0 &= (1, \sqrt{3}), & \mathbf{u}_1 &= (\sqrt{3}, -1).
 \end{aligned} \tag{4.19}$$

Finally,

$$\Delta^2 \hat{E}_4 = \Delta^2 \hat{E}_5 = \frac{1}{2} \sum_{k=0}^{\lfloor N/2 \rfloor} |c_k|^2 k(k+1). \tag{4.20}$$

In the P and TF phases, the eigenvalues and eigenvectors of  $\Gamma$  can be easily evaluated analytically. The P state  $|0, N, 0\rangle$  corresponds to  $c_0 = 1$  and  $c_{k \neq 0} = 0$ . Therefore,  $\lambda_{\pm} = N/4$  and all other eigenvalues vanish. The optimal QFI thus amounts to  $F_Q^{(P)} = N$  and can be attained by any  $\hat{R}_{\text{opt}}^{(P)} = u_1 \hat{E}_1 + u_2 \hat{E}_2 + u_6 \hat{E}_6 + u_7 \hat{E}_7$  with  $u_j \in \mathbb{R}$  and  $u_1^2 + u_2^2 + u_6^2 + u_7^2 = 1$ . The TF state  $|N/2, 0, N/2\rangle$  with  $N$  even yields  $\lambda_0 = \lambda_1 = 0$ ,  $\lambda_{\pm} = N/8$ , and  $\Delta^2 \hat{E}_4 = \Delta^2 \hat{E}_5 = N(N+2)/8$ . For odd  $N$  and  $|\lfloor N/2 \rfloor, 1, \lfloor N/2 \rfloor\rangle$ , we get  $\lambda_0 = \lambda_1 = 0$ ,  $\lambda_{\pm} = (3N-1)/8$ , and  $\Delta^2 \hat{E}_4 = \Delta^2 \hat{E}_5 = (N-1)(N+1)/8$ . Thus, for  $N \gg 1$ , the maximal QFI of the generalized TF state  $|\lfloor N/2 \rfloor, N-2\lfloor N/2 \rfloor, \lfloor N/2 \rfloor\rangle$  is

$$F_Q^{(\text{TF})} = \left\lfloor \frac{N}{2} \right\rfloor \left( \left\lfloor \frac{N}{2} \right\rfloor + 1 \right). \tag{4.21}$$

Any normalized linear combination of  $\{\hat{E}_4, \hat{E}_5\}$  provides an optimal phase-imprinting operator,

$$\begin{aligned}
 \hat{R}_{\text{opt}}^{(\text{TF})} &= u_4 \hat{E}_4 + u_5 \hat{E}_5, & u_4^2 + u_5^2 &= 1 \\
 &= \cos(\varphi) \hat{J}_x + \sin(\varphi) \hat{J}_y \equiv \hat{J}_{\varphi}.
 \end{aligned} \tag{4.22}$$

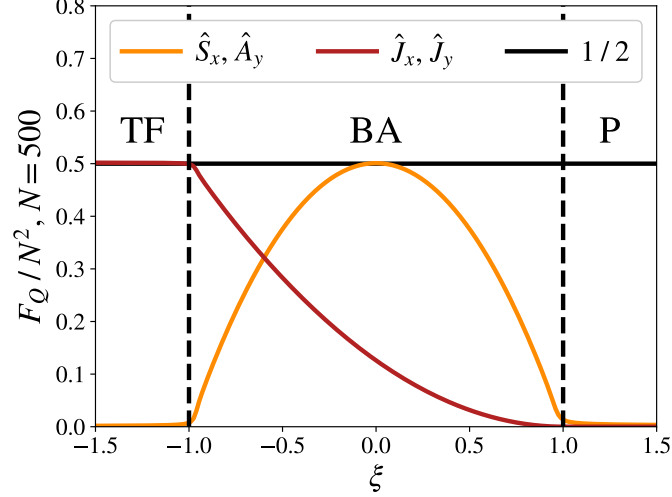


**Figure 4.2:** Ground-state QFI  $F_Q$  as a function of the control parameter  $\xi$ . The depicted QFI is obtained for any phase-imprinting operator  $\hat{R} = \cos(\varphi)\hat{R}_x + \sin(\varphi)\hat{R}_y$  with  $\hat{R}_{x/y}$  given in the legend. The solid horizontal line marks  $1/2$  of the HL. Dashed vertical lines indicate the QPTs.

The collective pseudospin-1/2 operator  $\hat{\mathbf{J}} \equiv (\hat{J}_x, \hat{J}_y, \hat{J}_z)$  has been introduced in Eq. (3.50).

To investigate the QFI in the BA phase and confirm our analytical results for the P and TF phases, we determine the  $\xi$ -dependent ground state  $|\psi_0^{(N)}\rangle$  for  $N = 500$  atoms by exact diagonalization of Hamiltonian (4.1) in the  $D = 0$  subspace. Then we numerically evaluate  $\tilde{\lambda}_\pm$ ,  $\lambda_1$ , and  $\Delta^2\hat{E}_4 = \Delta^2\hat{E}_5$  for the obtained  $|\psi_0^{(500)}\rangle$ . We consider  $\tilde{\lambda}_\pm$  instead of  $\lambda_\pm$  because all matrix elements  $\langle k, N - 2k, k | \hat{H} | l, N - 2l, l \rangle$  of the Hamiltonian  $\hat{H}$  are real and, hence, also the ground-state coefficients can be chosen as  $c_k \in \mathbb{R}$ . We observe that only  $\tilde{\lambda}_+$  and  $\Delta^2\hat{E}_4 = \Delta^2\hat{E}_5$  exceed  $N$ . The corresponding QFI is depicted in Fig. 4.2. Note that, for both kinds of phase imprinting, the QFI constitutes an order parameter of the two QPTs. Remarkably,  $\tilde{\lambda}_+$  becomes maximal at  $\xi = 0$ , i. e., for the CBA state, where it provides a QFI of

$$F_Q^{(\text{CBA})} = \frac{N(N+1)}{2}. \quad (4.23)$$

The corresponding space of optimal phase-imprinting operators can be read off from Eq. (4.18):

$$\begin{aligned} \hat{R}_{\text{opt}}^{(\text{CBA})} &= \frac{u_{16}}{\sqrt{2}}(\hat{E}_1 + \hat{E}_6) + \frac{u_{27}}{\sqrt{2}}(\hat{E}_2 + \hat{E}_7), \quad u_{16}^2 + u_{27}^2 = 1 \\ &= \cos(\varphi)\hat{S}_x + \sin(\varphi)\hat{A}_y \\ &= \frac{1}{2} \left( \cos(\varphi)\hat{L}_x + \sin(\varphi)\hat{L}_y \right) \equiv \frac{1}{2}\hat{L}_\varphi \end{aligned} \quad (4.24)$$

For the definition of the collective pseudospin-1/2 operators  $\hat{\mathbf{S}}$  and  $\hat{\mathbf{A}}$  confer, again, Eq. (3.50). As we have seen in Section 3.5,  $\hat{R}_{\text{opt}}^{(\text{CBA})}$  can be realized by a radiofrequency pulse that couples the  $m = 0$  spin state of each boson with its  $m = \pm 1$  spin states.

Quantum-enhanced interferometry requires, see Section 2.2.3, that the QFI exceeds the standard quantum limit (SQL):  $F_Q > (r_+ - r_-)^2 N$ . Here,  $r_\pm$  denote the maximum and minimum eigenvalue of the single-particle phase-imprinting operator  $\hat{r}$ . For  $\hat{R}_{\text{opt}}^{\text{TF}}$  and  $\hat{R}_{\text{opt}}^{\text{CBA}}$ ,  $r_+ - r_- = 1$ . More generally, note that  $\hat{R} = \sum_j u_j \hat{E}_j$  corresponds to  $\hat{r} = \sum_j u_j \hat{e}_j$  with the  $\hat{e}_j$  introduced in

Eq. (3.45). For  $\|\mathbf{u}\|_2 = 1$ , we then have

$$|r_+ - r_-| \leq 2\|\hat{r}\| \leq 2 \sum_{j=1}^8 |u_j| \|\hat{e}_j\| = \sum_{j=1}^7 |u_j| + \frac{2}{\sqrt{3}}|u_8| \leq \frac{5}{\sqrt{3}} < 3. \quad (4.25)$$

Hence, for sufficiently large  $N$ ,  $F_Q^{(\text{CBA})}$  and  $F_Q^{(\text{TF})}$  clearly exceed the SQL. Recall from Section 2.1.8 that the QFI is tightly bound from above by the Heisenberg limit (HL),  $F_Q \leq (r_+ - r_-)^2 N^2$ . Importantly,  $F_Q^{(\text{CBA})}$  and  $F_Q^{(\text{TF})}$  exhibit Heisenberg scaling, i. e., are essentially proportional to  $N^2$ .

### 4.3 Optimal Measurement

We characterize an ideal interferometer, see Section 2.2.2, by the probe state  $\hat{\rho}$ , the phase-imprinting operator  $\hat{R}$ , and a positive operator-valued measurement (POVM) that is applied to  $\hat{\rho}(\theta)$ . For a given POVM, the interferometric precision is limited by the Cramér-Rao bound (2.46), which is a simple function of the classical Fisher information (CFI). The best precision is obtained for a POVM that maximizes the CFI. The CFI for the optimal POVM equals the QFI. In this section we show that both  $F_Q^{(\text{CBA})}$  and  $F_Q^{(\text{TF})}$  can be attained by measuring the magnetization  $\hat{D}$ . Typically, experiments with spin-1 BECs give access to the occupation of the spin states,  $\hat{N}_m$  with  $m \in \{1, 0, -1\}$ , and thus to  $\hat{D} \equiv \hat{N}_1 - \hat{N}_{-1}$ .

We consider the probe states

$$|\psi\rangle \in \left\{ |\text{CBA}\rangle \equiv |l = N, m_1 = 0\rangle, |\text{TF}\rangle \equiv |[N/2], N - 2[N/2], [N/2]\rangle \right\} \quad (4.26)$$

along with the respective  $\hat{R}_{\text{opt}}$  defining  $|\psi(\theta)\rangle = e^{-i\theta\hat{R}_{\text{opt}}} |\psi\rangle$ . First, we set

$$\hat{R}_{\text{opt}}^{(\text{CBA})} = \hat{S}_x, \quad \hat{R}_{\text{opt}}^{(\text{TF})} = \hat{J}_x \quad (4.27)$$

and show that measuring  $(\hat{N}_1, \hat{N}_{-1})$  is optimal for any interferometric phase  $\theta$ . Note that our probe states are pure. Furthermore, the projections  $\hat{P}_{N_1, N_{-1}} \equiv |N_1, N - N_1 - N_{-1}, N_{-1}\rangle \langle N_1, N - N_1 - N_{-1}, N_{-1}|$  onto the eigenstates of  $(\hat{N}_+, \hat{N}_-)$  are 1-dimensional. Finally,

$$|\partial_\theta \psi(\theta)\rangle \equiv \partial_\theta |\psi(\theta)\rangle = -i\theta \hat{R}_{\text{opt}} |\psi(\theta)\rangle, \quad \langle \psi(\theta) | \partial_\theta \psi(\theta) \rangle = -i\theta \langle \psi | \hat{R}_{\text{opt}} | \psi \rangle = 0, \quad (4.28)$$

and thus

$$|\partial_\theta \psi_\perp(\theta)\rangle \equiv \left( \mathbb{1} - |\psi(\theta)\rangle \langle \psi(\theta)| \right) |\partial_\theta \psi(\theta)\rangle = |\partial_\theta \psi(\theta)\rangle = -i\theta \hat{R}_{\text{opt}} |\psi(\theta)\rangle. \quad (4.29)$$

Therefore, according to Eq. (2.14), measuring  $(\hat{N}_1, \hat{N}_{-1})$  is optimal for all  $\theta$  if and only if

$$\theta \text{Re} \left( \langle \psi(\theta) | \hat{P}_{N_1, N_{-1}} \hat{R}_{\text{opt}} | \psi(\theta) \rangle \right) = 0 \quad \forall N_1, N_{-1}, \theta. \quad (4.30)$$

We observe that for any  $n \in \mathbb{N}_0$

$$\begin{aligned} \langle N_1, N - N_1 - N_{-1} | \hat{S}_x^{2n+1} | \text{CBA} \rangle &= 0 \quad \text{for } N_1 - N_{-1} \text{ even,} \\ \langle N_1, N - N_1 - N_{-1} | \hat{S}_x^{2n} | \text{CBA} \rangle &= 0 \quad \text{for } N_1 - N_{-1} \text{ odd,} \\ \langle N_1, N - N_1 - N_{-1} | \hat{J}_x^{2n+1} | \text{TF} \rangle &= 0 \quad \text{for } N_1 - [N/2] \text{ even (or } N_{-1} - [N/2] \text{ even),} \\ \langle N_1, N - N_1 - N_{-1} | \hat{J}_x^{2n} | \text{TF} \rangle &= 0 \quad \text{for } N_1 - [N/2] \text{ odd (or } N_{-1} - [N/2] \text{ odd).} \end{aligned} \quad (4.31)$$

This entails

$$\langle \psi | \hat{R}_{\text{opt}}^{2n} \hat{P}_{N_1, N-1} \hat{R}_{\text{opt}}^{2m+1} | \psi \rangle = 0, \quad \langle \psi | \hat{R}_{\text{opt}}^{2m+1} \hat{P}_{N_1, N-1} \hat{R}_{\text{opt}}^{2n} | \psi \rangle = 0 \quad \forall n, m \in \mathbb{N}_0. \quad (4.32)$$

We can use Eq. (4.32) to write

$$\begin{aligned} \langle \psi(\theta) | \hat{P}_{N_1, N-1} \hat{R}_{\text{opt}} | \psi(\theta) \rangle &= i \sum_{j, l=0}^{\infty} \frac{(-1)^{j+l}}{(2j)!(2l)!} \theta^{2(j+l)+1} \\ &\times \left( \frac{1}{2j+1} \langle \psi | \hat{R}_{\text{opt}}^{2j+1} \hat{P}_{N_1, N-1} \hat{R}_{\text{opt}}^{2l+1} | \psi \rangle - \frac{1}{2l+1} \langle \psi | \hat{R}_{\text{opt}}^{2j} \hat{P}_{N_1, N-1} \hat{R}_{\text{opt}}^{2l+2} | \psi \rangle \right). \end{aligned} \quad (4.33)$$

Since the Fock-basis coefficients of  $|\psi\rangle$  (with an appropriate global phase) and the matrix elements of  $\hat{R}_{\text{opt}}$  are real, Eq. (4.33) implies  $\langle \psi(\theta) | \hat{P}_{N_1, N-1} \hat{R}_{\text{opt}} | \psi(\theta) \rangle \in i\mathbb{R}$  and, hence, Condition (4.30).

Next, we show that it is sufficient to measure  $\hat{D}$ . The projection onto an eigenspace of  $\hat{D}$  with eigenvalue  $D$  is  $\hat{P}_D = \sum_{N_1 - N_{-1} = D} \hat{P}_{N_1, N-1}$ . Therefore, Condition (4.30) holds also when  $\hat{P}_{N_1, N-1}$  is substituted by  $\hat{P}_D$ . However, this does not imply that measuring  $\hat{D}$  is optimal, because the  $\hat{P}_D$  are, in general, not 1-dimensional. To solve this problem, we identify restricted Hilbert spaces  $\tilde{\mathcal{H}}_N \subset \mathcal{H}_N$  such that  $\hat{R}_{\text{opt}}^n | \psi \rangle \in \tilde{\mathcal{H}}_N$  for all  $n \in \mathbb{N}_0$  and, at the same time,  $\hat{P}_D \tilde{\mathcal{H}}_N$  is 1-dimensional. Let us start with the TF state. Since  $[\hat{J}_x, \hat{N}_0] = 0$  and  $\hat{N}_0 | \text{TF} \rangle = N - 2 \lfloor N/2 \rfloor$ ,

$$\tilde{\mathcal{H}}_N^{(\text{TF})} \equiv \left( \sum_{N_1=0}^{2 \lfloor N/2 \rfloor} \hat{P}_{N_1, 2 \lfloor N/2 \rfloor - N_1} \right) \mathcal{H}_N \quad (4.34)$$

contains all  $\hat{J}_x^n | \text{TF} \rangle$ . Furthermore,  $\hat{P}_D \tilde{\mathcal{H}}_N^{(\text{TF})} = \hat{P}_{\lfloor N/2 \rfloor + D/2, \lfloor N/2 \rfloor - D/2} \mathcal{H}_N$  is clearly 1-dimensional. For the CBA state, we have  $[\hat{S}_x, \hat{\mathbf{L}}^2] = \frac{1}{2} [\hat{L}_x, \hat{\mathbf{L}}^2] = 0$  and  $\hat{\mathbf{L}}^2 | \text{CBA} \rangle = N(N+1) | \text{CBA} \rangle$ . Therefore, for any  $n \in \mathbb{N}_0$ ,

$$\hat{S}_x^n | \text{CBA} \rangle \in \left( \sum_{m_1=-N}^N |l=N, m_1\rangle \langle l=N, m_1| \right) \mathcal{H}_N \equiv \tilde{\mathcal{H}}_N^{(\text{CBA})}. \quad (4.35)$$

Since  $\hat{D} = -\hat{L}_z$ , also  $\hat{P}_D \tilde{\mathcal{H}}_N^{(\text{CBA})} = |l=N, m_1=-D\rangle \langle l=N, m_1=-D| \mathcal{H}_N$  is 1-dimensional.

Finally, we generalize our results to arbitrary  $\hat{R}_{\text{opt}}^{(\text{TF})} = \hat{J}_\varphi$  and  $\hat{R}_{\text{opt}}^{(\text{CBA})} = \frac{1}{2} \hat{L}_\varphi$ , cf. Eqs. (4.22) and (4.24). The transformation rule (3.55) for vector operators yields

$$\begin{aligned} \hat{J}_\varphi &= e^{-i\varphi \hat{J}_z} \hat{J}_x e^{i\varphi \hat{J}_z} = e^{-2i\varphi \hat{D}} \hat{J}_x e^{2i\varphi \hat{D}}, \\ \hat{L}_\varphi &= e^{-i\varphi \hat{L}_z} \hat{L}_x e^{i\varphi \hat{L}_z} = e^{-i\varphi \hat{D}} \hat{L}_x e^{i\varphi \hat{D}} = 2 e^{-i\varphi \hat{D}} \hat{S}_x e^{i\varphi \hat{D}}. \end{aligned} \quad (4.36)$$

Since  $\hat{D} | \psi \rangle = 0$ ,

$$\begin{aligned} e^{-i\theta \hat{J}_\varphi} | \text{TF} \rangle &= e^{-2i\varphi \hat{D}} e^{-i\theta \hat{J}_x} | \text{TF} \rangle, \\ e^{-\frac{i}{2} \theta \hat{L}_\varphi} | \text{CBA} \rangle &= e^{-i\varphi \hat{D}} e^{-i\theta \hat{S}_x} | \text{CBA} \rangle. \end{aligned} \quad (4.37)$$

The CFI is defined via  $\langle \psi(\theta) | \hat{P}_D | \psi(\theta) \rangle$ , see Eq. (2.4), and  $e^{2i\varphi \hat{D}} \hat{P}_D e^{-2i\varphi \hat{D}} = e^{i\varphi \hat{D}} \hat{P}_D e^{-i\varphi \hat{D}} = \hat{P}_D$ . Therefore, the CFI does not depend on  $\varphi$ .

## 4.4 Central Broken-Axisymmetry State

The QFI of the TF state subject to phase imprinting by  $\hat{J}_\varphi$  is well known [9]. Conversely, the large QFI  $F_Q^{(\text{CBA})}$  in Eq. (4.23) provided by the CBA state and the phase-imprinting operator  $\hat{L}_\varphi/2$  is, to the best of our knowledge, a novel result. In Section 4.2, the value of  $F_Q^{(\text{CBA})}$  has been obtained numerically. Let us now confirm it by an analytical derivation.

We want to compute

$$F_Q^{(\text{CBA})} = 4\Delta^2 \langle \hat{L}_\varphi/2 \rangle = \langle \text{CBA} | \hat{L}_\varphi^2 | \text{CBA} \rangle - \langle \text{CBA} | \hat{L}_\varphi | \text{CBA} \rangle^2, \quad (4.38)$$

cf. Eq. (2.27). First we note that, because of Eq. (4.36) and  $\hat{D}|\text{CBA}\rangle = 0$ , the expectation values do not depend on  $\varphi$ . Recall that  $|\text{CBA}\rangle \equiv |l = N, m_l = 0\rangle$  and  $(\hat{L}_x \pm i\hat{L}_y)|l, m_l\rangle \propto |l, m_l \pm 1\rangle$ . Therefore,

$$\langle \text{CBA} | \hat{L}_\varphi | \text{CBA} \rangle = 0. \quad (4.39)$$

Furthermore,

$$\begin{aligned} \langle l = N, m_l = 0 | \hat{L}_x^2 | l = N, m_l = 0 \rangle &= \frac{1}{2} \langle l = N, m_l = 0 | \hat{L}_x^2 + \hat{L}_y^2 | l = N, m_l = 0 \rangle \\ &= \frac{1}{2} \langle l = N, m_l = 0 | \hat{\mathbf{L}}^2 | l = N, m_l = 0 \rangle \\ &= \frac{1}{2} N(N+1). \end{aligned} \quad (4.40)$$

This yields, in accordance with Eq. (4.23),

$$F_Q^{(\text{CBA})} = \frac{N(N+1)}{2}. \quad (4.41)$$

Let us expand the CBA state in the Fock basis, which we often use for explicit calculations. The CBA state can be expressed as [176]

$$|\text{CBA}\rangle = \frac{1}{\sqrt{(2N)!}} \hat{L}_+^N |l = N, m_l = -N\rangle = \frac{1}{\sqrt{(2N)!}} \hat{L}_+^N |N_1 = N, N_0 = 0, N_{-1} = 0\rangle, \quad (4.42)$$

where  $\hat{L}_+ \equiv \hat{L}_x + i\hat{L}_y = \sqrt{2}(\hat{a}_0^\dagger \hat{a}_1 + \hat{a}_{-1}^\dagger \hat{a}_0)$  acts as  $\hat{L}_+ |l, m_l\rangle = \sqrt{(N-m_l)(N+m_l+1)} |l, m_l+1\rangle$ . We can rewrite Eq. (4.42) as<sup>3</sup>

$$|\text{CBA}\rangle = \frac{1}{\sqrt{(2N)!}} \partial_s^N e^{s\hat{L}_+} |N, 0, 0\rangle \Big|_{s=0}. \quad (4.43)$$

Note that  $[\hat{a}_0^\dagger \hat{a}_1, \hat{a}_{-1}^\dagger \hat{a}_0] = -\hat{a}_{-1}^\dagger \hat{a}_1$  and  $[\hat{a}_0^\dagger \hat{a}_1, \hat{a}_{-1}^\dagger \hat{a}_1] = [\hat{a}_{-1}^\dagger \hat{a}_0, \hat{a}_{-1}^\dagger \hat{a}_1] = 0$ . Therefore, we can use the Baker-Campbell-Hausdorff (BCH) formula in the form

$$e^{\hat{A}+\hat{B}} = e^{\hat{A}} e^{\hat{B}} e^{-[\hat{A}, \hat{B}]/2} \quad (4.44)$$

to obtain

$$e^{s\hat{L}_+} = e^{\sqrt{2}s\hat{a}_0^\dagger \hat{a}_1} e^{\sqrt{2}s\hat{a}_{-1}^\dagger \hat{a}_0} e^{s^2\hat{a}_{-1}^\dagger \hat{a}_1} = e^{s^2\hat{a}_{-1}^\dagger \hat{a}_1} e^{\sqrt{2}s\hat{a}_0^\dagger \hat{a}_1} e^{\sqrt{2}s\hat{a}_{-1}^\dagger \hat{a}_0}. \quad (4.45)$$

<sup>3</sup>This elegant approach has been pointed out to us by T. J. Volkoff from Konkuk University. Our original derivation was combinatorial and can be found in Ref. [222].



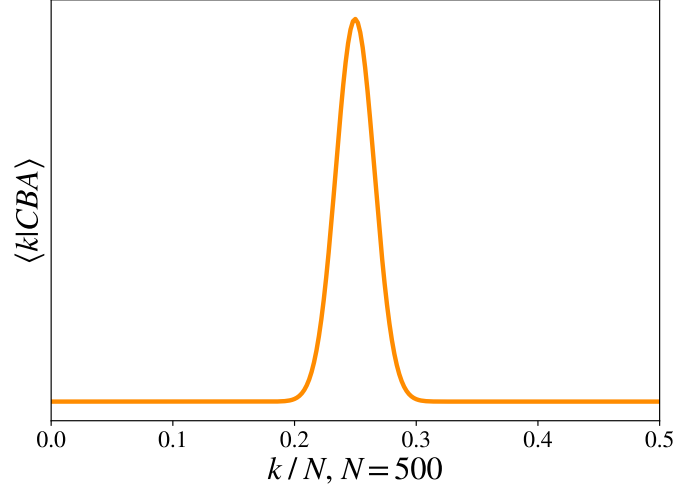


**Figure 4.3:** Coefficients of the CBA state in the Fock basis  $|k\rangle \equiv |k, N - 2k, k\rangle$  of the  $D = 0$  subspace.

Plugging Eq. (4.45) into Eq. (4.43) yields

$$\begin{aligned}
 |CBA\rangle &= \frac{1}{\sqrt{(2N)!}} \partial_s^N e^{s^2 \hat{a}_{-1}^\dagger \hat{a}_1} e^{\sqrt{2}s \hat{a}_0^\dagger \hat{a}_1} |N, 0, 0\rangle \Big|_{s=0} \\
 &= \frac{1}{\sqrt{(2N)!}} \partial_s^N \sum_{j,k=0}^{\infty} \frac{\sqrt{2}^j s^{j+2k}}{j!k!} \hat{a}_0^{\dagger j} \hat{a}_{-1}^{\dagger k} \hat{a}_1^{j+k} |N, 0, 0\rangle \Big|_{s=0} \\
 &= \sqrt{\frac{2^N (N!)^3}{(2N)!}} \sum_{k=0}^{\lfloor N/2 \rfloor} \frac{1}{2^k k! 2(N-2k)!} \hat{a}_0^{\dagger(N-2k)} (\hat{a}_1^\dagger \hat{a}_{-1}^\dagger)^k |0\rangle \\
 &= \sqrt{\frac{2^N (N!)^3}{(2N)!}} \sum_{k=0}^{\lfloor N/2 \rfloor} \frac{1}{2^k k! \sqrt{(N-2k)!}} |k, N - 2k, k\rangle.
 \end{aligned} \tag{4.46}$$

In Eq. (3.49), we have introduced the symmetric ( $g$ ) and antisymmetric ( $h$ ) creation and annihilation operators

$$\hat{g}^{(\dagger)} \equiv \frac{1}{\sqrt{2}} (\hat{a}_1^{(\dagger)} + \hat{a}_{-1}^{(\dagger)}), \quad \hat{h}^{(\dagger)} \equiv \frac{1}{\sqrt{2}} (\hat{a}_1^{(\dagger)} - \hat{a}_{-1}^{(\dagger)}). \tag{4.47}$$

They give rise to another useful Fock basis, which consists of the states  $|N_g, N_0, N_h\rangle$  characterized by the eigenvalues of  $\hat{N}_g \equiv \hat{g}^\dagger \hat{g}$  and  $\hat{N}_h \equiv \hat{h}^\dagger \hat{h}$ . To expand a state from the  $D = 0$  subspace in this basis, note that

$$\hat{a}_1^\dagger \hat{a}_{-1}^\dagger = \frac{1}{2} (\hat{g}^{\dagger 2} - \hat{h}^{\dagger 2}). \tag{4.48}$$

Figure 4.3 displays the expansion coefficients obtained in Eq. (4.46). A large QFI can be usually attributed to fine structures in an appropriate representation of the state. The expansion of  $|CBA\rangle$  in the Fock states  $|k, N - 2k, k\rangle$  does not exhibit such features. This is because we do not visualize the entire Hilbert space  $\mathcal{H}_N$  but expand in a basis of the  $D = 0$  subspace only. Meanwhile, the confinement of the CBA state to the  $D = 0$  subspace can be considered crucial for its large QFI and, thus, interferometric sensitivity. Indeed, an infinitesimal interferometric

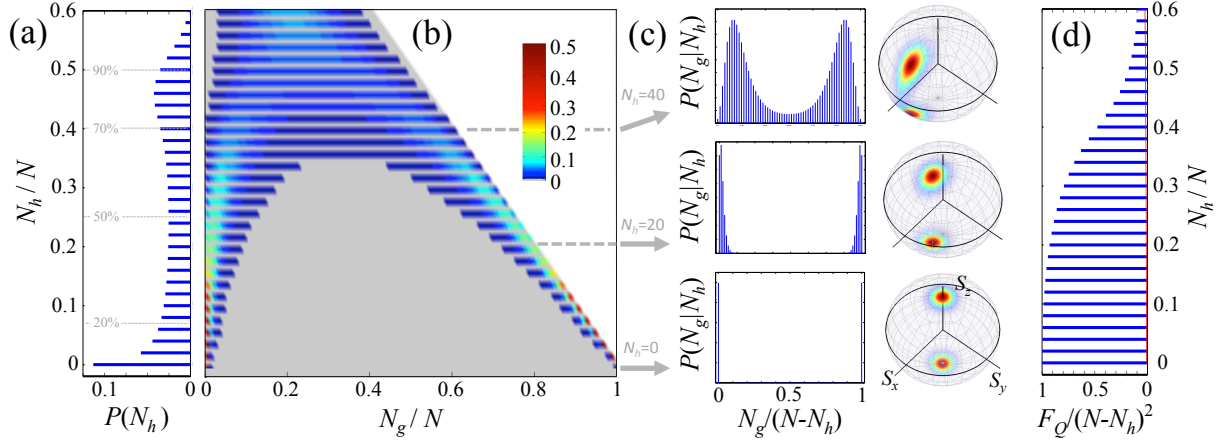


**Figure 4.4:** Two-mode MSSs within the three-mode rotated CBA state  $|\psi\rangle \equiv e^{-i\frac{\pi}{2}\hat{S}_y} |\text{CBA}\rangle$ . (a) Probability  $P(N_h)$  to find  $N_h$  atoms in the antisymmetric mode of  $|\psi\rangle$ . The dashed lines indicate cumulative probabilities. A measurement of  $\hat{N}_h$  with outcome  $N_h$  prepares the state  $|\phi_{N_h}\rangle \otimes |N_h\rangle$ . (b) Conditional probabilities  $P(N_g|N_h) = |\langle N_g, N - N_g - N_h | \phi_{N_h}\rangle|^2$ . Note that  $N_g + N_h \leq N$ . The two branches for  $N_h \lesssim N/2$  correspond to MSSs. (c) Exemplary  $|\phi_{N_h}\rangle$ :  $P(N_g|N_h)$  and the Husimi distributions of  $|\phi_{N_h}\rangle$  resemble NOON states. (d) QFI of  $|\phi_{N_h}\rangle$  subject to phase-imprinting by  $\hat{S}_z$ . For small  $N_h$ , the QFI reaches the HL. The red line indicates the SQL. In all panels  $N = 100$ .

phase  $\delta\theta$  changes the CBA state by  $\delta|\text{CBA}\rangle \equiv -i\delta\theta\hat{L}_\varphi/2|\text{CBA}\rangle$ , which can be well distinguished from the original state because the projection of  $\delta|\text{CBA}\rangle$  on the  $D = 0$  subspace vanishes.

Another way to understand the large QFI of the CBA state is provided by its relation to MSSs, which we discuss in the following section.

## 4.5 Macroscopic Superposition States

In this section we consider the rotated CBA state  $|\psi\rangle \equiv e^{-i\frac{\pi}{2}\hat{S}_y} |\text{CBA}\rangle$ . Figure 4.4b displays, for  $N = 100$  atoms, the conditional probability  $P(N_g|N_h)$  to find  $N_g$  atoms in the symmetric mode after having measured  $N_h$  atoms in the antisymmetric mode,

$$P(N_g|N_h) = \frac{P(N_g, N_h)}{P(N_h)}, \quad P(N_g, N_h) \equiv |\langle N_g, N - N_g - N_h, N_h | \psi \rangle|^2, \quad P(N_h) \equiv \sum_{N_g} P(N_g, N_h). \quad (4.49)$$

In accordance with Eq. (4.48), odd values of  $N_h$  have zero probability, so that  $P(N_g|N_h \text{ odd})$  is not defined. At small fixed values of  $N_h$ , there is a large probability to find all or, on the contrary, none of the remaining  $N - N_h$  atoms in the symmetric mode, cf. Fig. 4.4c. This hints at superpositions of macroscopically distinct states.

A measurement of  $\hat{N}_h$  with outcome  $N_h$  prepares a pure state  $|\phi_{N_h}\rangle$  in the symmetric and the  $m = 0$  mode:

$$|\phi_{N_h}\rangle \otimes |N_h\rangle \equiv \frac{1}{\sqrt{P(N_h)}} \sum_{N_g=0}^{N-N_h} \langle N_g, N - N_g - N_h, N_h | \psi \rangle |N_g, N - N_g - N_h, N_h\rangle, \quad (4.50)$$

where  $|N_h\rangle \equiv \hat{h}^\dagger{}^{N_h}|0\rangle/\sqrt{N_h!}$ , and the probability  $P(N_h)$  of finding  $N_h$  atoms in the antisymmetric

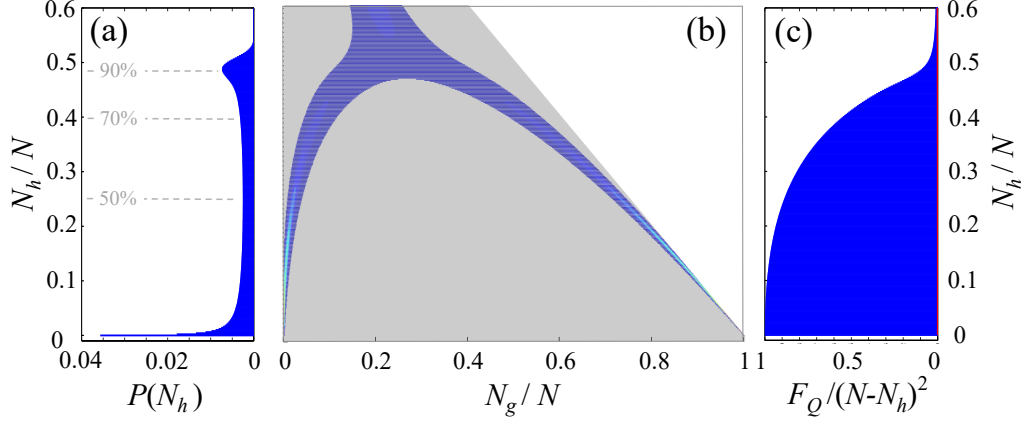


**Figure 4.5:** The same as Figs. 4.4a, b, and d, but for  $N = 1000$  atoms.

mode normalizes  $|\phi_{N_h}\rangle$ . Figure 4.4a shows that the most probable measurement outcome is  $N_h = 0$ . The state  $|\phi_0\rangle$  closely resembles a NOON state,

$$|\phi_0\rangle \approx \frac{1}{\sqrt{2}} \left( |N_g = N, N_0 = 0\rangle + |N_g = 0, N_0 = N\rangle \right). \quad (4.51)$$

This is confirmed by  $P(N_g|N_h) \equiv |\langle N_g, N - N_g - N_h | \phi_{N_h} \rangle|^2$  for  $N_h = 0$  and the Husimi distribution [177] of  $|\phi_0\rangle$ , see Fig. 4.4c. Furthermore, just as the QFI of a NOON state, the QFI of  $|\phi_0\rangle$  subject to phase-imprinting by  $\hat{S}_z$  reaches the HL, see Fig. 4.4d. For  $N = 500$ , the fidelity of  $|\phi_0\rangle$  with the NOON state in Eq. (4.51) exceeds 99%.

The resemblance between  $|\phi_{N_h}\rangle$  and NOON states decreases with increasing  $N_h$ . However, for  $N_h \lesssim N/2$ ,  $P(N_g|N_h)$  continues to exhibit a double-peaked shape, see Fig. 4.4b–c. Furthermore, the QFI depicted in Fig. 4.4d stays far above the SQL. Figure 4.5 shows that for an increased number of  $N = 1000$  atoms these features become even more pronounced. The overall probability to prepare  $|\phi_{N_h}\rangle$  with  $N_h \leq N/2$  by measuring  $\hat{N}_h$  is about 90%, as indicated in Figs. 4.4a and 4.5a.

The large QFI of the  $|\phi_{N_h}\rangle$  explains the large QFI of the CBA state. Recall that

$$F_Q^{(\text{CBA})} = 4\Delta^2 \hat{S}_x = 4\langle \text{CBA} | \hat{S}_x^2 | \text{CBA} \rangle, \quad (4.52)$$

where we have used that  $\langle \text{CBA} | \hat{S}_x | \text{CBA} \rangle = 0$ , cf. Eq. (4.39). Furthermore,

$$\begin{aligned} \langle \text{CBA} | \hat{S}_x^2 | \text{CBA} \rangle &= \langle \text{CBA} | e^{i\frac{\pi}{2}\hat{S}_y} \hat{S}_z^2 e^{-i\frac{\pi}{2}\hat{S}_y} | \text{CBA} \rangle \\ &= \langle \psi | \hat{S}_z^2 | \psi \rangle \\ &= \sum_{N_h, N'_h} \sqrt{P(N_h)P(N'_h)} \langle \phi_{N_h} | \hat{S}_z^2 | \phi_{N'_h} \rangle \langle N_h | N'_h \rangle \\ &= \sum_{N_h} P(N_h) \langle \phi_{N_h} | \hat{S}_z^2 | \phi_{N_h} \rangle. \end{aligned} \quad (4.53)$$

The QFI of  $|\phi_{N_h}\rangle$  with respect to  $\hat{S}_z$  is

$$F_Q^{(N_h)} \equiv 4 \left( \langle \phi_{N_h} | \hat{S}_z^2 | \phi_{N_h} \rangle - \langle \phi_{N_h} | \hat{S}_z | \phi_{N_h} \rangle^2 \right). \quad (4.54)$$

However, since  $\langle N_g, N - N_g - N_h | e^{i\frac{\pi}{2}\hat{S}_y} | \phi_{N_h} \rangle$  vanishes for odd  $N_g$ , and  $\hat{S}_x$  changes  $N_g$  by  $\pm 1$ ,

$$\langle \phi_{N_h} | \hat{S}_z | \phi_{N_h} \rangle = \langle \phi_{N_h} | e^{-i\frac{\pi}{2}\hat{S}_y} \hat{S}_x e^{i\frac{\pi}{2}\hat{S}_y} | \phi_{N_h} \rangle = 0. \quad (4.55)$$

Hence,  $F_Q^{(N_h)} = 4\langle \phi_{N_h} | \hat{S}_z^2 | \phi_{N_h} \rangle$  and

$$F_Q^{(\text{CBA})} = \sum_{N_h} P(N_h) F_Q^{(N_h)}. \quad (4.56)$$

In Eq. (2.51), we have introduced the effective size of a quantum state,

$$\mathcal{N}(\hat{\rho}) \equiv \frac{1}{N} \max_{\hat{r}: \|\hat{r}\|=1/2} F_Q[\hat{\rho}, \hat{r}], \quad (4.57)$$

where  $F_Q[\hat{\rho}, \hat{r}]$  denotes the QFI of  $\hat{\rho}$  with respect to the phase-imprinting operator  $\hat{R} = \sum_{l=1}^N \hat{r}^{(l)}$ . We call a state  $\hat{\rho}$  a MSS if  $1 \ll \mathcal{N}(\hat{\rho}) \ll N$ . The effective size of  $|\phi_{N_h}\rangle$  is lower bounded by its QFI with respect to  $\hat{S}_z$ ,

$$\mathcal{N}(|\phi_{N_h}\rangle\langle\phi_{N_h}|) \geq \frac{1}{N - N_h} F_Q^{(N_h)}. \quad (4.58)$$

As we have discussed, measuring  $\hat{N}_h$  prepares the BEC in a state  $|\phi_{N_h}\rangle \otimes |N_h\rangle$ . With a large probability, the measurement outcome is  $N_h \lesssim N/2$ , whereupon

$$\frac{1}{N - N_h} \ll \frac{1}{(N - N_h)^2} F_Q^{(N_h)} \ll 1, \quad (4.59)$$

cf. Figs. 4.4d and 4.5c, and  $|\phi_{N_h}\rangle$  is a MSS. Thus,  $N_h \lesssim N/2$  heralds the preparation of a MSS  $|\phi_{N_h}\rangle$ .

According to our definition, also |CBA> and |TF> are MSSs. However, for small values of  $N_h$  the effective size of  $|\phi_{N_h}\rangle$  exceeds the one of |CBA> and |TF>. An even more important advantage of the  $|\phi_{N_h}\rangle$  is their resemblance to NOON states, which constitute a paradigmatic example of MSSs.

In general, the ground state of a gapped quantum phase cannot have a double-peaked probability distribution with respect to a collective observable [226]. Yet, in this section we have demonstrated that a non-degenerate ground state can be used for the heralded stochastic preparation of such MSSs. One might remark that, without restriction to the  $D = 0$  subspace, the CBA state belongs to a  $(2N + 1)$ -dimensional ground-state space of the Hamiltonian (4.1) at  $\xi = 0$  [176]. However, in practice this degeneracy is typically lifted (in the stationary frame) by an effective linear Zeeman shift.

## 4.6 Proposal

The CBA state can be obtained from the P state by adiabatically changing the effective quadratic Zeeman shift from  $\xi_0 > 1$  across the QPT at  $\xi = 1$  to  $\xi = 0$ , cf. Figs. 4.6a and 4.1. First, electromagnetic pulses transfer the BEC to the P state  $|N_1 = 0, N_0 = N, N_{-1} = 0\rangle$  [25, 35]. At  $\xi_0$ , this is (at finite  $N$  approximately) the spin ground state of the BEC. According to the adiabatic theorem [34], a system initialized in the ground state of an infinitely slowly varying Hamiltonian  $\hat{H}(t)$  and evolving with  $\hat{H}(t)$  remains in the instantaneous ground state of  $\hat{H}(t)$ . Therefore, we expect that a slow sweep of  $\xi$  from  $\xi_0$  to  $\xi = 0$  prepares the CBA state. In the simplest case, the ramp  $\xi(\tau)$  is linear,

$$\xi(\tau) = \xi_0 - Q\tau, \quad (4.60)$$

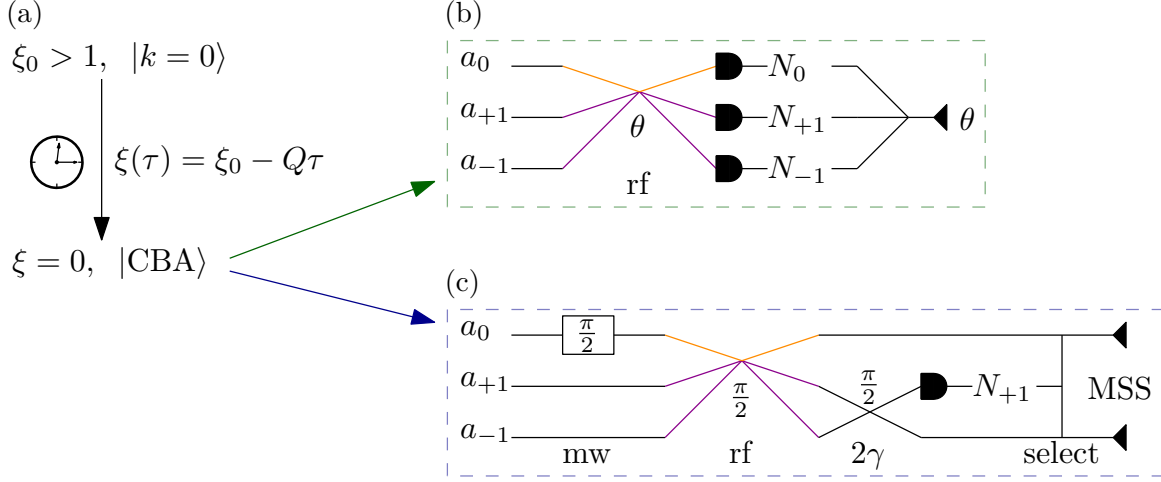


**Figure 4.6:** Proposed applications of the CBA state. (a) Quasiadiabatic preparation of the CBA state. The BEC is initialized in the ground state  $|k=0\rangle \equiv |N_1=0, N_0=N, N_{-1}=0\rangle$  of the P phase at  $\xi_0 > 1$ . A slow passage from  $\xi_0$  to  $\xi = 0$  prepares the ground state at  $\xi = 0$ , which is the CBA state. (b) Quantum-enhanced interferometry. A radio-frequency pulse imprints a phase  $\theta$  on  $|CBA\rangle$ . Measuring  $\hat{N}_{0,\pm 1}$  reveals  $\theta$  with quantum-enhanced precision. (c) Heralded stochastic generation of MSSs. The CBA state is subjected to a microwave pulse imposing the phase shift  $e^{i\frac{\pi}{2}\hat{N}_0}$ , a  $\pi/2$  radio-frequency pulse  $e^{-i\frac{\pi}{2}\hat{S}_x}$ , and a  $\pi/2$  two-photon coupling  $e^{-i\frac{\pi}{2}\hat{J}_y}$ . Then measuring  $\hat{N}_1$  yields  $e^{i\frac{\pi}{2}\hat{N}_0}|\phi_{N_h=N_1}\rangle$  with  $\hat{g}^\dagger$  and  $\hat{h}^\dagger$  replaced by  $\hat{a}_{\mp 1}^\dagger$ , respectively. With up to 90% probability the measurement outcome is  $N_1 \lesssim N/2$  and the state prepared in the  $m=0$  and  $m=-1$  modes thus resembles a NOON state.

where  $\tau \equiv |c|t/\hbar$  and  $Q$  are the dimensionless time and ramping speed, respectively. An ideally adiabatic transition corresponds to  $Q \rightarrow 0$ . This limit cannot be attained at finite times. We call a slow transition at nonvanishing speed quasiadiabatic.

The quasiadiabatic preparation of the CBA state has been proposed in Ref. [32]. Particularly, numerical results confirmed that a large entanglement depth could be attained at a realistic  $Q > 0$ . Reference [35] has proven the experimental feasibility of this approach: the TF ground state at  $\xi < -1$  was successfully prepared by driving the P ground state of a spin-1 BEC across both QPTs at  $\xi = \pm 1$ .

Based on our findings in the preceding Sections, we propose two applications of the quasiadiabatically generated CBA state. First, it can serve as a probe state for quantum-enhanced interferometry, as illustrated in Fig. 4.6b. A phase  $\theta$  imprinted by the operator  $\hat{R}_{\text{opt}}^{(CBA)}$ , see Eq. (4.24), can be revealed with quantum-enhanced precision by measuring the particle numbers  $\hat{N}_0$  and  $\hat{N}_{\pm 1}$  or the magnetization  $\hat{D}$ . Recall that, according to Eq. (3.79),  $\hat{R}_{\text{opt}}^{(CBA)}$  can be realized by a radio-frequency pulse. Furthermore, note that the quantum-enhanced microwave clock presented in Ref. [25] corresponds to a phase imprinting by  $\hat{R}_{\text{opt}}^{(CBA)}$ , yet onto a different probe state.

Alternatively, the CBA state can be used for the heralded stochastic generation of MSSs similar to NOON states. The experimental protocol is detailed in Fig. 4.6c. Starting from the CBA state, a microwave pulse imposes a  $\pi/2$  phase shift  $e^{i\frac{\pi}{2}\hat{N}_0}$  on the  $m=0$  mode, as explained in Section 3.5.1. Next, a  $\pi/2$  radio-frequency pulse with  $\phi=0$ , cf. Section 3.5.2, applies  $e^{-i\frac{\pi}{2}\hat{S}_x}$ . This yields

$$e^{-i\frac{\pi}{2}\hat{S}_x} e^{i\frac{\pi}{2}\hat{N}_0} |CBA\rangle = e^{i\frac{\pi}{2}\hat{N}_0} e^{-i\frac{\pi}{2}\hat{S}_y} |CBA\rangle = e^{i\frac{\pi}{2}\hat{N}_0} |\psi\rangle, \quad (4.61)$$

where  $|\psi\rangle$  denotes the same state as in the previous section. To prepare a two-mode MSS from  $|\psi\rangle$ , we would like to measure  $\hat{N}_h$ . However, usually only the atom numbers  $N_0$  and  $N_{\pm 1}$  are directly accessible. Note that

$$e^{-i\frac{\pi}{2}\hat{J}_y} \hat{g}^\dagger e^{i\frac{\pi}{2}\hat{J}_y} = \hat{a}_{-1}^\dagger, \quad e^{-i\frac{\pi}{2}\hat{J}_y} \hat{h}^\dagger e^{i\frac{\pi}{2}\hat{J}_y} = \hat{a}_1^\dagger. \quad (4.62)$$

Therefore,  $e^{-i\frac{\pi}{2}\hat{J}_y} |\psi\rangle$  is the same as  $|\psi\rangle$  with  $\hat{g}^\dagger$  and  $\hat{h}^\dagger$  replaced by  $\hat{a}_{\mp 1}^\dagger$ , respectively. Hence, measuring  $\hat{N}_1$  with outcome  $N_1$  in the state

$$e^{-i\frac{\pi}{2}\hat{J}_y} e^{-i\frac{\pi}{2}\hat{S}_x} e^{i\frac{\pi}{2}\hat{N}_0} |\text{CBA}\rangle = e^{i\frac{\pi}{2}\hat{N}_0} e^{-i\frac{\pi}{2}\hat{J}_y} |\psi\rangle \quad (4.63)$$

yields  $e^{i\frac{\pi}{2}\hat{N}_0} e^{-i\frac{\pi}{2}\hat{J}_y} |\phi_{N_h=N_1}\rangle$ , which is  $e^{i\frac{\pi}{2}\hat{N}_0} |\phi_{N_h=N_1}\rangle$  with  $\hat{g}^\dagger$  and  $\hat{h}^\dagger$  replaced by  $\hat{a}_{\mp 1}^\dagger$ . In Section 3.5.2 we have briefly discussed how  $\hat{J}_y$  can be implemented by a two-photon coupling. If desired, the phase  $e^{i\frac{\pi}{2}\hat{N}_0}$  can be compensated for by another microwave pulse. As we have seen in the previous section, the observed value of  $N_1$  signals whether the corresponding  $|\phi_{N_h=N_1}\rangle$  is a MSS. The overall probability that the state prepared in the  $m = 0$  and  $m = -1$  modes resembles a NOON state is about 90 %.

T. J. Volkoff from Konkuk University has suggested an alternative to the quasiadiabatic preparation of the CBA state. Starting from the P state, a  $\pi/2$  radio-frequency pulse yields the separable, coherent state

$$|(\alpha_1 = 1/2, \alpha_0 = 1/\sqrt{2}, \alpha_{-1} = 1/2), N\rangle = \frac{1}{\sqrt{2^N N!}} (\hat{a}_0^\dagger + \hat{g}^\dagger)^N |0\rangle. \quad (4.64)$$

Let  $\hat{P}_D$  with  $D = 0$  denote the projection onto the magnetization-free subspace. Then

$$\hat{P}_0 |(1/2, 1/\sqrt{2}, 1/2), N\rangle = \sqrt{\frac{(2N)!}{4^N (N!)^2}} |\text{CBA}\rangle. \quad (4.65)$$

Hence, a measurement of  $\hat{D}$  with outcome  $D = 0$  prepares the CBA state<sup>4</sup>. The probability of the desired measurement outcome is

$$P_0 \equiv \langle (1/2, 1/\sqrt{2}, 1/2), N | \hat{P}_0 |(1/2, 1/\sqrt{2}, 1/2), N\rangle = \frac{(2N)!}{4^N (N!)^2}. \quad (4.66)$$

Unfortunately,  $P_0$  vanishes in the limit  $N \rightarrow \infty$ . It falls below, e. g., 5 % at  $N \approx 125$  atoms.

## 4.7 Experimental Feasibility

Reference [35] reports on the quasiadiabatic preparation of the TF state. The CBA state is, in terms of  $\xi$ , halfway between the P and the TF state. It is thus natural to assume that attaining the CBA state is less demanding. All further experimental techniques required for our proposal in Fig. 4.6 have also been demonstrated [25, 191]. Therefore, theoretically analyzing the experimental feasibility of our proposal might seem redundant. However, the quasiadiabatic passage in Ref. [35] populated, besides the desired ground state of the final Hamiltonian, a significant number of excited states. The experiment was facilitated by the properties of these excited states. Such an advantageous relation between the ground and the low-lying excited states might not apply to the CBA state or the Fisher information (FI). Furthermore, the experimental

<sup>4</sup>Note that  $\hat{D}$  must not be measured via  $\hat{N}_{\pm 1}$ , which would yield a Fock state instead of the CBA state.

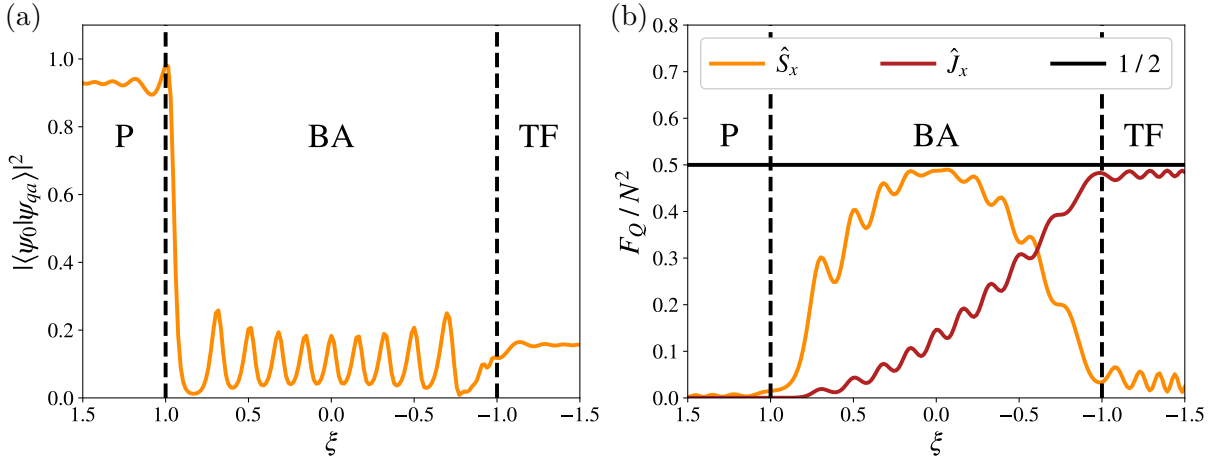


**Figure 4.7:** Quasiadiabatically evolved P state  $|\psi_{\text{qa}}(\xi)\rangle$ . (a) Fidelity with the instantaneous ground state  $|\psi_0(\xi)\rangle$ . (b) QFI  $F_Q$  with respect to the phase-imprinting operator indicated in the legend. The solid horizontal line marks 1/2 of the HL. Both panels are obtained for  $N = 500$  atoms and a linear ramp  $\xi(\tau)$  with speed  $Q = 0.05$ . Dashed vertical lines indicate the QPTs.

imperfections of the operations following on the preparation of the CBA state might prevent quantum-enhanced interferometry or the generation of MSSs.

In the following, we therefore investigate the FI of the CBA and the TF state and the generation of MSSs from the CBA state under realistic experimental conditions. First, we focus on the quasiadiabatic state preparation, discussing the deviation from ideal adiabaticity in Section 4.7.1 and adding atom loss in Section 4.7.2. Imprecise atom counting is considered in Section 4.7.3. For all of these aspects, we pay attention to the question of scalability. According to the analysis below, our proposal is suited for present experiments.

### 4.7.1 Quasiadiabaticity

As we have mentioned in Section 4.6, the adiabatic theorem assumes an infinitely slow sweep of  $\xi$ . Increasing the transition speed reduces the probability to follow the instantaneous ground state. The smaller the energy gap  $\Delta E$  between the ground and the first excited state, the lower is the speed providing a fixed ground-state probability [177, 218]. Recall from Fig. 4.1c that the minimal  $\Delta E$  is observed at the QPTs, where it closes with increasing atom number  $N$  as  $\Delta E/|c| \approx 7.4N^{-1/3}$  [32]. The quasiadiabatic passage starting from the P phase and targeting the CBA or TF state crosses one or both QPTs, respectively. Furthermore, we are particularly interested in large  $N$ . However, the coherence time in experiments with BECs is typically limited to few seconds [35]. This raises two questions: whether there is a quasiadiabatic passage that is fast enough to not exceed the coherence time of the BEC but slow enough to admit a large QFI and the generation of NOON-like MSSs, and whether our proposal is scalable.

We numerically evolve the P state with the Hamiltonian (4.1), where  $\xi$  is considered as an injective function of the dimensionless time  $\tau$ , and  $\xi(0) \equiv \xi_0$ . This defines the state  $|\psi_{\text{qa}}(\xi)\rangle$  with  $|\psi_{\text{qa}}(\xi_0)\rangle = |0, N, 0\rangle$ . First, we consider the linear ramp  $\xi(\tau)$  from Eq. (4.60) with  $\xi_0 = 1.5$ .

Figure 4.7a depicts the fidelity  $|\langle \psi_0(\xi) | \psi_{\text{qa}}(\xi) \rangle|^2$  of  $|\psi_{\text{qa}}\rangle$  with the instantaneous ground state  $|\psi_0\rangle$ , assuming  $N = 500$  atoms and a ramping speed of  $Q = 0.05$ . For comparison, the linear ramp in Ref. [35] corresponds to  $Q = 0.057 \pm 0.002$ . Typical atom numbers range between  $10^2$  and  $10^5$  [9]. The ground-state fidelity nosedives at the first QPT. In accordance with Ref. [35] crossing the second QPT has little further impact. However, Fig. 4.7b demonstrates that the



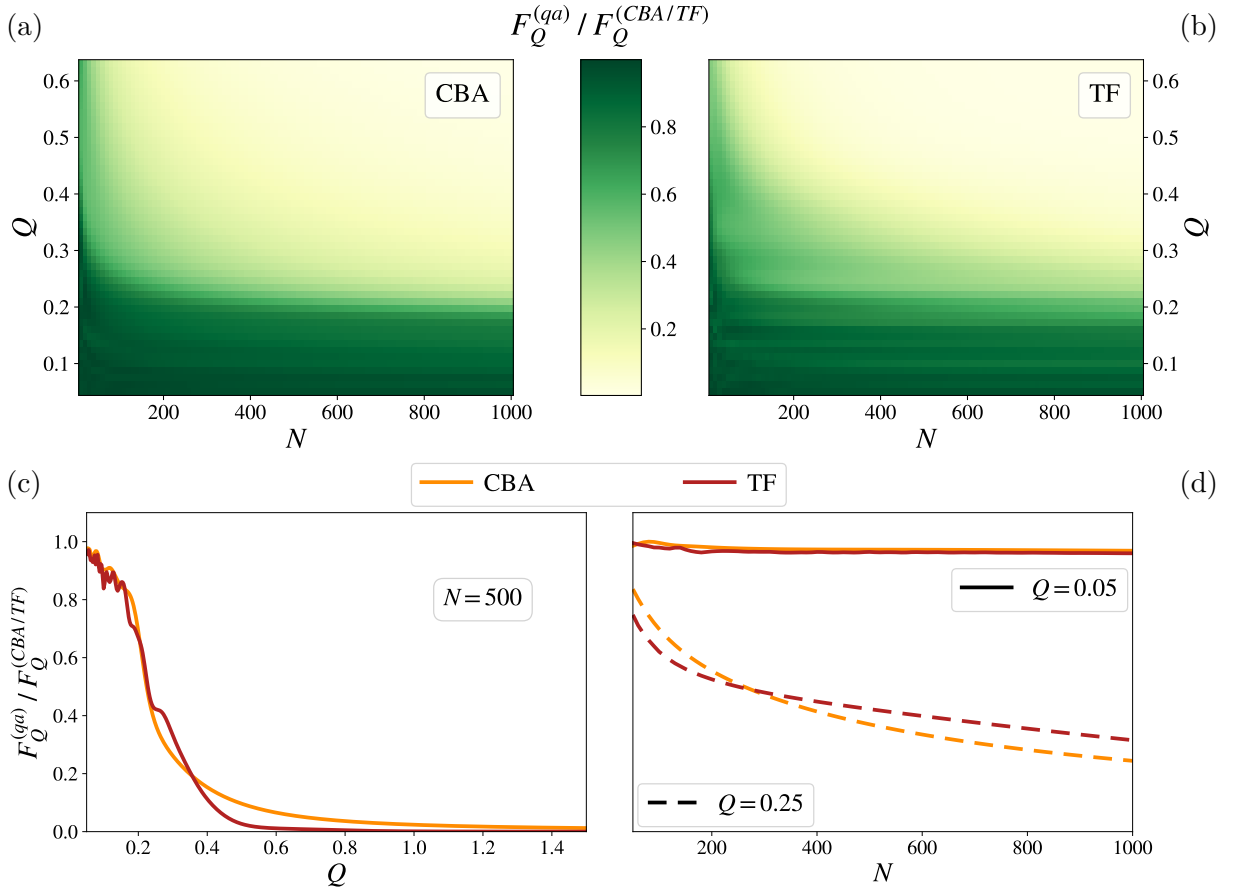


**Figure 4.8:** QFI  $F_Q^{(qa)}$  of the quasiadiabatically prepared state  $|\psi_{qa}(\xi)\rangle$  as a function of atom number  $N$  and ramping speed  $Q$ . CBA:  $|\psi_{qa}(\xi = 0)\rangle$ , phase imprinting by  $\hat{S}_x$ , and  $F_Q^{(qa)}$  is normalized to  $F_Q^{(CBA)}$ . TF:  $|\psi_{qa}(\xi = -1.5)\rangle$ , phase imprinting by  $\hat{J}_x$ , and  $F_Q^{(qa)}$  is normalized to  $F_Q^{(TF)}$ . Panels (c)–(d) show slices through (a)–(b). The fluctuations visible in panels (c)–(d) originate from the oscillations in Fig. 4.7.

QFI of  $|\psi_{qa}(\xi)\rangle$  almost coincides with the QFI of  $|\psi_0(\xi)\rangle$  depicted in Fig. 4.2. This resembles the observation in Ref. [32] that a large entanglement depth can be attained even at a small ground-state fidelity. The oscillations in Fig. 4.7 correspond to oscillations in the experimental data of Ref. [35].

We expect that increasing  $N$  or  $Q$  reduces the fidelity of  $|\psi_{qa}(\xi)\rangle$  with  $|\psi_0(\xi)\rangle$ . Figure 4.8 analyzes how the QFI  $F_Q^{(qa)}$  of  $|\psi_{qa}(\xi)\rangle$  at  $\xi = 0$  and  $\xi = -1.5$  for phase imprinting by  $\hat{S}_x$  and  $\hat{J}_x$ , respectively, depends on  $N$  and  $Q$ . We normalize  $F_Q^{(qa)}$  at  $\xi = 0$  and  $\xi = -1.5$  to  $F_Q^{(CBA)}$  and  $F_Q^{(TF)}$ , respectively. A large relative QFI is found for  $Q \lesssim 0.2$ , see Fig. 4.8a–c. In this region, the dependence of the relative QFI on  $N$  is particularly weak, as can be seen in Fig. 4.8a, b, and d. Similarly, Ref. [32] showed that the ramping time required to maintain another lower bound on the entanglement depth than the QFI grows just moderately with  $N$ . According to Fig. 4.8, quasiadiabatic passages terminated in the BA phase at  $\xi = 0$  or in the TF phase at  $\xi = -1.5$  yield almost the same QFI. Note that  $Q$  determines the duration of the ramp in terms of the dimensionless time  $\tau \equiv |c|t/\hbar$ . The physical ramping time  $T$  is, at a fixed  $Q$ , inversely



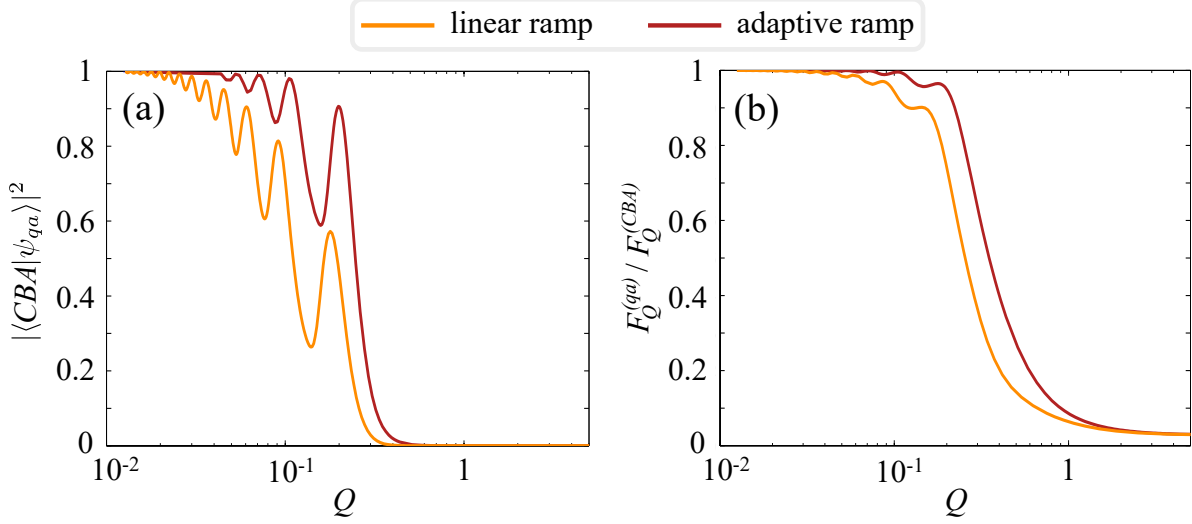


**Figure 4.9:** Adaptive versus linear quasiadiabatic sweep of  $\xi$  from  $\xi_0 = 1.5$  to  $\xi = 0$ , cf. Eqs. (4.60) and (4.67). The duration  $T$  of both ramps is equal and parameterized by the speed  $Q$  of the linear ramp as  $T = \frac{\hbar\xi_0}{|c|Q}$ . (a) Fidelity of the quasiadiabatically prepared state  $|\psi_{qa}(\xi = 0)\rangle$  with the CBA state. (b) Relative QFI  $F_Q^{(qa)} / F_Q^{(CBA)}$  of  $|\psi_{qa}(\xi = 0)\rangle$  subject to phase-imprinting by  $\hat{S}_x$ .

proportional to  $|c|$  and thus, approximately, to the density of the BEC.

We have already mentioned that attaining a given ground-state fidelity at a smaller gap  $\Delta E$  requires a slower sweep of  $\xi$ . Therefore, a quasiadiabatic ramp of a fixed duration can be improved by changing the ramping speed as a function of the instantaneous  $\Delta E$ . We consider the adaptive ramp

$$\xi(\tau) = \xi_0 - \nu \frac{\Delta E}{|c|} \tau, \quad (4.67)$$

where the dimensionless parameter  $\nu$  determines the overall ramping time  $T$ . Figure 4.9 compares, for a quasiadiabatic passage from  $\xi_0 = 1.5$  to  $\xi = 0$  within  $T = \frac{\hbar\xi_0}{|c|Q}$ , the adaptive ramp with the linear ramp in Eq. (4.60). The adaptive ramp clearly outperforms the linear ramp, both in terms of ground-state fidelity and relative QFI.

Figure 4.10 analyzes the generation of MSSs from the state  $|\psi_{qa}(\xi = 0)\rangle$  that is obtained by an adaptive quasiadiabatic passage of length  $T = \frac{\hbar\xi_0}{|c|Q}$  starting at  $\xi_0 = 1.5$ . For an interaction strength of, e. g.,  $|c|/\hbar = 2\pi \times 3$  Hz,  $Q = 0.15$  in Fig. 4.10a–d and  $Q = 0.075$  in Fig. 4.10e–h correspond to the experimentally feasible [35] times  $T \approx 0.5$  s and  $T \approx 1.1$  s, respectively. The most noticeable difference between Fig. 4.4 and Fig. 4.10 is the broadening of the double-peaked conditional probability distributions  $P(N_g|N_h)$  in Fig. 4.10b–c. This slightly reduces the probability to generate a two-mode MSS when measuring  $\hat{N}_h$ .

We conclude that the deviation of a realistic quasiadiabatic passage from ideal adiabaticity only weakly impairs the generation of a large QFI and NOON-like MSSs. Figure 4.8 suggests that this holds also for larger atom numbers than covered by the numerical results in the present section.

Before proceeding, we would like to highlight that the quasiadiabatic state preparation is insensitive to fluctuations of the effective linear Zeeman shift, and thus to the first-order effect of

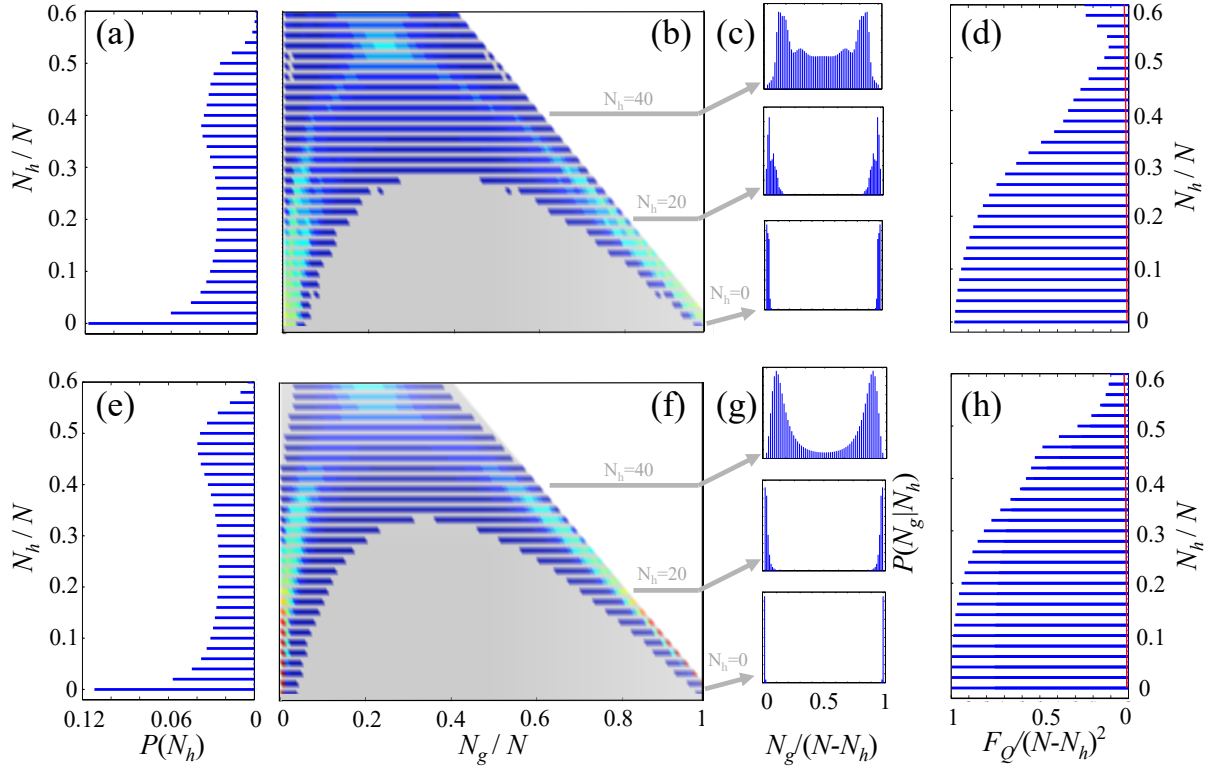


**Figure 4.10:** The same as Fig. 4.4a–d, but with  $|\text{CBA}\rangle$  replaced by the state  $|\psi_{\text{qa}}(\xi = 0)\rangle$  prepared by an adaptive quasiadiabatic passage of length  $T = \frac{\hbar\xi_0}{|c|Q}$  from  $\xi_0 = 1.5$ . (a)–(d):  $Q = 0.15$ , (e)–(h):  $Q = 0.075$ .

magnetic noise. The effective linear Zeeman shift contributes  $-p\hat{D}$  to the Hamiltonian (3.27) in the stationary frame. The quasiadiabatic evolution commutes with  $\hat{D}$ . Therefore, an eigenstate of  $\hat{D}$  with eigenvalue  $D$  evolves within the  $D$ -eigenspace, and  $p$  affects only the irrelevant global phase of the evolved state. This holds, particularly, for the quasiadiabatic evolution under consideration, since  $\hat{D}|\psi_{\text{qa}}(\xi_0)\rangle = 0$ . Note also that because of  $\hat{D}|\psi_{\text{qa}}(\xi)\rangle = 0$  the phase  $\phi$ , cf. Eq. (3.79), of the radio-frequency pulse in Fig. 4.6b is arbitrary.

## 4.7.2 Atom Loss

In Section 4.5, we have shown that the large QFI of the CBA state directly follows from the large QFI of the two-mode MSSs  $|\phi_{N_h \lesssim N/2}\rangle$ . The large QFI of these  $|\phi_{N_h}\rangle$  can, in turn, be explained by their resemblance to NOON states. Let us introduce

$$|\{K_1, K_2\}\rangle \equiv \frac{1}{\sqrt{2}} \left( |N_g = K_1, N_0 = K_2\rangle + |N_g = K_2, N_0 = K_1\rangle \right). \quad (4.68)$$

Then  $|\{N, 0\}\rangle$  is an ideal NOON state. The QFI of  $|\{N, 0\}\rangle$  with respect to  $\hat{S}_z$  saturates the HL  $F_Q = N^2$ , cf. Eq. (2.27). However, losing a single arbitrary atom transforms  $|\{N, 0\}\rangle$  into the

separable state

$$\begin{aligned}\hat{\rho} &= \frac{1}{N} \left( \hat{a}_0 | \{N, 0\} \rangle \langle \{N, 0\} | \hat{a}_0^\dagger + \hat{g} | \{N, 0\} \rangle \langle \{N, 0\} | \hat{g}^\dagger \right) \\ &= \frac{1}{2} \left( |0, N-1\rangle \langle 0, N-1| + |N-1, 0\rangle \langle N-1, 0| \right).\end{aligned}\quad (4.69)$$

Equation (2.26) yields a QFI of zero for  $\hat{\rho}$  subject to phase imprinting by  $\hat{S}_z$ . Hence, the QFI of the  $|\phi_{N_h}\rangle$  and, thus, also of |CBA) might be highly susceptible to atom loss. This raises the question whether the quasiadiabatic preparation of the CBA state can be both slow enough to stay sufficiently close to adiabaticity, see Section 4.7.1, and fast enough to admit a large QFI in the presence of atom loss.

To address this question, we simulate the quasiadiabatic preparation of the CBA state in the presence of atom loss by means of the Monte-Carlo wave-function (MCWF) method introduced in Section 3.6. We consider an optically trapped BEC of  $N = 100$   $^{87}\text{Rb}$  atoms in their ground state with hyperfine spin  $f = 1$  subject to a linear sweep of  $\xi$ , see Eq. (4.60), from  $\xi_0 = 1.5$  to  $\xi = 0$ . Atom loss from a BEC in an optical trap is dominated by one-body and three-body processes [193–195], cf. Section 3.6. We assume an ambitious but realistic one-body loss rate of  $\Gamma_1 = 0.005$  Hz. The three-body loss rate  $\Gamma_3 \equiv G_k \langle n^3 \rangle \equiv \frac{1}{N} G_3 \int d^3r n^3(\mathbf{r})$  depends on the rate constant  $G_3$  and the particle density  $n(\mathbf{r})$  of the BEC. For Bose-condensed  $^{87}\text{Rb}$  atoms in the hyperfine state  $|f = 1, m = -1\rangle$ ,  $G_3 \approx 5.8 \times 10^{-30}$  cm<sup>6</sup>/s [194]. We assume that  $\Gamma_1$  and  $G_3$  do not depend on  $m$ , define  $\Gamma \equiv \Gamma_1 + \Gamma_3$ , and treat it as an effective one-body loss rate. Keeping  $\Gamma$  constant throughout the MCWF evolution, we ignore the dependence of  $\Gamma_3$  on the particle density, which is decreased by atom loss. This is an appropriate approximation as long as only a small part of  $N$  is lost. Overestimating the loss, it never embellishes our results.

Rewriting the Lindblad equation (3.82) in terms of the dimensionless time  $\tau \equiv |c|t/\hbar$  and Hamiltonian  $\hat{H}/|c|$ , we observe that the loss rate enters via the dimensionless parameter  $\gamma \equiv \hbar\Gamma/|c|$ . Within the Thomas-Fermi approximation, Eq. (3.43) yields

$$\frac{1}{N} \int d^3r n^3(\mathbf{r}) = \frac{7}{6} \left( \frac{3M}{4\pi\hbar^2(a_2 - a_0)} \right)^2 c^2, \quad (4.70)$$

where  $M$  is the mass and  $a_{\mathcal{F}}$  are the scattering lengths of the atoms. Hence,  $\Gamma_3 \propto c^2$  and  $\gamma$  can be minimized by choosing  $|c|$  such that  $\Gamma_1 = \Gamma_3$ . For  $^{87}\text{Rb}$  atoms in their hyperfine ground state [29], this leads to an optimal interaction strength of  $c/\hbar \approx -2\pi \times 1$  Hz, which can be readily chosen in current experiments [25, 35]. Therefore, we set  $\Gamma = 0.01$  Hz.

In the presence of atom loss, we evaluate the CFI instead of the QFI, cf. Section 2.1. Recall that the CFI of a state  $\hat{\rho}$  subject to phase imprinting by  $\hat{R}$  depends on the measurement performed on  $\hat{\rho}(\theta) = e^{-i\theta\hat{R}} \hat{\rho} e^{i\theta\hat{R}}$ . Optimizing over all possible measurements yields the QFI. We assume that  $\hat{R} = \hat{S}_x$  and the measurement counts the atom numbers ( $\tilde{N} = N_1 + N_0 + N_{-1}, N_1, N_{-1}$ ), which is optimal for the ideal CBA state, as we have seen in Section 4.3. Considering the CFI has two advantages. First, our results immediately apply to a well-defined experimental situation. Second, in contrast to the QFI, the CFI can be computed without diagonalizing the density matrix  $\hat{\rho}_{\text{mc}}$  that comes out of the MCWF method. Since all MCWFs are eigenstates of  $\hat{N}$ , we can write

$$\hat{\rho}_{\text{mc}} = \frac{1}{r} \sum_{\tilde{N}=0}^N \sum_{k=1}^{r_{\tilde{N}}} |\psi_{\tilde{N},k}\rangle \langle \psi_{\tilde{N},k}| \equiv \frac{1}{r} \sum_{\tilde{N}=0}^N r_{\tilde{N}} \hat{\rho}_{\tilde{N}}, \quad (4.71)$$

where  $|\psi_{\tilde{N},k}\rangle$  are the individual MCWFs,  $\hat{N}|\psi_{\tilde{N},k}\rangle = \tilde{N}|\psi_{\tilde{N},k}\rangle$ ,  $r_{\tilde{N}}$  is the number of MCWFs with  $\tilde{N}$  atoms, and  $r = \sum_{\tilde{N}} r_{\tilde{N}}$  is the overall iteration number of the MCWF algorithm. Let us

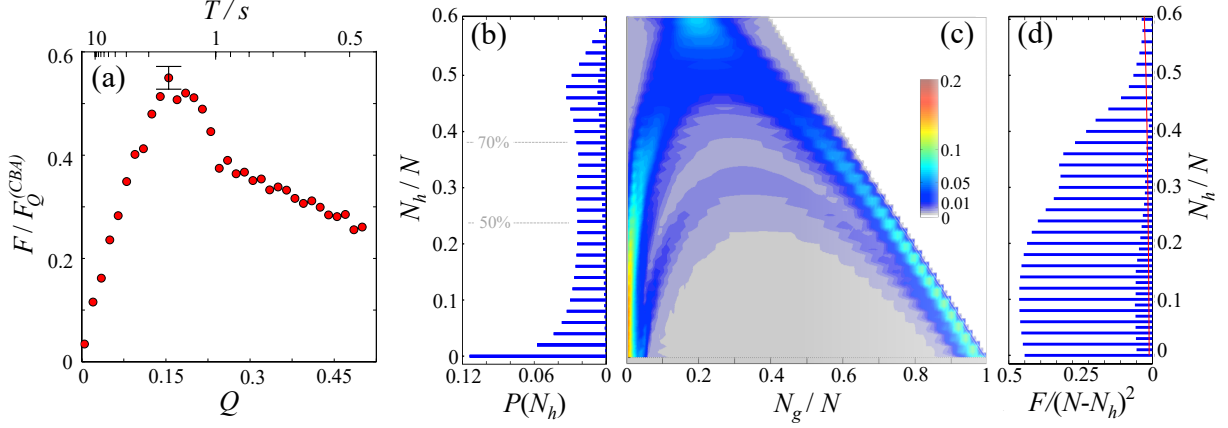


**Figure 4.11:** Quasiadiabatic preparation of the CBA state in the presence of atom loss. The state  $\hat{\rho}_{\text{mc}}$  obtained by a linear sweep from  $\xi_0 = 1.5$  to  $\xi = 0$  with speed  $Q$  is computed by the MCWF method with loss rate  $\Gamma = 0.01$  Hz and  $|c|/\hbar = 2\pi \times 1$  Hz. (a) CFI of  $\hat{\rho}_{\text{mc}}$ , for phase imprinting by  $\hat{S}_x$ , measurement of  $(\hat{N}, \hat{N}_1, \hat{N}_{-1})$ , and optimal imprinted phase  $\theta_{\text{opt}}$ , as a function of  $Q$ . The panels (b)–(d) refer to the optimal point in (a). (b) Probability  $P(N_h) \equiv \sum_{\tilde{N}, N_g} \langle N_g, \tilde{N} - N_g - N_h, N_h | \hat{\rho}_{\text{mc}} | N_g, \tilde{N} - N_g - N_h, N_h \rangle$ . The dashed lines indicate cumulative probabilities. Measuring  $\hat{N}_h$  with outcome  $N_h$  prepares  $\hat{\rho}_{\text{mc}}^{(N_h)}$  from  $\hat{\rho}_{\text{mc}}$ . (c) Conditional probabilities  $P(N_g|N_h) \equiv \sum_{\tilde{N}} \langle N_g, \tilde{N} - N_g - N_h | e^{-i\frac{\pi}{2}\hat{S}_y} \hat{\rho}_{\text{mc}}^{(N_h)} e^{i\frac{\pi}{2}\hat{S}_y} | N_g, \tilde{N} - N_g - N_h \rangle$ . (d) CFI of  $\hat{\rho}_{\text{mc}}^{(N_h)}$  for phase imprinting by  $\hat{S}_x$ , measurement of  $(\hat{N}, \hat{N}_1, \hat{N}_{-1})$ , and imprinted phase  $\theta_{\text{opt}}$ . The red line indicates the SQL. In all panels  $N = 100$ .

introduce the projections

$$\hat{P}_{\tilde{N}, N_1, N_{-1}} \equiv |N_1, \tilde{N} - N_1 - N_{-1}, N_{-1}\rangle \langle N_1, \tilde{N} - N_1 - N_{-1}, N_{-1}| \quad (4.72)$$

and  $\hat{P}_{N_1, N_{-1}} \equiv \sum_{\tilde{N}} \hat{P}_{\tilde{N}, N_1, N_{-1}}$ . Then, according to Eq. (2.24), the CFI is

$$\begin{aligned} F(\theta) &= - \sum_{\tilde{N}=0}^N \sum_{N_1+N_{-1} \leq \tilde{N}} \frac{\text{Tr}^2[\hat{\rho}_{\text{mc}}(\theta)[\hat{S}_x, \hat{P}_{\tilde{N}, N_1, N_{-1}}]]}{\text{Tr}[\hat{\rho}_{\text{mc}}(\theta)\hat{P}_{\tilde{N}, N_1, N_{-1}}]} \\ &= - \frac{1}{r} \sum_{\tilde{N}=0}^N r_{\tilde{N}} \sum_{N_1+N_{-1} \leq \tilde{N}} \frac{\text{Tr}^2[\hat{\rho}_{\tilde{N}}(\theta)[\hat{S}_x, \hat{P}_{N_1, N_{-1}}]]}{\text{Tr}[\hat{\rho}_{\tilde{N}}(\theta)\hat{P}_{N_1, N_{-1}}]} \\ &= - \frac{1}{r} \sum_{\tilde{N}=0}^N \sum_{N_1+N_{-1} \leq \tilde{N}} \frac{\left( \sum_{k=1}^{r_{\tilde{N}}} \langle \psi_{\tilde{N}, k}(\theta) | [\hat{S}_x, \hat{P}_{N_1, N_{-1}}] | \psi_{\tilde{N}, k}(\theta) \rangle \right)^2}{\sum_{k=1}^{r_{\tilde{N}}} \langle \psi_{\tilde{N}, k}(\theta) | \hat{P}_{N_1, N_{-1}} | \psi_{\tilde{N}, k}(\theta) \rangle} \end{aligned} \quad (4.73)$$

with  $\hat{\rho}_{\text{mc}}(\theta) \equiv e^{-i\theta\hat{S}_x} \hat{\rho}_{\text{mc}} e^{i\theta\hat{S}_x}$ ,  $\hat{\rho}_{\tilde{N}}(\theta) \equiv e^{-i\theta\hat{S}_x} \hat{\rho}_{\tilde{N}} e^{i\theta\hat{S}_x}$ , and  $|\psi_{\tilde{N}, k}(\theta)\rangle \equiv e^{-i\theta\hat{S}_x} |\psi_{\tilde{N}, k}\rangle$ . The CFI depends on  $\theta$ . We choose  $\theta_{\text{opt}}$  such that it maximizes the CFI of the entire quasiadiabatically prepared state  $\hat{\rho}_{\text{mc}}$ . Guided by experimental feasibility, we refrain from optimizing the CFI for individual two-mode states generated by measurements of  $\hat{N}_h$ .

Figure 4.11 is obtained with the following parameters of the MCWF algorithm. The sweep from  $\xi_0 = 1.5$  to  $\xi = 0$  is divided into 5000 time steps, and each density matrix is constructed from  $r = 500$  stochastic evolutions of the P state. The number of time steps is sufficiently large

to ensure a small quantum jump probability  $j(t) \leq 0.1$  throughout the evolution. Furthermore, the MCWF evolution with  $\Gamma = 0$  has been checked against the solution of the time-dependent Schrödinger equation obtained by `scipy.integrate.odeint` for Python. The iteration number  $r$  is justified by a sufficiently small statistical error of the CFI. The error bar in Fig. 4.11a is computed from 20 values of the CFI, obtained from  $r = 500$  MCWFs each.

Figure 4.11a displays  $F(\theta_{\text{opt}})$  as a function of the ramping speed  $Q$ . Let us repeat that a small  $Q$  brings us closer to adiabaticity, while a large  $Q$  reduces the number of lost atoms. As a result of this competition, the CFI presents a maximum at  $Q_{\text{opt}} = 0.155$ , where  $F = (0.55 \pm 0.02)F_Q^{(\text{CBA})}$ . For the assumed interaction strength of  $|c|/\hbar = 2\pi \times 1$  Hz,  $Q_{\text{opt}}$  corresponds to a ramping time of  $T \approx 1.54$  s. On average, the quasiadiabatic passage with speed  $Q_{\text{opt}}$  leads to the loss of about 1.5 atoms.

Figures 4.11b–d address the generation of NOON-like MSSs from  $\hat{\rho}_{\text{mc}}$  for  $Q_{\text{opt}}$ . The CFI of the two-mode states obtained by measuring  $\hat{N}_{\text{h}}$ , see Fig. 4.11d, is smaller than without atom loss but remains, for a large range of measurement outcomes  $N_{\text{h}}$ , far above the SQL. This clearly indicates that the two branches in Fig. 4.11c are still in a coherent superposition. Thus, MSSs are heralded by measurement outcomes  $N_{\text{h}} \lesssim 0.4N$ , which occur with an overall probability of about 70 %.

To have a glance at the scalability in the presence of atom loss, we have repeated the analysis in Fig. 4.11a for  $N = 200$  instead of  $N = 100$  atoms. We have found an optimal CFI of  $F \approx 0.42F_Q^{(\text{CBA})}$  at  $Q_{\text{opt}} = 0.165$ . This corresponds to an increase of the CFI with  $N$  that is much faster than linear.

It might be possible to identify bosons that admit a smaller loss parameter  $\gamma$  than  $^{87}\text{Rb}$  atoms in their ground state with hyperfine spin 1. This would increase the CFI, reduce  $Q_{\text{opt}}$ , and improve the scalability, cf. Fig. 4.8. Furthermore, according to Fig. 4.9, the results of the present section could be enhanced by a nonlinear sweep of  $\xi$ .

Altogether, the FI of the CBA state turns out to be much less sensitive to atom loss than could have been expected from the argument at the beginning of the section. This calls for an explanation. The first third of the quasiadiabatic evolution takes place within the P phase. Since the P state is coherent, atom loss does not affect it beyond reducing the total atom number. We thus may introduce an effective loss rate  $\Gamma' = \frac{2}{3}\Gamma$  that accounts only for the evolution within the BA phase. At the end of the quasiadiabatic passage, atom loss from the antisymmetric mode merely shifts the two-mode states generated by measuring  $\hat{N}_{\text{h}}$  to lower heralding particle numbers  $N_{\text{h}}$ . Averaging over the quasiadiabatic evolution within the BA phase gives  $\lim_{N \rightarrow \infty} \frac{1}{N} \int d\xi \langle \psi_0^{(N)}(\xi) | \hat{N}_{\text{h}} | \psi_0^{(N)}(\xi) \rangle = 1/8$  for the occupation of the antisymmetric mode. Therefore, we set  $\Gamma'' = \frac{7}{8}\Gamma'$  and estimate the probability that no “relevant” of the  $N = 100$  atoms has been lost within the ramping time  $T \approx 1.54$  s to be  $e^{-\Gamma''NT} \approx 0.4$ . This coincides very well with the relative CFI of the state heralded by  $N_{\text{h}} = 0$  in Fig. 4.11d.

To understand why the CFI in Fig. 4.11d gets even slightly larger for  $0 < N_{\text{h}} \lesssim 0.2N$ , let us have a closer look at the ideal two-mode states  $|\phi_{N_{\text{h}}}\rangle$ . While  $|\phi_{N_{\text{h}}=0}\rangle$  is indeed an almost perfect NOON state, the MSSs  $|\phi_{0 < N_{\text{h}} \lesssim N/2}\rangle$  resemble rather states of the form  $|\{K_1, K_2\}\rangle$ , see Eq. (4.68), with  $0 < K_2 \ll K_1$  and  $K_1 + K_2 = N - N_{\text{h}}$ . Before atom loss, such states have an almost maximal QFI with respect to  $\hat{S}_z$ :

$$F_Q = 4 \left( \langle \{K_1, K_2\} | \hat{S}_z^2 | \{K_1, K_2\} \rangle - \langle \{K_1, K_2\} | \hat{S}_z | \{K_1, K_2\} \rangle^2 \right) = (K_1 - K_2)^2 \approx (N - N_{\text{h}})^2. \quad (4.74)$$

After the loss of a single arbitrary atom, the state  $|\{K_1, K_2\}\rangle$  becomes

$$\hat{\rho} = \frac{1}{K} \left( \hat{a}_0 |\{K_1, K_2\}\rangle \langle \{K_1, K_2\}| \hat{a}_0^\dagger + \hat{g} |\{K_1, K_2\}\rangle \langle \{K_1, K_2\}| \hat{g}^\dagger \right). \quad (4.75)$$

Equation (2.26) yields

$$F_Q = 4 \frac{K_1 K_2 (K_1 - K_2)^2}{(N - N_h)^2} \approx 4 K_2 (N - N_h) \quad (4.76)$$

for the QFI of  $\hat{\rho}$ , which thus exceeds the SQL for any  $K_2 > 0$ .

Note that the CBA state contains more “relevant” atoms than on average present during the quasiadiabatic passage. Indeed, exposing the ideal CBA state to atom loss for the duration of the optimal ramp leaves us with a CFI of  $F \approx 0.32 F_Q^{(\text{CBA})}$ , which is significantly less than obtained by quasiadiabatic state preparation. However, typical experimental time scales are much shorter [25, 49]. After as long as 0.1 s, the CFI of the CBA state still amounts to  $F \approx 0.93 F_Q^{(\text{CBA})}$ .

### 4.7.3 Atom-Counting Uncertainty

In Section 4.3 we have demonstrated that measuring  $(\hat{N}_1, \hat{N}_{-1})$  or  $\hat{D} \equiv \hat{N}_1 - \hat{N}_{-1}$  gives access to the ultimate sensitivity of the states  $|\text{CBA}\rangle$  and  $|\text{TF}\rangle$ . Thus, an obvious way to realize the optimal measurement is to count the number of atoms in the modes  $m = \pm 1$ . Besides this, counting the atoms in the antisymmetric mode (mapped to the  $m = 1$  mode, see Fig. 4.6) is central to the proposed generation of MSSs. However, counting Bose-condensed atoms with single-particle resolution is very challenging [227]. Therefore, we study the CFI of  $|\text{CBA}\rangle$  and  $|\text{TF}\rangle$  and the generation of MSSs from  $|\text{CBA}\rangle$  in the case of finite atom-counting precision. Note that, in this section, we disregard quasiadiabaticity and atom loss.

First, we consider the CFI of

$$|\psi(\theta)\rangle \in \left\{ e^{-i\theta \hat{S}_x} |\text{CBA}\rangle, e^{-i\theta \hat{J}_x} |\text{TF}\rangle \right\} \quad (4.77)$$

with respect to the observable  $\hat{D}$ . For an ideal measurement, the CFI (2.4) is completely determined by the probability distribution

$$P_\theta(D) = \langle \psi(\theta) | \hat{P}_D | \psi(\theta) \rangle, \quad (4.78)$$

where  $\hat{P}_D$ , as usual, denotes the projection onto the Fock states  $|N_1, N - N_1 - N_{-1}, N_{-1}\rangle$  with  $N_1 - N_{-1} = D$ . We assume that the magnetization  $D$  is experimentally determined by measuring  $\hat{N}_{\pm 1}$ . To incorporate the uncertainty of atom counting, we introduce the probability  $P(n_{\pm 1} | N_{\pm 1})$  of mistaking an atom number  $N_{\pm 1}$  for  $n_{\pm 1}$ . We model  $P(n_{\pm 1} | N_{\pm 1})$  as a Gaussian distribution with mean  $N_{\pm 1}$  and variance  $\sigma^2$ :

$$P(n_{\pm 1} | N_{\pm 1}) = g_\sigma(n_{\pm 1} - N_{\pm 1}), \quad g_\sigma(x) = A e^{-\frac{x^2}{2\sigma^2}}. \quad (4.79)$$

The constant  $A$  is fixed by the normalization condition<sup>5</sup>

$$\sum_{x=-\infty}^{\infty} g_\sigma(x) = 1. \quad (4.80)$$

Thus, the probability to observe a magnetization of  $d$  when measuring  $\hat{D}$  in the state  $|\psi(\theta)\rangle$  becomes

$$P_\theta(d) = \sum_{D=-N}^N P(d|D) P_\theta(D), \quad P(d|D) = g_{\sqrt{2}\sigma}(d - D). \quad (4.81)$$

<sup>5</sup>For our numerical results, we approximate  $A$  by  $A(N_{\pm 1})$  satisfying  $\sum_{n_{\pm 1}=-5\lceil\sigma\rceil}^{N+5\lceil\sigma\rceil} P(n_{\pm 1} | N_{\pm 1}) = 1$ .

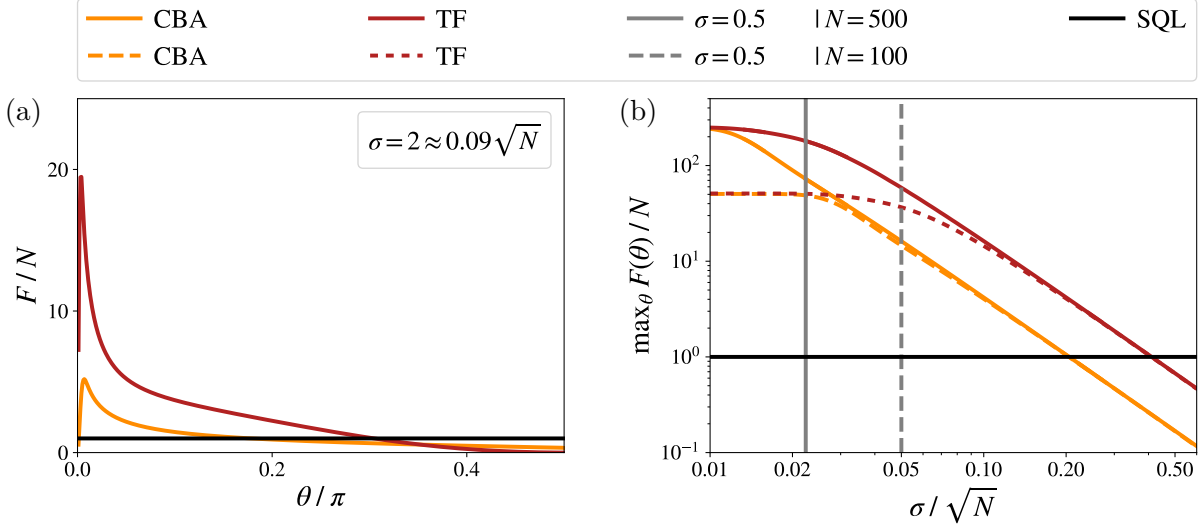


**Figure 4.12:** CFI of  $|CBA\rangle$  and  $|TF\rangle$  for Gaussian atom-counting uncertainty with variance  $\sigma^2$ . Solid lines correspond to  $N = 500$ , dashed lines to  $N = 100$ . (a) Typical behavior of the CFI  $F(\theta)$ , which exhibits a peak reaching far above the SQL. (b) Peak value of  $F/N$  as a function of  $\sigma/\sqrt{N}$ . Gray vertical lines indicate single-particle resolution.

To compute the CFI with atom-counting uncertainty, we replace  $P_{\theta}(D)$  in Eq. (2.4) by  $P_{\theta}(d)$ .

The typical behavior of the CFI evaluated by imprecise atom-counting is depicted, both for the CBA and TF state, in Fig. 4.12a. Recall that an ideal measurement would yield a CFI of  $F_Q^{(CBA/TF)} \approx N^2/2$  at any  $\theta$ . We observe that the atom-counting uncertainty strongly damps the CFI. However,  $F(\theta)$  exhibits a peak that remains far above the SQL. Figure 4.12b analyses how the peak value  $F_{\max} \equiv \max_{\theta} F(\theta)$  depends on the width  $\sigma$  of the Gaussian measurement uncertainty. Beyond single-particle resolution, i. e., for  $\sigma \gtrsim 0.5$ , an increasing  $\sigma$  reduces  $F_{\max}$  according to

$$\frac{F_{\max}}{N} \approx \frac{N}{\sigma^2} F_0 \quad (4.82)$$

with  $F_0 \approx 0.042$  for the CBA state and  $F_0 \approx 0.168$  for the TF state. As we see from Fig. 4.12b, this result seems to be independent of  $N$ . The TF state is thus less sensitive to atom-counting uncertainty than the CBA state. However, the CBA state requires only a two times smaller value of  $\sigma/\sqrt{N}$  to surpass the SQL. Ref. [113] has experimentally demonstrated a peak interferometric sensitivity above the SQL for the TF state of Bose-condensed  $^{87}\text{Rb}$  atoms. Note that, by Eq. (4.82), a CFI that scales with  $N$  better than linearly requires that  $\sigma/\sqrt{N}$  decreases with  $N$ .

When investigating, in Section 4.5, the generation of MSSs from  $|\psi\rangle \equiv e^{-i\frac{\pi}{2}\hat{S}_y} |CBA\rangle$ , we payed particular attention to the probability distributions

$$P(N_h) \equiv \sum_{N_g} P(N_g, N_h), \quad P(N_g|N_h) \equiv \frac{1}{P(N_h)} P(N_g, N_h) \quad (4.83)$$

derived from

$$P(N_g, N_h) \equiv |\langle N_g, N_0, N_h | \psi \rangle|^2, \quad (4.84)$$

see Fig. 4.4a–c. Now we assume that the measurement of  $\hat{N}_h$ , which prepares the two-mode



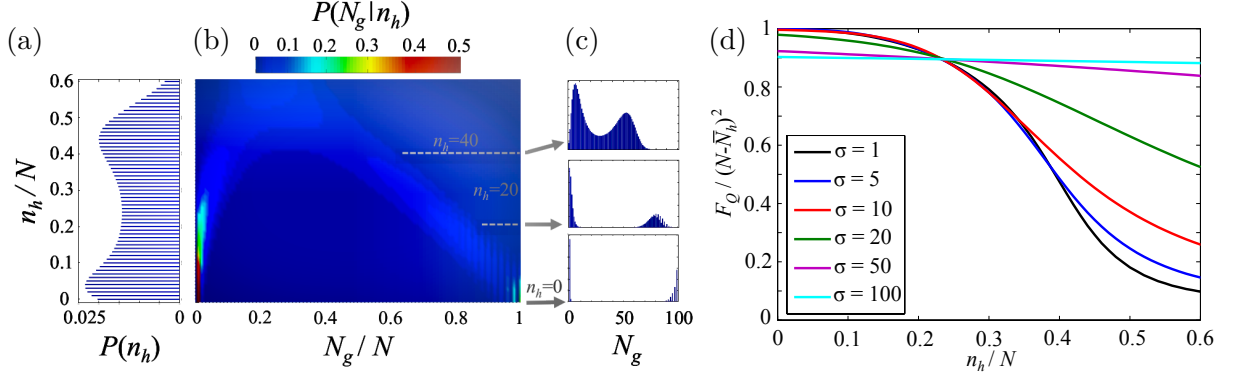


**Figure 4.13:** Generating MSSs from  $|\psi\rangle \equiv e^{-i\frac{\pi}{2}\hat{S}_y} |\text{CBA}\rangle$  by measuring  $\hat{N}_h$  with atom-counting uncertainty  $\sigma$ . (a) Probability  $P(n_h)$  to read off  $n_h$  and generate  $\hat{\rho}_{n_h}$ . (b)–(c) Conditional probabilities  $P(N_g|n_h) = \sum_{\tilde{N}=0}^N \langle N_g, \tilde{N} - N_g | \hat{\rho}_{n_h} | N_g, \tilde{N} - N_g \rangle$ . (d) Relative QFI  $F_Q/(N - \bar{N}_h)^2$  of  $\hat{\rho}_{n_h}$  with  $\bar{N}_h \equiv \sum_{N_h} P(N_h|n_h)N_h$  for various  $\sigma$ . For  $\sigma \rightarrow \infty$ , the relative QFI tends to  $8/9$ .

MSSs, is subject to atom-counting errors described by<sup>6</sup>

$$P(n_h|N_h) = g_\sigma(n_h - N_h). \quad (4.85)$$

The probability distributions of interest thus become

$$\begin{aligned} P(N_g, n_h) &= \sum_{N_h} P(n_h|N_h)P(N_g, N_h), \\ P(n_h) &= \sum_{N_g} P(N_g, n_h) = \sum_{N_h} P(n_h|N_h)P(N_h), \\ P(N_g|n_h) &= \frac{1}{P(n_h)}P(N_g, n_h) = \sum_{N_h} P(N_h|n_h)P(N_g|N_h). \end{aligned} \quad (4.86)$$

In the last line, we have used Bayes' theorem

$$P(N_h|n_h) = \frac{P(n_h|N_h)P(N_h)}{P(n_h)}, \quad (4.87)$$

where  $P(N_h|n_h)$  is the probability that a measurement with readout  $n_h$  prepares  $N_h$  atoms in the antisymmetric mode. The probability distributions  $P(n_h)$  and  $P(N_g|n_h)$  are depicted in Fig. 4.13a–c.  $P(N_h)$  and  $P(N_g|N_h)$  get visibly blurred by the convolution with  $P(n_h|N_h)$  and  $P(N_h|n_h)$ , respectively. The right peak of  $P(N_g|N_h)$  gets particularly broadened since its position strongly depends on  $N_h$ . The asymmetry of  $P(N_g|n_h)$  is the most noticeable effect of the measurement uncertainty on the probability distributions.

An imperfect measurement of  $\hat{N}_h$  in  $|\psi\rangle$  with readout  $n_h$  prepares the two-mode state

$$\hat{\rho}_{n_h} \equiv \sum_{N_h} P(N_h|n_h) |\phi_{N_h}\rangle \langle \phi_{N_h}| \quad (4.88)$$

with  $|\phi_{N_h}\rangle$  defined in Eq. (4.50). We are interested in the QFI of  $\hat{\rho}_{n_h}$  for phase imprinting by  $\hat{S}_z$ . Recall that  $|\phi_{N_h}\rangle$  consists of  $N - N_h$  atoms. Therefore,  $\langle \phi_{N_h} | \phi_{N'_h} \rangle = \langle \phi_{N_h} | \hat{S}_z | \phi_{N'_h} \rangle = 0$  for

<sup>6</sup>In the context of MSSs, we use the normalization condition  $\sum_{n_h=0}^N P(n_h|N_h) = 1$ . This corresponds to the situation when the experimentalist knows  $N$  and discards all  $n_h < 0$  and  $n_h > N$ .



$N_h \neq N'_h$ , and the QFI (2.26) of  $\hat{\rho}_{n_h}$  can be expressed in terms of the QFI of the  $|\phi_{N_h}\rangle$  as

$$F_Q^{(n_h)} = \sum_{N_h} P(N_h|n_h) F_Q^{(N_h)} = 4 \sum_{N_h} P(N_h|n_h) \langle \phi_{N_h} | \hat{S}_z^2 | \phi_{N_h} \rangle. \quad (4.89)$$

Thus, also the QFI is simply smeared over close values of  $N_h$ . Figure 4.13d displays the relative QFI  $F_Q^{(n_h)}/(N - \bar{N}_h)^2$  with  $\bar{N}_h \equiv \sum_{N_h} P(N_h|n_h) N_h$  as a function of  $n_h$ . The largest values of the relative QFI get, of course, decreased by atom-counting uncertainty. However, this effect is rather small, as becomes particularly obvious from the worst case limit. For  $N \gg 1$ ,  $\sigma \rightarrow \infty$  leads to

$$\frac{P(n_h|N_h)}{P(n_h)} = 1 \Rightarrow F_Q^{(n_h)} = \sum_{N_h} P(N_h) F_Q^{(N_h)} = F_Q^{(\text{CBA})}, \quad (4.90)$$

cf. Eq. (4.56). Since  $\bar{N}_h$  becomes  $\sum_{N_h} P(N_h) N_h \approx N/4$ , we end up with the  $n_h$ -independent

$$\frac{F_Q^{(n_h)}}{(N - \bar{N}_h)^2} \approx \frac{8}{9} \quad \text{for } N \gg 1, \sigma \rightarrow \infty. \quad (4.91)$$

A measurement with  $\sigma \rightarrow \infty$  means that the antisymmetric mode is simply disregarded, i. e., traced out. The large limiting value of  $F_Q^{(n_h)}/(N - \bar{N}_h)^2$  is a consequence of the high cumulative probability to generate  $|\phi_{N_h}\rangle$  with a large QFI.

In summary, the CFI of the states |CBA) and |TF) exceeds the SQL for ambitious but feasible atom-counting uncertainty. The preparation of two-mode MSSs suffers only weakly from an imprecise generating measurement of  $\hat{N}_h$ .

## 4.8 Quenching

Preparing the P ground state and then instantaneously quenching  $\xi$  into the BA phase exposes the P state to entangling spin-changing collisions [151–153]. Since this is a popular method for the generation of entanglement in spinor BECs [9, 30], we compare the QFI of the (quasiadiabatically prepared) CBA and TF state to the QFI attainable by quenching.

Recall that the P state is  $|N_1 = 0, N_0 = N, N_{-1} = 0\rangle$ . After the quench, spin-changing collisions start to populate the spin modes  $m = \pm 1$ . Because of technical limitations—particularly, phase noise [159]—the evolution is typically terminated before  $N_0 \gg 1$  gets notably depleted [25, 228, 229]. Thus  $N_0 \approx N \gg 1$ , and  $\hat{a}_0^{(\dagger)}$  can be approximately replaced by  $\sqrt{N}$ . Then the spin Hamiltonian (4.1) in the subspace with magnetization  $D = 0$  becomes

$$\frac{\hat{H}}{|c|} \approx 2\xi(\hat{N}_1 + \hat{N}_{-1}) - \left[ \hat{a}_1 \hat{a}_{-1} + \hat{a}_1^\dagger \hat{a}_{-1}^\dagger + \hat{N}_1 + \hat{N}_{-1} + \frac{1}{2} \right] = \frac{1}{|c|} (\hat{H}_g + \hat{H}_h) - 2\xi + \frac{1}{2} \quad (4.92)$$

with

$$\begin{aligned} \frac{\hat{H}_g}{|c|} &\equiv (2\xi - 1) \left( \hat{N}_g + \frac{1}{2} \right) - \frac{1}{2} (\hat{g}^{\dagger 2} + \hat{g}^2), \\ \frac{\hat{H}_h}{|c|} &\equiv (2\xi - 1) \left( \hat{N}_h + \frac{1}{2} \right) + \frac{1}{2} (\hat{h}^{\dagger 2} + \hat{h}^2), \end{aligned} \quad (4.93)$$

where we have used Eqs. (4.47) and (4.48). Let us introduce the generators of  $\mathfrak{su}(1, 1)$  [230]

$$\hat{G}_0^{(a)} = \frac{1}{4} (2\hat{a}^\dagger \hat{a} + 1), \quad \hat{G}_+^{(a)} = \frac{1}{2} \hat{a}^{\dagger 2}, \quad \hat{G}_-^{(a)} = \frac{1}{2} \hat{a}^2 \quad (4.94)$$

constructed from some bosonic creation and annihilation operator  $\hat{a}^{(\dagger)}$ . Then

$$\frac{\hat{H}_{g/h}}{|c|} = 2(2\xi - 1)\hat{G}_0^{(g/h)} \mp (\hat{G}_+^{(g/h)} + \hat{G}_-^{(g/h)}). \quad (4.95)$$

Within the low-depletion approximation, the initial P state is described by the vacuum state  $|\psi(0)\rangle = |N_g = 0\rangle \otimes |N_h = 0\rangle$ . Since  $[\hat{H}_g, \hat{H}_h] = 0$ , evolving  $|\psi(0)\rangle$  for a time  $\tau = |c|t/\hbar$  after the quench of  $\xi$  produces a state  $|\psi(\tau)\rangle = |\psi_g(\tau)\rangle \otimes |\psi_h(\tau)\rangle$  with  $|\psi_{g/h}\rangle \equiv e^{-i\tau\hat{H}_{g/h}/|c|} |N_{g/h} = 0\rangle$ . To derive the Fock basis coefficients of  $|\psi_{g/h}(\tau)\rangle$ , we make use of the BCH relation [230]

$$e^{(2ir\hat{G}_0 + z\hat{G}_+ - z^*\hat{G}_-)\tau} = e^{p_+\hat{G}_+} e^{p_0\hat{G}_0} e^{p_-\hat{G}_-} \quad \text{for } \tau, r \in \mathbb{R}, z \in \mathbb{C}, \quad (4.96)$$

where

$$\begin{aligned} p_+ &= \frac{z\tau_0}{C} \sinh(\tau/\tau_0), \quad p_0 = -2 \ln C, \quad p_- = -\frac{z^*\tau_0}{C} \sinh(\tau/\tau_0), \\ C &= \cosh(\tau/\tau_0) - ir\tau_0 \sinh(\tau/\tau_0), \quad \tau_0 = \frac{1}{\sqrt{|z|^2 - r^2}}. \end{aligned} \quad (4.97)$$

The coefficients  $p_{0,\pm}$  for  $|z|^2 = r^2$  can be obtained by taking the corresponding limit. Equation (4.96) yields

$$|\psi_{g/h}\rangle \equiv e^{-i\tau\hat{H}_{g/h}/|c|} |N_{g/h} = 0\rangle = \frac{1}{\sqrt{C}} \sum_{k=0}^{\infty} \epsilon_{g/h}^k \sqrt{\binom{2k}{k} \left(\frac{p_+}{2}\right)^k} |N_{g/h} = 2k\rangle \quad (4.98)$$

with  $z = i$ ,  $r = 1 - 2\xi$ ,  $\epsilon_g = 1$ , and  $\epsilon_h = -1$ .

Knowing  $|\psi(\tau)\rangle$ , we want to compute its QFI for optimal collective unitary phase imprinting. In the low-depletion limit, a phase-imprinting operator  $\hat{R}$  has to act on the  $m = 0$  mode in order to provide a large QFI. Therefore, we consider

$$\hat{R} = \sum_k u_k \hat{R}_k, \quad \hat{R}_k \in \{\hat{S}_x, \hat{S}_y, \hat{S}_z, \hat{A}_x, \hat{A}_y, \hat{A}_z\}, \quad u_k \in \mathbb{R}, \quad \sum_k u_k^2 = 1, \quad (4.99)$$

cf. Eqs. (3.47) and (3.50). According to Section 2.1.6, the optimal QFI is four times the largest eigenvalue of the covariance matrix  $\Gamma$  with elements

$$\Gamma_{kl} = \frac{1}{2} \langle \psi(\tau) | \hat{R}_k \hat{R}_l + \hat{R}_l \hat{R}_k | \psi(\tau) \rangle - \langle \psi(\tau) | \hat{R}_k | \psi(\tau) \rangle \langle \psi(\tau) | \hat{R}_l | \psi(\tau) \rangle. \quad (4.100)$$

The low depletion approximation of the  $\hat{R}_k$  is

$$\begin{aligned} \hat{S}_x &\approx \frac{\sqrt{N}}{2} (\hat{g} + \hat{g}^\dagger), \quad \hat{S}_y \approx \frac{\sqrt{N}}{2i} (\hat{g} - \hat{g}^\dagger), \quad \hat{S}_z \approx \frac{1}{2} (N - \hat{N}_g), \\ \hat{A}_x &\approx \frac{\sqrt{N}}{2} (\hat{h} + \hat{h}^\dagger), \quad \hat{A}_y \approx \frac{\sqrt{N}}{2i} (\hat{h} - \hat{h}^\dagger), \quad \hat{A}_z \approx \frac{1}{2} (N - \hat{N}_h). \end{aligned} \quad (4.101)$$

Hence,

$$\begin{aligned} &\frac{1}{2} \langle \psi(\tau) | \hat{S}_k \hat{A}_l + \hat{A}_l \hat{S}_k | \psi(\tau) \rangle - \langle \psi(\tau) | \hat{S}_k | \psi(\tau) \rangle \langle \psi(\tau) | \hat{A}_l | \psi(\tau) \rangle \\ &\approx \langle \psi_g(\tau) | \hat{S}_k | \psi_g(\tau) \rangle \langle \psi_h(\tau) | \hat{A}_l | \psi_h(\tau) \rangle - \langle \psi_g(\tau) | \hat{S}_k | \psi_g(\tau) \rangle \langle \psi_h(\tau) | \hat{A}_l | \psi_h(\tau) \rangle = 0 \end{aligned} \quad (4.102)$$

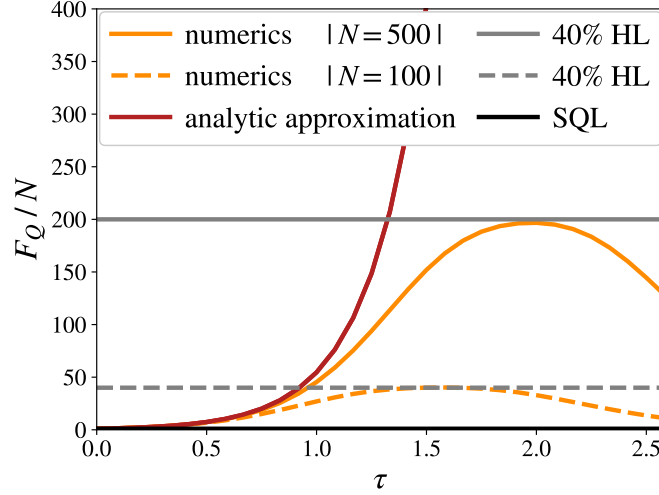


**Figure 4.14:** QFI of the P state evolving at  $\xi_r = 1/2$  for time  $\tau$ . The QFI is optimized over phase imprinting by  $\hat{\mathbf{S}}$  (numeric) or  $\hat{\mathbf{S}}$  and  $\hat{\mathbf{A}}$  (analytic). Experiments usually explore the low-depletion (small  $\tau$ ) regime, which is well described by the analytic approximation. The low-depletion QFI scales linearly with  $N$ . Beyond the low-depletion regime, the QFI reaches roughly 40% of the HL.

and  $\Gamma$  decomposes into two diagonal blocks,  $\Gamma = \Gamma^{(g)} \oplus \Gamma^{(h)}$ , for  $\hat{\mathbf{S}}$  with  $|\psi_g\rangle$  and  $\hat{\mathbf{A}}$  with  $|\psi_h\rangle$ , respectively.

Let us first focus on  $\Gamma^{(g)}$ . It further decomposes into the variance of  $\hat{S}_z$ ,

$$\lambda_z^{(g)} = \frac{1}{4} \Delta^2 \hat{N}_g = \frac{1}{4} \left( \langle \psi_g(\tau) | \hat{N}_g^2 | \psi_g(\tau) \rangle - \langle \hat{N}_g \rangle^2 \right), \quad \langle \hat{N}_g \rangle \equiv \langle \psi_g(\tau) | \hat{N}_g | \psi_g(\tau) \rangle, \quad (4.103)$$

and the covariance matrix of  $\hat{S}_x$  and  $\hat{S}_y$  with eigenvalues

$$\lambda_{\pm}^{(g)} = \frac{N}{4} \left( 1 + 2\langle \hat{N}_g \rangle \pm \sqrt{2} \Delta \hat{N}_g \right). \quad (4.104)$$

Since low depletion implies  $\Delta \hat{N}_g \ll N$ , the maximal QFI for phase imprinting by  $\hat{\mathbf{S}}$  amounts to

$$F_Q = 4\lambda_+^{(g)} = N \left( 1 + 2\langle \hat{N}_g \rangle + \sqrt{2} \Delta \hat{N}_g \right). \quad (4.105)$$

The corresponding optimal phase-imprinting operator is  $\hat{R}^{(g)} \equiv u_x^{(g)} \hat{S}_x + u_y^{(g)} \hat{S}_y + u_z^{(g)} \hat{S}_z$  with

$$\mathbf{u}^{(g)} \equiv \frac{1}{\sqrt{2}} \left( \sqrt{1 + \sqrt{2}(1 - 2\xi)^2 \frac{\langle \hat{N}_g \rangle}{\Delta \hat{N}_g}}, -\sqrt{1 - \sqrt{2}(1 - 2\xi)^2 \frac{\langle \hat{N}_g \rangle}{\Delta \hat{N}_g}}, 0 \right). \quad (4.106)$$

To evaluate  $\langle \hat{N}_g \rangle$  and  $\Delta^2 \hat{N}_g$ , we employ the generating function

$$f(x) \equiv \sum_{k=0}^{\infty} \binom{2k}{k} \left( \frac{|p_+|}{2} \right)^{2k} e^{kx} = \frac{1}{\sqrt{1 - |p_+|^2 e^x}} \quad \forall x \in \mathbb{R}, |p_+|^2 e^x < 1, \quad (4.107)$$

in terms of which

$$\langle \hat{N}_g \rangle = \frac{2}{|C|} \partial_x f(x)|_{x=0}, \quad \Delta^2 \hat{N}_g = \frac{4}{|C|} \partial_x^2 f(x)|_{x=0} - \langle \hat{N}_g \rangle^2. \quad (4.108)$$

Squeezed states of spinor BECs are generated by quenching  $\xi$  to a positive value in the BA phase,  $0 < \xi < 1$ . This range of  $\xi$  is equivalent to  $\tau_0 \in \mathbb{R}$ , which is called the non-oscillatory regime. Equation (4.108) then yields

$$\langle \hat{N}_g \rangle = \tau_0^2 \sinh^2(\tau/\tau_0), \quad \Delta^2 \hat{N}_g = 2 \langle \hat{N}_g \rangle (\langle \hat{N}_g \rangle + 1), \quad (4.109)$$

and the maximal QFI becomes

$$F_Q = N \left[ 1 + 2 \left( \langle \hat{N}_g \rangle + \sqrt{\langle \hat{N}_g \rangle (\langle \hat{N}_g \rangle + 1)} \right) \right]. \quad (4.110)$$

$F_Q$  depends via  $\tau_0$  on the value of  $\xi$  targeted by the quench. The largest QFI is obtained when, after the quench,  $\hat{G}_0^{(g)}$  does not contribute to  $\hat{H}_g$ , which defines the resonance condition  $\xi_r = 1/2$  with  $\tau_0 = 1$ . At resonance,  $|\psi_g(\tau)\rangle$  becomes a squeezed vacuum state [177] with the squeezing amplitude  $\zeta = \tau e^{-i\pi/2}$ .

The results for  $\Gamma^{(g)}$  can be easily transferred to  $\Gamma^{(h)}$ . We observe that the replacement

$$\hat{g}^\dagger \leftrightarrow i\hat{h}^\dagger, \quad \hat{g} \leftrightarrow -i\hat{h} \quad (4.111)$$

leaves  $|\psi(0)\rangle$  and  $\hat{H}$  invariant, while transforming  $\hat{S}_x$ ,  $\hat{S}_y$ , and  $\hat{S}_z$  into  $\hat{A}_y$ ,  $-\hat{A}_x$ , and  $\hat{A}_z$ , respectively. Hence, the eigenvalues of  $\Gamma^{(g)}$  and  $\Gamma^{(h)}$  coincide, and the QFI in Eq. (4.110) gives the maximum over all phase-imprinting operators from Eq. (4.99). Besides  $\hat{R}^{(g)}$ , also  $\hat{R}^{(h)} \equiv u_x^{(h)} \hat{A}_x + u_y^{(h)} \hat{A}_y + u_z^{(h)} \hat{A}_z$  with  $\mathbf{u}^{(h)} \equiv (-u_y^{(g)}, u_x^{(g)}, 0)$  provides optimal phase imprinting.

The QFI in Eq. (4.110) scales only linearly with  $N$ , see also Fig. 4.14. By contrast, the QFI of the ideal CBA and TF state exhibits Heisenberg scaling. Even for a quasiadiabatic preparation in the presence of atom loss, we have found that the QFI of the CBA state scales much better than linearly. The interaction strengths, evolution times, and atom numbers in Refs. [25, 159, 228, 229] correspond to a QFI with  $5 \lesssim F_Q/N \lesssim 700$  and  $0.02\% \lesssim F_Q/N^2 \lesssim 3\%$ . According to Section 4.7.2, we expect that  $N = 200$  atoms can be, despite atom loss, quasiadiabatically transferred into a state with  $F_Q/N \approx 40$  and  $F_Q/N^2 > 20\%$ . In general, we assume that a quasiadiabatic passage is favorable, as compared to quenching, when aiming at a large QFI with respect to the HL.

The evolution time after quenching may be limited by the effect of phase noise [159] on a squeezing parameter. By contrast, we are interested in the QFI instead of a squeezing parameter and have not included phase noise in our simulations of quasiadiabatic state preparation. Therefore, limiting our comparison to the low-depletion approximation may seem inappropriate. To investigate a quench to  $\xi_r$  beyond the low-depletion limit, we numerically evolve the P state and optimize its QFI over phase-imprinting operators  $\hat{R} = u_x \hat{S}_x + u_y \hat{S}_y + u_z \hat{S}_z$ <sup>7</sup>. Figure 4.14 shows that the QFI attains a (local) maximum with  $F_Q \approx 0.4N^2$  but does not reach  $F_Q^{(\text{CBA/TF})} \approx N^2/2$ .

## 4.9 Conclusion

A ferromagnetic spin-1 BEC can be quasiadiabatically driven across a QPT from a P state into the CBA state. We propose two applications of the CBA state. First, it can serve as the probe state for quantum-enhanced interferometry. Second, it can be used for the heralded stochastic generation of MSSs similar to NOON states. Both applications tolerate a reasonably swift quasiadiabatic passage in the presence of atom loss and uncertainties of atom counting.

<sup>7</sup>Our choice of  $\hat{R}$  is motivated by the low-depletion analysis. Other phase-imprinting operators from the Schwinger representation of  $\mathfrak{su}(3)$  might, in principle, yield a larger QFI. Combining our general discussion in Section 4.2 with findings from Ref. [220] reveals that the QFI for phase imprinting by  $\hat{R} = u_x \hat{J}_x + u_y \hat{J}_y + u_z \hat{J}_z$  is smaller.

In parallel to our theoretical study, the quantum-enhanced interferometric sensitivity of the CBA state has been experimentally demonstrated in a spin-1 BEC of over 10 000  $^{87}\text{Rb}$  atoms [49]. The coupling to the environment that is most sensitively probed by the CBA state corresponds to a radio-frequency pulse. By transferring the entangled atoms to different internal states, the optimal coupling can be modified. In this way, the CBA state can be used, e. g., to operate a microwave atomic clock beyond the SQL [25]. However, because of the comparatively low frequency of microwave radiation, such clocks are not able to compete with optical atomic clocks<sup>8</sup>. Alternatively, one can think of applications that are intrinsically related to radio-frequency radiation, such as, e. g., radio telescopes.

An experimental realization of our second proposal, regarding the generation of MSSs, is pending. Admittedly, we have not discussed how to characterize the produced MSSs, which is essential to prove experimental success. However, methods for characterization can probably be adapted from related experiments [49, 113]. Greenberger-Horne-Zeilinger (GHZ) states and NOON states represent closely related paradigmatic examples of entangled MSSs. So far, such states have been prepared with no more than 30 massive particles [36–39]. By contrast, our proposal promises NOON-like MSSs of  $10^2$ - $10^5$  atoms.

---

<sup>8</sup>Microwave Rb clocks are widely used as a secondary frequency standard. However, their main advantages, which include low cost and compactness, would considerably suffer from targeting quantum enhancement. An optical clock based on  $^{87}\text{Rb}$  has been recently presented in Ref. [231].



## 5 Excited-State Quantum Phase Transitions

In Chapter 4, we have demonstrated how ground-state quantum phase transitions (ground-state QPTs) in spinor Bose-Einstein condensates (BECs) can be used for quantum-state engineering. Though our proposal concerned exclusively the ground state, its experimental feasibility significantly depended on favorable properties of low-lying excited states. This is just one of many examples for the relevance of excited eigenstates beyond their thermal mixtures. Currently, there is much interest in quantum many-body systems out of equilibrium [232, 233]. The corresponding dynamics depends on the properties of excited states. Regarding quantum-state engineering, all Hamiltonian eigenstates share the advantage of being pure and stationary. Depending on their further properties, it may be favorable to target certain excited states. Experimentally obtained excited states include, e. g., single-photon states [234, 235], atomic clock states [23], motional Fock states [236], excited bands of ultracold atoms in optical lattices [237], and highest excited states in spinor BECs [161]. Ongoing progress towards the generation of arbitrary quantum states increases, particularly, the accessibility of excited states [238]. Moreover, predictions of intriguing excited-state properties would certainly trigger dedicated experiments. Hence, it is highly desirable to extend investigations of ground-state QPTs towards excited states.

As recently as 2006, excited-state quantum phase transitions (ESQPTs) have been introduced in Refs. [41, 239, 240]. The general concept regarding phases of matter, outlined at the beginning of Chapter 4, pertains also to Hamiltonian eigenstates. Just as for ground-state QPTs, one has to identify appropriate signatures. Because the first investigations of ESQPTs concerned nuclear and molecular physics [41, 241], much attention has been paid to spectral properties. A common spectral signature of ground-state QPTs consists in a closing gap between the lowest and the next higher eigenenergy. Transferring this to excited states is straightforward: closing energy gaps occur also further up the spectrum. More generally, ESQPTs are associated with singularities in the density of states (DOS) [42]. We treat this as the defining signature of ESQPTs. Excited-state phase diagrams are usually at least two-dimensional: one control parameter is given by a Hamiltonian coupling coefficient  $\lambda$ , and the other one by the energy density  $\eta$ . Typically, continuous critical curves  $\eta_*(\lambda)$  of singular DOS divide the  $\lambda$ - $\eta$  plane into excited-state phases. At the lower bound of the spectrum, one recovers the ground-state phase diagram.

ESQPTs have been theoretically investigated in various quantum many-body systems with small numbers of collective degrees of freedom. Examples include the Lipkin-Meshkov-Glick (LMG) model [242, 243], the Dicke model [244–247], interacting boson models for nuclei [41, 248] and molecules [47, 241], two-site Bose-Hubbard models [249], and driven systems [250]. A general analysis of ESQPTs in systems with two collective degrees of freedom is performed in Refs. [248, 251, 252]. From the very beginning, ESQPTs have been related to properties of classical models describing the infinite-size limit of the quantum system under consideration [41]. Reference [253] elaborates on this relation and presents a classification of ESQPTs. Beyond spectral signatures, much attention has been devoted to the effect of ESQPTs on thermodynamics [254–257] and dynamics [258–261]. Experimentally, signatures of ESQPTs have been so far observed in molecular spectra [47, 262, 263], in the dynamics of spinor BECs [43, 44, 46], and in microwave photonic crystals [45]. Recently, a dynamical QPT in a spinor BEC has been traced back to an ESQPT in the highest excited state [161]. For a review on ESQPTs, see Ref. [42].

The number of theory papers on ESQPTs tremendously exceeds the amount of experimental

contributions. Based on the mean-field model [29, 149], it is generally assumed that spinor BECs exhibit ESQPTs. However, there have been so far neither theoretical nor experimental studies dedicated to the investigation of these ESQPTs. The experiments cited above [43, 44, 46] demonstrated the mean-field dynamics, and some of the observations were later attributed to ESQPTs. We believe that ESQPTs in spinor BECs deserve more attention. Spinor BECs offer excellent experimental control and can, thus, help to fill the lack of experiments on ESQPTs.

Order parameters are crucial for the concept of phases. Moreover, they constitute an important link to quantum-state engineering. Therefore, it is surprising how rarely order parameters are discussed in the literature on ESQPTs. Instead, much attention is paid to singularities marking the transitions. Most probably, a universal method for constructing order parameters of ESQPTs does not exist [42]. Just as ground-state QPTs, ESQPTs can go along with spontaneous symmetry breaking. This aids the definition of both static [245] and dynamic [264–266] order parameters. Reference [45] suggests the f-sum rule as a quasiorder parameter. However, in general, identifying order parameters of ESQPTs remains a highly relevant open problem.

Chapter 4 was concerned with the ground-state QPTs in a magnetization-free ferromagnetic spin-1 BEC. Below, we extend the ground-state phase diagram across the spectrum. We begin, in Section 5.1, by postulating the excited-state phases. Section 5.2 provides some details on the mean-field model fundamental to the entire chapter. In Section 5.3, we prove that the DOS diverges at the ESQPTs. This confirms the excited-state phases. Further signatures of the ESQPTs are outlined in Section 5.4. Particularly, we identify a winding number, see Sections 5.4 and 5.5, that classifies the mean-field phase-space trajectories according to the excited-state phases. Based on this observation, we introduce an order parameter (Section 5.5) that can be extracted by interferometry (Section 5.6). According to our analysis in Section 5.7, such an interferometric measurement is feasible but requires an outstanding control over magnetic-field fluctuations. Section 5.8 highlights that our findings apply to a large class of quantum models with the same mean-field limit. A spinor BEC can be, thus, considered as a quantum simulator of ESQPTs in different physical systems. We conclude in Section 5.9.

In this chapter we elaborate on our results presented in Ref. [208].

## 5.1 Phases

The spin degrees of freedom of a ferromagnetic spin-1 BEC can be modeled by the Hamiltonian density

$$\frac{\hat{h}}{|c|} = \xi \left( 1 - \frac{2\hat{N}_0}{N} \right) - \frac{1}{N^2} \left[ \hat{a}_0^{\dagger 2} \hat{a}_1 \hat{a}_{-1} + \hat{a}_1^{\dagger} \hat{a}_{-1}^{\dagger} \hat{a}_0^2 + \hat{N}_0 \left( \hat{N}_1 + \hat{N}_{-1} + \frac{1}{2} \right) + \frac{\hat{D}^2}{2} \right], \quad (5.1)$$

cf. Chapter 3. Recall that the magnetization  $\hat{D} \equiv \hat{N}_1 - \hat{N}_{-1}$  is conserved,  $[\hat{h}, \hat{D}] = 0$ . We consider the eigenspace of  $\hat{D}$  with eigenvalue  $D = 0$ . Figure 5.1 depicts, for  $N = 100$  bosons, the spectrum of  $\hat{h}/|c|$  as a function of the dimensionless effective quadratic Zeeman shift  $\xi$ <sup>1</sup>. The ground-state QPTs discussed in the previous chapter are located at  $\xi = \pm 1$ . They delimit three ground-state quantum phases: the Twin-Fock (TF) phase for  $\xi < -1$ , the polar (P) phase for  $\xi > 1$ , and the broken-axisymmetry (BA) phase for  $|\xi| < 1$ .

Figure 5.1 hints at the existence of a critical dimensionless energy density  $\eta_*(\xi) \equiv -|\xi|$ . At  $|\xi| \leq 1$ , the eigenvalues of  $\hat{h}/|c|$  cluster around  $\eta_*(\xi)$ . For  $|\xi| > 1$ ,  $\eta_*(\xi)$  follows the energy density of the ground state, cf. Eq. (4.6). By contrast,  $\eta_*(0)$  touches the energy density of the highest excited state. Thus,  $\eta_*(\xi)$  with  $|\xi| \leq 1$  cuts the spectrum into three regions, each of which

<sup>1</sup>Note that for finite  $N$  the apparent mirror symmetry with respect to  $\xi = 0$  is not exact.



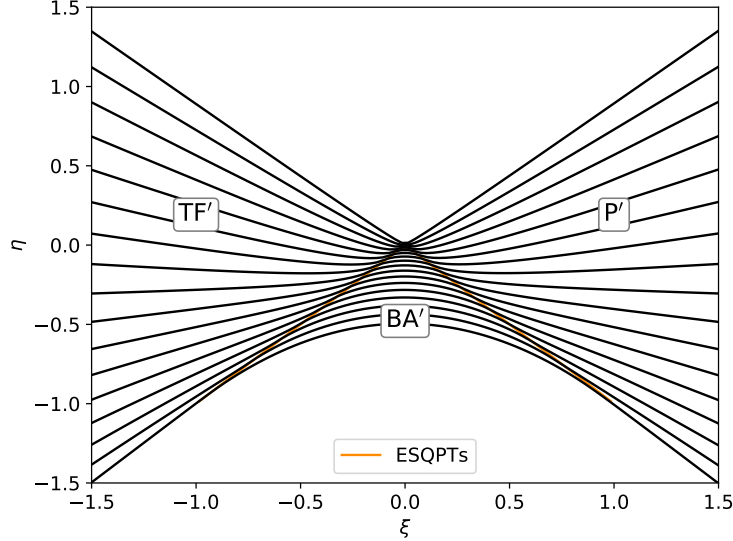


**Figure 5.1:** Excited-state quantum phases in the magnetization-free subspace of a ferromagnetic spin-1 BEC. We depict every third eigenvalue of the Hamiltonian density  $\hat{h}/|c|$  for  $N = 100$  bosons as a function of the effective quadratic Zeeman shift  $\xi$ . Avoided crossings lead to a clustering of eigenvalues around  $\eta_*(\xi) \equiv -|\xi|$  with  $|\xi| \leq 1$  (orange line). This points at ESQPTs that divide the spectrum into three phases, by analogy with the ground-state quantum phases called the TF', P', and BA' phase.

contains one ground-state quantum phase. The clustering of the spectrum suggests that, in the mean-field limit  $N \rightarrow \infty$ , the DOS diverges at  $\eta_*(\xi)$  with  $|\xi| \leq 1$ . We understand a singular DOS as the defining property of ESQPTs. Hence, we introduce three excited-state quantum phases: the TF' phase for  $\eta > \eta_*(\xi)$  and  $\xi < 0$ , the P' phase for  $\eta > \eta_*(\xi)$  and  $\xi > 0$ , and the BA' phase for  $\eta < \eta_*(\xi)$ , implying  $|\xi| < 1$ . Below, we confirm the divergence of the DOS and further analyze the excited-state quantum phases.

## 5.2 Mean-Field Model

Phase transitions constitute a property of infinite systems. Therefore, we study the model (5.1) in the limit of  $N \rightarrow \infty$  bosons. More precisely, we consider the mean-field limit that we have discussed in Section 3.7. Recall the  $N$ -particle coherent states

$$|\boldsymbol{\alpha}, N\rangle = \frac{1}{\sqrt{N!}} \left( \sum_{m=-1}^1 \alpha_m \hat{a}_m^\dagger \right)^N |0\rangle \quad (5.2)$$

with  $\alpha_m \equiv \sqrt{n_m} e^{i\phi_m}$ ,  $n_m \geq 0$ ,  $\phi_m \in \mathbb{R} \bmod 2\pi$ , and  $\sum_m n_m = 1$ . To obtain the mean-field symbol  $A_{\text{mf}}(\boldsymbol{\alpha})$  of a suitable operator  $\hat{A}$ , one substitutes  $\hat{a}_m^{(\dagger)}$  by  $\sqrt{N}\alpha_m^{(*)}$  and takes the  $N \rightarrow \infty$  limit, see Definition 2. Then, according to Lemma 3,

$$\lim_{N \rightarrow \infty} \langle \boldsymbol{\alpha}, N | \hat{A} | \boldsymbol{\alpha}, N \rangle = A_{\text{mf}}(\boldsymbol{\alpha}). \quad (5.3)$$

We focus on coherent states with zero magnetization,  $\frac{1}{N}\langle\boldsymbol{\alpha}, N|\hat{D}|\boldsymbol{\alpha}, N\rangle = n_1 - n_{-1} \equiv d = 0$ . For such states, the mean-field symbol of the Hamiltonian density 5.1 becomes

$$\frac{h_{\text{mf}}}{|c|} = \xi(1 - 2n_0) - 2n_0(1 - n_0) \cos^2(\phi) \quad (5.4)$$

with  $\phi \equiv \phi_0 - (\phi_1 + \phi_{-1})/2$ , see Eq. (3.100). We call  $h_{\text{mf}}$  the mean-field Hamiltonian. Note that  $h_{\text{mf}}$  respects the symmetries  $h_{\text{mf}}(\phi \pm \pi) = h_{\text{mf}}(\phi)$ ,  $h_{\text{mf}}(-\phi) = h_{\text{mf}}(\phi)$ , and  $h_{\text{mf}}(-\xi, 1 - n_0) = h_{\text{mf}}(\xi, n_0)$ . The evolution with  $\hat{h}$  leads to a dynamics of mean-field symbols that is, for  $d = 0$  states, governed by the Hamiltonian equations

$$\begin{aligned} \frac{d}{d\tau} n_0 &= \frac{\partial}{\partial \phi} \frac{h_{\text{mf}}}{|c|} = 4n_0(1 - n_0) \cos(\phi) \sin(\phi), \\ \frac{d}{d\tau} \phi &= -\frac{\partial}{\partial n_0} \frac{h_{\text{mf}}}{|c|} = 2\xi + 2(1 - 2n_0) \cos^2(\phi) \end{aligned} \quad (5.5)$$

with  $\tau \equiv |c|t/\hbar$  and by  $\frac{d}{d\tau} d = \frac{d}{d\tau} \Delta\phi = 0$  with  $\Delta\phi \equiv (\phi_1 - \phi_{-1})/2$ , cf. Eq. (3.120). In the present section we provide, for later use, some details on the mean-field model defined by Eqs. (5.4) and (5.5).

### 5.2.1 Phase Space

The phase space of the mean-field model consists of all tuples  $(n_0, \phi)$  of the generalized coordinate  $n_0 \in [0, 1]$  and the conjugate momentum  $\phi \in [0, 2\pi)$ . A given tuple  $(n_0, \phi)$  corresponds to the coherent state, see Eq. (5.2), with

$$\alpha_0 = \sqrt{n_0} e^{i\phi_0}, \quad \alpha_1 = \sqrt{\frac{1 - n_0}{2}} e^{i(\phi_0 - \phi + \Delta\phi)}, \quad \alpha_{-1} = \sqrt{\frac{1 - n_0}{2}} e^{i(\phi_0 - \phi - \Delta\phi)}. \quad (5.6)$$

Here,  $\phi_0$  is an irrelevant global phase and  $\Delta\phi \in \mathbb{R} \bmod 2\pi$  is fixed by the initial conditions. For  $n_0 \in \{0, 1\}$ , the coherent state does not depend, up to a global phase, on the value of  $\phi$ . Therefore, the phase space is isomorphic to a sphere with  $z$ -axis  $n_0$  and azimuthal angle  $\phi$ , see Fig. 5.2. The north pole is located at  $n_0 = 1$  and the south pole at  $n_0 = 0$ . Up to the sign of  $\phi$ , the phase space coincides with the Bloch sphere for the modes  $\hat{a}_0^\dagger$  and  $\frac{1}{2}(e^{i\Delta\phi} \hat{a}_1^\dagger + e^{-i\Delta\phi} \hat{a}_{-1}^\dagger)$ , cf. Eq. (2.38).

### 5.2.2 Stationary Points

The stationary points of  $h_{\text{mf}}$  are defined by

$$\frac{\partial}{\partial n_0} \frac{h_{\text{mf}}}{|c|} = -\frac{d}{d\tau} \phi = 0, \quad \frac{\partial}{\partial \phi} \frac{h_{\text{mf}}}{|c|} = \frac{d}{d\tau} n_0 = 0. \quad (5.7)$$

Equations (5.4) and (5.5) yield the following stationary points:

$n_0$	0	1	$\frac{1}{2}(\xi + 1)$	any
$\cos^2(\phi)$	$ \xi $	$ \xi $	1	0
for	$-1 \leq \xi \leq 0$	$0 \leq \xi \leq 1$	$-1 \leq \xi \leq 1$	$\xi = 0$
$\eta$	$- \xi $	$- \xi $	$-\frac{1}{2}(\xi^2 + 1)$	0

Here,  $\eta$  denotes the value of  $h_{\text{mf}}/|c|$ . Note that the first two stationary points have an energy density of  $\eta_*(\xi)$ . The third column corresponds to the ground state at  $-1 \leq \xi \leq 1$ , cf. Eqs. (4.5) and (4.6). In the following, we refrain from discussing the forth, special, case  $\xi = 0$ .

The dynamics in the vicinity of a stationary point is determined by the corresponding Hessian matrix  $H$  of  $h_{\text{mf}}/|c|$ :

$$H \equiv \begin{pmatrix} \partial_{n_0}^2 & \partial_{n_0} \partial_\phi \\ \partial_\phi \partial_{n_0} & \partial_\phi^2 \end{pmatrix} \frac{h_{\text{mf}}}{|c|} = \begin{pmatrix} 4 \cos^2(\phi) & 2(1 - 2n_0) \sin(2\phi) \\ 2(1 - 2n_0) \sin(2\phi) & 4n_0(1 - n_0) \cos(2\phi) \end{pmatrix} \quad (5.8)$$

The Hessian matrices at  $n_0 \in \{0, 1\}$  are

$$H = 4 \cos(\phi) \begin{pmatrix} \cos(\phi) & \pm \sin(\phi) \\ \pm \sin(\phi) & 0 \end{pmatrix} \quad (5.9)$$

with the positive sign applying to  $n_0 = 0$ . At the corresponding stationary points,  $\cos^2(\phi) = |\xi|$  and the eigenvalues of  $H$  become

$$\lambda_{\pm} = 2\sqrt{|\xi|} \left( \sqrt{|\xi|} \pm \sqrt{4 - 3|\xi|} \right). \quad (5.10)$$

For  $0 < |\xi| < 1$ ,  $\lambda_- < 0$  and  $\lambda_+ > 0$  imply that the first two stationary points are saddle points of  $h_{\text{mf}}$ <sup>2</sup>. The Hessian matrix at the ground-state stationary points is diagonal with eigenvalues  $\lambda_{n_0} = 4$  and  $\lambda_\phi = 1 - \xi^2$ . Hence, for  $|\xi| < 1$  both eigenvalues are positive, marking a minimum of  $h_{\text{mf}}$ <sup>3</sup>.

In summary, there are three stationary points of  $h_{\text{mf}}$  at any  $|\xi| \in (0, 1)$ : two ground-state minima at  $n_0 = \frac{1}{2}(\xi + 1)$  and  $\phi \in \{0, \pi\}$  with an energy density of  $\eta = \eta_0 = -\frac{1}{2}(\xi^2 + 1)$  and a saddle point at the north ( $\xi > 0$ ) or south ( $\xi < 0$ ) pole of the phase space with  $\eta = \eta_* = -|\xi|$ , cf. Fig. 5.2. Note that admitting an arbitrary magnetization  $d$ , see Eqs. (3.99) and (3.119), does not change the set of stationary points for  $\xi \neq 0$ . This further justifies our focus on  $d = 0$  states.

### 5.2.3 Energy Hypersurfaces

Consider the mean-field model at a fixed value of  $\xi$ . The phase-space points  $(n_0, \phi)$  satisfying

$$\eta = \xi(1 - 2n_0) - 2n_0(1 - n_0) \cos^2(\phi) \quad (5.11)$$

constitute a level set of  $h_{\text{mf}}$ , which we call the energy hypersurface with energy density  $\eta$ . The largest value of  $\eta$  that corresponds to a non-empty level set is  $\eta_{\text{max}} \equiv |\xi|$ , and the smallest one is the ground-state energy density  $\eta_0$  in Eq. (4.6),

$$\eta_0 = \begin{cases} \xi & \text{for } \xi \leq -1 \\ -\frac{1}{2}(\xi^2 + 1) & \text{for } -1 < \xi < 1 \\ -\xi & \text{for } \xi \geq 1 \end{cases}. \quad (5.12)$$

For  $\xi \neq 0$ , solving Eq. (5.11) for  $n_0$  yields

$$n_0(\phi) = \begin{cases} \begin{cases} n_+(\phi) \quad \forall \phi & \text{for } \xi < 0 \\ n_-(\phi) \quad \forall \phi & \text{for } \xi > 0 \end{cases} & \text{for } \eta > \eta_* \\ n_{\pm}(\phi) \quad \forall \cos^2(\phi) \geq \sqrt{\eta^2 - \xi^2} - \eta & \text{for } \eta < \eta_* \\ \begin{cases} \frac{1}{2} \left( 1 - \frac{\xi}{|\xi|} \right) + \frac{\xi}{\cos^2(\phi)} & \forall \cos^2(\phi) \geq |\xi| \\ \frac{1}{2} \left( 1 + \frac{\xi}{|\xi|} \right) & \forall \phi \end{cases} & \text{for } \eta = \eta_* \end{cases} \quad (5.13)$$

<sup>2</sup>For  $|\xi| = 0$  we get  $\lambda_{\pm} = 0$ , and  $|\xi| = 1$  yields  $\lambda_- = 0$ ,  $\lambda_+ = 4$ .

<sup>3</sup>For  $|\xi| = 1$ ,  $\lambda_\phi = 0$ .

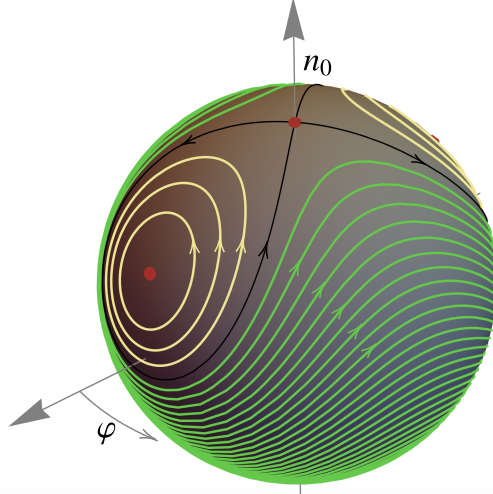


**Figure 5.2:** Phase-space trajectories of the mean-field model for  $\xi = 0.5$ . North and south pole of the phase space are at  $n_0 = 1$  and  $n_0 = 0$ , respectively. Stationary points of  $h_{\text{mf}}$  are marked in red. The separatrix (black) separates trajectories in the P' phase ( $\eta > \eta_*$ , green) from trajectories in the BA' phase ( $\eta < \eta_*$ , yellow). In the P' phase, each energy hypersurface is the image of a single trajectory. In the BA' phase, it subsumes one trajectory at the front and one at the back of the phase space.

with

$$n_{\pm}(\phi) \equiv \frac{1}{2 \cos^2(\phi)} \left( \cos^2(\phi) + \xi \pm \sqrt{\Delta} \right), \quad \Delta \equiv \cos^4(\phi) + 2\eta \cos^2(\phi) + \xi^2. \quad (5.14)$$

The value of  $n_0(\phi)$  at  $\phi \in \{\pi/2, 3\pi/2\}$  is obtained by taking the limit  $\cos^2(\phi) \rightarrow 0$  in Eq. (5.14).

Let us discuss some implications of Eqs. (5.13) and (5.14). For  $\eta_* < \eta < \eta_{\text{max}}$ , each energy hypersurface constitutes a closed loop around the  $n_0$ -axis of the phase space (green curves in Fig. 5.2). Towards  $\eta_{\text{max}}$ , this loop shrinks to a pole of the phase space, which is opposite to the saddle point (for  $|\xi| < 1$ ) or ground state (for  $|\xi| \geq 1$ ) of  $h_{\text{mf}}$ . For  $\eta < \eta_*$ , we first note that Eq. (5.12) implies  $|\xi| < 1$ . Furthermore,  $f(\xi, \eta)$  in  $\cos^2(\phi) \geq \sqrt{\eta^2 - \xi^2} - \eta \equiv f(\xi, \eta)$ , see Eq. (5.13), satisfies  $f(\xi, \eta) > 0$  and  $f(\xi, \eta) = 1 \Leftrightarrow \eta = \eta_0$ . Within the admitted range of  $\phi$ ,  $n_+(\phi) = n_-(\phi)$  is equivalent to  $\cos^2(\phi) = f(\xi, \eta)$ . Additionally, we observe that  $n_0(\phi)$  does not attain the values  $\{0, 1\}$ . Hence, for  $\eta_0 < \eta < \eta_*$ , each energy hypersurface consists of two disconnected loops (yellow curves in Fig. 5.2), none of which encircles the  $n_0$ -axis or includes a pole of the phase space. At  $\eta_0$ , we recover the ground-state stationary points. The energy hypersurface with energy density  $\eta_*(\xi) \equiv -|\xi|$  at  $|\xi| < 1$  includes the saddle point of  $h_{\text{mf}}$  and is therefore called a “separatrix” (black line in Fig. 5.2). It is a closed curve with an intersection at the stationary point. For  $|\xi| \geq 1$ , the energy hypersurfaces at  $\eta_*$  is confined to the phase-space pole corresponding to the respective ground state, cf. Eq. (4.5).

All energy hypersurfaces necessarily reflect the symmetries of the mean-field Hamiltonian, such as  $h_{\text{mf}}(\phi \pm \pi) = h_{\text{mf}}(\phi)$ ,  $h_{\text{mf}}(-\phi) = h_{\text{mf}}(\phi)$ , and  $h_{\text{mf}}(-\xi, 1 - n_0) = h_{\text{mf}}(\xi, n_0)$ .

### 5.2.4 Trajectories

Let  $(n_0(\tau), \phi(\tau))$  with  $\tau \in \mathbb{R}$  be a solution of the equations of motion (EOMs) in Eq. (5.5). Then  $(n_0(\tau + \tau_0), \phi(\tau + \tau_0))$  with any  $\tau_0 \in \mathbb{R}$  also solves the EOMs. We say that all  $(n_0(\tau + \tau_0), \phi(\tau + \tau_0))$

represent the same trajectory. Since all representatives have the same image, we can refer to it as the image of the trajectory.

The mean-field Hamiltonian is time-independent so that the EOMs conserve the energy density  $\eta$ . Therefore, the image of a trajectory is always part of an energy hypersurface. More precisely, if we exclude all stationary points from an energy hypersurface, each connected component of the remaining set becomes the image of a trajectory. Every stationary point defines its own trajectory. Hence, energy hypersurfaces with  $\eta_* < \eta \leq \eta_{\max}$  directly correspond to trajectories (green curves in Fig. 5.2), while for  $\eta_0 \leq \eta < \eta_*$  each energy hypersurface is made up of two trajectories with the same energy density (yellow curves). The separatrix consists of three trajectories.

The parameterization of  $(n_0(\tau), \phi(\tau))$  by  $\tau$  assigns the direction of increasing  $\tau$  to the trajectories. For  $\eta \neq \eta_*$ , it can be readily determined by observing that for  $\cos^2(\phi) = 1$

$$\frac{d}{d\tau}\phi = \begin{cases} -2\sqrt{1+2\eta+\xi^2} \leq 0 & \text{for } n_0(\phi) = n_+(\phi) \\ 2\sqrt{1+2\eta+\xi^2} \geq 0 & \text{for } n_0(\phi) = n_-(\phi) \end{cases}. \quad (5.15)$$

For the separatrix at  $\cos^2(\phi) = 1$ , we find

$$\frac{d}{d\tau}\phi = 2\frac{\xi}{|\xi|}(1-|\xi|) \begin{cases} < 0 & \text{for } \xi < 0 \\ > 0 & \text{for } \xi > 0 \end{cases}. \quad (5.16)$$

Figure 5.2 depicts exemplary trajectories for  $\xi = 0.5$ .

### 5.2.5 Dynamics

In Section 3.7.5, we have reviewed some general results on the evolution  $n_0(\tau)$  determined by the mean-field EOMs for a spin-1 BEC. Here, we focus on the model (5.1), i. e., a ferromagnetic interaction,  $c < 0$ , and zero magnetization,  $d = 0$ .

Using the conservation of  $\eta$ , we find that for  $\xi \neq 0$

$$\left(\frac{d}{d\tau}n_0\right)^2 = 16\xi(n_0 - z_0)(n_0 - z_+)(n_0 - z_-) \quad (5.17)$$

with  $z_0 = \frac{1}{2}(1 - \eta/\xi)$  and  $z_{\pm} = \frac{1}{2}(1 + \xi \pm \sqrt{1 + \xi^2 + 2\eta})$ . Recall that we have divided the  $(\xi, \eta)$ -plane into the TF' phase for  $\eta > \eta_*$  and  $\xi < 0$ , the P' phase for  $\eta > \eta_*$  and  $\xi > 0$ , and the BA' phase for  $\eta < \eta_*$ . At  $\eta_*$  and in the TF' and P' phases  $z_- \leq z_0 \leq z_+$ , while in the BA' phase  $z_0 \leq z_- \leq z_+$  for  $\xi < 0$  and  $z_- \leq z_+ \leq z_0$  for  $\xi > 0$ . Let us introduce

$$\begin{aligned} x_1 &\equiv \frac{1}{2}(1 + |\xi| - \sqrt{1 + \xi^2 + 2\eta}), \\ x_2 &\equiv \begin{cases} \frac{1}{2}(1 + |\xi| + \sqrt{1 + \xi^2 + 2\eta}) & \text{for } \eta < \eta_* \\ \frac{1}{2}(1 - \eta/|\xi|) & \text{for } \eta \geq \eta_* \end{cases}, \\ x_3 &\equiv \begin{cases} \frac{1}{2}(1 - \eta/|\xi|) & \text{for } \eta < \eta_* \\ \frac{1}{2}(1 + |\xi| + \sqrt{1 + \xi^2 + 2\eta}) & \text{for } \eta \geq \eta_* \end{cases} \end{aligned} \quad (5.18)$$

with  $x_1 \leq x_2 \leq x_3$ . For  $\xi > 0$ , the  $x_i$  coincide with the appropriately ordered zeroes  $z_0$  and  $z_{\pm}$ . However, in contrast to the  $z_i$  the  $x_i$  do not depend on the sign of  $\xi$ .

For  $\xi > 0$ , according to Eq. (3.123),  $n_0$  evolves as

$$n_0(\tau) = x_2 - (x_2 - x_1) \text{cn}^2\left(2\sqrt{|\xi|(x_3 - x_1)}\tau + v, \frac{x_2 - x_1}{x_3 - x_1}\right) \equiv \tilde{n}_0(\tau), \quad (5.19)$$

where  $\text{cn}(w; k^2)$  is the Jacobi elliptic cosine and  $v$  accounts for the initial conditions<sup>4</sup>. If  $(n_0(\tau), \phi(\tau))$  solves the EOMs (5.5) for some  $\xi > 0$ , the symmetries  $h_{\text{mf}}(-\xi, 1 - n_0) = h_{\text{mf}}(\xi, n_0)$  and  $h_{\text{mf}}(-\phi) = h_{\text{mf}}(\phi)$  imply that  $(1 - n_0(-\tau), -\phi(\tau))$  solves the EOMs for  $-\xi < 0$ . Since additionally  $\text{cn}(-w; k^2) = \text{cn}(w; k^2)$ ,  $n_0(\tau)$  for  $\xi < 0$  can be expressed as

$$n_0(\tau) = 1 - \tilde{n}_0(\tau). \quad (5.20)$$

Hence,  $n_0(\tau)$  oscillates between  $x_1$  and  $x_2$ . The period is, see Eq. (3.124),

$$\mathcal{T} = \frac{1}{\sqrt{|\xi|(x_3 - x_1)}} K\left(\frac{x_2 - x_1}{x_3 - x_1}\right) = \begin{cases} \sqrt{y}^{-1} K(x/y) & \text{for } \eta < \eta_* \\ \sqrt{x}^{-1} K(y/x) & \text{for } \eta > \eta_* \end{cases}, \quad (5.21)$$

where  $K(k^2) = \int_0^{\pi/2} d\gamma \sqrt{1 - k^2 \sin^2 \gamma}^{-1}$  is the complete elliptic integral of the first kind,  $x \equiv |\xi| \sqrt{1 + \xi^2 + 2\eta}$ , and  $y \equiv \frac{1}{2}(x - \xi^2 - \eta)$ . For  $0 < |\xi| \leq 1$ , the period diverges at  $\eta_*$ : when  $\eta$  approaches  $\eta_*$  from above,  $y/x$  converges from below to unity and  $K(y/x)$  goes to infinity.

### 5.3 Density of States

The central signature of an ESQPT is a singularity in the DOS. Here, the DOS has to be evaluated in the limit of an infinitely large system. For a ferromagnetic spin-1 BEC with zero magnetization, the finite-size spectrum in Fig. 5.1 suggests that, in the limit of  $N \rightarrow \infty$  atoms, the DOS diverges at  $\eta_*(\xi) \equiv -|\xi|$  with  $|\xi| \leq 1$ . To verify this, we study the DOS of the mean-field model discussed in the previous section.

Equation (3.103) provides a concise expression for the DOS of a spin-1 BEC in the mean-field limit. However, this DOS takes into account states with an arbitrary magnetization. The derivation of Eq. (3.103) is based on coherent states that are, in general, no eigenstates of the magnetization  $\hat{D}$ . It is therefore not obvious how to restrict the DOS to the zero-magnetization subspace. In Section 5.3.1 we prove that this restriction can be realized by an intuitive modification of the DOS in Eq. (3.103). We evaluate the restricted DOS in Section 5.3.2. We demonstrate that the DOS, indeed, diverges at  $\eta_*(\xi)$  with  $0 < |\xi| < 1$ .

#### 5.3.1 Restriction to Magnetization-Free Subspace

In terms of the Fock basis states  $|N_1, N_0, N_{-1}\rangle$  with  $\sum_m N_m = N$  of the  $N$ -particle Hilbert space  $\mathcal{H}_N$ , the projection onto the eigenspace of  $\hat{D} \equiv \hat{N}_1 - \hat{N}_{-1}$  with eigenvalue  $D = 0$  reads

$$\hat{P}_N = \sum_{k=0}^{\lfloor N/2 \rfloor} |k, N - 2k, k\rangle \langle k, N - 2k, k|. \quad (5.22)$$

We define the DOS restricted to the magnetization-free subspace of  $\mathcal{H}_N$  by

$$\mathcal{F}[\tilde{\nu}_N](\zeta) \equiv \int d\eta e^{i\zeta\eta} \tilde{\nu}_N(\eta) \equiv \text{Tr}_N \hat{P}_N e^{i\zeta \hat{h}/|c|} \quad \text{with } \zeta \in \mathbb{R}, \quad (5.23)$$

where  $\hat{h}/|c|$  is the dimensionless Hamiltonian density in Eq. (5.1),  $\eta$  the corresponding energy density, and  $\mathcal{F}$  denotes the Fourier transformation. Below, we show that

$$\lim_{N \rightarrow \infty} \frac{1}{N} \text{Tr}_N \hat{P}_N e^{i\zeta \hat{h}/|c|} = \int \mathcal{D}\alpha \delta(n_1 - n_{-1}) e^{i\zeta h_{\text{mf}}(\alpha)/|c|} \quad (5.24)$$

<sup>4</sup>Note that at  $(|\xi| = 1, \eta = -1)$  the denominator  $x_3 - x_1$  vanishes, so that  $\tilde{n}_0(\tau)$  has to be computed by taking the appropriate limit.

with  $\mathcal{D}\boldsymbol{\alpha} \equiv \frac{1}{(2\pi)^3} \prod_m dn_m d\phi_m \delta(\sum_m n_m - 1)$ . This yields, in the same way as in Section 3.7.3,

$$\lim_{N \rightarrow \infty} \frac{\tilde{\nu}(\eta)}{N} = \int \mathcal{D}\boldsymbol{\alpha} \delta(n_1 - n_{-1}) \delta\left(\frac{h_{\text{mf}}(\boldsymbol{\alpha})}{|c|} - \eta\right) \quad (5.25)$$

for the mean-field limit of the restricted DOS. Thus, the restriction to  $D = 0$  can be essentially implemented by multiplying the coherent-state measure by  $\delta(d)$ , as might have been expected [245].

Our following proof of Eq. (5.24) relies on the framework introduced in Refs. [203–206]. Let us therefore review some central ideas of this approach. For the details, please consult the original works.

Let  $\mathcal{A}_N$  be the set of linear operators on  $\mathcal{H}_N$ . Here,  $\mathcal{H}_1$  is the single-particle Hilbert space and  $\mathcal{H}_N$  the symmetric subspace of  $\mathcal{H}_1^{\otimes N}$ . We denote the projection from  $\mathcal{H}_1^{\otimes N}$  onto  $\mathcal{H}_N$  by  $\hat{F}_N$ .  $\mathcal{A}_M$  and  $\mathcal{A}_N$  with  $M < N$  can be related by

$$j_{NM} : \mathcal{A}_M \rightarrow \mathcal{A}_N, \quad \hat{A}_M \mapsto \hat{F}_N \text{sym}_N(\hat{A}_M \otimes \mathbb{1}_{N-M})\hat{F}_N, \quad (5.26)$$

where  $\mathbb{1}_{N-M}$  is the identity on  $\mathcal{H}_1^{\otimes(N-M)}$ . The symmetrization operator  $\text{sym}_N$  averages over all permutations of the single-particle Hilbert spaces constituting  $\mathcal{H}_1^{\otimes N}$ . A uniformly bounded sequence  $\hat{A}_N$  of  $\hat{A}_N \in \mathcal{A}_N$  with  $N \in \mathbb{N}$  is called  $j$ -convergent if

$$\lim_{M \rightarrow \infty} \limsup_{N \rightarrow \infty} \|\hat{A}_N - j_{NM}(\hat{A}_M)\| = 0. \quad (5.27)$$

We denote the set of  $j$ -convergent sequences by  $\mathfrak{J}$ , and the  $N \rightarrow \infty$  limit of  $\hat{A}_N$  by  $A_\infty$ . The  $j$ -convergent sequences with  $\|\hat{A}_\infty\| = 0$  constitute the set of null sequences  $\mathfrak{J}_0$ . Note that applying a complex analytic function  $f \in \mathcal{C}(\mathbb{C}^r)$  to  $\hat{A}_N^{(s)} \in \mathfrak{J}$  with  $s \in \{1, \dots, r\}$  yields the  $j$ -convergent sequence  $\lim_{N \rightarrow \infty} f(\hat{A}_N^{(1)}, \dots, \hat{A}_N^{(r)}) = f(A_\infty^{(1)}, \dots, A_\infty^{(r)})$ .

The space of limiting operators  $A_\infty$  is isomorphic to

$$\mathcal{A}_\infty \equiv \tilde{\mathfrak{J}}/\mathfrak{J}_0. \quad (5.28)$$

$\mathcal{A}_\infty$  is a commutative  $C^*$ -algebra. The state or dual space  $\mathcal{A}_\infty^*$  of  $\mathcal{A}_\infty$  is a weak\* compact convex set. The set  $\Omega$  of pure or extremal states in  $\mathcal{A}_\infty^*$  coincides with the set of multiplicative states. By Gelfand's representation,  $\mathcal{A}_\infty$  is isomorphic to the space of continuous functions on  $\Omega$ .

The pure states in  $\mathcal{A}_\infty^*$  turn out to be bijectively related to coherent states. For any  $\Phi \in \Omega$  and  $A_\infty \in \mathcal{A}_\infty$ , there is an  $\boldsymbol{\alpha} \in \mathbb{C}^3$  with  $\sum_m |\alpha_m|^2 = 1$  such that

$$\Phi(A_\infty) = \lim_{N \rightarrow \infty} \langle \boldsymbol{\alpha}, N | \hat{A}_N | \boldsymbol{\alpha}, N \rangle \quad \forall \hat{A}_N \in \mathfrak{J} : \lim_{N \rightarrow \infty} \hat{A}_N = A_\infty. \quad (5.29)$$

Vice versa, for any normalized  $\boldsymbol{\alpha} \in \mathbb{C}^3$  and  $\hat{A}_N \in \mathfrak{J}$ , there is a  $\Phi \in \Omega$  such that

$$\lim_{N \rightarrow \infty} \langle \boldsymbol{\alpha}, N | \hat{A}_N | \boldsymbol{\alpha}, N \rangle = \Phi(A_\infty). \quad (5.30)$$

We can, thus, conclude that any  $\Psi \in \mathcal{A}_\infty^*$  acts as

$$\Psi(\hat{A}_\infty) = \int \prod_m dn_m d\phi_m \mu(\boldsymbol{\alpha}) A_\infty(\boldsymbol{\alpha}), \quad (5.31)$$

where  $A_\infty(\boldsymbol{\alpha}) \equiv \lim_{N \rightarrow \infty} \langle \boldsymbol{\alpha}, N | \hat{A}_N | \boldsymbol{\alpha}, N \rangle$  and  $\mu(\boldsymbol{\alpha})$  defines a probability measure.

We are now ready to show that

$$\lim_{N \rightarrow \infty} \frac{1}{N} \text{Tr} \hat{P}_N f(\hat{A}_N) = \int \mathcal{D}\alpha \delta(n_1 - n_{-1}) f(A_\infty(\alpha)) \quad \forall f \in \mathcal{C}(\mathbb{C}), \hat{A}_N \in \mathfrak{J}. \quad (5.32)$$

Restricting  $\hat{h}$  to  $\mathcal{H}_N$  defines a sequence of  $j$ -convergent operators with  $h_\infty(\alpha) = h_{\text{mf}}(\alpha)$ , cf. Definition 1 and Lemma 3. Therefore, Eq. (5.32) immediately implies Eq. (5.24).

To prove Eq. (5.32), we introduce the sequence  $\hat{\rho}_N$  of states

$$\hat{\rho}_N \equiv \frac{1}{\lfloor N/2 \rfloor + 1} \hat{P}_N. \quad (5.33)$$

If  $\hat{\rho}_N$  is weakly convergent, then for any  $\hat{A}_N \in \mathfrak{J}$

$$\lim_{N \rightarrow \infty} \frac{1}{N} \text{Tr} \hat{P}_N \hat{A}_N = \frac{1}{2} \lim_{N \rightarrow \infty} \text{Tr} \hat{\rho}_N \hat{A}_N. \quad (5.34)$$

The states

$$\hat{\rho}_N : \mathcal{A}_N \rightarrow \mathbb{C}, \quad \hat{A}_N \mapsto \text{Tr} \hat{\rho}_N \hat{A}_N \quad (5.35)$$

can be thought of as being embedded in the weak\* compact space  $\mathcal{A}_\infty^*$ . Therefore, the sequence  $\hat{\rho}_N$  must have at least one convergent subsequence. If all convergent subsequences converge to the same limit, the entire sequence converges to this limit.

The limit of any convergent subsequence  $\hat{\rho}_{M(N)}$  of  $\hat{\rho}_N$  must be of the form

$$\lim_{N \rightarrow \infty} \text{Tr} \hat{\rho}_{M(N)} \hat{A}_{M(N)} = \int \prod_m dn_m d\phi_m \mu(\alpha) A_\infty(\alpha) \quad \forall \hat{A}_N \in \mathfrak{J}, \quad (5.36)$$

see Eq. (5.31). We observe that the  $\hat{\rho}_N$  are invariant under phase shifts:

$$e^{-i\theta \hat{N}_m} \hat{\rho}_N e^{i\theta \hat{N}_m} = \hat{\rho}_N \Rightarrow \text{Tr} \hat{\rho}_N f(e^{i\theta \hat{N}_m} \hat{A}_N e^{-i\theta \hat{N}_m}) = \text{Tr} \hat{\rho}_N f(\hat{A}_N) \quad \forall m, \theta \quad (5.37)$$

Note that  $\langle \alpha, N | e^{i\theta \hat{N}_l} \hat{A}_N e^{-i\theta \hat{N}_l} | \alpha, N \rangle = \langle \alpha', N | \hat{A}_N | \alpha', N \rangle$  with  $n'_m = n_m$ ,  $\phi'_{m \neq l} = \phi_m$ , and  $\phi'_l = \phi_l - \theta$ . Hence,  $\mu(\alpha)$  cannot depend on any of the  $\phi_m$ . Furthermore, applying  $f \in \mathcal{C}(\mathbb{C})$  to  $\hat{u}_N \equiv (\hat{N}_1 + \hat{N}_0 + \hat{N}_{-1})/N$ , we find that

$$\lim_{N \rightarrow \infty} \text{Tr} \hat{\rho}_{M(N)} f(\hat{u}_{M(N)}) = \lim_{N \rightarrow \infty} \frac{1}{\lfloor M(N)/2 \rfloor + 1} \sum_{k=0}^{\lfloor M(N)/2 \rfloor} f(1) = f(1). \quad (5.38)$$

Similarly, for functions of  $\hat{d}_N \equiv \hat{D}/N$ ,

$$\lim_{N \rightarrow \infty} \text{Tr} \hat{\rho}_{M(N)} f(\hat{d}_{M(N)}) = f(0). \quad (5.39)$$

Hence,  $\mu(\alpha) = \tilde{\mu}(n_0) \delta(\sum_m n_m - 1) \delta(n_1 - n_{-1})$ . To determine  $\tilde{\mu}(n_0)$ , we consider functions of  $\hat{n}_N \equiv \hat{N}_0/N$ :

$$\lim_{N \rightarrow \infty} \text{Tr} \hat{\rho}_{M(N)} f(\hat{n}_{M(N)}) = \lim_{N \rightarrow \infty} \frac{1}{\lfloor M(N)/2 \rfloor + 1} \sum_{k=0}^{\lfloor M(N)/2 \rfloor} f\left(\frac{M(N) - 2k}{M(N)}\right) = \int dn_0 f(n_0). \quad (5.40)$$

This, finally, yields  $\mu(\alpha) = \frac{2}{(2\pi)^3} \delta(\sum_m n_m - 1) \delta(n_1 - n_{-1})$  independently of the specific convergent subsequence of  $\hat{\rho}_N$ . We have thus proven

$$\lim_{N \rightarrow \infty} \text{Tr} \hat{\rho}_N f(\hat{A}_N) = 2 \int \mathcal{D}\alpha \delta(n_1 - n_{-1}) f(A_\infty(\alpha)) \quad \forall f \in \mathcal{C}(\mathbb{C}), \hat{A}_N \in \mathfrak{J}, \quad (5.41)$$

from which Eq. (5.32) follows via Eq. (5.34), and Eq. (5.24) as a special case of Eq. (5.32).



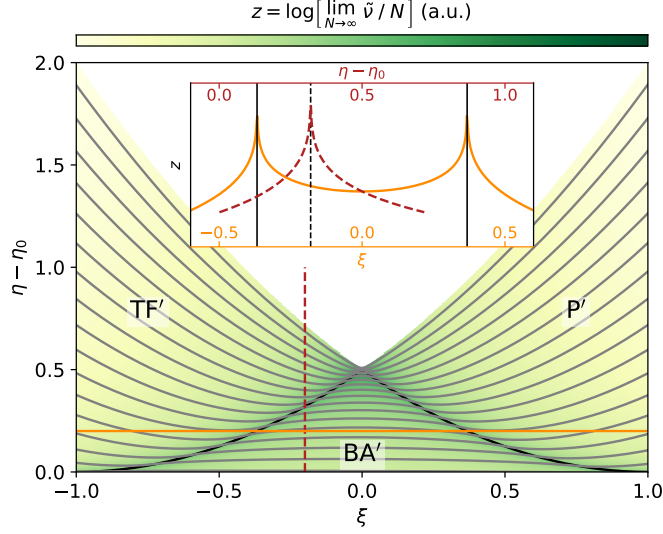


**Figure 5.3:** DOS in the mean-field limit as a function of  $\xi$  and  $\eta - \eta_0$ , where  $\eta_0 = -\frac{1}{2}(\xi^2 + 1)$  is the ground-state energy density. The DOS diverges at  $\eta_* \equiv -|\xi|$  (black), defining ESQPTs between the TF' phase, the P' phase, and the BA' phase. The inset shows the DOS along lines of constant  $\xi = -0.2$  (red, dashed) and  $\eta - \eta_0 = 0.2$  (orange, solid). The spectrum of a BEC of  $N = 100$  atoms (gray, every third eigenvalue) exhibits avoided crossings at the ESQPTs.

### 5.3.2 Divergence at Excited-State Quantum Phase Transitions

Since the mean-field Hamiltonian (5.4) depends only on  $n_0$  and  $\phi \equiv \phi_0 - (\phi_1 + \phi_{-1})/2$ , we can rewrite the restricted DOS in Eq. (5.25) as

$$\lim_{N \rightarrow \infty} \frac{\tilde{\nu}(\eta)}{N} = \frac{1}{4\pi} \int_0^1 dn_0 \int_0^{2\pi} d\phi \delta\left(\frac{h_{\text{mf}}(n_0, \phi)}{|c|} - \eta\right). \quad (5.42)$$

First, we integrate over  $n_0$ , using the familiar identity  $\delta(g(x)) = \sum_i \frac{\delta(x-z_i)}{|g'(z_i)|}$ , where  $z_i$  are the zeroes of  $g(x)$ . With the expressions for the energy hypersurfaces in Eq. (5.13), this yields for  $\xi \neq 0$ :

$$\lim_{N \rightarrow \infty} \frac{\tilde{\nu}(\eta)}{N} = \frac{1}{4\pi} \times \begin{cases} \int d\phi \left| \frac{1}{\partial_{n_0} h_{\text{mf}}/|c|} \right|_{n_0=n_+(\phi)} & \text{for } \xi < 0 \\ \int d\phi \left| \frac{1}{\partial_{n_0} h_{\text{mf}}/|c|} \right|_{n_0=n_-(\phi)} & \text{for } \xi > 0 \end{cases} \quad \text{for } \eta > \eta_* \\ \int d\phi \Theta(\cos^2(\phi) - \sqrt{\eta^2 - \xi^2} + \eta) \left( \left| \frac{1}{\partial_{n_0} h_{\text{mf}}/|c|} \right|_{n_0=n_+(\phi)} + \left| \frac{1}{\partial_{n_0} h_{\text{mf}}/|c|} \right|_{n_0=n_-(\phi)} \right) & \text{for } \eta < \eta_* \\ \int d\phi \left( \Theta(\cos^2(\phi) - |\xi|) \left| \frac{1}{\partial_{n_0} h_{\text{mf}}/|c|} \right|_{n_0=\tilde{n}_*(\phi)} + \frac{1}{2} \left| \frac{1}{\partial_{n_0} h_{\text{mf}}/|c|} \right|_{n_0=n_*} \right) & \text{for } \eta = \eta_* \end{cases} \quad (5.43)$$

Here,  $\partial_{n_0} \frac{h_{\text{mf}}}{|c|} = -2\xi - 2(1 - 2n_0) \cos^2(\phi)$ ,  $n_{\pm}(\phi) \equiv \frac{1}{2\cos^2(\phi)}(\cos^2(\phi) + \xi \pm \sqrt{\Delta})$ ,  $\Delta \equiv \cos^4(\phi) + 2\eta \cos^2(\phi) + \xi^2$ ,  $\tilde{n}_*(\phi) \equiv \frac{1}{2}(1 - \xi/|\xi|) + \xi/\cos^2(\phi)$ , and  $n_* \equiv \frac{1}{2}(1 + \xi/|\xi|)$ . The factor  $\frac{1}{2}$  in front of the second term for  $\eta_*$  in Eq. (5.43) accounts for the fact that  $n_*$  always coincides with a limit

of the integration over  $n_0$ . Substituting  $x$  for  $\cos^2(\phi)$ , we explicitly get:

$$\lim_{N \rightarrow \infty} \frac{\tilde{\nu}(\eta)}{N} = \begin{cases} \frac{1}{4\pi} \int_0^1 dx \sqrt{x(1-x)(x^2 + 2\eta x + \xi^2)}^{-1} & \text{for } \eta > \eta_* \\ \frac{1}{2\pi} \int_{\sqrt{\eta^2 - \xi^2} - \eta}^1 dx \sqrt{x(1-x)(x^2 + 2\eta x + \xi^2)}^{-1} & \text{for } \eta < \eta_* \\ \frac{1}{8\pi} \int_0^{|\xi|} dx \left[ \sqrt{x(1-x)}(|\xi| - x) \right]^{-1} + \frac{3}{8\pi} \int_{|\xi|}^1 dx \left[ \sqrt{x(1-x)}(x - |\xi|) \right]^{-1} & \text{for } \eta = \eta_* \end{cases} \quad (5.44)$$

Figure 5.3 depicts the restricted DOS.

At stationary points of  $h_{\text{mf}}$ , the integrand in Eq. (5.42) becomes singular. This can lead to a divergence of the DOS. We have seen in Section 5.2.2 that, for any  $0 < |\xi| < 1$ ,  $h_{\text{mf}}$  has a saddle point at  $\eta_*$ ,  $n_*$ , and  $\cos^2(\phi) = |\xi|$ . Let us analyze how this saddle point affects the integrals for the DOS at  $\eta_*$  in Eq. (5.44). Taylor expanding the denominator of the first integral around  $x = |\xi|$  yields, for small  $0 < \epsilon_1 < \epsilon_2$ ,

$$\int_{|\xi| - \epsilon_2}^{|\xi| - \epsilon_1} dx \left[ \sqrt{x(1-x)}(|\xi| - x) \right]^{-1} \approx \frac{1}{\sqrt{|\xi|(1-|\xi|)}} \int_{\epsilon_1}^{\epsilon_2} \frac{dy}{y} = \frac{1}{\sqrt{|\xi|(1-|\xi|)}} \ln(y) \Big|_{\epsilon_1}^{\epsilon_2} \xrightarrow{\epsilon_1 \rightarrow 0} \infty. \quad (5.45)$$

The same happens at the lower bound of the second integral<sup>5</sup>. Hence, the restricted DOS diverges at  $\eta_* \equiv -|\xi|$  with  $0 < |\xi| < 1$ , cf. Fig. 5.3.

Reference [253] classifies the singularities in the DOS that arise from non-degenerate stationary points of the Hamiltonian. Here, non-degenerate means that the corresponding Hessian matrix does not have zero eigenvalues. The singularities can be characterized by the dimensionality of the phase space and the number of negative eigenvalues of the Hessian matrix. Particularly, saddle points on a two-dimensional phase space lead to a DOS tending to  $+\infty$ . Our findings coincide with this general result. Additionally, Ref. [253] proves that such a divergence is always logarithmic in  $|\eta - \eta_*|$ .

## 5.4 Further Signatures

We have identified ESQPTs at  $\eta_* = -|\xi|$  with  $0 < |\xi| < 1$ . The DOS diverges at the ESQPTs but does not distinguish the excited-state phases from each other. In this section, we discuss some properties that qualitatively change at the ESQPTs.

As we have seen in Section 5.2.3, each energy hypersurface with  $\eta > \eta_*$  is a single closed loop (or point), whereas for  $\eta < \eta_*$  it consists of two disconnected loops (or points). Thus, the topology of energy hypersurfaces abruptly changes from the TF' and P' phases to the BA' phase. Such a signature of ESQPTs has been also observed in the LMG model [243].

Every connected component of an energy hypersurface with  $\eta \neq \eta_*$  corresponds to a trajectory of the mean-field dynamics, cf. Section 5.2.4. The energy hypersurfaces always respect the symmetries of the mean-field Hamiltonian. However, if an energy hypersurface consists of several connected components, each of them may break these symmetries. Since, for  $\eta > \eta_*$ , there is only one trajectory per energy hypersurface, these trajectories share the Hamiltonian symmetry  $h_{\text{mf}}(\phi \pm \pi) = h_{\text{mf}}(\phi)$ . By contrast, all trajectories with  $\eta < \eta_*$  break this symmetry. Recall that the mean-field symmetry  $h_{\text{mf}}(\phi \pm \pi) = h_{\text{mf}}(\phi)$  arises from the quantum conservation of  $\hat{I} \equiv (-1)^{\hat{N}_0}$ . However, all eigenstates of the magnetization  $\hat{D}$  with the same eigenvalue  $D$  belong

<sup>5</sup>Note that the integrands in Eq. (5.44) for  $\eta_*$  are also singular at  $x \in \{0, 1\}$ . However, the integrals do not diverge in the neighborhood of these values.

to a single eigenspace of  $\hat{I}$ . Therefore, the quantum symmetry cannot be broken within the zero-magnetization subspace. We understand the mean-field symmetry breaking as an artifact which is caused by the fact that we study the  $D = 0$  subspace in terms of coherent states from the Hilbert space comprising arbitrary  $D$ .

In the TF' and P' phases, the trajectories encircle the  $n_0$ -axis (green curves in Fig. 5.2)—clockwise in the TF' phase and counterclockwise in the P' phase. By contrast, the trajectories in the BA' phase do not enclose the  $n_0$ -axis (yellow curves). This observation lays the foundation for the order parameter that we introduce in the next section.

## 5.5 Order Parameter

An order parameter has to qualitatively distinguish between excited-state phases. Moreover, we wish it to be experimentally well accessible. For the ground-state phases, see Chapter 4, both requirements are satisfied by the relative occupation  $n_0$  of the  $m = 0$  spin state. To generalize this observable to excited states, we define [245]

$$n_0(\xi, \eta) \equiv \lim_{N \rightarrow \infty} \frac{\sum_j \langle \eta_j, N | \hat{N}_0 / N | \eta_j, N \rangle \delta(\eta_j - \eta)}{\sum_j \delta(\eta_j - \eta)}. \quad (5.46)$$

The index  $j$  labels the  $N$ -particle eigenstates of the Hamiltonian density,  $\frac{\hat{h}}{|c|} |\eta_j, N\rangle = \eta_j |\eta_j, N\rangle$ , with  $\hat{D} |\eta_j, N\rangle = 0$ . We know from Section 5.3 that

$$\lim_{N \rightarrow \infty} \frac{1}{N} \sum_j \delta(\eta_j - \eta) \equiv \lim_{N \rightarrow \infty} \frac{\tilde{\nu}(\eta)}{N} = \frac{1}{4\pi} \int_0^1 dn_0 \int_0^{2\pi} d\phi \delta\left(\frac{h_{\text{mf}}(n_0, \phi)}{|c|} - \eta\right). \quad (5.47)$$

One can analogously show that

$$\begin{aligned} \lim_{N \rightarrow \infty} \frac{1}{N} \sum_j \langle \eta_j, N | \hat{N}_0 / N | \eta_j, N \rangle \delta(\eta_j - \eta) &= \mathcal{F}^{-1} \left[ \lim_{N \rightarrow \infty} \frac{1}{N} \text{Tr}_N \hat{P}_N \frac{\hat{N}_0}{N} e^{i\zeta \hat{h}/|c|} \right] (\eta) \\ &= \frac{1}{4\pi} \int_0^1 dn_0 \int_0^{2\pi} d\phi n_0 \delta\left(\frac{h_{\text{mf}}(n_0, \phi)}{|c|} - \eta\right). \end{aligned} \quad (5.48)$$

Recall that, here,  $\hat{P}_N$  denotes the projection onto the  $N$ -particle eigenspace of  $\hat{D}$  with eigenvalue  $D = 0$ . Equation (5.48) can be evaluated<sup>6</sup> similarly to the DOS, see Eq. (5.43). Explicitly, we find

$$n_0(\xi, \eta) = \left( \lim_{N \rightarrow \infty} \frac{\tilde{\nu}(\eta)}{N} \right)^{-1} \times \begin{cases} \frac{1}{8\pi} \int_0^1 dx \frac{x + \xi + \sqrt{\Delta}}{x \sqrt{x(1-x)\Delta}} & \text{for } \eta > \eta_*, \xi < 0 \\ \frac{1}{8\pi} \int_0^1 dx \frac{x + \xi - \sqrt{\Delta}}{x \sqrt{x(1-x)\Delta}} & \text{for } \eta > \eta_*, \xi > 0 \\ \frac{1}{4\pi} \int_{\sqrt{\eta^2 - \xi^2} - \eta}^1 dx \frac{x + \xi}{x \sqrt{x(1-x)\Delta}} & \text{for } \eta < \eta_* \end{cases} \quad (5.49)$$

with  $\Delta \equiv x^2 + 2\eta x + \xi^2$ .

Figure 5.4 shows that, just as the DOS,  $n_0(\xi, \eta)$  becomes singular at the ESQPTs but detects no qualitative difference between the excited-state phases. Hence, we need another approach to the search for an order parameter. Already Ref. [41] emphasizes that ESQPTs are related to mean-field dynamics. Following this direction, we succeed in constructing an order parameter that is experimentally well accessible.

<sup>6</sup>Note that Eq. (5.48) is essentially a  $\tau$ -integral over the mean-field dynamics  $n_0(\tau)$ .

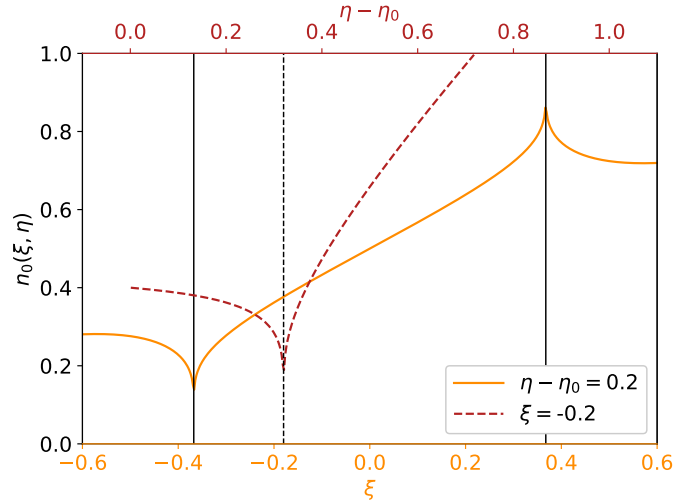


**Figure 5.4:** Mean-field limit  $n_0(\xi, \eta)$  of  $\langle \hat{N}_0/N \rangle$  in the eigenstates of  $\hat{h}(\xi)/|c|$  with eigenvalue  $\eta$ . At the ESQPTs (black lines),  $n_0(\xi, \eta)$  exhibits singularities. Though  $n_0(\xi, \eta)$  is an order parameter of the ground-state quantum phases, it fails to qualitatively distinguish the excited-state phases. Thus,  $n_0(\xi, \eta)$  does not qualify for being an order parameter of the ESQPTs.

All trajectories with  $\eta_0 < \eta < \eta_*$  or  $\eta_* < \eta < \eta_{\max}$  trace closed loops in phase space, see Section 5.2.4. This means that the corresponding dynamics  $(n_0(\tau), \phi(\tau))$  is periodic. We denote the period by  $\tilde{\mathcal{T}}$ . The winding number

$$w \equiv \frac{1}{2\pi} \int_0^{\tilde{\mathcal{T}}} d\tau \phi'(\tau) \quad (5.50)$$

counts how often  $\phi(\tau)$  counterclockwise encircles the  $n_0$ -axis during  $\tilde{\mathcal{T}}$ . Its value does not depend on the precise functional form of  $\phi(\tau)$ . We already know from Sections 5.2.3 and 5.4 that

$$w = \begin{cases} -1 & \text{for } \eta_* < \eta < \eta_{\max}, \quad \xi < 0 \\ 0 & \text{for } \eta_0 < \eta < \eta_* \\ 1 & \text{for } \eta_* < \eta < \eta_{\max}, \quad \xi > 0 \end{cases}. \quad (5.51)$$

Hence,  $w$  constitutes an order parameter that distinguishes the phases TF' ( $w = -1$ ), BA' ( $w = 0$ ), and P' ( $w = 1$ ) from each other. Note, however, that the winding number is not defined for the point-like trajectories at the lower and upper bound of the energy spectrum.

In Section 5.2.5, we have derived an expression for the period  $\mathcal{T}$  of  $n_0(\tau)$ .  $\tilde{\mathcal{T}}$  is the least common multiple of  $\mathcal{T}$  and the period of  $\phi(\tau)$ . The conservation of energy density implies that, for  $n_0 \notin \{0, 1\}$ ,

$$\cos^2(\phi) = \frac{\xi(1 - 2n_0) - \eta}{2n_0(1 - n_0)} \quad (5.52)$$

satisfies  $\cos^2(\phi(\tau + \mathcal{T})) = \cos^2(\phi(\tau))$ . Recall from Section 5.2.4 that  $n_0 \in \{0, 1\}$  is attained only at  $\eta \in \{\eta_*, \eta_{\max}\}$ . Hence, for  $\eta \notin \{\eta_*, \eta_{\max}\}$ ,  $\phi(\tau + \mathcal{T}) = \phi(\tau) + \pi z$  with  $z \in \mathbb{Z}$  independent of  $\tau$ . An even  $z$  implies  $\tilde{\mathcal{T}} = \mathcal{T}$ , whereas an odd  $z$  entails  $\tilde{\mathcal{T}} = 2\mathcal{T}$ . In the BA' phase,  $\phi(\tau) + \pi z$  with  $z$  odd belongs to another trajectory than  $\phi(\tau)$ , see Section 5.2.4. Therefore,  $z$  must be even and  $\tilde{\mathcal{T}} = \mathcal{T}$ . On the other hand, the trajectories in the TF' and P' phases respect the Hamiltonian

symmetry  $h_{\text{mf}}(\phi \pm \pi) = h_{\text{mf}}(\phi)$ . This entails that the period of  $\phi(\tau)$  is at least two times  $\mathcal{T}$  and, hence,  $\tilde{\mathcal{T}} = 2\mathcal{T}$ . According to the EOMs (5.5),  $\phi'(\tau)$  is  $\mathcal{T}$ -periodic. Therefore, we can rewrite the winding number as

$$w = \begin{cases} \frac{1}{\pi} \int_0^{\mathcal{T}} \phi'(\tau) = \frac{\phi(\mathcal{T}) - \phi(0)}{\pi} & \text{for TF', P'} \\ \frac{1}{2\pi} \int_0^{\mathcal{T}} \phi'(\tau) = \frac{\phi(\mathcal{T}) - \phi(0)}{2\pi} & \text{for BA'} \end{cases}. \quad (5.53)$$

Here,  $\phi(\tau)$  is considered as a function to  $\mathbb{R}$  rather than to  $\mathbb{R} \bmod 2\pi$ . Since, in the BA' phase,  $\phi(\mathcal{T}) - \phi(0) = 0$ , we may simplify our expression for  $w$  to

$$w = \frac{\phi(\mathcal{T}) - \phi(0)}{\pi}. \quad (5.54)$$

There is no measurable difference between  $\phi(\tilde{\mathcal{T}})$  and  $\phi(0)$ . Therefore, Eq. (5.51) might lead to the impression that  $w$  can be deduced only by monitoring the entire evolution of  $\phi$ . However, the values 0 and  $\pm\pi$  attained by  $\phi(\mathcal{T}) - \phi(0)$  in Eq. (5.54) are physically distinct. In the following section, we present an interferometric protocol that gives access to the order parameter

$$p \equiv \cos(\phi(\mathcal{T}) - \phi(0)) = \cos(\pi w) = \begin{cases} -1 & \text{for TF', P'} \\ 1 & \text{for BA'} \end{cases}. \quad (5.55)$$

Note that, though  $p$  does not tell apart all three excited-state phases, it still distinguishes the adjacent ones.

## 5.6 Proposal

The order parameter  $p \equiv \cos(\phi(\mathcal{T}) - \phi(0))$  introduced in the previous section can be measured interferometrically. First, one has to decide on an instance of  $(\xi, \eta)$  at which  $p$  shall be determined. This fixes an energy hypersurface of the mean-field model, from which one chooses a starting point  $(n_0(0), \phi(0))$ . The experiment begins by preparing, at an effective quadratic Zeeman shift of  $q = 2|c|\xi$ , a coherent state  $|\psi(0)\rangle$  that is specified by  $d = 0$ ,  $\phi_1 - \phi_{-1} = 0$ , and the chosen  $(n_0(0), \phi(0))$ . After a free evolution<sup>7</sup> for one period  $T \equiv \hbar\mathcal{T}/|c|$  of  $n_0(t)$ , the spin states with  $m = 0$  and  $m = \pm 1$  are coupled by the symmetric beamsplitter  $e^{-i\frac{\pi}{2}\hat{S}_\vartheta}$  with  $\hat{S}_\theta \equiv \cos(\theta)\hat{S}_x + \sin(\theta)\hat{S}_y$  and  $\vartheta \equiv \pi/2 - \phi(0)$ . The definition of  $\hat{S}_{x/y}$  can be found in Eq. (3.50). Each iteration of the experiment ends with a measurement of  $\hat{N}_0/N$ .

The order parameter  $p$  is encoded in the expectation value

$$\langle \hat{N}_0/N \rangle \equiv \frac{1}{N} \langle \psi(T) | e^{i\frac{\pi}{2}\hat{S}_\vartheta} \hat{N}_0 e^{-i\frac{\pi}{2}\hat{S}_\vartheta} | \psi(T) \rangle. \quad (5.56)$$

The relation between  $\langle \hat{N}_0/N \rangle$  and  $p$  reveals itself in the mean-field limit. Using Eq. (3.53) and  $\hat{g}^{(\dagger)} \equiv \frac{1}{\sqrt{2}}(\hat{a}_1^{(\dagger)} + \hat{a}_{-1}^{(\dagger)})$ , we obtain

$$\begin{aligned} e^{i\frac{\pi}{2}\hat{S}_\vartheta} \hat{N}_0 e^{-i\frac{\pi}{2}\hat{S}_\vartheta} &= \frac{1}{2}(\hat{a}_0^\dagger - e^{-i\phi(0)} \hat{g}^\dagger)(\hat{a}_0 - e^{i\phi(0)} \hat{g}) \\ &= \frac{1}{4}(N - \hat{N}_0 + \hat{a}_1^\dagger \hat{a}_{-1} + \hat{a}_{-1}^\dagger \hat{a}_1) \\ &\quad - \frac{1}{2\sqrt{2}} \left[ e^{-i\phi(0)} (\hat{a}_1^\dagger + \hat{a}_{-1}^\dagger) \hat{a}_0 + e^{i\phi(0)} \hat{a}_0^\dagger (\hat{a}_1 + \hat{a}_{-1}) \right]. \end{aligned} \quad (5.57)$$

<sup>7</sup>Here, ‘‘free evolution’’ means the evolution with the many-body Hamiltonian (5.1).

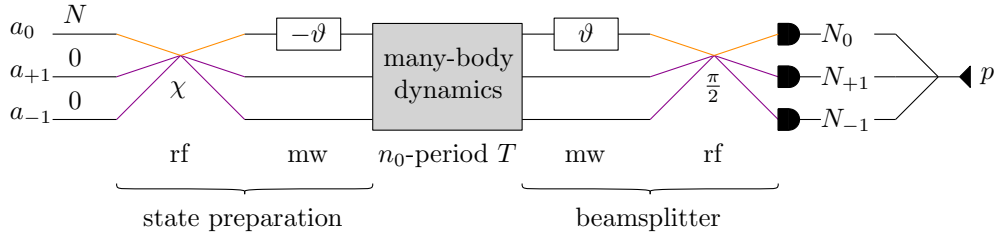


**Figure 5.5:** Measuring the order parameter  $p$  of ESQPTs in a spin-1  $^{87}\text{Rb}$  BEC. Starting from the P state, the coherent state  $|\psi(0)\rangle$  with energy density  $\eta$  is prepared at  $\xi$  by a radio-frequency (rf) pulse of amplitude  $\chi$ ,  $\cos^2(\chi/2) = n_0(0)$ , and a microwave (mw) pulse of amplitude  $-\vartheta \equiv \phi(0) - \pi/2$ . The state  $|\psi(0)\rangle$  freely evolves for one period  $T$  of  $n_0(t)$ . A beamsplitter composed from another mw and rf pulse encodes the phase  $\phi(T) - \phi(0)$  into atom numbers. Counting the atoms in different spin states reveals  $\langle N_0/N \rangle$  and, thus,  $p$ .

Since  $|\psi(0)\rangle$  is a coherent state, we can evaluate  $\lim_{N \rightarrow \infty} \langle \hat{N}_0/N \rangle$  according to Eq. (3.111): substituting  $\hat{a}_m$  and  $\hat{a}_m^\dagger$  by  $\sqrt{N n_m(T)} e^{i\phi_m(T)}$  and  $\sqrt{N n_m(T)} e^{-i\phi_m(T)}$ , respectively, yields

$$\begin{aligned} \lim_{N \rightarrow \infty} \frac{1}{N} \langle \psi(T) | e^{i\frac{\pi}{2}\hat{S}_\vartheta} \hat{N}_0 e^{-i\frac{\pi}{2}\hat{S}_\vartheta} | \psi(T) \rangle &= \frac{1}{2} \left( 1 - 2\sqrt{n_0(T)(1-n_0(T))} \cos(\phi(T) - \phi(0)) \right) \\ &= \frac{1}{2} \left( 1 - 2\sqrt{n_0(0)(1-n_0(0))} \right) p \\ &\equiv \frac{1}{2}(1 - Vp). \end{aligned} \quad (5.58)$$

The visibility  $V \equiv 2\sqrt{1-n_0(0)}\sqrt{n_0(0)}$  vanishes only for  $n_0(0) \in \{0, 1\}$ . Recall that these values of  $n_0$  correspond to point-like trajectories, for which  $p$  is not defined. Hence, for all  $(\xi, \eta)$  with well-defined  $p$ , the proposed experimental protocol, indeed, extracts the value of the order parameter.

Our proposal requires three experimental techniques: preparing a specific coherent state, implementing the internal-state beamsplitter  $e^{-i\frac{\pi}{2}\hat{S}_\vartheta}$ , and measuring  $\hat{N}_0$ . Assume that the spin-1 BEC is initialized in the P state  $\hat{a}_0^{\dagger N} |0\rangle / \sqrt{N!}$  [25, 35]. The coherent state  $|\psi(0)\rangle$  can be then obtained by applying  $e^{-i\chi\hat{S}_\vartheta}$  with  $\cos^2(\chi/2) = n_0(0)$ . Thus, both the state preparation and the beamsplitter correspond to operators of the form

$$e^{-i\zeta\hat{S}_\vartheta} = e^{-i\vartheta\hat{N}_0} e^{-i\zeta\hat{S}_x} e^{i\vartheta\hat{N}_0}. \quad (5.59)$$

For a BEC of  $^{87}\text{Rb}$  atoms in their hyperfine ground state, we have seen in Section 3.5 that  $e^{i\vartheta\hat{N}_0}$  and  $e^{-i\zeta\hat{S}_x}$  can be implemented by a microwave or radio-frequency pulse, respectively. Note that applying  $e^{i\vartheta\hat{N}_0}$  to the P state affects only its global phase, and that  $e^{i\vartheta\hat{N}_0} \hat{N}_0 e^{-i\vartheta\hat{N}_0} = \hat{N}_0$ . Therefore, the first of the three pulses for state preparation and the last one of the beamsplitter can be omitted. The resulting experimental sequence is summarized in Fig. 5.5. To measure  $\hat{N}_0$  one can, e. g., spatially separate the different spin states by a magnetic-field gradient and then perform absorptive imaging [267].

## 5.7 Experimental Feasibility

Our proposal for measuring the order parameter  $p$  of the ESQPTs is based on the mean-field properties of spinor BECs. Therefore, one might expect that it is comparatively easy to realize—

the more so as the mean-field dynamics has been already explored experimentally [46, 149]. Nevertheless, the proposal raises several questions regarding its feasibility.

Below we show, in Section 5.7.1, how to ensure a high visibility of the interferometric signal. Furthermore, we find that neither realistic coherence times (Section 5.7.2) nor realistic system sizes (Section 5.7.3) significantly impair the proposed measurement. Our analysis in Section 5.7.4 identifies magnetic-field stability as the central experimental challenge in extracting  $p$ .

We pay particular attention to the case of  $^{87}\text{Rb}$  atoms [25, 49]. However, most of our discussion applies to any ferromagnetic spin-1 BEC.

### 5.7.1 Visibility

In Section 5.6, we have introduced the visibility

$$V \equiv 2\sqrt{1 - n_0(0)}\sqrt{n_0(0)} \in [0, 1]. \quad (5.60)$$

A large value of  $V$  increases the confidence with which an order parameter of  $p = 1$  can be experimentally distinguished from  $p = -1$ . To maximize the visibility,  $n_0(0)$  has to be chosen as close to  $1/2$  as possible.

Not every phase-space trajectory passes through a point with  $n_0 = 1/2$ . We want to identify the optimal  $n_0(0)$  for given  $\xi$  and  $\eta$ . Recall from Section 5.2.5 that, for  $\xi > 0$ ,  $n_0(t)$  oscillates between  $x_1$  and  $x_2 \geq x_1$ ,

$$\begin{aligned} x_1 &\equiv \frac{1}{2}(1 + |\xi| - \sqrt{1 + \xi^2 + 2\eta}), \\ x_2 &\equiv \begin{cases} \frac{1}{2}(1 + |\xi| + \sqrt{1 + \xi^2 + 2\eta}) & \text{for } \eta < \eta_* \\ \frac{1}{2}(1 - \eta/|\xi|) & \text{for } \eta \geq \eta_* \end{cases}. \end{aligned} \quad (5.61)$$

We observe that

$$\begin{aligned} x_1 \leq \frac{1}{2} &\Leftrightarrow \eta \geq -\frac{1}{2}, \\ x_2 \geq \frac{1}{2} &\Leftrightarrow \begin{cases} \text{always} & \text{for } \eta < \eta_* \\ \eta \leq 0 & \text{for } \eta \geq \eta_* \end{cases}. \end{aligned} \quad (5.62)$$

Hence, for  $\xi > 0$ , the optimal visibility is attained by setting  $n_0(0)$  to

$$n_{\text{opt}}^{(+)} = \begin{cases} x_1 & \text{for } \eta < -\frac{1}{2} \\ \frac{1}{2} & \text{for } -\frac{1}{2} \leq \eta \leq 0 \\ \frac{1}{2}(1 - \eta/|\xi|) & \text{for } 0 < \eta \end{cases} \quad (5.63)$$

As discussed in Section 5.2.5, we can express  $n_0(t)$  for  $\xi < 0$  in terms of  $n_0(t)$  for  $|\xi|$  as  $n_0(\xi < 0; t) = 1 - n_0(|\xi|; t)$ . For  $\xi < 0$ , the inequalities (5.62) therefore imply an optimal  $n_0(0)$  of

$$n_{\text{opt}}^{(-)} = \begin{cases} 1 - x_1 & \text{for } \eta < -\frac{1}{2} \\ \frac{1}{2} & \text{for } -\frac{1}{2} \leq \eta \leq 0 \\ 1 - \frac{1}{2}(1 - \eta/|\xi|) & \text{for } 0 < \eta \end{cases} \quad (5.64)$$

The expressions for  $n_{\text{opt}}^{(+)}$  and  $n_{\text{opt}}^{(-)}$  can be combined into an  $n_{\text{opt}}$  valid for arbitrary  $\xi \neq 0$ :

$$n_{\text{opt}} = \begin{cases} \frac{1}{2}(1 + \xi - \frac{\xi}{|\xi|}\sqrt{1 + 2\eta + \xi^2}) & \text{for } \eta < -\frac{1}{2} \\ \frac{1}{2} & \text{for } -\frac{1}{2} \leq \eta \leq 0 \\ \frac{1}{2}(1 - \eta/\xi) & \text{for } 0 < \eta \end{cases} \quad (5.65)$$



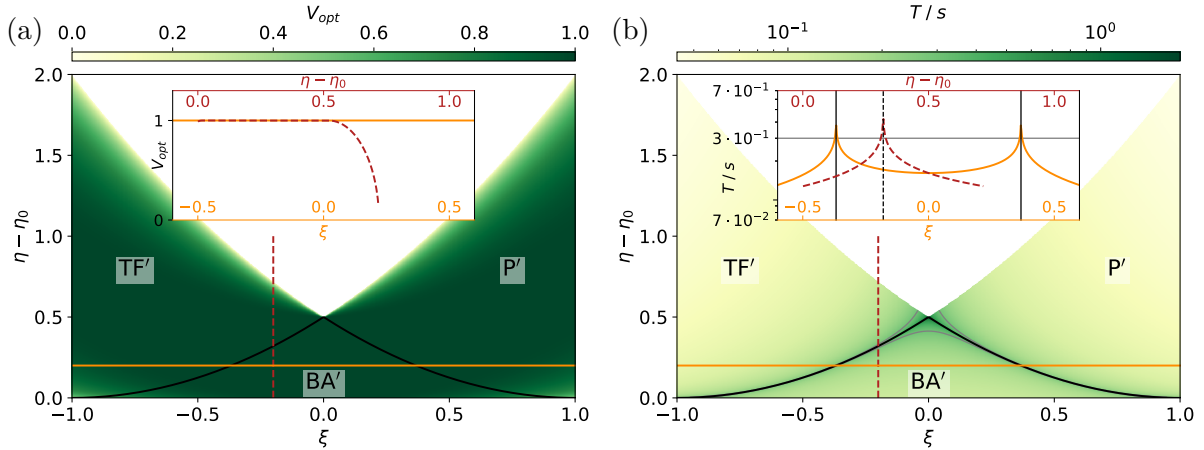


**Figure 5.6:** Measuring the order parameter  $p$  benefits from a large visibility  $V_{\text{opt}}$  and a short period  $T$ . (a)  $V_{\text{opt}}$  is large throughout the vast majority of the phase diagram. (b)  $T$  for  $|c|/\hbar = 2\pi \times 4$  Hz. A moderate value of 0.3 s (gray) is surpassed only in the immediate vicinity of the ESQPTs. (a)–(b) Black lines mark the ESQPTs. The insets show  $V_{\text{opt}}$  and  $T$  along lines of constant  $\xi = -0.2$  (red, dashed) and  $n - n_0 = 0.2$  (orange, solid).

The phase  $\phi_{\text{opt}}$  at which the trajectory specified by  $\xi$  and  $\eta$  passes  $n_{\text{opt}}$  is determined by the conservation of energy density,

$$\cos^2(\phi_{\text{opt}}) = \frac{\xi(1 - 2n_{\text{opt}}) - \eta}{2n_{\text{opt}}(1 - n_{\text{opt}})}. \quad (5.66)$$

Figure 5.6a depicts the optimal visibility  $V_{\text{opt}}$  corresponding to  $n_{\text{opt}}$ . It shows that  $V_{\text{opt}}$  is large throughout the vast majority of the phase diagram. In the proposed experiment, the optimal visibility is attained by choosing  $(n_0(0), \phi(0)) = (n_{\text{opt}}, \phi_{\text{opt}})$  in the coherent state preparation.

### 5.7.2 Finite Time

The duration of the experiment proposed in Section 5.6 is essentially determined by the period  $T$  of the mean-field evolution  $n_0(t)$ . Hence, measuring the order parameter  $p$  requires an experimental coherence time of the BEC that is greater than  $T$ . The coherence time is usually limited to few seconds [35, 149]. Based on the expression for  $\mathcal{T} \equiv |c|T/\hbar$  in Eq. (5.21), Fig. 5.6b displays  $T$  for a typical interaction strength of  $|c|/\hbar = 2\pi \times 4$  Hz [25, 35]. As discussed in Section 5.2.5,  $T$  diverges at the ESQPTs. However, fortunately, acceptable values of  $T$  are exceeded only in the immediate vicinity of the ESQPTs. In Fig. 5.6b, this is illustrated by the gray lines indicating  $T = 0.3$  s.

### 5.7.3 Finite Size

So far, we have always considered the mean-field limit, i. e., BECs of  $N \rightarrow \infty$  atoms. It is crucial to examine whether the mean-field predictions provide a sufficiently accurate description of realistic finite-size systems. In typical BEC experiments,  $N$  is of the order of  $10^4$  [25, 49]. Simulating, for  $N = 100$ , a measurement of the order parameter  $p$  by exact diagonalization of the Hamiltonian density (5.1) yields Fig. 5.7. In the mean-field limit,  $p$  jumps at the ESQPTs from  $p = -1$  in the TF' and P' phases to  $p = 1$  in the BA' phase. As expected, proceeding to finite  $N$  smooths these discontinuities. Note that, according to the inset in Fig. 5.7, small features in  $p$



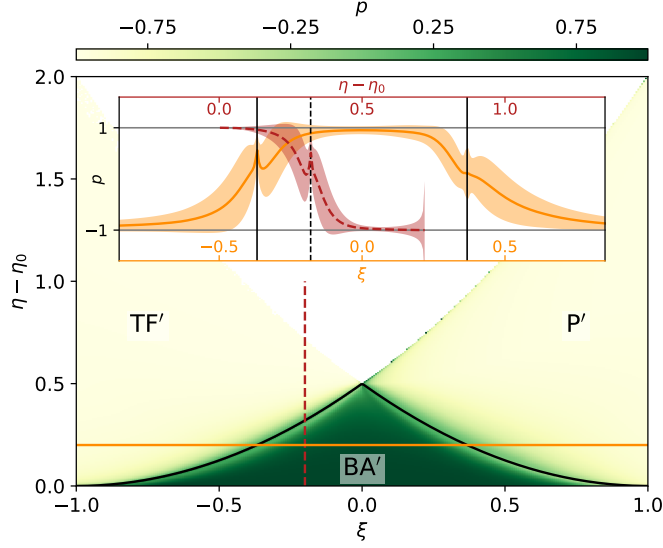


**Figure 5.7:** Measuring  $p$  in a BEC of  $N = 100$  atoms. The finite-size results closely resemble the mean-field limit, where  $p = 1$  in the  $BA'$  phase and  $p = -1$  in the  $TF'$  and  $P'$  phases. Black lines mark the ESQPTs. The inset shows  $p$  along lines of constant  $\xi = -0.2$  (red, dashed) and  $\eta - \eta_0 = 0.2$  (orange, solid). The shaded regions indicate the standard deviation.

give nonetheless access to the exact position of the ESQPTs. But most importantly, the  $BA'$  phase can be still clearly distinguished from the  $TF'$  and  $P'$  phases. For typical  $N \sim 10^4$ , an even much closer resemblance to the mean-field predictions can be expected.

#### 5.7.4 Magnetic-Field Fluctuations

Magnetic-field fluctuations probably pose the only serious challenge to our proposal. Recall that we are describing the BEC in a rotating reference frame, cf. Sections 3.3.1 and 3.5.2. This rotating frame absorbs the constant linear Zeeman effect corresponding to the intended magnetic field  $B_0$ . For atoms with electronic spin  $s = 1/2$  and orbital angular momentum  $l = 0$ , fluctuations  $B(t)$  on top of  $B_0$  contribute, to first order,

$$\hat{H}_B(t) \equiv -(-1)^{f-i+1/2} \frac{g_j \mu_B}{2i+1} B(t) \hat{D} \quad (5.67)$$

to the Hamiltonian of the BEC. Here,  $f$  is the hyperfine spin,  $i$  the nuclear spin,  $\mu_B$  the Bohr magneton, and  $g_j \approx 2$  the Landé g-factor, cf. Eq. (3.18).  $\hat{H}_B$  commutes with the Hamiltonian density in Eq. (5.1). Therefore, in the presence of magnetic-field fluctuations, the Hamiltonian evolution in our proposal yields

$$|\tilde{\psi}(T)\rangle \equiv e^{-i\beta \hat{D}} |\psi(T)\rangle, \quad \beta \equiv -(-1)^{f-i+1/2} \frac{g_j \mu_B}{(2i+1)\hbar} \int_0^T dt B(t). \quad (5.68)$$

The expectation value of the measurement outcome thus becomes

$$\overline{\lim_{N \rightarrow \infty} \frac{1}{N} \langle \tilde{\psi}(T) | e^{i\frac{\pi}{2} \hat{S}_\vartheta} \hat{N}_0 e^{-i\frac{\pi}{2} \hat{S}_\vartheta} | \tilde{\psi}(T) \rangle} = \frac{1}{4} (1 + \overline{\cos(\beta)}) + \frac{1}{4} n_0 (1 - \overline{\cos(\beta)}) - \frac{V}{2} \overline{\cos(\beta)} p, \quad (5.69)$$

where the bars indicate averages over  $\beta$ .

Equation (5.69) imposes, basically, the requirement  $|\beta| \ll 2\pi$ . To benchmark the stability of the magnetic field needed for  $^{87}\text{Rb}$  atoms in their hyperfine ground state, we set  $i = 3/2$  and assume a constant  $B(t) \equiv b$  and an evolution time of  $T = 0.3\text{ s}$ , cf. Section 5.7.2. Then

$$|\beta| \ll 2\pi \Leftrightarrow |b| \ll 5\ \mu\text{G}. \quad (5.70)$$

This is ambitious: we are not aware of any BEC experiment with a magnetic-field stability beating the level of  $20\ \mu\text{G}$  [49]. However, Ref. [49] did not especially strike for low magnetic-field noise. We expect that a further improvement is demanding but technically feasible. Furthermore, this issue can be addressed not only by stabilizing the magnetic field. For example, one can diminish  $T \equiv \hbar\mathcal{T}/|c|$  by increasing the density of the BEC and, thus,  $|c|$ . Staying further away from the ESQPTs also limits the relevant periods  $T$  to shorter times. Note that the sign of  $\hat{H}_B$  in Eq. (5.67) depends on  $f$ . Therefore, in a  $^{87}\text{Rb}$  BEC with hyperfine spin  $f = 1$ , a variation of  $B(t)$  that is much slower than  $T$  could be possibly compensated by an echo protocol employing  $f = 2$  states. To design a suitable protocol, one has to carefully account for the dynamics in both  $f = 1$  and  $f = 2$  states.

## 5.8 Bosonic Two-Level Pairing Models

Most of our observations on ESQPTs in magnetization-free ferromagnetic spin-1 BECs ensue from the mean-field model in Eq. (5.4). Thus, they also hold for any other quantum system with the same mean-field limit.

Let us introduce a class of bosonic two-level pairing models with Hamiltonian densities

$$\frac{\hat{h}_{\text{sb}}}{|c|} = \frac{\xi}{N}(N - 2\hat{N}_s) + \frac{1}{N^2} \left[ (-1)^j \hat{N}_s(N - \hat{N}_s) + \frac{1}{2} \sum_{\mu} (-1)^{\mu} (\hat{s}^{\dagger 2} \hat{b}_{\mu} \hat{b}_{-\mu} + \hat{b}_{\mu}^{\dagger} \hat{b}_{-\mu}^{\dagger} \hat{s}^2) \right]. \quad (5.71)$$

Here,  $\hat{s}^{(\dagger)}$  and  $\hat{b}_{\mu}^{(\dagger)}$  are bosonic creation and annihilation operators,  $\hat{N}_s \equiv \hat{s}^{\dagger} \hat{s}$ ,  $\sum_{\mu} \hat{b}_{\mu}^{\dagger} \hat{b}_{\mu} + \hat{N}_s = N$ , and  $j \in \mathbb{N}_0$ . The sum over  $\mu \in \{j, j-1, \dots, -j\}$  may or may not include  $\mu = 0$ . According to Ref. [241], all models defined by Eq. (5.71) exhibit an  $SO(n)$  symmetry, where  $n = 2j$  if  $\mu \neq 0$  or  $n = 2j + 1$  otherwise. This leads to the conservation of a generalized angular momentum operator  $\hat{C}$ . Remarkably, restricted to the respective eigenspace of  $\hat{C}$  with eigenvalue  $C = 0$ , the mean-field limits of all models in Eq. (5.71) coincide.

For  $j = 1$  and  $\mu \neq 0$ , the angular momentum operator becomes  $\hat{C} = \hat{b}_1^{\dagger} \hat{b}_1 - \hat{b}_{-1}^{\dagger} \hat{b}_{-1}$ . Identifying  $\hat{s}^{(\dagger)}$  with  $\hat{a}_0^{(\dagger)}$  and  $\hat{b}_{\pm 1}^{(\dagger)}$  with  $\hat{a}_{\pm 1}^{(\dagger)}$ , we immediately observe that the mean-field limit of  $\hat{h}_{\text{sb}}$  with  $C = 0$  yields precisely the model studied throughout the present chapter. Hence, our results are applicable to all  $\hat{h}_{\text{sb}}$  in the  $C = 0$  subspace. Reference [241] is devoted to ESQPTs in bosonic two-level pairing models with the opposite sign of interaction, i. e., a minus sign in front of the square bracket in Eq. (5.71). Therefore, our investigation complements Ref. [241].

In summary, a spin-1 BEC simulates the large- $N$  behavior of all bosonic two-level pairing models from the class (5.71) with zero angular momentum. Such models appear in various physical contexts: for example, if  $\mu = 0$  is included,  $j = 0$  yields an LMG model,  $j = 1$  a vibron model for molecules, and  $j = 2$  an interacting boson model for nuclei.

## 5.9 Conclusion

Extending the ground-state phase diagram for magnetization-free ferromagnetic spin-1 BECs across the spectrum, we have identified three excited-state phases. They can be distinguished by

the value of a winding number characterizing the mean-field dynamics. The winding number gives rise to an order parameter of the ESQPTs that can be extracted by interferometry. Remarkably, spinor BECs simulate the mean-field driven ESQPT physics of a large class of quantum systems.

Our work facilitates the experimental investigation of ESQPTs in spinor BECs. This has a threefold value since experiments on ESQPTs are rare, spinor BECs offer particularly good experimental control, and the ESQPTs in spinor BECs are prototypical for a large class of quantum systems. In contrast to most other studies on ESQPTs, we introduce an experimentally accessible order parameter. This is an important contribution to the characterization of excited-state phases. A thorough characterization of phases can, in turn, reveal potential applications of ESQPTs in quantum-state engineering.

The interferometric extraction of the order parameter is feasible. However, the proposed experiment is highly susceptible to magnetic-field fluctuations. Though the required magnetic-field stability seems to be within reach, it would be desirable to develop a more robust experimental protocol or to find a more convenient order parameter. For example, it might be advantageous to follow Ref. [44] and consider the time average of  $\langle \psi(t) | \hat{S}_x | \psi(t) \rangle$ , where  $\hat{S}$  is a collective pseudospin-1/2 operator introduced in Eq. (3.50) and  $|\psi(0)\rangle$  an initial coherent state as in Section 5.6.

In Chapter 4, we have identified the quantum Fisher information (QFI) as an order parameter of the ground-state QPTs. So far, we have not examined whether the QFI distinguishes also the excited-state phases. Because of the great importance of the QFI for quantum-state engineering, this is a particularly relevant question. We expect that it can be addressed by the method employed at the beginning of Section 5.5.

Another topic that we have not yet explored concerns the quench dynamics related to ESQPTs in spinor BECs. Let us remark that squeezed states of spinor BECs are commonly generated by quenching [151–153], cf. also Section 4.8. These quenches are performed precisely along an ESQPT.



## 6 Conclusion and Outlook

Experiment is the supreme judge of all and every physical theory.

---

L. Landau and Y. Rumer  
in *What is the theory of relativity*

We have investigated ferromagnetic spin-1 Bose-Einstein condensates (BECs) with zero magnetization, focusing on the ground- and excited-state quantum phases with respect to the effective quadratic Zeeman shift as a control parameter.

Chapter 4 was devoted to the ground-state phase diagram. We have evaluated the quantum Fisher information (QFI) for collective unitary phase imprinting and identified optimal phase-imprinting and measurement operators. The QFI constitutes an order parameter of the ground-state quantum phase transitions (QPTs). Its maximal value—amounting to about half the Heisenberg limit (HL)—is attained by the central broken-axisymmetry (CBA) and the Twin-Fock (TF) state. These highly entangled states can be accessed by adiabatically driving a BEC from the non-entangled polar (P) state across one—for the CBA state—or two—for the TF state—QPTs. We have focused on the less known and, in terms of adiabatic driving, closer CBA state and have developed two proposals. First, the CBA state can serve as a probe for quantum-enhanced interferometry. Second, measuring the atom number in one out of three spin modes generates, with high probability and heralded by the measurement outcome, macroscopic superposition states (MSSs).

In Chapter 5, we have extended the ground-state phase diagram across the spectrum. There are three excited-state phases, each of which ensues from one of the three ground-state phases. The excited-state quantum phase transitions (ESQPTs) are signaled by a diverging density of states (DOS). A winding number that can be assigned to the mean-field phase-space trajectories is in one-to-one correspondence to the excited-state phases and, thus, constitutes an order parameter of the ESQPTs. We have proposed an interferometric scheme that measures a related order parameter encoded in the evolution of coherent states. The mean-field model governing the ESQPTs in a spin-1 BEC with zero magnetization describes also the infinite-size limit of many other quantum models, which are relevant for, e. g., molecular and nuclear physics. Because of the superior experimental control, spinor BECs can be considered as simulators for the ESQPTs in other systems from the same universality class.

This thesis contains three proposals. We are highly interested in their experimental realization. Quantum-enhanced interferometry based on the CBA state of over 10 000  $^{87}\text{Rb}$  atoms has been already demonstrated in Ref. [49]. This proof-of-principle experiment establishes the adiabatic state preparation across QPTs as a valuable tool for quantum-enhanced metrology. Furthermore, it can be regarded as an important step towards the interferometry with more than two internal modes. The proof-of-principle experiment in Ref. [49] does not measure any relevant physical quantity. Combining it with the experiment in Ref. [25] would yield a quantum-enhanced microwave atomic clock. However, its precision would not be competitive with state-of-the-art clocks. It is thus an open and intriguing question whether the CBA state can provide the basis for some quantum-enhanced technology such as, e. g., quantum-enhanced radio telescopes. Another interesting task is to identify further applications of the adiabatic state preparation across QPTs.

Generalizing our analysis of the ground-state QFI to spinor BECs with larger spins would further contribute to the investigation of multi-mode quantum-enhanced interferometry.

Our second proposal concerns the generation of NOON-like MSSs. Greenberger-Horne-Zeilinger (GHZ) and NOON states constitute a paradigmatic class of entangled MSSs. So far, experimental realizations of such states have been limited to less than 30 massive particles [36–39]. By contrast, our proposal aims at  $10^2$ - $10^5$  atoms. The experimental protocol is ambitious, but all required technologies have been already demonstrated. Moreover, our numerical analysis shows that the generation of MSSs tolerates both a reasonably swift quasiadiabatic passage in the presence of atom loss and uncertainties of atom counting. So far, we have not elaborated on the characterization of the generated MSSs, which is a prerequisite for any experimental realization. We expect that it is possible to adapt methods from related experiments [49, 113]. A detailed investigation of entanglement decay in the MSSs could be used to probe the validity of quantum physics for ensembles of many atoms.

Third, we have proposed an interferometric scheme that measures an order parameter of the ESQPTs. This addresses both the lack of experimental results on ESQPTs and the scarcity of order parameters distinguishing the excited-state phases. According to our analysis, the interferometric measurement is feasible but requires an outstanding control over magnetic-field noise. The necessary level of magnetic-field stability can be reduced by increasing the density of the BEC or by restricting oneself to appropriate regions of the phase diagram. However, a more robust experimental protocol remains desirable. Maybe, some other order parameter would be easier to measure. In any case, identifying further order parameters would contribute to the characterization of the excited-state phases. This, in turn, could lead on to applications in quantum-state engineering. In this regard, the QFI is an especially relevant potential order parameter that needs to be investigated. Another topic that this thesis has barely touched upon is the quench dynamics related to ESQPTs. This is particularly interesting in the context of quantum many-body systems out of equilibrium. However, the mean-field model of spin-1 BECs is integrable [268], whereas out-of-equilibrium dynamics is mainly studied in non-integrable systems. Therefore, the excited-state phase diagrams of spinor BECs with larger spins promise qualitatively different insights. Beyond spinor BECs, we are curious whether our order parameter will inspire similar constructions in different quantum systems.

In summary, this thesis investigates spinor BECs and contributes to the fields of quantum-state engineering, quantum-enhanced interferometry, and excited-state quantum phases.

## 7 Acknowledgment

A Russian proverb says: “A single ember won’t burn even in the stove but two will blaze even in the field.” My doctorate would not have been successful without the guidance, inspiration, and support by many others.

First and foremost, I would like to thank Prof. Luis Santos for introducing me to the fascinating fields of ultracold atoms and quantum-enhanced metrology. His invariable readiness to proficiently answer all of my questions has given me an invaluable feeling of safety. I consider it a great privilege that this safety has been accompanied by a significant degree of academic freedom. On a personal level, I am very grateful to Prof. Luis Santos for his cordial, wise, and plain style of communication.

To my co-advisor Prof. Augusto Smerzi, I am particularly indebted for interesting research topics. He has given me valuable orientation in judging the impact of scientific results. His sincere fascination with beautiful physics has always been a source of motivation.

Almost all my doctorate projects were inspired by an experimental setup in the laboratory of Prof. Carsten Klempt and would not have been possible without his guidance. I very much enjoyed a couple of weeks spent at his laboratory, which significantly advanced my understanding of the experiment. Collaborating with Prof. Carsten Klempt has always been a pleasure. Additionally, I would like to thank him for all kinds of valuable advice shared along the way.

Following the discussions of Prof. Luis Santos, Prof. Augusto Smerzi, and Prof. Carsten Klempt has given me precious insights into the work of great scientists.

When visiting the group of Prof. Augusto Smerzi, I had the delightful opportunity to meet Dr. Luca Pezzè and Dr. Manuel Gessner. I owe great thanks to Dr. Luca Pezzè for his work on macroscopic superposition states. Dr. Manuel Gessner has initiated the project on excited-state quantum phase transitions. I am grateful for the fruitful collaboration and hope that we will continue to work together.

During my doctoral studies, I have very much benefited from the collaborative atmosphere at the Institute of Theoretical Physics in Hanover. I particularly appreciate the incredible patience with which Prof. Reinhard Werner has been answering my questions on mean-field theory. Prof. Tobias Osborne has introduced me to the field of quantum machine learning. I would also like to thank Prof. Domenico Giulini for his advice on algebra.

I am grateful to the administrative staff of the Institute of Theoretical Physics and of DQ-mat for their help with all bureaucratic issues.

Before the coronavirus pandemic, I had enjoyed numerous travels—to schools, conferences, and for research visits. This has been enabled by Prof. Luis Santos, Prof. Augusto Smerzi, Dr. Manuel Gessner, and the collaborative research center DQ-mat. Many thanks for these enriching experiences!

The various meetings organized by DQ-mat, headed by Prof. Piet O. Schmidt, have contributed a lot to my scientific development. They have been providing a convenient opportunity to widen my horizon and to discuss with colleagues from different groups. Beyond that, I will keep them in good memory because this is where I have met my dear husband.

I cannot imagine scientific productivity without inspiring company. During the years of doctoral studies, my life has been greatly embellished by many colleagues and friends. I would like to particularly thank Fabian for sharing his experimental expertise with me, Daniel for solving

all my computer problems, Doro for interesting scientific conversations and for her friendship, Marco for entertaining me in Florence and for his incredible patience in teaching me Italian, Meghana, Lorenzo, and Nikolay for the fun time in Hanover, as well as Anna and Friederike for their friendship and continuous support. I also very much appreciate the overall kindness I have been encountering in the groups of Prof. Luis Santos and Prof. Hendrik Weimer, Prof. Carsten Klempt, Prof. Reinhard Werner and Prof. Tobias Osborne, and Prof. Augusto Smerzi.

Finally, I would like to express my deepest gratitude to my dear family—particularly, to my mother, my brother, and my husband—for their loving companionship. Dmytro has not only made my life a lot more fulfilled and happy. He has introduced me to quantum information theory. His broad interest in physics has helped me to gain an overview of the scientific landscape. We have collaborated on several projects, and Dmytro has been patiently discussing with me also all the others. Moreover, working, due to the pandemic, from home would have been bleak alone but has been delightful together.



# Bibliography

- [1] A. Einstein, B. Podolsky, and N. Rosen, “Can quantum-mechanical description of physical reality be considered complete?”, *Phys. Rev.* **47**, 777 (1935).
- [2] E. Schrödinger, “Discussion of probability relations between separated systems”, *Math. Proc. Camb. Phil. Soc.* **31**, 555 (1935).
- [3] *D-wave*, <https://www.dwavesys.com/>.
- [4] *ID Quantique*, <https://www.idquantique.com/>.
- [5] H. Grote, K. Danzmann, K. L. Dooley, R. Schnabel, J. Slutsky, and H. Vahlbruch, “First long-term application of squeezed states of light in a gravitational-wave observatory”, *Phys. Rev. Lett.* **110**, 181101 (2013).
- [6] M. Tse et al., “Quantum-enhanced advanced LIGO detectors in the era of gravitational-wave astronomy”, *Phys. Rev. Lett.* **123**, 231107 (2019).
- [7] F. Acernese et al., “Increasing the astrophysical reach of the advanced Virgo detector via the application of squeezed vacuum states of light”, *Phys. Rev. Lett.* **123**, 231108 (2019).
- [8] C. L. Degen, F. Reinhard, and P. Cappellaro, “Quantum sensing”, *Rev. Mod. Phys.* **89**, 035002 (2017).
- [9] L. Pezzè, A. Smerzi, M. K. Oberthaler, R. Schmied, and P. Treutlein, “Quantum metrology with nonclassical states of atomic ensembles”, *Rev. Mod. Phys.* **90**, 035005 (2018).
- [10] M. Krenn, M. Malik, T. Scheidl, R. Ursin, and A. Zeilinger, “Quantum communication with photons”, *Optics in Our Time*, 455 (2016).
- [11] S. Pirandola, U. L. Andersen, L. Banchi, M. Berta, D. Bunandar, R. Colbeck, D. Englund, T. Gehring, C. Lupo, C. Ottaviani, J. Pereira, M. Razavi, J. S. Shaari, M. Tomamichel, V. C. Usenko, G. Vallone, P. Villoresi, and P. Wallden, *Advances in quantum cryptography*, [arXiv:1906.01645](https://arxiv.org/abs/1906.01645), 2019.
- [12] F. Xu, X. Ma, Q. Zhang, H.-K. Lo, and J.-W. Pan, “Secure quantum key distribution with realistic devices”, *Rev. Mod. Phys.* **92**, 025002 (2020).
- [13] I. M. Georgescu, S. Ashhab, and F. Nori, “Quantum simulation”, *Rev. Mod. Phys.* **86**, 153 (2014).
- [14] M. C. Banuls, R. Blatt, J. Catani, A. Celi, J. I. Cirac, M. Dalmonte, L. Fallani, K. Jansen, M. Lewenstein, S. Montangero, C. A. Muschik, B. Reznik, E. Rico, L. Tagliacozzo, K. van Acoleyen, F. Verstraete, U.-J. Wiese, M. Wingate, J. Zakrzewski, and P. Zoller, “Simulating lattice gauge theories within quantum technologies”, *Eur. Phys. J. D* **74**, 1 (2020).
- [15] G. Wendin, “Quantum information processing with superconducting circuits: a review”, *Rep. Prog. Phys.* **80**, 106001 (2017).
- [16] J. Preskill, “Quantum computing in the NISQ era and beyond”, *Quantum* **2**, 79 (2018).
- [17] S. Slussarenko and G. J. Pryde, “Photonic quantum information processing: a concise review”, *Appl. Phys. Rev.* **6**, 041303 (2019).

- [18] C. D. Bruzewicz, J. Chiaverini, R. McConnell, and J. M. Sage, “Trapped-ion quantum computing: progress and challenges”, *Appl. Phys. Rev.* **6**, 021314 (2019).
- [19] B. Zeng, X. Chen, D.-L. Zhou, and X.-G. Wen, *Quantum information meets quantum matter – from quantum entanglement to topological phase in many-body systems*, arXiv:1508.02595, 2018.
- [20] R. A. Fisher, “Theory of statistical estimation”, *Math. Proc. Camb. Phil. Soc.* **22**, 700 (1925).
- [21] F. Fröwis and W. Dür, “Measures of macroscopicity for quantum spin systems”, *New J. Phys.* **14**, 093039 (2012).
- [22] F. Fröwis, P. Sekatski, W. Dür, N. Gisin, and N. Sangouard, “Macroscopic quantum states: measures, fragility, and implementations”, *Rev. Mod. Phys.* **90**, 025004 (2018).
- [23] A. D. Ludlow, M. M. Boyd, J. Ye, E. Peik, and P. O. Schmidt, “Optical atomic clocks”, *Rev. Mod. Phys.* **87**, 637 (2015).
- [24] I. D. Leroux, M. H. Schleier-Smith, and V. Vuletić, “Orientation-dependent entanglement lifetime in a squeezed atomic clock”, *Phys. Rev. Lett.* **104**, 250801 (2010).
- [25] I. Kruse, K. Lange, J. Peise, B. Lücke, L. Pezzè, J. Arlt, W. Ertmer, C. Lisdat, L. Santos, A. Smerzi, and C. Klempt, “Improvement of an atomic clock using squeezed vacuum”, *Phys. Rev. Lett.* **117**, 143004 (2016).
- [26] O. Hosten, N. J. Engelsen, R. Krishnakumar, and M. A. Kasevich, “Measurement noise 100 times lower than the quantum-projection limit using entangled atoms”, *Nature* **529**, 505 (2016).
- [27] E. Pedrozo-Peñafiel, S. Colombo, C. Shu, A. F. Adiyatullin, Z. Li, E. Mendez, B. Braverman, A. Kawasaki, D. Akamatsu, Y. Xiao, and V. Vuletić, “Entanglement on an optical atomic-clock transition”, *Nature* **588**, 414 (2020).
- [28] L. Pitaevskii and S. Stringari, *Bose-Einstein condensation* (Clarendon Press, Oxford, 2004).
- [29] Y. Kawaguchi and M. Ueda, “Spinor Bose–Einstein condensates”, *Physics Reports* **520**, 253 (2012).
- [30] D. M. Stamper-Kurn and M. Ueda, “Spinor Bose gases: symmetries, magnetism, and quantum dynamics”, *Rev. Mod. Phys.* **85**, 1191 (2013).
- [31] F. Anders, A. Idel, P. Feldmann, D. Bondarenko, S. Loriani, K. Lange, J. Peise, M. Gersemann, B. Meyer, S. Abend, N. Gaaloul, C. Schubert, D. Schlippert, L. Santos, E. Rasel, and C. Klempt, *Momentum entanglement for atom interferometry*, arXiv:2010.15796, 2020.
- [32] Z. Zhang and L.-M. Duan, “Generation of massive entanglement through an adiabatic quantum phase transition in a spinor condensate”, *Phys. Rev. Lett.* **111**, 180401 (2013).
- [33] E. M. Bookjans, A. Vinit, and C. Raman, “Quantum phase transition in an antiferromagnetic spinor Bose-Einstein condensate”, *Phys. Rev. Lett.* **107**, 195306 (2011).
- [34] M. Born and V. Fock, “Beweis des Adiabatsatzes”, *Z. Physik* **51**, 165 (1928).
- [35] X.-Y. Luo, Y.-Q. Zou, L.-N. Wu, Q. Liu, M.-F. Han, M. K. Tey, and L. You, “Deterministic entanglement generation from driving through quantum phase transitions”, *Science* **355**, 620 (2017).

- 
- [36] T. Monz, P. Schindler, J. T. Barreiro, M. Chwalla, D. Nigg, W. A. Coish, M. Harlander, W. Hänsel, M. Hennrich, and R. Blatt, “14-qubit entanglement: creation and coherence”, *Phys. Rev. Lett.* **106**, 130506 (2011).
- [37] A. Omran, H. Levine, A. Keesling, G. Semeghini, T. T. Wang, S. Ebadi, H. Bernien, A. S. Zibrov, H. Pichler, S. Choi, J. Cui, M. Rossignolo, P. Rembold, S. Montangero, T. Calarco, M. Endres, M. Greiner, V. Vuletić, and M. D. Lukin, “Generation and manipulation of Schrödinger cat states in Rydberg atom arrays”, *Science* **365**, 570 (2019).
- [38] I. Pogorelov, T. Feldker, C. D. Marciniak, G. Jacob, V. Podlesnic, M. Meth, V. Negnevitsky, M. Stadler, K. Lakhmanskii, R. Blatt, P. Schindler, and T. Monz, *A compact ion-trap quantum computing demonstrator*, [arXiv:2101.11390](https://arxiv.org/abs/2101.11390), Jan. 2021.
- [39] G. J. Mooney, G. A. L. White, C. D. Hill, and L. C. L. Hollenberg, *Generation and verification of 27-qubit Greenberger-Horne-Zeilinger states in a superconducting quantum computer*, [arXiv:2101.08946](https://arxiv.org/abs/2101.08946), Jan. 2021.
- [40] S. Sachdev, *Quantum phase transitions*, 2nd ed. (Cambridge University Press, Cambridge, 2011).
- [41] P. Cejnar, M. Macek, S. Heinze, J. Jolie, and J. Dobeš, “Monodromy and excited-state quantum phase transitions in integrable systems: collective vibrations of nuclei”, *J. Phys. A* **39**, L515 (2006).
- [42] P. Cejnar, P. Stránský, M. Macek, and M. Kloc, “Excited-state quantum phase transitions”, *J. Phys. A* **54**, 133001 (2021).
- [43] M.-S. Chang, Q. Qin, W. Zhang, L. You, and M. S. Chapman, “Coherent spinor dynamics in a spin-1 Bose condensate”, *Nat. Phys.* **1**, 111 (2005).
- [44] T. Zibold, E. Nicklas, C. Gross, and M. K. Oberthaler, “Classical bifurcation at the transition from Rabi to Josephson dynamics”, *Phys. Rev. Lett.* **105**, 204101 (2010).
- [45] B. Dietz, F. Iachello, M. Miski-Oglu, N. Pietralla, A. Richter, L. v. Smekal, and J. Wambach, “Lifshitz and excited-state quantum phase transitions in microwave Dirac billiards”, *Phys. Rev. B* **88**, 104101 (2013).
- [46] L. Zhao, J. Jiang, T. Tang, M. Webb, and Y. Liu, “Dynamics in spinor condensates tuned by a microwave dressing field”, *Phys. Rev. A* **89**, 023608 (2014).
- [47] J. Khalouf-Rivera, F. Pérez-Bernal, and M. Carvajal, *Excited state quantum phase transitions in the bending spectra of molecules*, *J. Quant. Spectrosc. Radiat. Transf.* in press, 2020.
- [48] R. Horodecki, P. Horodecki, M. Horodecki, and K. Horodecki, “Quantum entanglement”, *Rev. Mod. Phys.* **81**, 865 (2009).
- [49] Y.-Q. Zou, L.-N. Wu, Q. Liu, X.-Y. Luo, S.-F. Guo, J.-H. Cao, M. K. Tey, and L. You, “Beating the classical precision limit with spin-1 Dicke states of more than 10,000 atoms”, *Proceedings of the National Academy of Sciences* **115**, 6381 (2018).
- [50] W. Wang, Y. Wu, Y. Ma, W. Cai, L. Hu, X. Mu, Y. Xu, Z.-J. Chen, H. Wang, Y. P. Song, H. Yuan, L.-M. Duan, and L. Sun, “Heisenberg-limited single-mode quantum metrology in a superconducting circuit”, *Nature communications* **10**, 1 (2019).

- [51] J. Yin, Y.-H. Li, S.-K. Liao, M. Yang, Y. Cao, L. Zhang, J.-G. Ren, W.-Q. Cai, W.-Y. Liu, S.-L. Li, R. Shu, Y.-M. Huang, L. Deng, L. Li, Q. Zhang, N.-L. Liu, Y.-A. Chen, C.-Y. Lu, X.-B. Wang, F. Xu, J.-Y. Wang, C.-Z. Peng, A. K. Ekert, and J.-W. Pan, “Entanglement-based secure quantum cryptography over 1120 kilometres”, *Nature* **582**, 1 (2020).
- [52] M. K. Bhaskar, R. Riedinger, B. Machielse, D. S. Levonian, C. T. Nguyen, E. N. Knall, H. Park, D. Englund, M. Lončar, D. D. Sukachev, and M. D. Lukin, “Experimental demonstration of memory-enhanced quantum communication”, *Nature* **580**, 60 (2020).
- [53] A. Keesling, A. Omran, H. Levine, H. Bernien, H. Pichler, S. Choi, R. Samajdar, S. Schwartz, P. Silvi, S. Sachdev, P. Zoller, M. Endres, M. Greiner, V. Vuletić, and M. D. Lukin, “Quantum Kibble-Zurek mechanism and critical dynamics on a programmable Rydberg simulator”, *Nature* **568**, 207 (2019).
- [54] C. Kokail, C. Maier, R. van Bijnen, T. Brydges, M. K. Joshi, P. Jurcevic, C. A. Muschik, P. Silvi, R. Blatt, C. F. Roos, and P. Zoller, “Self-verifying variational quantum simulation of lattice models”, *Nature* **569**, 355 (2019).
- [55] F. Arute et al., “Quantum supremacy using a programmable superconducting processor”, *Nature* **574**, 505 (2019).
- [56] D. Inoue, A. Okada, T. Matsumori, K. Aihara, and H. Yoshida, *Traffic signal optimization on a square lattice using the D-Wave quantum annealer*, [arXiv:2003.07527](https://arxiv.org/abs/2003.07527), 2020.
- [57] O. Gühne and G. Tóth, “Entanglement detection”, *Physics Reports* **474**, 1 (2009).
- [58] L. Pezzé and A. Smerzi, “Entanglement, nonlinear dynamics, and the Heisenberg limit”, *Phys. Rev. Lett.* **102**, 100401 (2009).
- [59] P. Hyllus, W. Laskowski, R. Krischek, C. Schwemmer, W. Wieczorek, H. Weinfurter, L. Pezzé, and A. Smerzi, “Fisher information and multiparticle entanglement”, *Phys. Rev. A* **85**, 022321 (2012).
- [60] G. Tóth, “Multipartite entanglement and high-precision metrology”, *Phys. Rev. A* **85**, 022322 (2012).
- [61] L. Pezzè and A. Smerzi, *Quantum theory of phase estimation*, [arXiv:1411.5164](https://arxiv.org/abs/1411.5164), Nov. 2014.
- [62] L. Pezzè and A. Smerzi, “Quantum theory of phase estimation”, in *Atom interferometry*, Vol. 188, Proceedings of the international school of physics Enrico Fermi (2014), pp. 691–741.
- [63] M. Gessner and A. Smerzi, “Statistical speed of quantum states: generalized quantum Fisher information and Schatten speed”, *Phys. Rev. A* **97**, 022109 (2018).
- [64] S. L. Braunstein and C. M. Caves, “Statistical distance and the geometry of quantum states”, *Phys. Rev. Lett.* **72**, 3439 (1994).
- [65] O. E. Barndorff-Nielsen and R. D. Gill, “Fisher information in quantum statistics”, *J. Phys. A* **33**, 4481 (2000).
- [66] A. A. Michelson and E. W. Morley, “On the relative motion of the Earth and the luminiferous ether”, *Am. J. Sci.* **34**, 333.
- [67] L. Zehnder, “Ein neuer Interferenzrefraktor”, *Zeitschr. Instrumentenk.* **11**, 275 (1891).
- [68] L. Mach, “Ueber einen Interferenzrefraktor”, *Zeitschr. Instrumentenk.* **12**, 89 (1892).
- [69] N. F. Ramsey, “A molecular beam resonance method with separated oscillating fields”, *Phys. Rev.* **78**, 695 (1950).

- 
- [70] R. Geiger, A. Landragin, S. Merlet, and F. P. d. Santos, *High-accuracy inertial measurements with cold-atom sensors*, [arXiv:2003.12516](https://arxiv.org/abs/2003.12516), 2020.
- [71] M. Kasevich and S. Chu, “Atomic interferometry using stimulated Raman transitions”, *Phys. Rev. Lett.* **67**, 181 (1991).
- [72] F. Riehle, T. Kisters, A. Witte, J. Helmcke, and C. J. Bordé, “Optical Ramsey spectroscopy in a rotating frame: Sagnac effect in a matter-wave interferometer”, *Phys. Rev. Lett.* **67**, 177 (1991).
- [73] B. P. Abbott et al., “Observation of gravitational waves from a binary black hole merger”, *Phys. Rev. Lett.* **116**, 061102 (2016).
- [74] S. Weyers, V. Gerginov, M. Kazda, J. Rahm, B. Lipphardt, G. Dobrev, and K. Gibble, “Advances in the accuracy, stability, and reliability of the PTB primary fountain clocks”, *Metrologia* **55**, 789 (2018).
- [75] T. L. Nicholson, S. L. Campbell, R. B. Hutson, G. E. Marti, B. J. Bloom, R. L. McNally, W. Zhang, M. D. Barrett, M. S. Safronova, G. F. Strouse, and J. Ye, “Systematic evaluation of an atomic clock at  $2 \times 10^{-18}$  total uncertainty”, *Nat. Comm.* **6**, 1 (2015).
- [76] N. Huntemann, C. Sanner, B. Lipphardt, C. Tamm, and E. Peik, “Single-ion atomic clock with  $3 \times 10^{-18}$  systematic uncertainty”, *Phys. Rev. Lett.* **116**, 063001 (2016).
- [77] W. F. McGrew, X. Zhang, R. J. Fasano, S. A. Schäffer, K. Beloy, D. Nicolodi, R. C. Brown, N. Hinkley, G. Milani, M. Schioppo, T. H. Yoon, and A. D. Ludlow, “Atomic clock performance enabling geodesy below the centimetre level”, *Nature* **564**, 87 (2018).
- [78] S. M. Brewer, J.-S. Chen, A. M. Hankin, E. R. Clements, C. W. Chou, D. J. Wineland, D. B. Hume, and D. R. Leibbrandt, “ $^{27}\text{Al}^+$  quantum-logic clock with a systematic uncertainty below  $10^{-18}$ ”, *Phys. Rev. Lett.* **123**, 033201 (2019).
- [79] P. Gillot, O. Francis, A. Landragin, F. P. dos Santos, and S. Merlet, “Stability comparison of two absolute gravimeters: optical versus atomic interferometers”, *Metrologia* **51**, L15 (2014).
- [80] C. Freier, M. Hauth, V. Schkolnik, B. Leykauf, M. Schilling, H. Wziontek, H.-G. Scherneck, J. Müller, and A. Peters, “Mobile quantum gravity sensor with unprecedented stability”, *J. Phys. Conf. Ser.* **723**, 012050 (2016).
- [81] D. Savoie, M. Altorio, B. Fang, L. A. Sidorenkov, R. Geiger, and A. Landragin, “Interleaved atom interferometry for high-sensitivity inertial measurements”, *Science Advances* **4**, 12 (2018).
- [82] V. Ménot, P. Vermeulen, N. Le Moigne, S. Bonvalot, P. Bouyer, A. Landragin, and B. Desruelle, “Gravity measurements below  $10^{-9}g$  with a transportable absolute quantum gravimeter”, *Scientific reports* **8**, 1 (2018).
- [83] P. Cheiney, L. Fouché, S. Templier, F. Napolitano, B. Battelier, P. Bouyer, and B. Barrett, “Navigation-compatible hybrid quantum accelerometer using a Kalman filter”, *Phys. Rev. Applied* **10**, 034030 (2018).
- [84] B. Barrett, P. Cheiney, B. Battelier, F. Napolitano, and P. Bouyer, “Multidimensional atom optics and interferometry”, *Phys. Rev. Lett.* **122**, 043604 (2019).
- [85] M. S. Safronova, D. Budker, D. DeMille, D. F. J. Kimball, A. Derevianko, and C. W. Clark, “Search for new physics with atoms and molecules”, *Rev. Mod. Phys.* **90**, 025008 (2018).
- [86] P. Hamilton, M. Jaffe, P. Haslinger, Q. Simmons, H. Müller, and J. Khoury, “Atom-interferometry constraints on dark energy”, *Science* **349**, 849 (2015).

- [87] R. H. Parker, C. Yu, W. Zhong, B. Estey, and H. Müller, “Measurement of the fine-structure constant as a test of the Standard Model”, *Science* **360**, 191 (2018).
- [88] C. Sanner, N. Huntemann, R. Lange, C. Tamm, E. Peik, M. S. Safronova, and S. G. Porsev, “Optical clock comparison for Lorentz symmetry testing”, *Nature* **567**, 204 (2019).
- [89] B. M. Roberts et al., “Search for transient variations of the fine structure constant and dark matter using fiber-linked optical atomic clocks”, *New J. Phys.* **22**, 093010 (2020).
- [90] M. Fréchet, “Sur l’extension de certaines évaluations statistiques au cas de petits échantillons”, *Revue de l’Institut International de Statistique* **11**, 182 (1943).
- [91] H. Cramér, *Mathematical methods of statistics* (Almqvist & Wiksells, Uppsala, 1945).
- [92] C. R. Rao, “Information and the accuracy attainable in the estimation of statistical parameters”, *Bull. Calcutta Math. Soc.* **37**, 81 (1945).
- [93] C. M. Caves, “Quantum-mechanical noise in an interferometer”, *Phys. Rev. D* **23**, 1693 (1981).
- [94] V. Giovannetti, S. Lloyd, and L. Maccone, “Quantum metrology”, *Phys. Rev. Lett.* **96**, 010401 (2006).
- [95] M.-Z. Huang, T. Mazzoni, C. L. G. Alzar, and J. Reichel, “Towards a quantum-enhanced trapped-atom clock on a chip”, in *Quantum information and measurement (QIM) V: quantum technologies* (2019), T5A.32.
- [96] P. He, M. A. Perlin, S. R. Muleady, R. J. Lewis-Swan, R. B. Hutson, J. Ye, and A. M. Rey, “Engineering spin squeezing in a 3D optical lattice with interacting spin-orbit-coupled fermions”, *Phys. Rev. Research* **1**, 033075 (2019).
- [97] L. Salvi, N. Poli, V. Vuletić, and G. M. Tino, “Squeezing on momentum states for atom interferometry”, *Phys. Rev. Lett.* **120**, 033601 (2018).
- [98] M. Kritsotakis, J. A. Dunningham, and S. A. Haine, *Spin squeezing of a Bose-Einstein condensate via quantum non-demolition measurement for quantum-enhanced atom interferometry*, [arXiv:2005.00299](https://arxiv.org/abs/2005.00299), 2020.
- [99] Y. Wu, R. Krishnakumar, J. Martínez-Rincón, B. K. Malia, O. Hosten, and M. A. Kasevich, “Retrieval of cavity-generated atomic spin squeezing after free-space release”, *Phys. Rev. A* **102**, 012224 (2020).
- [100] M. Schulte, C. Lisdat, P. O. Schmidt, U. Sterr, and K. Hammerer, *Prospects and challenges for squeezing-enhanced optical atomic clocks*, [arXiv:1911.00882](https://arxiv.org/abs/1911.00882), 2020.
- [101] S. S. Szigeti, O. Hosten, and S. A. Haine, *Will quantum-enhanced atom interferometry ever be useful? Prospects for improving cold-atom sensors with quantum entanglement*, [arXiv:2010.09168](https://arxiv.org/abs/2010.09168), 2020.
- [102] E. L. Lehmann and G. Casella, *Theory of point estimation*, 2nd ed. (Springer, New York, NY, 1998).
- [103] E. Schroedinger, “Die gegenwärtige Situation in der Quantenmechanik”, *Naturw.* **23**, 807 (1935).
- [104] W. H. Zurek, “Decoherence, einselection, and the quantum origins of the classical”, *Rev. Mod. Phys.* **75**, 715 (2003).
- [105] E. Joos, H. D. Zeh, C. Kiefer, D. J. W. Giulini, J. Kupsch, and I.-O. Stamatescu, *Decoherence and the appearance of a classical world in quantum theory*, 2nd ed. (Springer, Berlin, Heidelberg, 2003).



- 
- [106] A. Bassi, K. Lochan, S. Satin, T. P. Singh, and H. Ulbricht, “Models of wave-function collapse, underlying theories, and experimental tests”, *Rev. Mod. Phys.* **85**, 471 (2013).
- [107] F. Karolyhazy, “Gravitation and quantum mechanics of macroscopic objects”, *Nuovo Cimento A* **42**, 390 (1966).
- [108] L. Diósi, “A universal master equation for the gravitational violation of quantum mechanics”, *Phys. Lett. A* **120**, 377 (1987).
- [109] R. Penrose, “On gravity’s role in quantum state reduction”, *Gen. Relat. Gravit.* **28**, 581 (1996).
- [110] F. Laloë, “A model of quantum collapse induced by gravity”, *Eur. Phys. J. D* **74**, 25 (2020).
- [111] H. Vahlbruch, M. Mehmet, K. Danzmann, and R. Schnabel, “Detection of 15 dB squeezed states of light and their application for the absolute calibration of photoelectric quantum efficiency”, *Phys. Rev. Lett.* **117**, 110801 (2016).
- [112] C. Wang, Y. Y. Gao, P. Reinhold, R. W. Heeres, N. Ofek, K. Chou, C. Axline, M. Reagor, J. Blumoff, K. M. Sliwa, L. Frunzio, S. M. Girvin, L. Jiang, M. Mirrahimi, M. H. Devoret, and R. J. Schoelkopf, “A Schrödinger cat living in two boxes”, *Science* **352**, 1087 (2016).
- [113] B. Lücke, M. Scherer, J. Kruse, L. Pezzé, F. Deuretzbacher, P. Hyllus, O. Topic, J. Peise, W. Ertmer, J. Arlt, L. Santos, A. Smerzi, and C. Klempt, “Twin matter waves for interferometry beyond the classical limit”, *Science* **334**, 773 (2011).
- [114] T. Kovachy, P. Asenbaum, C. Overstreet, C. A. Donnelly, S. M. Dickerson, A. Sugarbaker, J. M. Hogan, and M. A. Kasevich, “Quantum superposition at the half-metre scale”, *Nature* **528**, 530 (2015).
- [115] S. Eibenberger, S. Gerlich, M. Arndt, M. Mayor, and J. Tüxen, “Matter–wave interference of particles selected from a molecular library with masses exceeding 10 000 amu”, *Phys. Chem. Chem. Phys.* **15**, 14696 (2013).
- [116] J. Millen, T. S. Monteiro, R. Pettit, and A. N. Vamivakas, “Optomechanics with levitated particles”, *Rep. Prog. Phys.* **83**, 026401 (2020).
- [117] M. Carlesso, A. Bassi, M. Paternostro, and H. Ulbricht, “Testing the gravitational field generated by a quantum superposition”, *New J. Phys.* **21**, 093052 (2019).
- [118] U. Delić, M. Reisenbauer, K. Dare, D. Grass, V. Vuletić, N. Kiesel, and M. Aspelmeyer, “Cooling of a levitated nanoparticle to the motional quantum ground state”, *Science* **367**, 892 (2020).
- [119] A. J. Leggett, “Macroscopic quantum systems and the quantum theory of measurement”, *Prog. Theor. Phys. Supp.* **69**, 80 (1980).
- [120] A. Shimizu and T. Morimae, “Detection of macroscopic entanglement by correlation of local observables”, *Phys. Rev. Lett.* **95**, 090401 (2005).
- [121] E. G. Cavalcanti and M. D. Reid, “Criteria for generalized macroscopic and mesoscopic quantum coherence”, *Phys. Rev. A* **77**, 062108 (2008).
- [122] G. Björk and P. G. L. Mana, “A size criterion for macroscopic superposition states”, *J. Opt. B* **6**, 429 (2004).
- [123] J. I. Korsbakken, K. B. Whaley, J. Dubois, and J. I. Cirac, “Measurement-based measure of the size of macroscopic quantum superpositions”, *Phys. Rev. A* **75**, 042106 (2007).

- [124] S. Nimmrichter and K. Hornberger, “Macroscopicity of mechanical quantum superposition states”, *Phys. Rev. Lett.* **110**, 160403 (2013).
- [125] B. Yadin and V. Vedral, “Quantum macroscopicity versus distillation of macroscopic superpositions”, *Phys. Rev. A* **92**, 022356 (2015).
- [126] C.-W. Lee and H. Jeong, “Quantification of macroscopic quantum superpositions within phase space”, *Phys. Rev. Lett.* **106**, 220401 (2011).
- [127] P. Sekatski, N. Gisin, and N. Sangouard, “How difficult is it to prove the quantumness of macroscopic states?”, *Phys. Rev. Lett.* **113**, 090403 (2014).
- [128] H. Strobel, W. Muessel, D. Linnemann, T. Zibold, D. B. Hume, L. Pezzè, A. Smerzi, and M. K. Oberthaler, “Fisher information and entanglement of non-Gaussian spin states”, *Science* **345**, 424 (2014).
- [129] I. Apellaniz, M. Kleinmann, O. Gühne, and G. Tóth, “Optimal witnessing of the quantum Fisher information with few measurements”, *Phys. Rev. A* **95**, 032330 (2017).
- [130] F. Fröwis, “Lower bounds on the size of general Schrödinger-cat states from experimental data”, *J. Phys. A* **50**, 114003 (2017).
- [131] A. Einstein, “Quantentheorie des einatomigen idealen Gases. Zweite Abhandlung”, *Sitzungsberichte der Preussischen Akademie der Wissenschaften* **III**, 3 (1925).
- [132] P. Kapitza, “Viscosity of liquid helium below the  $\lambda$ -point”, *Nature* **141**, 74 (1938).
- [133] J. Allen and A. Misener, “Flow of liquid helium II”, *Nature* **141**, 75 (1938).
- [134] F. London, “The  $\lambda$ -phenomenon of liquid helium and the Bose-Einstein degeneracy”, *Nature* **141**, 643 (1938).
- [135] L. Tisza, “Transport phenomena in helium II”, *Nature* **141**, 913 (1938).
- [136] A. Griffin, “A brief history of our understanding of BEC: from Bose to Beliaev”, in *Bose-Einstein condensation in atomic gases*, edited by M. Inguscio, S. Stringari, and C. E. Wieman (IOS Press, Amsterdam, 1999), pp. 1–10.
- [137] K. B. Davis, M.-O. Mewes, M. R. Andrews, N. J. v. Druten, D. S. Durfee, D. M. Kurn, and W. Ketterle, “Bose-Einstein condensation in a gas of sodium atoms”, *Phys. Rev. Lett.* **75**, 3969 (1995).
- [138] C. C. Bradley, C. A. Sackett, J. J. Tollett, and R. G. Hulet, “Evidence of Bose-Einstein condensation in an atomic gas with attractive interactions”, *Phys. Rev. Lett.* **75**, 1687 (1995).
- [139] M. H. Anderson, J. R. Ensher, M. R. Matthews, C. E. Wieman, and E. A. Cornell, “Observation of Bose-Einstein condensation in a dilute atomic vapor”, *Science* **269**, 198 (1995).
- [140] A. Griffin, “High-momentum scattering and the condensate fraction”, in *Excitations in a Bose-condensed liquid*, Cambridge studies in low temperature physics (Cambridge University Press, Cambridge, 1993), pp. 67–91.
- [141] J. L. Lin and J. P. Wolfe, “Bose-Einstein condensation of paraexcitons in stressed  $\text{Cu}_2\text{O}$ ”, *Phys. Rev. Lett.* **71**, 1222 (1993).
- [142] C. J. Pethick and H. Smith, *Bose-Einstein condensation in dilute gases*, 2nd ed. (Cambridge University Press, Cambridge, 2008).
- [143] M. Greiner, C. Regal, and D. Jin, “Emergence of a molecular Bose-Einstein condensate from a Fermi gas”, *Nature* **426**, 537 (2003).



- 
- [144] M. W. Zwierlein, C. A. Stan, C. H. Schunck, S. M. F. Raupach, S. Gupta, Z. Hadzibabic, and W. Ketterle, “Observation of Bose-Einstein condensation of molecules”, *Phys. Rev. Lett.* **91**, 250401 (2003).
- [145] I. Carusotto and C. Ciuti, “Quantum fluids of light”, *Rev. Mod. Phys.* **85**, 299 (2013).
- [146] V. Zapf, M. Jaime, and C. D. Batista, “Bose-Einstein condensation in quantum magnets”, *Rev. Mod. Phys.* **86**, 563 (2014).
- [147] D. M. Stamper-Kurn, M. R. Andrews, A. P. Chikkatur, S. Inouye, H.-J. Miesner, J. Stenger, and W. Ketterle, “Optical confinement of a Bose-Einstein condensate”, *Phys. Rev. Lett.* **80**, 2027 (1998).
- [148] W. Zhang, S. Yi, and L. You, “Mean field ground state of a spin-1 condensate in a magnetic field”, *New J. Phys.* **5**, 77 (2003).
- [149] W. Zhang, D. L. Zhou, M.-S. Chang, M. S. Chapman, and L. You, “Coherent spin mixing dynamics in a spin-1 atomic condensate”, *Phys. Rev. A* **72**, 013602 (2005).
- [150] T. M. Hoang, H. M. Bharath, M. J. Boguslawski, M. Anquez, B. A. Robbins, and M. S. Chapman, “Adiabatic quenches and characterization of amplitude excitations in a continuous quantum phase transition”, *PNAS* **113**, 9475 (2016).
- [151] L.-M. Duan, A. Sørensen, J. I. Cirac, and P. Zoller, “Squeezing and entanglement of atomic beams”, *Phys. Rev. Lett.* **85**, 3991 (2000).
- [152] H. Pu and P. Meystre, “Creating macroscopic atomic Einstein-Podolsky-Rosen states from Bose-Einstein condensates”, *Phys. Rev. Lett.* **85**, 3987 (2000).
- [153] C. Klempt, O. Topic, G. Gebreyesus, M. Scherer, T. Henninger, P. Hyllus, W. Ertmer, L. Santos, and J. J. Arlt, “Parametric amplification of vacuum fluctuations in a spinor condensate”, *Phys. Rev. Lett.* **104**, 195303 (2010).
- [154] C. Gross, H. Strobel, E. Nicklas, T. Zibold, N. Bar-Gill, G. Kurizki, and M. K. Oberthaler, “Atomic homodyne detection of continuous-variable entangled twin-atom states”, *Nature* **480**, 219 (2011).
- [155] G. Colangelo, F. Martin Ciurana, G. Puentes, M. W. Mitchell, and R. J. Sewell, “Entanglement-enhanced phase estimation without prior phase information”, *Phys. Rev. Lett.* **118**, 233603 (2017).
- [156] K. Lange, J. Peise, B. Lücke, T. Gruber, A. Sala, A. Polls, W. Ertmer, B. Juliá-Díaz, L. Santos, and C. Klempt, “Creation of entangled atomic states by an analogue of the dynamical Casimir effect”, *New J. Phys.* **20**, 103017 (2018).
- [157] L. Sadler, J. Higbie, S. Leslie, M. Vengalattore, and D. M. Stamper-Kurn, “Spontaneous symmetry breaking in a quenched ferromagnetic spinor Bose-Einstein condensate”, *Nature* **443**, 312 (2006).
- [158] S. Sinha, R. Nath, and L. Santos, “Trapped two-dimensional condensates with synthetic spin-orbit coupling”, *Phys. Rev. Lett.* **107**, 270401 (2011).
- [159] J. Peise, B. Lücke, L. Pezzé, F. Deuretzbacher, W. Ertmer, J. Arlt, A. Smerzi, L. Santos, and C. Klempt, “Interaction-free measurements by quantum zeno stabilization of ultracold atoms”, *Nat. Comm.* **6**, 6811 (2015).
- [160] C. R. Cabrera, L. Tanzi, J. Sanz, B. Naylor, P. Thomas, P. Cheiney, and L. Tarruell, “Quantum liquid droplets in a mixture of Bose-Einstein condensates”, *Science* **359**, 301 (2018).

- [161] T. Tian, H.-X. Yang, L.-Y. Qiu, H.-Y. Liang, Y.-B. Yang, Y. Xu, and L.-M. Duan, “Observation of dynamical quantum phase transitions with correspondence in an excited state phase diagram”, *Phys. Rev. Lett.* **124**, 043001 (2020).
- [162] P. Gomez, F. Martin, C. Mazzinghi, D. Benedicto Orenes, S. Palacios, and M. W. Mitchell, “Bose-Einstein condensate comagnetometer”, *Phys. Rev. Lett.* **124**, 170401 (2020).
- [163] M.-S. Chang, C. D. Hamley, M. D. Barrett, J. A. Sauer, K. M. Fortier, W. Zhang, L. You, and M. S. Chapman, “Observation of spinor dynamics in optically trapped  $^{87}\text{Rb}$  Bose-Einstein condensates”, *Phys. Rev. Lett.* **92**, 140403 (2004).
- [164] S. N. Bose, “Plancks Gesetz und Lichtquantenhypothese”, *Z. Physik* **26**, 178 (1924).
- [165] L. D. Landau and E. M. Lifshitz, *Statistical physics*, 3rd ed., Vol. 5, Course of Theoretical Physics (Elsevier Butterworth-Heinemann, Oxford, 2013).
- [166] A. Einstein, “Quantentheorie des einatomigen idealen Gases”, *Sitzungsberichte der Preussischen Akademie der Wissenschaften* **XXII**, 261 (1924).
- [167] A. Einstein, “Zur Quantentheorie des idealen Gases.”, *Sitzungsberichte der Preussischen Akademie der Wissenschaften* **III**, 18 (1925).
- [168] J. J. Sakurai and J. Napolitano, *Modern quantum mechanics*, 2nd ed. (Cambridge University Press, Cambridge, 2017).
- [169] I. V. Hertel and C.-P. Schulz, *Atoms, molecules, and optical physics*, Vol. 1 (Springer, Berlin, Heidelberg, 2015).
- [170] T. Mayer-Kuckuk, *Atomphysik*, 5th ed. (Springer, Wiesbaden, 1997).
- [171] S. Weinberg, *The quantum theory of fields*, Vol. 1 (Cambridge University Press, Cambridge, 1995).
- [172] R. Grimm, M. Weidemüller, and Y.-B. Ovchinnikov, “Optical dipole traps for neutral atoms”, in *Advances in atomic, molecular, and optical physics*, Vol. 42, edited by B. Bederson and H. Walther (Academic Press, 2000), pp. 95–170.
- [173] G. Breit and I. I. Rabi, “Measurement of nuclear spin”, *Phys. Rev.* **38**, 2082 (1931).
- [174] L. Santos, M. Fattori, J. Stuhler, and T. Pfau, “Spinor condensates with a laser-induced quadratic Zeeman effect”, *Phys. Rev. A* **75**, 053606 (2007).
- [175] Wikipedia contributors, “Table of Clebsch-Gordan coefficients”, in *Wikipedia, The Free Encyclopedia* (Nov. 2020).
- [176] C. K. Law, H. Pu, and N. P. Bigelow, “Quantum spins mixing in spinor Bose-Einstein condensates”, *Phys. Rev. Lett.* **81**, 5257 (1998).
- [177] D. A. Steck, *Quantum and atom optics*, available online at <http://steck.us/teaching> (revision 0.13.4, 2020).
- [178] H. Pu, C. K. Law, S. Raghavan, J. H. Eberly, and N. P. Bigelow, “Spin-mixing dynamics of a spinor Bose-Einstein condensate”, *Phys. Rev. A* **60**, 1463 (1999).
- [179] H. Schmaljohann, M. Erhard, M. Kronjäger, K. Sengstock, and K. Bongs, “Dynamics and thermodynamics in spinor quantum gases”, *Appl. Phys. B* **79**, 1001 (2004).
- [180] S. Yi, O. E. Müstecaplıoğlu, C. P. Sun, and L. You, “Single-mode approximation in a spinor-1 atomic condensate”, *Phys. Rev. A* **66**, 011601 (2002).
- [181] G. Arfken, H. Weber, and F. E. Harris, *Mathematical methods for physicists*, 7th ed. (Elsevier Academic Press, Waltham, 2012).

- 
- [182] L. P. Pitaevskii, “Vortex lines in an imperfect Bose gas”, *Sov. Phys. JETP* **13**, 451 (1961).
- [183] E. P. Gross, “Structure of a quantized vortex in boson systems”, *Nuovo Cim.* **20**, 454 (1961).
- [184] E. H. Lieb and R. Seiringer, “Proof of Bose-Einstein condensation for dilute trapped gases”, *Phys. Rev. Lett.* **88**, 170409 (2002).
- [185] G. Baym and C. J. Pethick, “Ground-state properties of magnetically trapped Bose-condensed rubidium gas”, *Phys. Rev. Lett.* **76**, 6 (1996).
- [186] W. Greiner, L. Neise, and H. Stöcker, *Thermodynamics and statistical mechanics* (Springer, New York, 1995).
- [187] R. Gilmore, *Lie groups, physics, and geometry* (Cambridge University Press, New York, 2008).
- [188] F. Iachello, *Lie algebras and applications*, 2nd ed. (Springer, Berlin, Heidelberg, 2015).
- [189] B. C. Hall, *Lie groups, Lie algebras, and representations*, 2nd ed. (Springer, Cham, 2015).
- [190] J. Schwinger, *On angular momentum*, USAEC Report NYO-3071, 1952.
- [191] M. J. Boguslawski, “All-microwave control of hyperfine states in ultracold spin-1 rubidium”, PhD thesis (Georgia Institute of Technology, 2019).
- [192] D. A. Steck, *Rubidium 87 D line data*, available online at <http://steck.us/alkalidata> (revision 2.2.1, 2019).
- [193] E. A. Cornell and C. E. Wieman, “Nobel lecture: Bose-Einstein condensation in a dilute gas, the first 70 years and some recent experiments”, *Rev. Mod. Phys.* **74**, 875 (2002).
- [194] E. A. Burt, R. W. Ghrist, C. J. Myatt, M. J. Holland, E. A. Cornell, and C. E. Wieman, “Coherence, correlations, and collisions: what one learns about Bose-Einstein condensates from their decay”, *Phys. Rev. Lett.* **79**, 337 (1997).
- [195] J. Söding, D. Guéry-Odelin, P. Desbiolles, F. Chevy, H. Inamori, and J. Dalibard, “Three-body decay of a rubidium Bose-Einstein condensate”, *Appl. Phys. B* **69**, 257 (1999).
- [196] C. Gardiner and P. Zoller, *Quantum noise*, 3rd ed. (Springer, Berlin, Heidelberg, 2004).
- [197] A. Rivas and S. F. Huelga, *Open quantum systems* (Springer, Berlin, Heidelberg, 2012).
- [198] G. Lindblad, “On the generators of quantum dynamical semigroups”, *Commun. Math. Phys.* **48**, 119 (1975).
- [199] V. Gorini, A. Kossakowski, and E. C. G. Sudarshan, “Completely positive dynamical semigroups of n-level systems”, *J. Math. Phys.* **17**, 821 (1976).
- [200] K. Mølmer, Y. Castin, and J. Dalibard, “Monte Carlo wave-function method in quantum optics”, *J. Opt. Soc. Am. B* **10**, 524 (1993).
- [201] H. Weimer, A. Kshetrimayum, and R. Orús, *Simulation methods for open quantum many-body systems*, [arXiv:1907.07079](https://arxiv.org/abs/1907.07079), 2020.
- [202] L. G. Yaffe, “Large  $n$  limits as classical mechanics”, *Rev. Mod. Phys.* **54**, 407 (1982).
- [203] G. A. Raggio and R. F. Werner, “Quantum statistical mechanics of general mean field systems”, *Helv. Phys. Acta* **62**, 980 (1989).
- [204] N. G. Duffield and R. F. Werner, “Mean-field dynamical semigroups on  $C^*$ -algebras”, *Rev. Math. Phys.* **4**, 383 (1992).

- [205] N. G. Duffield and R. F. Werner, “Classical Hamiltonian dynamics for quantum Hamiltonian mean-field limits”, in *Stochastics and quantum mechanics*, edited by A. Truman and I. M. Davies, Proceedings of a conference held in Swansea, UK, 1986 (1992), pp. 115–129.
- [206] R. F. Werner, “Large deviations and mean-field quantum systems”, in *Quantum probability & related topics*, edited by L. Accardi, Conference proceedings (1992), pp. 349–381.
- [207] W.-M. Zhang, D. H. Feng, and R. Gilmore, “Coherent states: theory and some applications”, *Rev. Mod. Phys.* **62**, 867 (1990).
- [208] P. Feldmann, C. Klempt, A. Smerzi, L. Santos, and M. Gessner, *Excited-state quantum phase transitions in spinor Bose-Einstein condensates*, [arXiv:2011.02823](https://arxiv.org/abs/2011.02823), 2020.
- [209] P. Loya, *Amazing and aesthetic aspects of analysis* (Springer, New York, NY, 2017).
- [210] K. Königsberger, *Analysis*, 5th ed., Vol. 2 (Springer, Berlin, Heidelberg, 2004).
- [211] O. Forster, *Analysis*, 11th ed., Vol. 1 (Springer Spektrum, Wiesbaden, 2013).
- [212] Y. G. Sinai, *Theory of phase transitions: rigorous results* (Pergamon, Oxford, 1982).
- [213] O. Bratteli and D. W. Robinson, *Operator algebras and quantum statistical mechanics*, 2nd ed., Vol. 2 (Springer, Berlin, Heidelberg, 2002).
- [214] D. Guéry-Odelin, A. Ruschhaupt, A. Kiely, E. Torrontegui, S. Martínez-Garaot, and J. G. Muga, “Shortcuts to adiabaticity: concepts, methods, and applications”, *Rev. Mod. Phys.* **91**, 045001 (2019).
- [215] L. D. Landau, “A theory of energy transfer on collisions”, *Phys. Zs. Sowjet.* **1**, 88 (1932).
- [216] L. D. Landau, “A theory of energy transfer II”, *Phys. Zs. Sowjet.* **2**, 46 (1932).
- [217] C. Zener and R. H. Fowler, “Non-adiabatic crossing of energy levels”, *Proc. R. Soc. of Lond. A* **137**, 696 (1932).
- [218] C. Wittig, “The Landau-Zener formula”, *J. Phys. Chem. B* **109**, 8428 (2005).
- [219] M. Greiner, O. Mandel, T. Esslinger, T. W. Hänsch, and I. Bloch, “Quantum phase transition from a superfluid to a Mott insulator in a gas of ultracold atoms”, *Nature* **415**, 39 (2002).
- [220] L.-N. Wu and L. You, “Using the ground state of an antiferromagnetic spin-1 atomic condensate for Heisenberg-limited metrology”, *Phys. Rev. A* **93**, 033608 (2016).
- [221] D. Kajtoch, K. Pawłowski, and E. Witkowska, “Metrologically useful states of spin-1 Bose condensates with macroscopic magnetization”, *Phys. Rev. A* **97**, 023616 (2018).
- [222] P. Feldmann, M. Gessner, M. Gabbrielli, C. Klempt, L. Santos, L. Pezzè, and A. Smerzi, “Interferometric sensitivity and entanglement by scanning through quantum phase transitions in spinor Bose-Einstein condensates”, *Phys. Rev. A* **97**, 032339 (2018).
- [223] L. Pezzè, M. Gessner, P. Feldmann, C. Klempt, L. Santos, and A. Smerzi, “Heralded generation of macroscopic superposition states in a spinor Bose-Einstein condensate”, *Phys. Rev. Lett.* **123**, 260403 (2019).
- [224] F. Trimborn, R. F. Werner, and D. Witthaut, “Quantum de Finetti theorems and mean-field theory from quantum phase space representations”, *J. Phys. A* **49**, 135302 (2016).
- [225] L.-M. Duan, “Entanglement detection in the vicinity of arbitrary Dicke states”, *Phys. Rev. Lett.* **107**, 180502 (2011).
- [226] B. Dakić and M. Radonjić, “Macroscopic superpositions as quantum ground states”, *Phys. Rev. Lett.* **119**, 090401 (2017).

- 
- [227] A. Hüper, C. Pür, M. Hetzel, J. Geng, J. Peise, I. Kruse, M. A. Kristensen, W. Ertmer, J. Arlt, and C. Klempt, *Number-resolved preparation of mesoscopic atomic ensembles*, *New J. Phys.*, accepted manuscript, 2020.
- [228] C. Hamley, C. Gerving, T. Hoang, E. M. Bookjans, and M. S. Chapman, “Spin-nematic squeezed vacuum in a quantum gas”, *Nat. Phys.* **8**, 305 (2012).
- [229] D. Linnemann, H. Strobel, W. Muessel, J. Schulz, R. J. Lewis-Swan, K. V. Kheruntsyan, and M. K. Oberthaler, “Quantum-enhanced sensing based on time reversal of nonlinear dynamics”, *Phys. Rev. Lett.* **117**, 013001 (2016).
- [230] D. R. Truax, “Baker-Campbell-Hausdorff relations and unitarity of SU(2) and SU(1,1) squeeze operators”, *Phys. Rev. D* **31**, 1988 (1985).
- [231] K. W. Martin, G. Phelps, N. D. Lemke, M. S. Bigelow, B. Stuhl, M. Wojcik, M. Holt, I. Coddington, M. W. Bishop, and J. H. Burke, “Compact optical atomic clock based on a two-photon transition in rubidium”, *Phys. Rev. Applied* **9**, 014019 (2018).
- [232] A. Polkovnikov, K. Sengupta, A. Silva, and M. Vengalattore, “Colloquium: nonequilibrium dynamics of closed interacting quantum systems”, *Rev. Mod. Phys.* **83**, 863 (2011).
- [233] D. A. Abanin, E. Altman, I. Bloch, and M. Serbyn, “Colloquium: many-body localization, thermalization, and entanglement”, *Rev. Mod. Phys.* **91**, 021001 (2019).
- [234] M. D. Eisaman, J. Fan, A. Migdall, and S. V. Polyakov, “Invited review article: single-photon sources and detectors”, *Rev. Sci. Instrum.* **82**, 071101 (2011).
- [235] L. J. Diguna, L. Tjahjana, Y. Darma, S. Zeng, H. Wang, and M. D. Birowosuto, “Light-matter interaction of single quantum emitters with dielectric nanostructures”, *Photonics* **5**, 14 (2018).
- [236] F. Wolf, C. Shi, J. C. Heip, M. Gessner, L. Pezzè, A. Smerzi, M. Schulte, K. Hammerer, and P. O. Schmidt, “Motional Fock states for quantum-enhanced amplitude and phase measurements with trapped ions”, *Nat. Comm.* **10**, 2929 (2019).
- [237] M. Lohse, C. Schweizer, O. Zilberberg, M. Aidelsburger, and I. Bloch, “A Thouless quantum pump with ultracold bosonic atoms in an optical superlattice”, *Nat. Phys.* **12**, 350 (2016).
- [238] A. Roggero, C. Gu, A. Baroni, and T. Papenbrock, “Preparation of excited states for nuclear dynamics on a quantum computer”, *Phys. Rev. C* **102**, 064624 (2020).
- [239] S. Heinze, P. Cejnar, J. Jolie, and M. Macek, “Evolution of spectral properties along the O(6)-U(5) transition in the interacting boson model. I. Level dynamics”, *Phys. Rev. C* **73**, 014306 (2006).
- [240] M. Macek, P. Cejnar, J. Jolie, and S. Heinze, “Evolution of spectral properties along the O(6)-U(5) transition in the interacting boson model. II. Classical trajectories”, *Phys. Rev. C* **73**, 014307 (2006).
- [241] M. A. Caprio, P. Cejnar, and F. Iachello, “Excited state quantum phase transitions in many-body systems”, *Annals of Physics* **323**, 1106 (2008).
- [242] F. Leyvraz and W. D. Heiss, “Large- $n$  scaling behavior of the Lipkin-Meshkov-Glick model”, *Phys. Rev. Lett.* **95**, 050402 (2005).
- [243] P. Ribeiro, J. Vidal, and R. Mosseri, “Exact spectrum of the Lipkin-Meshkov-Glick model in the thermodynamic limit and finite-size corrections”, *Phys. Rev. E* **78**, 021106 (2008).



- [244] P. Pérez-Fernández, A. Relaño, J. M. Arias, P. Cejnar, J. Dukelsky, and J. E. García-Ramos, “Excited-state phase transition and onset of chaos in quantum optical models”, *Phys. Rev. E* **83**, 046208 (2011).
- [245] T. Brandes, “Excited-state quantum phase transitions in Dicke superradiance models”, *Phys. Rev. E* **88**, 032133 (2013).
- [246] M. A. Bastarrachea-Magnani, S. Lerma-Hernández, and J. G. Hirsch, “Comparative quantum and semiclassical analysis of atom-field systems. I. Density of states and excited-state quantum phase transitions”, *Phys. Rev. A* **89**, 032101 (2014).
- [247] M. A. Bastarrachea-Magnani, S. Lerma-Hernández, and J. G. Hirsch, “Comparative quantum and semiclassical analysis of atom-field systems. II. Chaos and regularity”, *Phys. Rev. A* **89**, 032102 (2014).
- [248] M. Macek, P. Stránský, A. Leviatan, and P. Cejnar, “Excited-state quantum phase transitions in systems with two degrees of freedom. III. Interacting boson systems”, *Phys. Rev. C* **99**, 064323 (2019).
- [249] A. Relaño, J. Dukelsky, P. Pérez-Fernández, and J. M. Arias, “Quantum phase transitions of atom-molecule Bose mixtures in a double-well potential”, *Phys. Rev. E* **90**, 042139 (2014).
- [250] V. M. Bastidas, P. Pérez-Fernández, M. Vogl, and T. Brandes, “Quantum criticality and dynamical instability in the kicked-top model”, *Phys. Rev. Lett.* **112**, 140408 (2014).
- [251] P. Stránský, M. Macek, and P. Cejnar, “Excited-state quantum phase transitions in systems with two degrees of freedom: level density, level dynamics, thermal properties”, *Ann. Phys.* **345**, 73 (2014).
- [252] P. Stránský, M. Macek, A. Leviatan, and P. Cejnar, “Excited-state quantum phase transitions in systems with two degrees of freedom: II. finite-size effects”, *Annals of Physics* **356**, 57 (2015).
- [253] P. Stránský and P. Cejnar, “Classification of excited-state quantum phase transitions for arbitrary number of degrees of freedom”, *Phys. Lett. A* **380**, 2637 (2016).
- [254] M. A. Bastarrachea-Magnani, S. Lerma-Hernández, and J. G. Hirsch, “Thermal and quantum phase transitions in atom-field systems: a microcanonical analysis”, *J. Stat. Mech.* **2016**, 093105 (2016).
- [255] P. Pérez-Fernández and A. Relaño, “From thermal to excited-state quantum phase transition: the Dicke model”, *Phys. Rev. E* **96**, 012121 (2017).
- [256] P. Cejnar and P. Stránský, “Heat capacity for systems with excited-state quantum phase transitions”, *Phys. Lett. A* **381**, 984 (2017).
- [257] M. Kloc, P. Cejnar, and G. Schaller, “Collective performance of a finite-time quantum Otto cycle”, *Phys. Rev. E* **100**, 042126 (2019).
- [258] P. Pérez-Fernández, P. Cejnar, J. M. Arias, J. Dukelsky, J. E. García-Ramos, and A. Relaño, “Quantum quench influenced by an excited-state phase transition”, *Phys. Rev. A* **83**, 033802 (2011).
- [259] L. F. Santos and F. Pérez-Bernal, “Structure of eigenstates and quench dynamics at an excited-state quantum phase transition”, *Phys. Rev. A* **92**, 050101(R) (2015).
- [260] R. Puebla, A. Smirne, S. F. Huelga, and M. B. Plenio, “Universal anti-Kibble-Zurek scaling in fully connected systems”, *Phys. Rev. Lett.* **124**, 230602 (2020).

- 
- [261] M. Kloc, D. Šimsa, F. Hanák, P. R. Kaprálová-Ž'ánská, P. Stránský, and P. Cejnar, *Quasiclassical approach to quantum quench dynamics in the presence of an excited-state quantum phase transition*, [arXiv:2010.07750](#), 2020.
- [262] D. Larese and F. Iachello, “A study of quantum phase transitions and quantum monodromy in the bending motion of non-rigid molecules”, *J. Mol. Struct.* **1006**, 611 (2011).
- [263] D. Larese, F. Pérez-Bernal, and F. Iachello, “Signatures of quantum phase transitions and excited state quantum phase transitions in the vibrational bending dynamics of triatomic molecules”, *J. Mol. Struct.* **1051**, 310 (2013).
- [264] R. Puebla, A. Relaño, and J. Retamosa, “Excited-state phase transition leading to symmetry-breaking steady states in the Dicke model”, *Phys. Rev. A* **87**, 023819 (2013).
- [265] R. Puebla and A. Relaño, “Non-thermal excited-state quantum phase transitions”, *EPL* **104**, 50007 (2013).
- [266] A. L. Corps and A. Relaño, *Constant of motion identifying excited-state quantum phases*, [arXiv:2103.10762](#), 2021.
- [267] B. Lücke, J. Peise, G. Vitagliano, J. Arlt, L. Santos, G. Tóth, and C. Klempt, “Detecting multiparticle entanglement of Dicke states”, *Phys. Rev. Lett.* **112**, 155304 (2014).
- [268] D. R. Romano and E. J. V. d. Passos, “Population and phase dynamics of  $f = 1$  spinor condensates in an external magnetic field”, *Phys. Rev. A* **70**, 043614 (2004).





# Curriculum Vitae

## Personal details

Name	Polina Feldmann
ORCID iD	<a href="https://orcid.org/0000-0002-9516-1899">https://orcid.org/0000-0002-9516-1899</a>
Gender	Female
Date of Birth	August 1993
Place of Birth	Moscow, Russia
Parents	Alexander and Valeria Feldmann
Nationalities	Russian, German
Civil Status	married

## Education

since 2016	Doctoral candidate, Institute of Theoretical Physics, Leibniz University Hanover, Germany
2016	<i>Master of Science in Physics,</i> <i>Friedrich Schiller University Jena, Germany</i>
2014–2016	Friedrich Schiller University Jena, Germany: Physics
2014	<i>Bachelor of Science in Physics,</i> <i>Friedrich Schiller University Jena, Germany</i>
2013–2014	Friedrich Schiller University Jena, Germany: Physics
2011–2013	Philipps University Marburg, Germany: Physics
2010–2011	Friedrich Schiller University Jena, Germany: Chemistry
2010	<i>high-school graduation, Marienschule Limburg, Germany</i>



# List of Publications

- P. Feldmann, C. Klempt, A. Smerzi, L. Santos, and M. Gessner, *Excited-state quantum phase transitions in spinor Bose-Einstein condensates*, [arXiv:2011.02823](#) (2020)
- F. Anders, A. Idel, P. Feldmann, D. Bondarenko, S. Loriani, K. Lange, J. Peise, M. Gersmann, B. Meyer, S. Abend, N. Gaaloul, C. Schubert, D. Schlippert, L. Santos, E. Rasel, and C. Klempt, *Momentum entanglement for atom interferometry*, [arXiv:2010.15796](#) (2020)
- D. Bondarenko and P. Feldmann, *Quantum autoencoders to denoise quantum data*, *Phys. Rev. Lett.* **124**, 130502 (2020)
- L. Pezzè, M. Gessner, P. Feldmann, C. Klempt, L. Santos, and A. Smerzi, *Heralded generation of macroscopic superposition states in a spinor Bose-Einstein condensate*, *Phys. Rev. Lett.* **123**, 260403 (2019)
- P. Feldmann, M. Gessner, M. Gabbrielli, C. Klempt, L. Santos, L. Pezzè, and A. Smerzi, *Interferometric sensitivity and entanglement by scanning through quantum phase transitions in spinor Bose-Einstein condensates*, *Phys. Rev. A* **97**, 032339 (2018)
- P. Feldmann, A. Wipf, and L. Zambelli, *Critical Wess-Zumino models with four supercharges in the functional renormalization group approach*, *Phys. Rev. D* **98**, 096005 (2018)
- A. Jost, E. Tolstik, P. Feldmann, K. Wicker, A. Sentenac, and R. Heintzmann, *Optical sectioning and high resolution in single-slice structured illumination microscopy by thick-slice blind-SIM reconstruction*, *PLoS ONE* **10**(7), e0132174 (2015)